UNIVERSIDADE DE BRASÍLIA
INSTITUTO DE GEOCIÊNCIAS

GEOCRONOLOGIA E SIGNIFICADO TECTÔNICO DE ROCHAS MÁFICAS DE ALTO GRAU METAMÓRFICO DA FAIXA BRASÍLIA

Maria Emilia Schutesky Della Giustina

Tese de Doutorado № 101

Brasília, DF

2010

UNIVERSIDADE DE BRASÍLIA
INSTITUTO DE GEOCIÊNCIAS

GEOCRONOLOGIA E SIGNIFICADO TECTÔNICO DE ROCHAS MÁFICAS DE ALTO GRAU METAMÓRFICO DA FAIXA BRASÍLIA

Maria Emilia Schutesky Della Giustina

Tese de Doutorado № 101

Orientador: Prof. Márcio Martins Pimentel
Co-orientador: Prof. Cesar Fonseca Ferreira Filho

Banca Examinadora: Prof. Reinhardt A. Fuck (UnB)
Prof. Nilson F. Botelho (UnB)
Prof.ª Renata Schmitt (UFRJ)
Prof. Claudio Valeriano (UERJ)
Suplente: Prof. Elton L. Dantas (UnB)

Brasília, DF, julho de 2010

Agradecimentos

A Deus, por me indicar o caminho.

Ao Christian e à minha mãe Georgete, em especial, e a toda a minha família, pelo incentivo e paciência.

Aos meus orientadores, pela confiança.

Ao meu "guru" Claudinei, por todos os palpites.

À Joseneusa e ao Sérgio, pelas longas conversas, e a todos os meus amigos, pela força.

À equipe do Laboratório de Geocronologia, minha segunda casa nos últimos anos, e a todos que por lá passaram e marcaram nossa vida.

À equipe da Geo Lógica Consultoria Ambiental, pelo carinho.

Ao CNPq, pela concessão da bolsa de doutorado e pelo apoio financeiro relativo ao projeto 477347/2007-0 (Edital MCT/CNPq Universal).

À International Nickel Ventures Ltd. e à Amazônia Mineração, por fornecer os testemunhos de sondagens das intrusões de Damolândia e Taquaral, bem como pelo suporte nos trabalhos de campo.

Ao Prof. Claudio Lamarão (UFPA), pelas imagens de catodoluminescência de zircão.

À Prof.ª Sandra Andrade (USP), pelas análises de elementos-traço em zircão.

Finalmente, a todos que contribuíram de alguma forma para a realização desta tese.

"*Se vi mais longe foi porque estava sobre o ombro de gigantes.*"

Isaac Newton

Resumo

Maria Emilia Schutesky Della Giustina. 2010. *Geocronologia e significado tectônico de rochas máficas de alto grau metamórfico da Faixa Brasília*. Tese de doutorado, Universidade de Brasília, Instituto de Geociências, Brasília, 121 p.

A interpretação das idades fornecidas por zircão de terrenos de alto grau tem se revelado complexa, visto que há processos que promovem a alteração do cristal ígneo em diferentes escalas durante o evento metamórfico, fornecendo, por vezes, informações geocronológicas ambíguas e pouco acuradas. Nesse sentido, o objetivo deste estudo é investigar a influência do metamorfismo de alto grau no sistema U-Pb de cristais de zircão dos complexos Anápolis-Itauçu e Serra da Malacacheta-Barro Alto, por meio da utilização de imageamento por catodoluminescência e de análises pontuais suplementares de isótopos de Hf e química de zircão. Com isso, pretende-se definir a *real-idade* geológica dos resultados obtidos e, assim, promover uma melhor compreensão do contexto geotectônico dos terrenos granulíticos mais expressivos da Faixa Brasília.

Os complexos acamadados de Damolândia e Taquaral, Goiás, encontram-se inseridos no Complexo Anápolis-Itauçu. Apesar do metamorfismo de fácies granulito superimposto, ainda se observam texturas e mineralogia primária nas duas intrusões e, portanto, os cristais de zircão devem revelar informações primárias e secundárias. Análises U-Pb revelam espalhamento de idades concordantes em intervalo de cerca de 80 Ma, com "interceptos" superiores de ~ 670 Ma. Entretanto, as razões iniciais de $^{176}Hf/^{177}Hf$ são homogêneas, tanto em escala cristalina quanto na população de zircão e não apresentam correlação com as idades U-Pb. Isso sugere que os cristais formaram-se em um único evento e, portanto, a dispersão observada nas idades reflete a perda parcial de informação do sistema U-Pb. Assim, conclui-se que as idades mais antigas, próximas a 670 Ma, são representativas do evento de cristalização ígnea dos complexos de Damolândia e Taquaral e, portanto, estas intrusões constituem episódio anterior de magmatismo máfico na Faixa Brasília. Este evento magmático mostra-se coevo ao metamorfismo de alto grau e, destarte, pode caracterizar a fonte adicional de calor necessária para o desenvolvimento das assembléias de temperatura ultra-alta dos granulitos do Complexo Anápolis-Itauçu.

O complexo Serra da Malacacheta-Barro Alto revela-se, ainda, um alvo adicional para a avaliação das alterações metamórficas em zircão, visto que também reúne rochas máfico-ultramáficas com metamorfismo de alto grau superimposto. Idades U-Pb revelam que o corpo acamadado constitui-se por duas intrusões distintas, caracterizadas pelos complexos Serra da Malcacheta (1,3 Ga) e Barro Alto (0,8 Ga). O metamorfismo de alto grau é datado por titanita e zircão recristalizado das duas unidades em c. 750 Ma, o que implica que ambas já se encontravam unidas neste episódio. Portanto, os novos dados confirmam a similaridade com os complexos Serra dos Borges e Niquelândia, expostos ao norte. Entretanto, os dados U-Pb em zircão são inconclusivos para o metanortosito e para o anfibolito Cafelândia. Em ambos os casos, a assinatura isotópica de Hf é homogênea e, consequentemente, implica em um único episódio de cristalização. Tal fato permite a reclassificação geocronológica das unidades, de modo que o metanortosito relaciona-se ao primeiro episódio magmático, enquanto que o anfibolito Cafelândia insere-se no segundo evento de magmatismo máfico.

Assim, o volumoso magmatismo máfico revela-se coevo ao metamorfismo de alto grau e sugere, portanto, que a Faixa Brasília represente um orógeno quente.

Palavras-chave: Faixa Brasília, zircão metamórfico, intrusões máficas-ultramáficas acamadadas, metamorfismo de alto grau, Complexo Anápolis-Itauçu, Complexo Serra da Malcacheta - Barro Alto.

Abstract

Maria Emilia Schutesky Della Giustina. 2010. *Geocronologia e significado tectônico de rochas máficas de alto grau metamórfico da Faixa Brasília*. Tese de doutorado, Universidade de Brasília, Instituto de Geociências, Brasília, 121 p.

The interpretation of U-Pb ages obtained in zircon grains from high-grade rocks have shown to be very complex, given that metamorphism might promote the alteration of igneous crystals in different scales, resulting in ambiguous and imprecise geochronological data. Therefore, the purpose of this study is to investigate the influence of the high-grade metamorphic imprint on the U-Pb isotopic system of zircon from the Anápolis-Itauçu and Serra da Malacacheta-Barro Alto complex, using additional information from cathodoluminescence imaging and *in-situ* isotopic and chemical analyses in order to define the geological meaning of U-Pb ages. Consequently, the new data provides a better comprehension of the geotectonic evolution of the most noteworthy granulite terranes in the Brasília Belt.

The Damolândia and Taquaral layered complexes, Goiás, are part of the Anápolis-Itauçu Complex. Besides of the superimposition of granulite-facies metamorphism, these intrusions still partially preserve igneous texture and mineralogy and, hence, zircon grains might enclose both primary and secondary geochronological information. U-Pb analyses reveal a spread of concordant ages spanning within an age interval of ~80 Ma, which suggests an "upper" intercept age of ~670 Ma. Nevertheless, Hf isotopic ratios are homogeneous within populations and also in crystal-scale domains in all samples and show correlation neither with U-Pb ages nor with Th/U ratios, suggesting that zircon grains crystallized during a single growth event. Therefore, it is suggested that the observed spread of concordant ages in reality reflects the partial reset of the U-Pb system and, thus, the older obtained ages, around 670 Ma, shall be representative of the igneous crystallization of the Damolândia and Taquaral intrusions. Consequently, the new data advocate for a previous episode of mafic magmatism in the Brasília Belt, which is coeval with the high-grade metamorphism in the Anápolis-Itauçu Complexes and, hence, characterizes the additional heat source to the development of ultra-high temperature assemblages.

The Serra da Malacacheta-Barro Alto constitutes an additional target to the investigation of metamorphic alteration processes on zircon, since it enclosures mafic-ultramafic rocks

metamorphosed under amphibolites to granulite facies conditions. U-Pb ages reveal that this composite intrusion is composed of two distinct intrusions, namely the Serra da Malacacheta (1.3 Ga) and Barro Alto complexes (0.8 Ga). The metamorphism is defined at ~750 Ma by titanite and recrystallized domains of zircon from both units, which implies that they were already combined by the time of the metamorphic imprint. Therefore, the new data confirms the similarity among the Serra da Malacacheta-Barro Alto Complex and the Serra dos Borges-Niquelândia complex, exposed to the north. However, U-Pb ages are themselves inconclusive in dating the metanorthosite and the Cafelândia amphibolite. Nevertheless, Hf isotopic signature of both samples is homogeneous and implies that zircon population has crystallized in a single episode, which allows the geochronological reclassification of these units. Thus, the metanorthosite characterizes the first event of mafic magmatism, while the Cafelândia amphibolite is attributed to the second magmatic episode.

Therefore, the voluminous mafic magmatism is coeval to high-grade metamorphism in both studied areas and thus, it suggests that the Brasília Belt typify a hot orogen.

Key-words: Brasília Belt, metamorphic zircon, layered mafic-ultramafic intrusions, high-grade metamorphism, Anápolis-Itauçu Complex, Serra da Malcacheta - Barro Alto Complex.

Lista de Figuras

Figura 1.1 – Mapa geológico esquemático da Faixa Brasília (modificado de Pimentel *et al.*, 2006). 3

Figura 1.2 – Ilustração do problema geocronológico no Complexo Anápolis-Itauçu. Dados U-Pb em zircão (TIMS, SHRIMP). a) Complexo Anápolis-Itauçu; para- e ortogranulitos félsicos (Piuzana, *et al.*, 2003; Baldwin & Brown, 2008; Moraes *et al.*, 2007). b) Complexos máficos-ultramáficos no domínio do Arco de Arenópolis (Hollanda *et al.*, 2003; Laux, *et al.* 2003). 4

Figura 1.3 – Ilustração do problema geocronológico para o Complexo Serra da Malacacheta-Barro Alto. A) SHRIMP U-Pb em zircão de metanortosito (modificado de Correia *et al.*, 2007). Os dados revelam idades entre 800 e 730 Ma e, portanto, não permitem a distinção entre a cristalização ígnea e o metamorfismo de alto-grau. B) Cristal de zircão de amostra do Complexo de Niquelândia, interpretado como equivalente ao norte do Complexo de Barro Alto (modificado de Pimentel *et al.*, 2004). Bordas metamórficas são nítidas e ocorrem como superfícies curvas quee obliteram a zonação primária. Verifica-se, ainda, que o núcleo apresenta idades mais novas que as bordas, o que sugere distúrbio da assinatura isotópica U-Pb. 5

Figura 2.1 - Aplicações do zircão (baseado em Belousova *et al.*, 2006, Valley, 2003; Watson *et al.*, 2006; Harley & Kelly, 2007; Gerdes & Zeh, 2009). 9

Figura 2.2 – Possíveis etapas de cristalização de zircão durante o metamorfismo em um orógeno quente, durante um período de tempo (Δt) da ordem de milhões de anos (modificado de Harley *et al.*, 2007). Vide texto para explicação. 11

Figura 2.3 - Morfologias externas e texturas internas típicas de zircão metamórfico. A) Morfologia ovóide, com faces e arestas arredondadas, resultantes da interação com fluidos insaturados em Zr (Hoskin & Schaltegger, 2003). B) Zircão euédrico, denominado "soccer-ball", descrito em leucossoma de fácies granulito (Schaltegger *et al.*, 1999). C) Sequência de estruturas geralmente observadas em zircão cristalizado no episódio metamórfico de alto-grau. O núcleo herdado (1) é envolto por uma zona de baixa luminescência (2), a qual é subsequentemente envolta por uma zona de alta catodoluminescência (Hoskin & Schaltegger, 2003). D) Zircão recristalizado no metamorfismo de alto-grau; nota-se um domínio externo com zonação caótica e não planar, bem como reentrâncias que migram da borda para o núcleo do grão (dimensão em torno de 200μm; Corfu *et al.*, 2003). 13

Figura 2.4 – Mobilidade de elementos traço em zircão durante o metamorfismo de alto-grau (modificado de Martin *et al.*, 2008). Em A, ilustra-se a situação na qual há uma nova cristalização, representada por bordas neoformadas ao redor de núcleos antigos, e em B observa-se um episódio de recristalização do zircão. Ressalta-se a presença de uma fase fluida em ambos os casos, a qual facilita a troca de elementos com o meio. 14

Figura 2.5 – Padrão de elementos terras raras de zircão metamórfico normalizados pelo condrito (Hoskin & Schaltegger 2003; Fraser *et al.* 1997). Ambas as curvas representam a cristalização de novos indivíduos ou o sobrecrescimento de bordas ao redor de núcleos herdados. 15

Figure 3.1 - A) Regional sketch map of the Brasilia Belt, in the eastern part of the Tocantins Province (modified from Giustina *et al.*, 2009). B) Geological map of the central part of the Anápolis-Itauçu Complex (modified from Piuzana *et al.*, 2003). The star represents the location of sample INHO-01. 22

Figure 3.2 - Geology of the Damolândia Complex (from unpublished report of International Nickel Venture Ltd.). 25

Figure 3.3 - A) View of the area close to the drill hole FSDM-07. Rare outcrops and abundant dark brownish termite mounts developed on soil from ultramafic rocks (close to drill hole FSDM-07). B) Orthopyroxenite with interstitial white plagioclase (close to drill hole FSDM-07). C) Harzburgite from drill hole FSDM-07. D) Photomicrograph of harzburgite consisting of cumulus olivine (Ol) enclosed in large orthopyroxene oikocryst (opx). E) Photomicrograph of norite consisting of cumulus orthopyroxene (opx) and plagioclase (Pl). F) Zircon-bearing hornblende gabbronorite. Sample DM-16 from drill hole FSDM-07. G) and H) Photomicrograph of partially recrystallized plagioclase-bearing orthopyroxenite. Large igneous orthopyroxene crystals are recrystallized into fine-grained granoblastic aggregates. 26

Figure 3.4 - Log, MgO content and εNd(T) for drill hole FSDM-07. 27

Figure 3.5 - Plot of MgO versus CaO, TiO_2, Cr and K_2O for the drill hole FSDM07. 28

Figure 3.6 - Geology of the northern area of the Taquaral Complex (from unpublished report of International Nickel Venture Ltd.). 30

Figure 3.7 - A) Boulder of highly foliated mafic granulite. The mineral assemblage consists of orthopyroxene, clinopyroxene, plagioclase, hornblende and magnetite. Abundant reddish termite mounts are developed on soil from mafic rocks (locality of sample TQ-22). B) Outcrop of highly foliated subvertical peridotite. Elongated pyroxene crystals and pyroxene aggregates become evident in the weathered surface. C) Sharp contact between peridotite (left side) and pyroxenite (right side) from drill core FSTQ-01. Large pyroxene crystals in the peridotite show up in lighter colors. D) Photomicrograph of peridotite consisting of partially serpentinized olivine crystals (Ol) associated with large orthopyroxene (opx) and chromite (Cr). E) Orthopyroxenite with interstitial sulfides from drill core FSTQ-01. 31

Figure 3.8 - Log, MgO content and εNd(T) for drill hole FSTQ-01 (see Fig. 6 for location). 32

Figure 3.9 - Plot of MgO versus CaO, TiO_2, Cr and K_2O for the drill hole FSTQ-01. 33

Figure 3.10 – CL images of zircon from sample DM-16 (A, B), sample DM-20 (C, D) and sample TQ-14 (E, F). Smaller spots (30 µm) represent the location of U-Pb analyses, whereas larger spots (40 µm) correspond to Hf isotopic investigation. 38

Figure 3.11 - LA-ICPMS (A-C), SHRIMP (D) and ID-TIMS (E-F) U-Pb plots for Damolândia (DM), Taquaral (TQ, TAQ) and Goianira-Trindade complexes (INHO). 39

Figure 3.12 - Zircon i*n situ* Hf isotopic data (A, $^{176}Hf/^{177}Hf_t$; B, ε_{Hft}) versus U-Pb age plots. 51

Figure 4.1 - Regional geotectonic setting of the Brasilia Belt, in the eastern part of the Tocantins Province (modified after Pimentel *et al.*, 2006; Giustina *et al.*, 2009). 60

Figure 4.2 – A) Geological sketch map of the Barro Alto and Serra da Malacacheta complexes showing sample locations. Geological sketch map (B) and geological section (A-A'; C) of the NNE-section of the Barro Alto and Serra da Malacacheta complexes in the Laguna-Barro Alto region (modified after Ferreira Filho *et al.*, 2010). 63

Figure 4.3 - CL images of zircon from the SMC and BAC. A, B) Sample BAL-09. (C-F) Sample CAFEL. G, H) Sample BAL-05. Smaller spots (30 µm) represent the location of U-Pb analyses, whereas larger spots (40 µm) correspond to Hf isotopic investigation. 69

Figure 4.4 - LA-ICPMS U-Pb diagrams for sample BAL-09 (A); sample BAL-04 (zircon, B; titanite, C); sample CAFEL (D); sample BAL-05 (E). 70

Figure 4.5 – Zircon REE normalized plots from samples BAL-09 (A), BAL-04 (B) and CAFEL (C). 81

Figure 4.6 - Zircon i*n situ* Hf isotopic data plotted against U-Pb systematics. Hf signature is homogeneous within individual samples and do not correlate with neither Lu-Hf ratios nor U-Pb ages, regardless of the concordance level. Additionally, Hf isotopic data reveal two distinct zircon crystallization events, the first at ca. 1.3 Ga and the second near 0.8 Ga. See text for discussion 87

Figure 4.7 - Ti-in-zircon temperatures plotted against U-Pb, Lu-Hf systematics and trace element contents. There is no correlation among Ti-in-zircon data and Th/U ratios, Hf isotopes or total REE contents. Additionally, the regular distribution of temperatures near 700°C is noteworthy. 91

Figura 5.1 - Ilustração esquemática dos processos de difusão (A) e dissolução-reprecipitação concomitante (B). No caso de difusão, a troca de elementos químicos se dá em estado sólido (A), enquanto que na dissolução-reprecipitação o fluido ou o magma facilitam a troca (B). Neste último caso, desenvolve-se uma borda de recristalização em ambos os minerais envolvidos, na qual se mantém preservada a orientação cristalográfica. O desenho não está em escala. 99

Figura 5.2 - Exemplos do processo de dissolução-reprecipitação concomitantes. A) Imagem de elétrons retro-espalhados em granada alterada pelo reequilíbrio com fluido hidrotermal (Pollock *et al.*, 2008). As porções escuras preservam a assinatura de facies granulito, enquanto que as bordas claras apresentam composição de granada eclogítica. B) Monazita de granulito básico da Zona Ivrea, Itália (Förster & Harlov, 1999). C) Cristal de monazita, inicialmente homogêneo, submetido àalteração por fluidos alcalinos (Harlov, 2009). As setas indicam as frentes de recristalização desenvolvidas sob condições de 900°C e 1000 MPa, após 25 dias de experimento. 101

Figura 5.3 - Processo de dissolução-reprecipitação concomitante (modificado de Geisler *et al.*, 2007). O processo envolve a dissolução de zircão rico em $MSiO_4$ e a concomitante precipitação de zircão puro e inclusões de $MSiO_4$. O zircão (amostra CAFEL) apresenta inclusões representadas por zonas com catodoluminescência mais elevada, feição característica deste tipo de recristalização. Ressalta-se que a recristalização se dá localmente (em escala de µm) e envolve transporte restrito. 103

Lista de Tabelas

Tabela 2.1- Principais substituições em zircão (Hoskin & Schaltegger, 2003). 16
Table 3.1 – U-Pb LA-ICPMS data for sample DM-16. 40
Table 3.2 - Summary of in situ Lu–Hf analyses for sample DM-16. 41
Table 3.3 - Sm-Nd data for the Damolândia Complex. 41
Table 3.4 - U-Pb LA-ICPMS data for sample DM-20. 42
Table 3.5 - Summary of in situ Lu–Hf analyses for sample DM-20. 42
Table 3.6 - U-Pb LA-ICPMS data for sample TQ-14. 43
Table 3.7 - Summary of in situ Lu–Hf analyses for sample TQ-14. 43
Table 3.8 - U-Pb SHRIMP data for sample TAQ-02. 44
Table 3.9 – U-Pb ID-TIMS data for sample TAQ-03. 44
Table 3.10 – Sm-Nd data for the Taquaral Complex. 45
Table 3.11 – U-Pb ID-TIMS data for sample INHO-01. 45
Table 3.12 - Sm-Nd data for the Goianira-Trindade Complex. 46
Table 4.1 - Instrumental and analytical parameters for LA-ICPMS trace-element analyses. 67
Table 4.2- Pb LA-ICPMS data for sample BAL-09. 71
Table 4.3 - Summary of in situ Lu–Hf analyses for sample BAL-09. 71
Table 4.4 - Trace element composition of zircon crystals from sample BAL-09. 72
Table 4.5 - U-Pb LA-ICPMS data for sample BAL-04. 74
Table 4.6 - Summary of in situ Lu–Hf analyses for sample BAL-04. 75
Table 4.7 - Trace element composition of zircon crystals from sample BAL-04. 75
Table 4.8 - U-Pb LA-ICPMS data for sample CAFEL. 77
Table 4.9 - Summary of in situ Lu–Hf analyses for sample CAFEL. 77
Table 4.10 - Trace element composition of zircon crystals from sample CAFEL. 78
Table 4.11 - U-Pb LA-ICPMS data for sample BAL-05. 80
Table 4.12 - Summary of in situ Lu–Hf analyses for sample BAL-05. 80

Sumário

AGRADECIMENTOS I

RESUMO III

ABSTRACT V

LISTA DE FIGURAS VII

LISTA DE TABELAS X

1. INTRODUÇÃO 1

1.1. Justificativa do tema 1

1.2. Objetivos 5

1.3. Estrutura da Tese 6

2. ZIRCÃO METAMÓRFICO 8

2.1. Introdução 8

2.2. Condições de formação de zircão no metamorfismo de alto grau 9

2.3. Características físicas 12

2.4. Assinatura Geoquímica 14

Cristalização de novos grãos/ sobrecrescimento metamórfico 15

Recristalização metamórfica de zircão 16

2.5. Considerações finais 17

3. DATING COEVAL MAFIC MAGMATISM AND ULTRAHIGH-TEMPERATURE METAMORPHISM IN THE ANÁPOLIS-ITAUÇU COMPLEX, CENTRAL BRAZIL 18

3.1. Introduction 19

3.2. Geological setting 20

3.3. Damolândia and Taquaral Layered Complexes 23

Damolândia 24

Taquaral 29

3.4. Methods 34

In situ zircon analyses 34

ID-TIMS analyses 36

3.5. Samples and results 37

Damolândia region 37

Taquaral area 47

Goianira-Trindade Complex 48

3.6. Discussion 49

"Metamorphic" zircon and the meaning of the spread of concordant U-Pb ages 49

Comparison between dating methods 53

Tectonic implications for the evolution of the Brasília Belt 54

3.7. Conclusions 55

3.8. Acknowledgments 56

4. HIGH-GRADE METAMORPHIC ALTERATION OF ZIRCON: A COMBINED LA-ICPMS ISOTOPIC AND TRACE ELEMENT STUDY OF A COMPOSITE MAFIC-ULTRAMAFIC LAYERED COMPLEX IN CENTRAL BRAZIL 57

4.1. Introduction 58

4.2. Regional Geological Setting 59

4.3. The Serra da Malacacheta and Barro Alto complexes 62

4.4. Methods **65**

4.5. Samples and Results **68**

Leucogabbro BAL-09 68

Metanorthosite BAL-04 82

Garnet-amphibolite CAFEL 83

Basic granulite BAL-05 84

4.6. Discussion **85**

High-grade metamorphic imprint and the interpretation of zircon U-Pb ages 85

Geological Implications 92

4.7. Conclusions **95**

4.8. Acknowledgments **97**

5. DISCUSSÃO **98**

5.1. Processos de recristalização mineral no metamorfismo **98**

5.2. Dissolução-reprecipitação concomitante em zircão **102**

5.3. Evidências dos complexos Anápolis-Itauçu e Serra da Malacacheta-Barro Alto **104**

6. CONCLUSÕES **107**

6.1. Implicações analíticas **108**

6.2. Implicações geotectônicas **109**

Complexo Anápolis-Itauçu 109

Complexos Serra da Malacacheta e Barro Alto 110

7. BIBLIOGRAFIA CONSULTADA **112**

1. INTRODUÇÃO

A datação de granulitos sempre despertou grande interesse na comunidade geológica, pois estas rochas evidenciam as condições mais extremas de pressão e temperatura por que passa um orógeno. O zircão é mineral comum em rochas ígneas e metamórficas, félsicas ou máficas, e, devido à sua resiliência mesmo sob condições de 1000°C e 20 kbar, ele permite adicionar informações geocronológicas aos estudos petrológicos. Entretanto, a interpretação das idades fornecidas por zircão de terrenos de alto grau é complexa e deve ser realizada com considerável cuidado, visto que há processos que promovem a alteração do cristal ígneo, em diferentes escalas, durante o evento metamórfico. Destarte, as informações geocronológicas providas podem ser ambíguas e pouco acuradas.

Conforme postulado por Rubatto & Hermann (2007), "não há varinha mágica para a interpretação das idades U-Pb em zircão; os estudos mais bem-sucedidos de datação são aqueles que combinam vários métodos para interpretar as idades U-Pb e que consideram a complexidade do sistema". Nesse contexto, o presente estudo abarca o problema geocronológico de datação de granulitos como prerrogativa para a interpretação da evolução geotectônica de um orógeno, exemplificado pela Faixa Brasília.

1.1.Justificativa do tema

Na Faixa Brasília, rochas metamórficas de alto grau são descritas essencialmente em duas áreas. O Complexo Anápolis-Itauçu, exposto em seu segmento meridional, constitui o núcleo metamórfico da Faixa Brasília (Pimentel *et al.*, 2000) e consiste de orto- e paragranulitos e granitos que compõem segmentos de orientação NW-SE, individualizados por zonas de cisalhamento de alto ângulo (Piuzana *et al.*, 2003).

Os complexos máfico-ultramáficos acamadados de Barro Alto, Niquelândia e Canabrava, por outro lado, encontram-se inseridos no Maciço de Goiás, o qual é interpretado como bloco alóctone incorporado à Província Tocantins durante a orogenia Brasiliana (Figura 1.1; Pimentel *et al.*, 2000). Os três complexos constituem uma faixa de aproximadamente 400 km na qual se exibem duas associações ígneas justapostas, metamorfisadas em fácies anfibolito a granulito.

Em ambas as áreas, granulitos com assembléias minerais de temperatura ultra-alta (>900°C; Harley, 1998) são descritos (Moraes & Fuck, 2000; Moraes *et al.*, 2002). Tais

condições metamórficas requerem ambiente crustal extremamente aquecido, o qual não é explicado pelos modelos numéricos disponíveis para orógenos colisionais (Jamieson *et al.*, 1998, 2004; Beaumont *et al.*, 2001, 2006). Dessa forma, uma fonte suplementar de calor é fundamental para o desenvolvimento destas assembléias minerais. Recentes artigos de revisão sobre granulitos de temperatura ultra-alta (Brown, 2007; Harley, 2008; Kelsey, 2008) discutem possíveis cenários geotectônicos para a formação destas rochas especiais e, atualmente, a hipótese dos orógenos acrescionários quentes ("hot orogens") é a mais aceita na comunidade científica como elucidativa de tais condições extremas (Collins, 2002; Hyndman *et al.*, 2005). Neste contexto, curtos episódios de extensão crustal durante o evento colisional resultam no afinamento da crosta e na ascensão da astenosfera, promovendo metamorfismo de alto-grau na base da crosta e a concomitante geração de grandes volumes de magma máfico, o qual poderia representar a fonte extra de calor (Pearce & Parkinson 1993; Jamieson *et al.*, 1998; Thompson *et al.*, 2001; Collins, 2002; Hyndman *et al.*, 2005).

Nos complexos Anápolis-Itauçu e Barro Alto observa-se a associação espacial entre granulitos de temperatura ultra-alta e rochas máficas e ultramáficas, porém dados disponíveis na literatura revelam um intervalo entre os episódios de metamorfismo e magmatismo que supera 20 Ma em ambos os casos. Conforme mencionado anteriormente, a superimposição do metamorfismo de alto-grau pode promover a alteração dos cristais de zircão, inclusive com perda da assinatura isotópica do sistema U-Pb (Ashwal *et al.*, 1999; Putins, 2002, 2009; Tomaschek *et al.*, 2003; Geisler *et al.*, 2007; Martin *et al.*, 2008). Logo, a diferença entre as idades de cristalização e de metamorfismo pode ser decorrente de um problema geocronológico e, portanto, uma investigação mais criteriosa se faz necessária a fim de determinar as reais idades dos episódios geológicos.

Nesse sentido, o Complexo Anápolis-Itauçu (CAI) constitui um objeto ideal para o estudo da atuação destas alterações em zircão, uma vez que inclui diversas intrusões máfico-ultramáficas nas quais ainda se observam texturas ígneas parcialmente preservadas, apesar do metamorfismo de alto-grau superimposto. Por conseguinte, o zircão dessas rochas deve preservar tanto informações primárias como secundárias. Adicionalmente, não há conhecimento geocronológico disponível para estas rochas e assume-se a idade de aproximadamente 630 Ma, obtida em intrusões acamadadas similares do domínio do Arco Magmático de Goiás, como

representativa do magmatismo máfico no Complexo Anápolis-Itauçu e, portanto, este episódio revela-se cerca de 20 Ma mais jovem que o pico do metamorfismo (Figura 1.2).

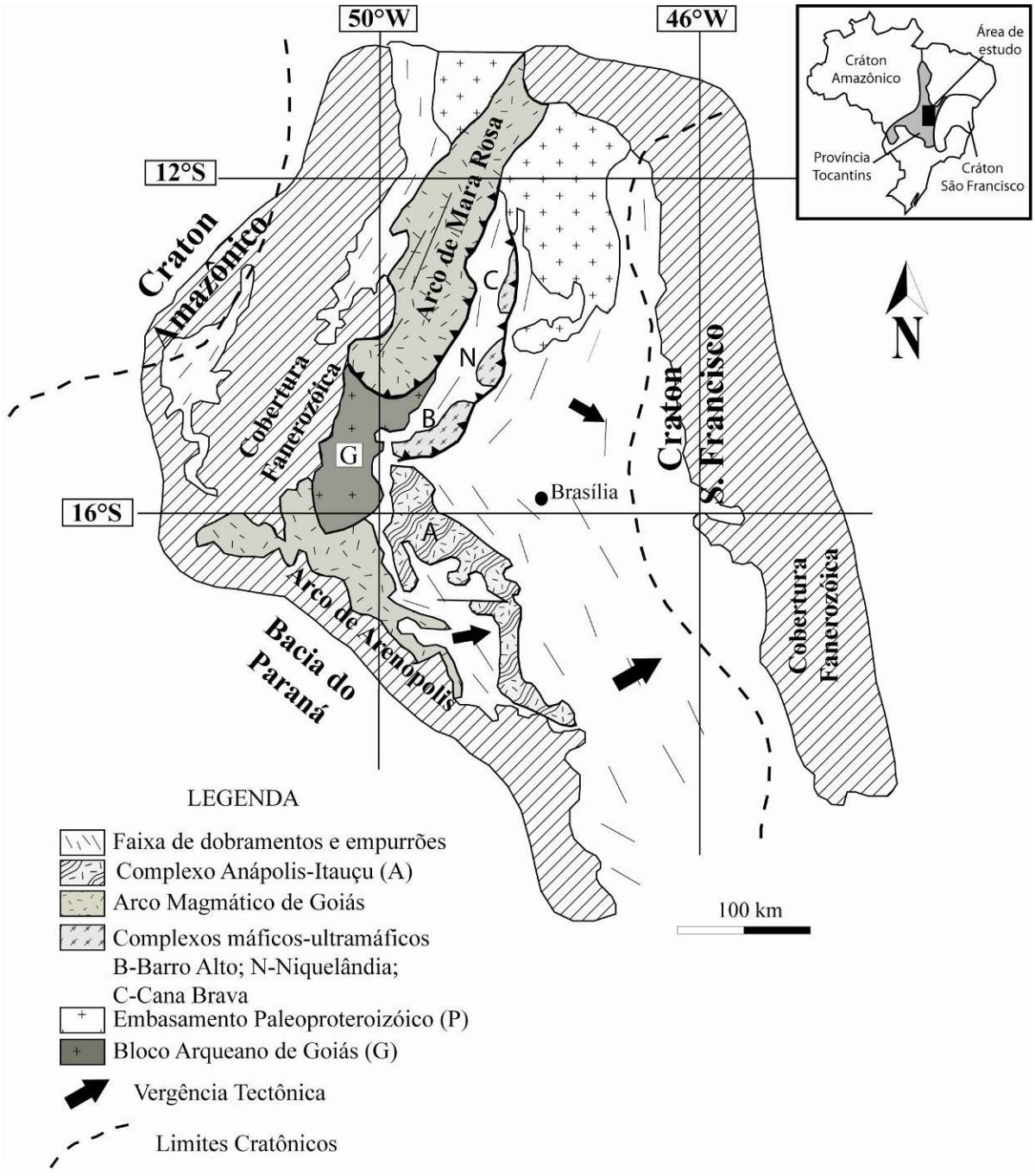

Figura 1.1 – Mapa geológico esquemático da Faixa Brasília (modificado de Pimentel *et al.*, 2006).

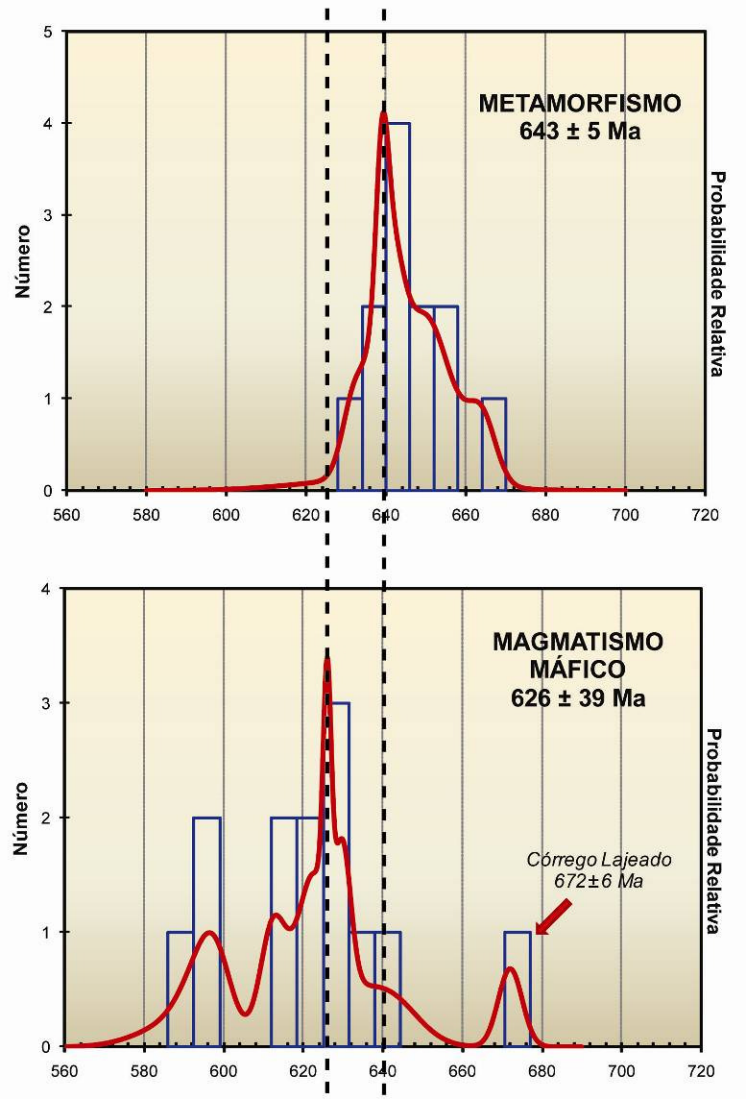

Figura 1.2 – Ilustração do problema geocronológico no Complexo Anápolis-Itauçu. Dados U-Pb em zircão (TIMS, SHRIMP). a) Complexo Anápolis-Itauçu; para- e ortogranulitos félsicos (Piuzana, *et al.*, 2003; Baldwin & Brown, 2008; Moraes *et al.*, 2007). b) Complexos máficos-ultramáficos no domínio do Arco de Arenópolis (Hollanda *et al.*, 2003; Laux, *et al.* 2003).

Adicionalmente, o Complexo de Barro Alto reúne condições geológicas similares aos corpos acamadados do Complexo Anápolis-Itauçu, nas quais as rochas máficas e ultramáficas apresentam metamorfismo de fácies granulito superimposto (Moraes *et al.*, 1994; Ferreira Filho, 1998). Dados de U-Pb em zircão para o Complexo de Barro Alto são escassos e indicam idades controversas, constituindo um comportamento análogo ao Complexo Anápolis-Itauçu (Figura 1.3a). Adicionalmente, o Complexo de Niquelândia, exposto ao norte, apresenta cristais de zircão nos quais a alteração é nítida e sugestiva de perda da informação isotópica (Figura 1.3b). Assim, feições similares devem estar presentes no Complexo de Barro Alto e, portanto, esta se

revela uma potencial área suplementar para a avaliação das alterações metamórficas de alto grau em cristais de zircão.

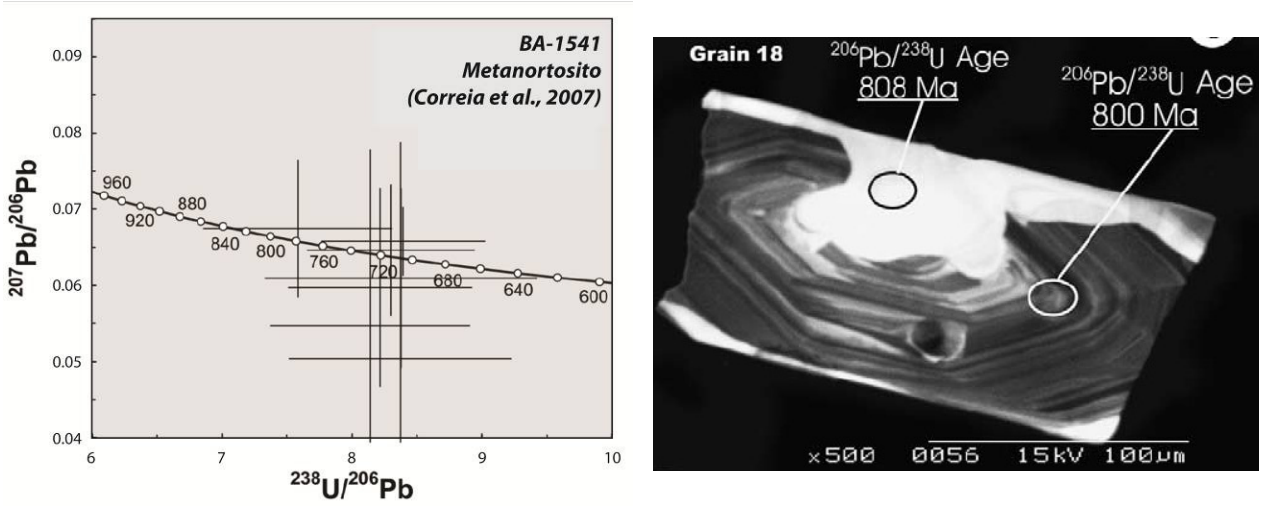

Figura 1.3 – Ilustração do problema geocronológico para o Complexo Serra da Malacacheta-Barro Alto. A) SHRIMP U-Pb em zircão de metanortosito (modificado de Correia *et al.*, 2007). Os dados revelam idades entre 800 e 730 Ma e, portanto, não permitem a distinção entre a cristalização ígnea e o metamorfismo de alto-grau. B) Cristal de zircão de amostra do Complexo de Niquelândia, interpretado como equivalente ao norte do Complexo de Barro Alto (modificado de Pimentel *et al.*, 2004). Bordas metamórficas são nítidas e ocorrem como superfícies curvas quee obliteram a zonação primária. Verifica-se, ainda, que o núcleo apresenta idades mais novas que as bordas, o que sugere distúrbio da assinatura isotópica U-Pb.

Dessa forma, o estudo das condições de alojamento crustal desse volumoso magmatismo máfico e de sua relação com o metamorfismo de alto grau torna-se crucial, dado que os complexos acamadados podem representar a fonte de calor para as paragêneses de temperatura ultra-alta observadas nos granulitos dos complexos Anápolis-Itauçu e Barro Alto.

1.2. Objetivos

O escopo desta tese é verificar qual a expressão do metamorfismo de alto grau nos cristais de zircão dos complexos Anápolis-Itauçu e Barro Alto e como esse processo influencia o sistema U-Pb. Com a resolução deste problema geocronológico, será possível definir a realidade geológica contida nas idades obtidas e, consequentemente, discorrer a respeito do contexto geotectônico dos terrenos granulíticos mais expressivos da Faixa Brasília.

Assim, no âmbito da Faixa Brasília, o estudo tem como objetivo específico responder às seguintes questões:

1. As idades U-Pb em zircão representam a cristalização ígnea, a superimposição do metamorfismo de alto grau, ou ainda um valor intermediário entre ambas?
2. Quantos eventos geológicos encontram-se registrados no zircão dessas rochas?
3. Quais as implicações dos resultados obtidos para o entendimento da evolução tectônica da Faixa Brasília?
4. E, por fim, qual é a relação entre o volumoso magmatismo máfico e o metamorfismo de temperatura ultra-alta?

Este estudo representa um avanço em termos de aplicação de diversas técnicas analíticas com vistas à resolução de problemas geológicos-geocronológicos na Faixa Brasília. Dessa forma, imagens de catodoluminescência revelarão a textura interna do grão, enquanto que análises *in-situ* de isótopos de Hf em zircão permitirão averiguar os episódios de cristalização aos quais o grão foi submetido. Por fim, a investigação da composição química de zircão contribuirá para a compreensão da relação entre este mineral e as demais fases metamórficas e, portanto, aliar-se-á informação petrológica às idades U-Pb.

Adicionalmente, este estudo promove um avanço para o entendimento da atuação do metamorfismo de alto grau sobre zircão e, assim, as informações aqui obtidas contribuem para a compreensão de feições similares, descritas em terrenos que apresentem cenário similar ao aqui exposto.

1.3. Estrutura da Tese

A tese encontra-se organizada em sete capítulos. Após este tópico introdutório, segue-se uma revisão teórica de questões relativas à formação de zircão metamórfico, com ênfase nas características físicas e químicas resultantes da superimposição do metamorfismo de alto-grau, a fim de acumular informações para posterior aplicação na interpretação do contexto geológico-geocronológico dos complexos Anápolis-Itauçu e Barro Alto.

Os resultados da tese são redigidos em formato próprio para divulgação em periódicos internacionais. Destarte, o Capítulo 3 discute os dados obtidos para o Complexo Anápolis-Itauçu, cujo artigo encontra-se aceito para publicação em volume especial do periódico *Lithos*, referente à conferência Granulites & Granulites 2009. O capítulo seguinte apresenta informações obtidas

para os complexos Serra da Malacacheta e Barro Alto, organizadas em trabalho submetido à *Precambrian Research*.

No Capítulo 5, discutem-se os processos físico-químicos de recristalização de minerais aplicados ao zircão, frente aos dados obtidos em ambas as áreas de estudo. Por fim, o Capítulo 6 apresenta as conclusões obtidas neste estudo.

As referências consultadas estão listadas no Capítulo 7.

No CD-ROM em anexo, encontram-se imagens de catodoluminescência dos grãos analisados neste estudo referenciados aos dados U-Pb em zircão.

2. ZIRCÃO METAMÓRFICO

2.1.Introdução

Zircão é o principal silicato de Zr tanto em rochas ígneas quanto metamórficas e, atualmente, é o mineral mais utilizado para datação pelo método U-Pb em função das características físico-químicas que admitem a substituição de Zr por íons tetravalentes (p.ex. U e Th) e ainda decorrem em baixas taxas de difusão iônica, permitindo assim o acúmulo de Pb durante o tempo geológico.

Na última década, vários estudos revelaram a aplicação deste mineral não somente para geocronologia, mas também para estudos petrogenéticos. Visto que geralmente são assimilados diversos outros elementos traço à estrutura cristalina, como Hf, REE, Y e Ti, zircão mostrou-se apropriado para investigações da fonte magmática e de processos de assimilação crustal, além de eventos geológicos posteriores à cristalização, como é o caso do metamorfismo (Figura 2.1).

Contudo, tais análises só se tornaram possíveis devido ao aprimoramento das ferramentas microanalíticas que, atualmente, propiciam resultados mais acurados em função da elevada resolução espacial e permitem a obtenção de dados robustos dos sistemas isotópicos U-Pb e Lu-Hf em zircão, bem como de concentrações de elementros-traço, que podem ser inferiores a 10 ppm (Hoskin & Schaltegger, 2003). Devido a tal progresso, diversos terrenos metamórficos de significado geológico-geocronológico complexo foram revisitados, com o intuito de avaliar o comportamento de zircão durante o metamorfismo de alto grau.

Nesse sentido, este capítulo dedica-se a uma revisão teórica sobre zircão metamórfico, a fim de adquirir as informações disponíveis na literatura e aplicá-las para melhor entendimento da evolução tectono-metamórfica dos complexos Anápolis-Itauçu e Serra da Malacacheta-Barro Alto.

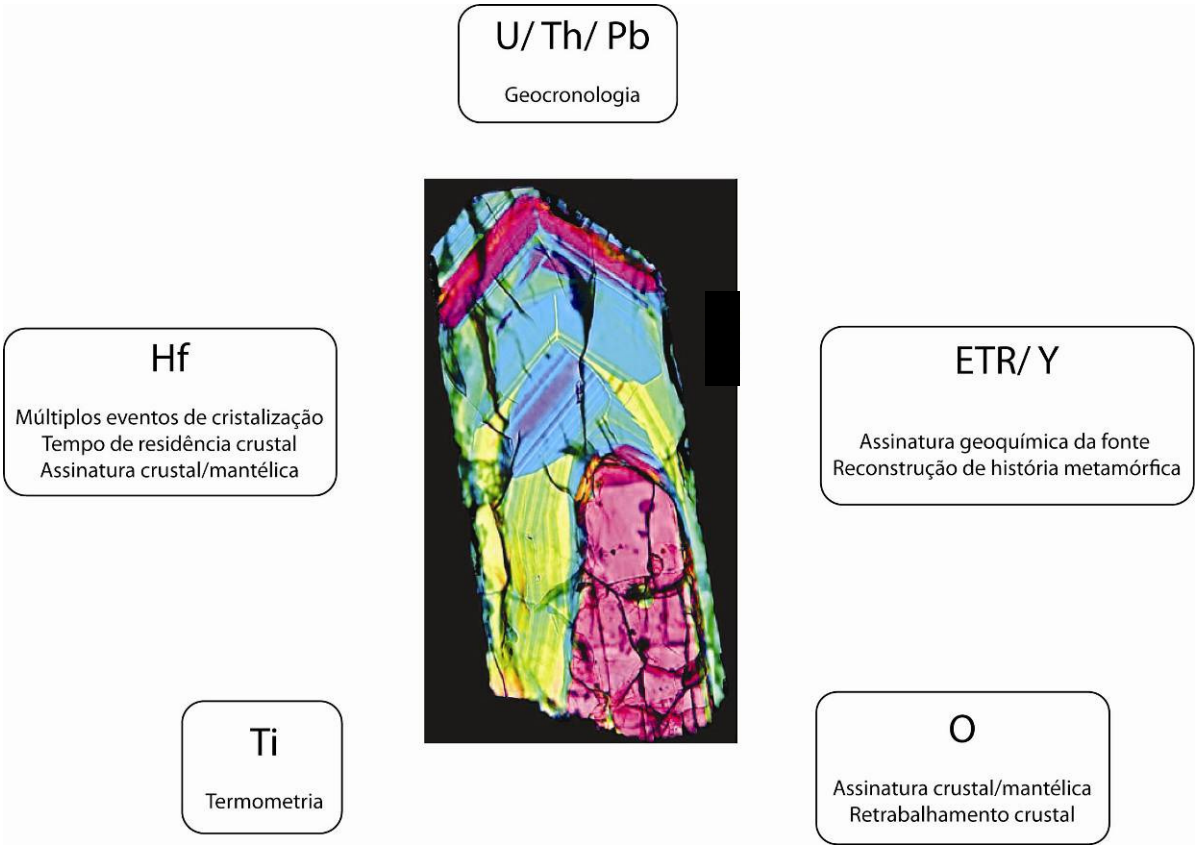

Figura 2.1 - Aplicações do zircão (baseado em Belousova *et al.*, 2006, Valley, 2003; Watson *et al.*, 2006; Harley & Kelly, 2007; Gerdes & Zeh, 2009).

2.2. Condições de formação de zircão no metamorfismo de alto grau

Durante o metamorfismo, zircão pode formar-se de dois modos distintos:

- Por ***cristalização***, a partir de fluidos ou magmas (Roberts & Finger, 1997; Schaltegger *et al.*, 1999; Vavra *et al.*, 1999; Rubatto, 2002, Rubatto & Hermann, 2007; entre outros) ou ainda em decorrência de reações metamórficas que envolvam a quebra de minerais portadores de Zr (Vavra *et al.*, 1996; Fraser *et al.*, 1997; Bingen *et al.*, 2001; Degeling *et al.*, 2001; Bea *et al.*, 2006). Esse processo resulta em bordas neoformadas ao redor de grãos remanescentes ou mesmo em novos cristais individuais. Portanto, trata-se de eventos de dissolução e cristalização temporal e espacialmente desconectados (Vavra *et al.*, 1999; Ayers *et al.*, 2003).

- Por ***recristalização***[1], induzida ou não por defeitos cristalinos oriundos de radiação, em um processo gradual que migra da borda para o núcleo do cristal e que promove o reequilíbrio físico-químico do zircão (Ashwal *et al.*, 1999; Hoskin & Black, 2000; Rubatto & Hermann, 2003; Tomaschek *et al.*, 2003; Geisler *et al.*, 2007; Martin *et al.*, 2008; Rubatto *et al.*, 2008; Gerdes & Zeh, 2009). Nesse caso fluidos metamórficos são responsáveis pela mobilidade dos elementos constituintes do zircão e, desta forma, esse tipo de alteração é capaz de induzir a perda parcial ou mesmo total de Pb. Por conseguinte, as idades obtidas podem não ter significado geológico.

Ambas as condições para formação de zircão metamórfico podem ser atribuídas tanto a etapas progressivas quanto retrometamórficas da evolução de um orógeno (Figura 2.2). Nas fases iniciais da trajetória P-T, predominam as reações de desidratação (Ms, Bt e/ou Hbl). Assim, os fluidos liberados promovem a fusão parcial da rocha (A), o que resulta na dissolução dos menores cristais de zircão e consequente sobrecrescimento nos grãos restantes (Figura 2.2B).

Com o aumento progressivo da temperatura, ao redor do pico do metamorfismo pode ocorrer o reequilíbrio do zircão primário ou previamente alterado. Nessa zona de recristalização os cristais que permanecerem em contato com o fluido ou magma podem gradualmente reordenar sua estrutura, que se encontra metaestável em função de defeitos induzidos por radiação ou devido à deformação do retículo cristalino derivada da incorporação de elementos traço. No primeiro caso, a recuperação se dá pela nucleação e recristalização à expensa dos domínios amorfos do grão e, dependendo da composição do fluido, elementos "non-formula", como Ca, Al, Fe e Pb comum, são incorporados ao cristal (Geisler *et al.*, 2003; 2007). No segundo caso, a diferença de solubilidade entre os dois extremos da solução sólida facilita a dissolução e a reprecipitação concomitante do zircão. Assim, quando o fluido atinge o eutético desse sistema, gera-se um domínio prístino, empobrecido em elementos-traço, além de inclusões de fases minerais formadas a partir dos compostos eliminados durante esse processo (Geisler *et al.*, 2007).

[1] O termo 'recristalização' refere-se à modificação parcial ou mesmo total de alguma feição de um mineral ou rocha, especialmente a sua composição química (Harley *et al.*, 2007).

Todavia, ressalta-se que somente será possível acessar idades representativas dessa etapa caso o zircão seja envolto por outro mineral, o qual atuará como escudo contra as posteriores alterações do retrometamorfismo.

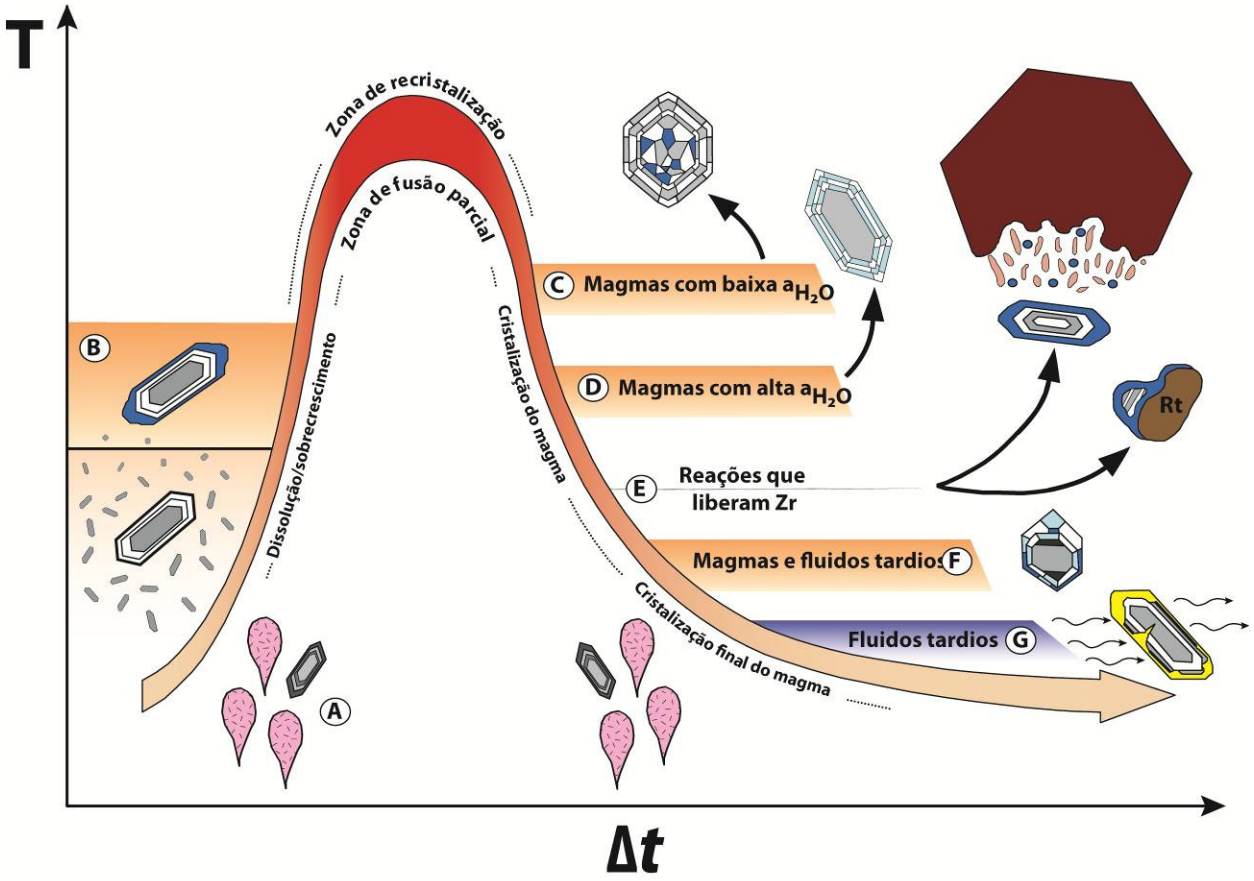

Figura 2.2 – Possíveis etapas de cristalização de zircão durante o metamorfismo em um orógeno quente, durante um período de tempo (Δt) da ordem de milhões de anos (modificado de Harley *et al.*, 2007). Vide texto para explicação.

Durante a trajetória de resfriamento, a composição do fluido/magma é, inicialmente, o principal fator que rege o momento de crescimento de novos grãos de zircão, visto que influencia diretamente a velocidade de cristalização (Figura 2.2C, D). Assim, fusões com baixa a_{H2O} cristalizam sob temperaturas mais elevadas e, além disso, o reduzido conteúdo de água diminui a difusão dos elementos nesse meio. Deste modo, uma feição atribuída a esse tipo de cristalização é a formação de prismas curtos que comumente apresentam zonação por setores (Schaltegger *et al.*, 1999; Hoskin & Schaltegger, 2003; Corfu *et al*, 2003). Por outro lado, minerais formados sob condições de elevada a_{H2O} revelam estruturas típicas de crescimento a partir do magma, como

hábito acicular a prismático e zonação oscilatória (Figura 2.2D; Corfu *et al.*, 2003; Nyström & Kriegsman, 2003).

As reações retrometamórficas promovem ainda a quebra de minerais portadores de Zr, como granada, rutilo, hornblenda e ilmenita, o que resulta na cristalização de novos indivíduos ou de bordas ao redor dos grãos restantes (Fraser *et al.*, 1997; Degeling *et al.*, 2001; Bingen *et al.*, 2001; Bea *et al.*, 2006; Figura 2.2E). Além disso, fusões parciais tardias, resultantes da descompressão isotérmica do orógeno, podem constituir uma população adicional de zircão (Figura 2.2F). Por fim, fluidos oriundos de magmas félsicos relacionados às etapas finais da evolução metamórfica reagem com as fases minerais presentes e, com isso, promovem a alteração hidrotermal das mesmas (Figura 2.2G).

Portanto, vê-se que o zircão sin-metamórfico pode ser neoformado ou recristalizado, em qualquer etapa da trajetória P-T de um orógeno, seja progressiva ou retrometamórfica. Tal fato implica em diferenças físicas e químicas significativas para cada situação, cuja análise torna-se imprescindível para a correta interpretação das idades U-Pb obtidas em zircão metamórfico. Deste modo, tais características serão discutidas nos tópicos seguintes.

2.3. Características físicas

Para a investigação da natureza do zircão, a descrição da morfologia externa e da textura interna é fundamental, visto que tais feições refletem a adaptação física do cristal à trama metamórfica, bem como à interação com fluidos e fusões.

Em geral, os grãos metamórficos são incolores, límpidos e pequenos, com dimensões comumente inferiores a 100 μm. Os cristais apresentam grau de arredondamento variável o que, por vezes, decorre em morfologia ovóide, interpretada como resultado da reabsorção diferencial por fluidos insaturados em Zr (Figura 2.3A; Hoskin & Schaltegger, 2003). Ainda, cristais euédricos e aproximadamente equidimensionais, denominados "soccer-ball", são também comuns em rochas de alto-grau (Figura 2.3B; Vavra *et al.*, 1999; Schaltegger *et al.*, 1999). O desenvolvimento desse hábito está relacionado à cristalização em arranjo granoblástico, em sistemas de elevada temperatura e ricos em fluidos, como é o caso de migmatitos (Oliver *et al.* 1999).

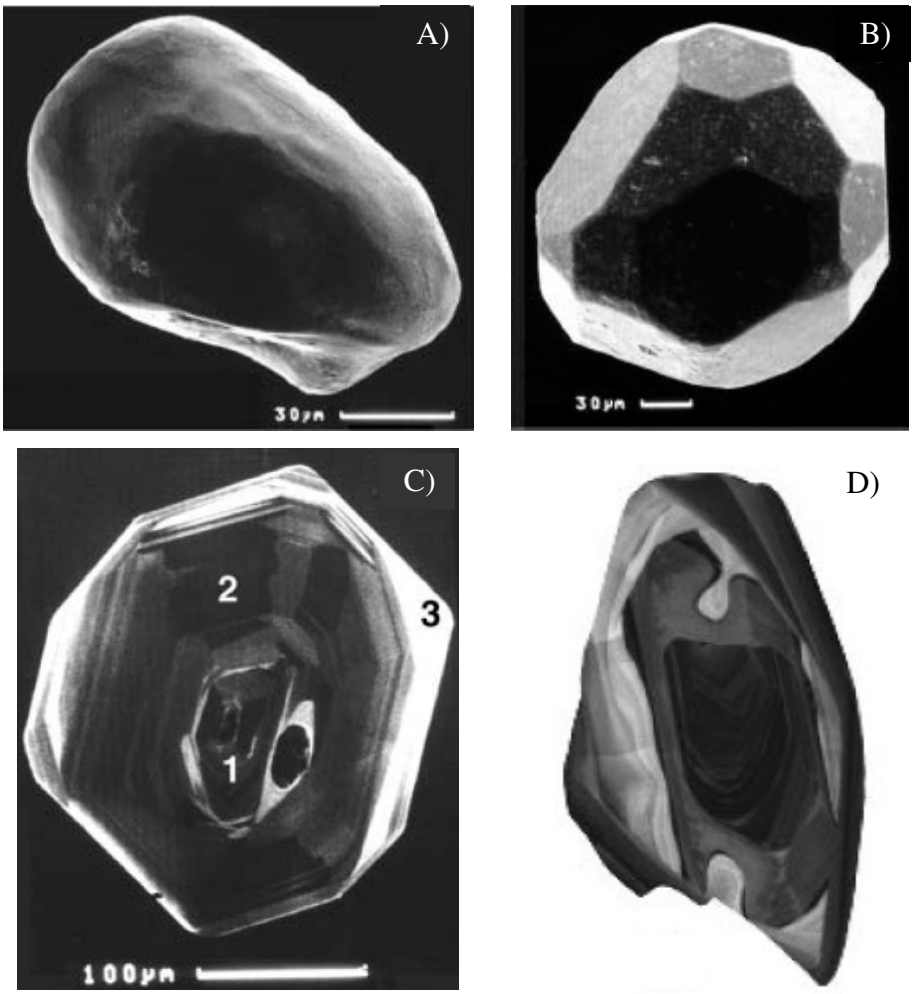

Figura 2.3 - Morfologias externas e texturas internas típicas de zircão metamórfico. A) Morfologia ovóide, com faces e arestas arredondadas, resultantes da interação com fluidos insaturados em Zr (Hoskin & Schaltegger, 2003). B) Zircão euédrico, denominado "soccer-ball", descrito em leucossoma de fácies granulito (Schaltegger *et al.*, 1999). C) Sequência de estruturas geralmente observadas em zircão cristalizado no episódio metamórfico de alto-grau. O núcleo herdado (1) é envolto por uma zona de baixa luminescência (2), a qual é subsequentemente envolta por uma zona de alta catodoluminescência (Hoskin & Schaltegger, 2003). D) Zircão recristalizado no metamorfismo de alto-grau; nota-se um domínio externo com zonação caótica e não planar, bem como reentrâncias que migram da borda para o núcleo do grão (dimensão em torno de 200µm; Corfu *et al.*, 2003).

O metamorfismo também promove modificações importantes na estrutura interna do zircão, de acordo com o mecanismo envolvido na formação ou recristalização do mesmo. Destarte, bordas neoformadas que envolvem núcleos antigos são os principais representantes de novo crescimento de zircão durante o metamorfismo (Figura 2.3C). Estes domínios apresentam composição homogênea e, por vezes, observa-se zonação oscilatória, típica de cristalização a partir do magma (Schaltegger *et al.*, 1999; Corfu *et al.*, 2003).

Por outro lado, a recristalização de zircão origina feições peculiares, irregulares e descontínuas, como reentrâncias e limites sinuosos entre domínios alterados e preservados do

grão (Figura 2.3D). Tais frentes de alteração formam-se predominantemente a partir das terminações do cristal, mas também ocorrem em regiões internas, sobretudo ao redor de inclusões minerais (Hoskin & Black, 2000; Hoskin & Schaltegger, 2003). São comuns texturas internas caóticas e zonações não planares e, em alguns grãos, a recristalização pode promover a obliteração total de estruturação, resultando em grãos internamente homogêneos (Hoskin & Black, 2000).

2.4.Assinatura Geoquímica

O metamorfismo de alto grau incorre não somente em feições texturais típicas no zircão, conforme visto no tópico anterior, mas também resulta em assinatura geoquímica modificada em relação à composição original. A Figura 2.4 ilustra as duas possíveis condições de formação de zircão metamórfico e ressalta, em ambas, as principais características químicas.

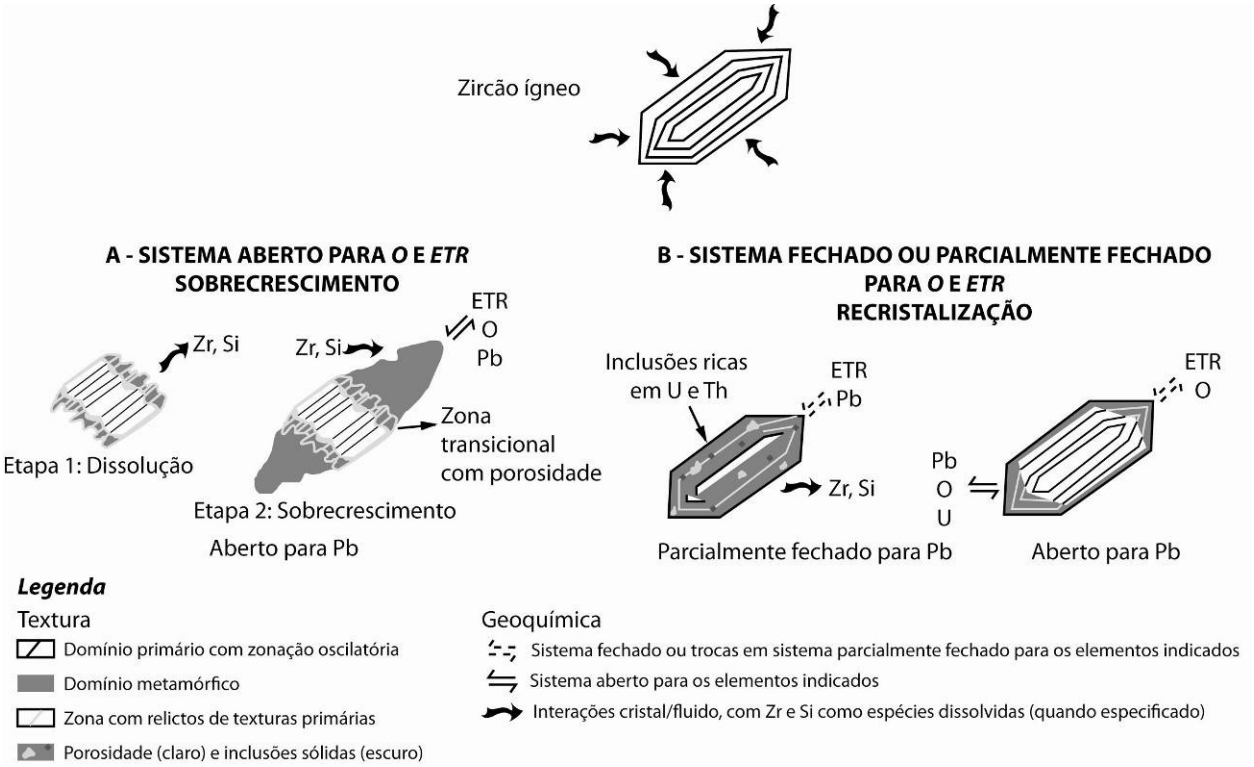

Figura 2.4 – Mobilidade de elementos traço em zircão durante o metamorfismo de alto-grau (modificado de Martin *et al.*, 2008). Em A, ilustra-se a situação na qual há uma nova cristalização, representada por bordas neoformadas ao redor de núcleos antigos, e em B observa-se um episódio de recristalização do zircão. Ressalta-se a presença de uma fase fluida em ambos os casos, a qual facilita a troca de elementos com o meio.

Cristalização de novos grãos/ sobrecrescimento metamórfico

No caso de cristalização de novos grãos ou bordas neoformadas, o sistema geoquímico do zircão é considerado aberto na escala do cristal, visto que a dissolução e o sobrecrescimento ocorrem em etapas díspares da trajetória P-T do orógeno (Figura 2.4A). Por conseguinte, este mineral desenvolve-se em equilíbrio com o magma ou fluido, bem como com as demais fases da assembléia metamórfica e, consequentemente, apresenta características isotópicas e composicionais distintas entre a borda neoformada e o núcleo do cristal.

Assim, o zircão formado a partir de fluidos ou fusões parciais (p. ex. migmatitos) apresenta a composição de elementos traço análoga ao magma e, portanto, o padrão de elementos terras raras assemelha-se a cristais ígneos. Observa-se uma distribuição enriquecida em ETR pesados em relação aos leves, resultando em razões Lu_N/La_N elevadas, além de anomalia positiva de Ce e negativa de Eu (Figura 2.5, curva A; Rubatto 2002; Hoskin & Schaltegger 2003).

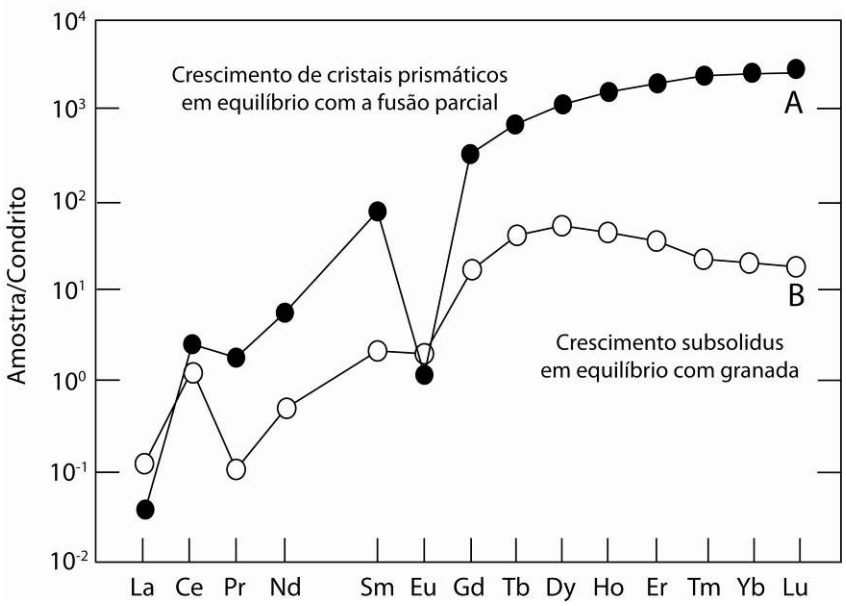

Figura 2.5 – Padrão de elementos terras raras de zircão metamórfico normalizados pelo condrito (Hoskin & Schaltegger 2003; Fraser *et al.* 1997). Ambas as curvas representam a cristalização de novos indivíduos ou o sobrecrescimento de bordas ao redor de núcleos herdados.

Todavia, os demais produtos metamórficos cristalizados em concomitância com zircão podem influenciar a partição dos elementos traço, modificando assim a assinatura geoquímica deste mineral (Fraser *et al.* 1997; Degeling *et al.* 2001; Bea *et al.* 2006). Granada é fase comum nas assembléias de alto-grau metamórfico e, devido aos elevados coeficientes de partição dos elementos terras raras pesados deste mineral, a cristalização em equilíbrio químico com o

fluido/magma resulta em padrões de distribuição horizontais ou mesmo negativos de ETR pesados no zircão, conforme ilustra a curva B da Figura 2.4 (Rubatto, 2002).

Recristalização metamórfica de zircão

Zircão incorpora uma série de elementos traço ao retículo cristalino durante a cristalização ígnea. O mecanismo de substituição pode envolver trocas simples, quando os cátions possuem a mesma valência que o Zr, ou acopladas, nas quais é necessário balanço de cargas para neutralizar a reação (Tabela 2.1). Entretanto, a diferença de raio iônico e de carga entre Zr e Si e os elementos traço incorporados em zircão cria uma tensão estrutural no cristal, tornando-o metaestável sob condições crustais.

Tabela 2.1- Principais substituições em zircão (Hoskin & Schaltegger, 2003).

Substituições simples	Substituições acopladas
Hf^{4+}, Th^{4+}, U^{4+}, Ti^{4+}, Sn^{4+} $= Zr^{4+}$	Em um sítio estrutural $(Y, REE)^{3+} + (Nb,Ta)^{5+} = 2\ Zr^{4+}$
	Em dois sítios estruturais $(Y, REE)^{3+} + P^{5+} = Zr^{4+} + Si^{4+}$ $Sc^{3+} + P^{5+} = Zr^{4+} + Si^{4+}$

Devido às elevadas temperaturas atingidas no metamorfismo de alto-grau, o zircão torna-se instável e, consequentemente, os constituintes não-essenciais são expulsos do retículo cristalino, por meio da recristalização (Hoskin & Schaltegger 2003). A supressão destes elementos se dá a partir de uma frente de alteração, a qual avança gradualmente rumo ao centro do zircão. Assim, evolui-se para um domínio externo pristino e praticamente puro que contém inclusões de fases minerais constituídas pelos elementos eliminados por esse processo, como xenotíma, coffinita e torita (Geisler *et al.* 2007).

Destarte, a recristalização promove a perda de elementos como Pb, Hf, REE e U (Geisler *et al.*, 2003; Geisler *et al.*, 2007). Ainda, o zircão recristalizado tende a ser relativamente empobrecido em elementos terras raras, porém a distribuição de ETR pesados é geralmente mantida e, assim, domínios preservados e alterados revelam razões Lu_N/La_N similares. Além

disso, quando o zircão apresenta defeitos induzidos por radiação, facilita-se a difusão dos elementos *non-formula* e pode haver ganho de cátions Al, Ca, Fe, Mg e Pb_{comum}, que ocuparão sítios intersticiais do retículo cristalino.

Caso a recristalização seja incompleta, o mineral ainda reterá parcialmente a assinatura geoquímica e isotópica primária e, portanto, as informações obtidas nesses domínios representam um valor intermediário entre a cristalização ígnea e o metamorfismo (Hoskin & Black, 2000; Möller *et al.*, 2003; Kelly & Harley, 2005; Harley *et al.*, 2007). Desta forma, na recristalização os sistemas geoquímico e isotópico são considerados apenas parcialmente fechados para determinados elementos e, consequentemente, não se atinge o equilíbrio completo com o restante da rocha (Martin *et al.* 2008).

2.5. Considerações finais

Conforme discutido nos tópicos anteriores, zircão pode ser alterado durante o metamorfismo de alto grau e esse processo resulta em distintas feições texturais e composicionais. A partir da integração da caracterização textural com dados isotópicos e geoquímicos, torna-se possível avaliar as condições de formação ou alteração destes grãos e recuperar informações a respeito do ambiente físico-químico de cristalização ou recristalização dos mesmos. Adicionalmente, esta avaliação multicriterial traz implicações importantes para a datação de rochas de alto-grau, visto que a assinatura geoquímica do zircão permite identificar em que momento da trajetória P-T este mineral se formou e, assim, diferenciam-se com mais precisão as etapas da evolução do orógeno.

Dessa forma, as informações aqui apresentadas fornecerão subsídios para a correta interpretação das idades obtidas em zircão de rochas dos complexos Anápolis-Itauçu e Barro Alto e, consequentemente, auxiliarão a elucidar a evolução tectônica da Faixa Brasília.

3. DATING COEVAL MAFIC MAGMATISM AND ULTRAHIGH-TEMPERATURE METAMORPHISM IN THE ANÁPOLIS-ITAUÇU COMPLEX, CENTRAL BRAZIL

Maria Emilia Schutesky Della Giustina[1]*

Márcio Martins Pimentel[1a]

Cesar Fonseca Ferreira Filho[1]

Maria Helena Bezerra Maia de Hollanda[2]

[1] Universidade de Brasilia, Instituto de Geociencias, 70910-900, Brasilia-DF-Brazil

*Correponding author: maria_emilia@unb.br;

Phone: +55-61-3307-1113; Fax: +55-61-3272-4286

[2] Universidade de São Paulo, Instituto de Geociências, Rua do Lago, 562, Cidade Universitária, 05508-900, São Paulo-SP-Brazil.

Abstract

Dating granulites has always been of great interest because they represent one of the most extreme settings of an orogen. Owing to the resilience of zircon, even in such severe environments, the link between P-T conditions and geological time is possible. However, a challenge to geochronologists is to define whether the growth of new zircon is related to pre- or post-P-T peak conditions and which processes might affect the (re)crystallization. In this context, the Anápolis-Itauçu Complex, a high-grade complex in central Brazil with ultra-high temperature (UHT) granulites, may provide valuable information within this topic.

The Anápolis-Itauçu Complex (AIC) includes ortho- and para-granulites, locally presenting UHT mineral assemblages, with igneous zircon ages varying between 760 and 650 Ma and metamorphic overgrowths dated at around 650-640 Ma. Also common in the Anápolis-Itauçu Complex are layered mafic-ultramafic complexes metamorphosed under high-grade conditions.

This article presents the first geological and geochronological constraints of three of these layered complexes within the AIC, the Damolândia, Taquaral and Goianira-Trindade complexes. U-Pb (LA-

[a] Present address: Universidade Federal do Rio Grande do Sul, Instituto de Geociências, 91501-970, Porto Alegre-RS-Brazil.

ICPMS, SHRIMP and ID-TIMS) zircon analyses reveal a spread of concordant ages spanning within an age interval of ~80 Ma, which suggests an "upper" intercept age of ~670 Ma. Under cathodoluminescence imaging, these crystals show partially preserved primary sector zoning, as well as internal textures typical of alteration during high-grade metamorphism, such as inward-moving boundaries. Zircon grains reveal homogeneous initial $^{176}Hf/^{177}Hf$ values within populations and also in crystal-scale domains in all samples. Moreover, Hf isotopic ratios show correlation neither with U-Pb ages nor with Th/U ratios, suggesting that zircon grains crystallized during a single growth event. It is suggested, therefore, that the observed spread of concordant U-Pb ages may be related to a memory effect due to coupled dissolution-reprecipitation process during high grade metamorphism. Thus, it is unlikely that the emplacement of the mafic-ultramafic complexes and UHT metamorphism in the Anápolis-Itauçu Complex represent unrelated geological episodes.

Therefore, understanding the emplacement and metamorphism of this voluminous mafic magmatism is crucial, given that they may characterize the additional heat source for the development of the ultra-high temperature paragenesis recorded in the paragranulites.

Key-words: Brasília Belt, metamorphic zircon, UHT metamorphism, hot orogen, Hf-in-zircon, coupled dissolution-reprecipitation process

3.1.Introduction

In recent years, petrological studies of granulite terranes have shown that these rocks can experience extreme P-T conditions, which may be substantially more vigorous than previously recognized. The so-called *ultra-high temperature granulites*, recording temperatures higher than 900°C in a moderate pressure environment, are present in most orogens. The origin of these rocks requires extremely hot crustal conditions, which cannot be explained by the numerical models currently available for collisional orogens (Jamieson *et al.*, 1998, 2004; Beaumont *et al.*, 2001, 2006; Collins, 2002) Even considering a large-hot orogen model, when compared to the real geological data there is still a thermal gap of about 100 to 200°C, which requires an additional heat source (Harley, 1998, 2004, 2008). Such supplementary thermal gradient might be found in accretionary orogens (Collins, 2002), where extensional intervals in the overall collisional setting promote lithospheric thinning and, consequently, the ascent of hot asthenospheric mantle generating elevated heat flow (Schott & Schmeling, 1998). This process

results in extensive mafic magmatism associated in space and time with high-temperature-low-pressure metamorphism (Sandiford & Powell, 1986; Schott & Schmeling, 1998).

In central Brazil, such scenario may be recognized in the Anápolis-Itauçu Complex (AIC), which represents the metamorphic nucleus of the Brasilia Belt. The geological framework, with UHT occurrences spatially associated with mafic granulites, suggests that the Brasilia Belt may correspond to a large, hot orogen, as suggested before (Pimentel *et al.*; 2003; Giustina *et al.*, 2009).

Previous studies combining geological and geochronological aspects of the UHT paragranulites of the AIC reveal the age of ~645 Ma for the peak of metamorphism (Moraes *et al.*, 2002; Piuzana *et al.*, 2003a; Baldwin & Brown, 2008). However, associated mafic complexes have never been the topic of such kind of research. The data available for the regional mafic magmatic event in the Brasilia Belt is limited to the arc terranes, exposed to the west of the AIC.

Therefore, this study aims at describing the geology of three layered mafic-ultramafic complexes, occurring within the Anápolis-Itauçu Complex, as well as discuss their isotopic and geochronological record, in order to verify the relationship between mafic magmatism and metamorphism in the AIC. Mafic intrusions emplaced into deep crustal levels represent the most suitable rock association for this study. The intrusions investigated here present partially preserved igneous textures and high-grade metamorphic imprint.

3.2. Geological setting

The Brasília Belt is a Neoproterozoic orogen in central Brazil, developed throughout island arc amalgamation and continental collision between the São Francisco-Congo and the Paranapanema continent to the south, covered by the Paraná Basin (Figure 3.1; Pimentel et al., 2000; Valeriano et al., 2008). It is part of a global network of Neoproterozoic orogenic belts which resulted in the final amalgamation of Gondwana. It may be divided into four domains: (i) in the easternmost part is a thrust-and-fold belt consisting of various Neoproterozoic metasedimentary sequences formed along the western margin of the São Francisco Craton, (ii) in the central part of the belt, the metamorphic core is exposed, comprising high-grade rocks and ultra-high temperature granulites – the Anápolis-Itauçu Complex, (iii) the Goiás Massif, interpreted as a microcontinent/exotic terrane accreted to the orogen at the end of the Neoproterozoic, and (iv) the Goiás Magmatic Arc, which represents a juvenile terrane forming

the westernmost part of the belt (Brito Neves & Cordani, 1991; Pimentel & Fuck, 1992; Fuck *et al.*, 1994; Pimentel *et al.* 2000; Figure 3.1A).

The Anápolis-Itauçu Complex (AIC) is located in the southern branch of the Brasília Belt (Figure 3.1B). It constitutes an elongated NW-SE zone of high-grade rocks exposed between the Goiás Magmatic Arc and lower-grade Neoproterozoic Araxá Group micaschists and quartzites. Geological contacts are marked by high-angle shear-zones, thus preventing the identification of clear stratigraphic or cross-cutting relationships between the different rock units. However, geochronological data support the interpretation that at least part of the AIC may represent high-grade equivalents of the Araxá Group (Piuzana *et al.*, 2003b) and, moreover, it might be an exposure of the root of the original mountain chain.

The AIC includes a variety of rock-types forming NW-oriented segment, in which three main rock associations may be recognized. The orthogranulites are represented by tonalitic to granodioritic gneisses, as well as by mafic rocks, exposed either as dioritic/gabbroic granulites or as mafic-ultramafic complexes. Such layered bodies are composed of peridotite, pyroxenite, gabbro and gabbro-anorthosite. Relict igneous textures and layering are usually observed. However, these complexes are often strongly foliated and metamorphosed under amphibolite to granulite facies conditions. Geochemical analysis point toward a tholeiitic parental magma, with LREE enrichment and a negative Eu anomaly, and the high-Al content of relict igneous pyroxenes suggests that the intrusion took place at deep levels in the crust (Silva, 1991, 1997; Nilson, 1992).

Example of these layered bodies are the Damolândia, Taquaral (Silva, 1997), Goianira-Trindade (Nilson & Motta, 1969) and Águas Claras complexes (Nilson, 1992), which are interpreted to be coeval with those exposed to the west, within the Goiás Magmatic Arc domain (Laux *et al.*, 2004).

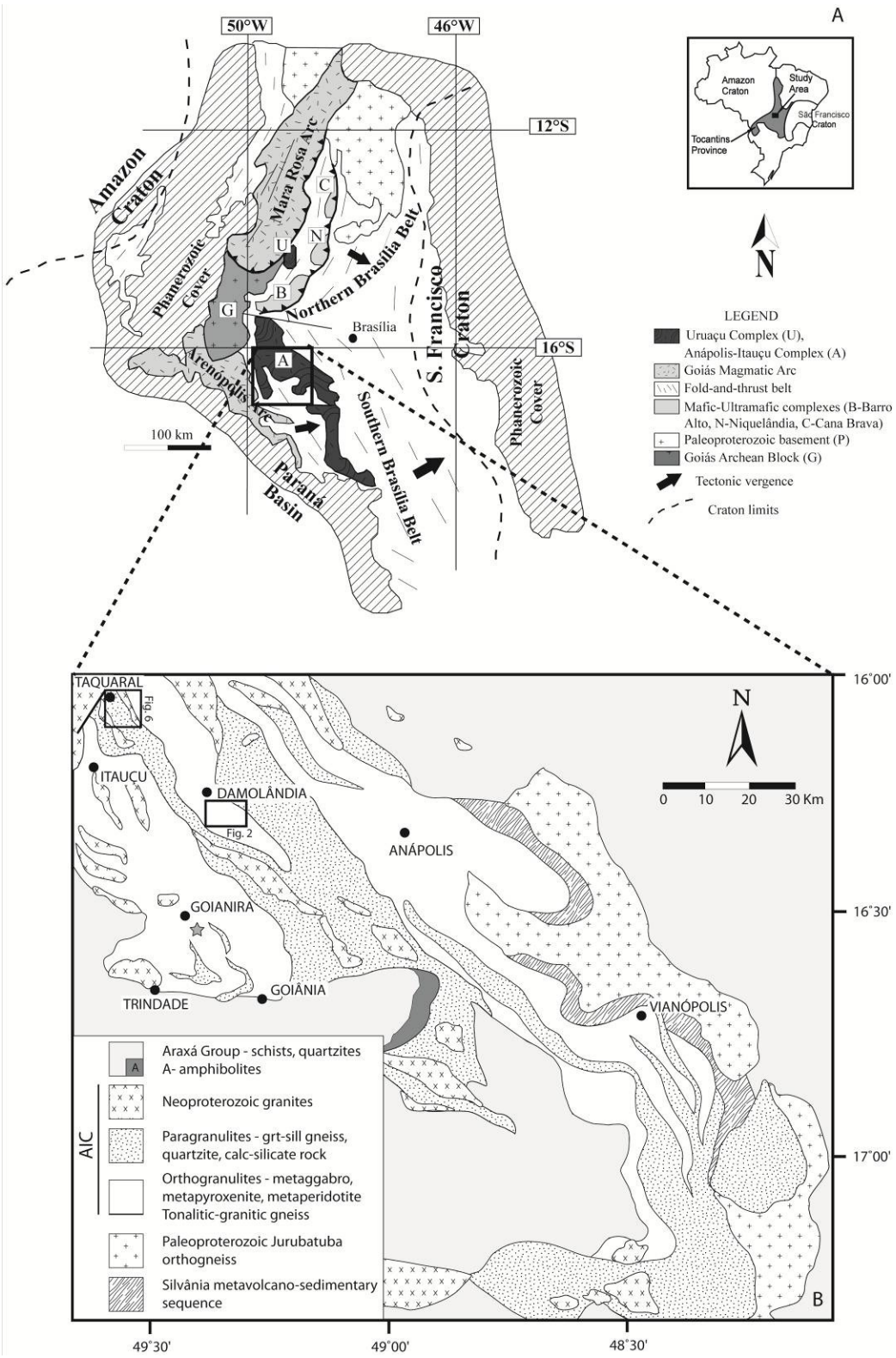

Figure 3.1 - A) Regional sketch map of the Brasilia Belt, in the eastern part of the Tocantins Province (modified from Giustina *et al.*, 2009). B) Geological map of the central part of the Anápolis-Itauçu Complex (modified from Piuzana *et al.*, 2003). The star represents the location of sample INHO-01.

Metasedimentary rocks are typically represented by aluminous granulites with variable amounts of sillimanite, garnet, spinel, cordierite and feldspars. Commonly, these rocks occur as massive outcrops or either form bands in stromatic migmatites, in which fine-grained mafic granulites, interpreted as metabasalts, are also observed (Winge, 1995). Calc-silicate rocks and impure quartzites are also recognized. Ultrahigh-temperature mineral assemblages, such as saphirine+quartz, orthopyroxene+sillimanite+quartz, wollastonite+scapolite and hercynite+quartz have been identified in several localities of the AIC (Moraes *et al.*, 2002, 2007; Baldwin *et al.*, 2005). The paragranulites preserve composite P-T paths, with a first near-isothermal decompressional phase, when the thermal peak is achieved, which is followed by a near-isobaric cooling stage (Moraes *et al.*, 2002; Baldwin & Brown, 2008).

A large number of granites also constitute the AIC (Figure 3.1B). They show variably deformational and metamorphic overprint, achieving even granulite facies conditions. Most of these granitic rocks are peraluminous and the Nd isotopic signature indicates that they may be the melting products of either the aluminous paragranulites of the AIC or metasedimentary rocks of the Araxá Group (Piuzana *et al.*, 2003a). In some of these bodies U-Pb ages for zircon igneous cores and metamorphic rims are identical and, therefore, the granites may be interpreted as representative of deep-crustal, syn-tectonic intrusions (Piuzana *et al.*, 2003a).

SHRIMP U-Pb ages of igneous zircon from felsic orthogranulites vary between 760 and 650 Ma and metamorphic overgrowths are dated at 650-640 Ma (Piuzana *et al.*, 2003a). T_{DM} Sm-Nd model ages of granulitic rocks fall into two age intervals, between 2.3-1.9 Ga and 1.7-1.4 Ga, and ε_{Nd} (T) values are negative, ranging from -9.3 to -1.4 (Piuzana *et al.*, 2003a). The younger T_{DM} values are in agreement with the zircon inheritance pattern observed in paragranulites (2.0 to 0.8 Ga). Both the Nd and the U-Pb data indicate an important Neoproterozoic sedimentary source.

3.3. Damolândia and Taquaral Layered Complexes

The Damolândia and Taquaral layered mafic-ultramafic complexes occurs within high-grade gneiss and granulites from the AIC. Both layered complexes were overprinted by heterogeneous high-grade metamorphism and associated tectonism. While primary igneous textures and mineralogy are largely preserved in rocks of the EW trending Damolândia Complex,

such features are just locally preserved in the NNW trending Taquaral Complex, which consists mainly of highly foliated and recrystallized mafic-ultramafic rocks.

Damolândia

The Damolândia Complex is a poorly exposed medium-size (ca 15 km^2) layered intrusion. Extensive mapping and mineral exploration data developed by International Nickel Venture Ltd. in 2006-2008 provided constraints on the geology and stratigraphy of the layered sequence (Figure 3.2). The host rocks of the Damolândia Complex were not investigated in detail, but regional mapping indicates that they consist mainly of basic to intermediate granulite in the north, and highly foliated leptynite[b] and felsic gneiss in the south (Figure 3.2). Mafic-ultramafic rocks of the Damolândia Complex form irregular domains of interlayered peridotite-pyroxenite-norite associated with domains of mafic rocks, mainly norite and gabbronorite, and domains where medium to coarse-grained diorite occur. Due to poor exposition of mafic and ultramafic rocks, the mapped domains are based on soil characteristics (Figure 3.3A) supported by scattered outcrops (Figure 3.3B) and soil geochemistry surveys. Layered rocks of the Damolândia Complex are heterogeneously tectonized and recrystallized in discrete zones, where primary igneous rocks were transformed into highly foliated mafic or ultramafic granulites.

Extensive drilling developed in the southwestern portion of the Damolândia Complex expose complete sections of the interlayered peridotite-pyroxenite-norite domain. A representative drill hole from this domain consists of a ca 200 meter-thick sequence of ultramafic cumulates within mafic cumulates (Figure 3.4). The facing of the layered sequence is not constrained by primary structures, but layering in the core defined by aligned prismatic pyroxenes indicates steep dip to the north. Norite and gabbronorite are orthopyroxene and plagioclase cumulates, with variable amounts of intercumulus clinopyroxene, hornblende and minor phlogopite. Pyroxenite consists of cumulus orthopyroxene, or orthopyroxene and chromite (ca 1-3 vol. %), with variable amounts of intercumulus plagioclase, clinopyroxene, hornblende and minor phlogopite. Textures of pyroxenite vary from medium- to coarse-grained adcumulate (orthopyroxenite), to mesocumulate and orthocumulates (usually websterite or melanorite). The transition from pyroxenite to norite is gradational and characterized by the increase of interstitial

[b] Leptynites are fine-grained leucocratic sill-grt gneisses with a granoblastic texture, probably of granitic nature (Winge & Danni, 1994).

plagioclase. Cyclic interlayering of peridotite (mainly harzburgite) and pyroxenite characterizes the central zone of ultramafic cumulates in drill hole FSDM-07 (Figure 3.4). Peridotite (Figure 3.3C and 3.3D) is an olivine and chromite (ca 1-3 vol. %) cumulate with variable amounts of intercumulus orthopyroxene and minor clinopyroxene, hornblende, plagioclase and phlogopite. Interlayered peridotite and pyroxenite form up to dozen of meter-thick layers with sharp contacts, splitting the ultramafic samples into one group of olivine-rich peridotite (MgO > 27 wt. %) and another of pyroxenite (MgO < 17 wt. %). Few discordant bodies of coarse-grained hornblende-bearing gabbronorite or hornblende diorite (Figure 3.3F) occur throughout the layered sequence. These bodies are usually few meter-wide and have accessory ilmenite, apatite and zircon, suggesting their crystallization from evolved magmas, possibly resulting from residual trapped liquids.

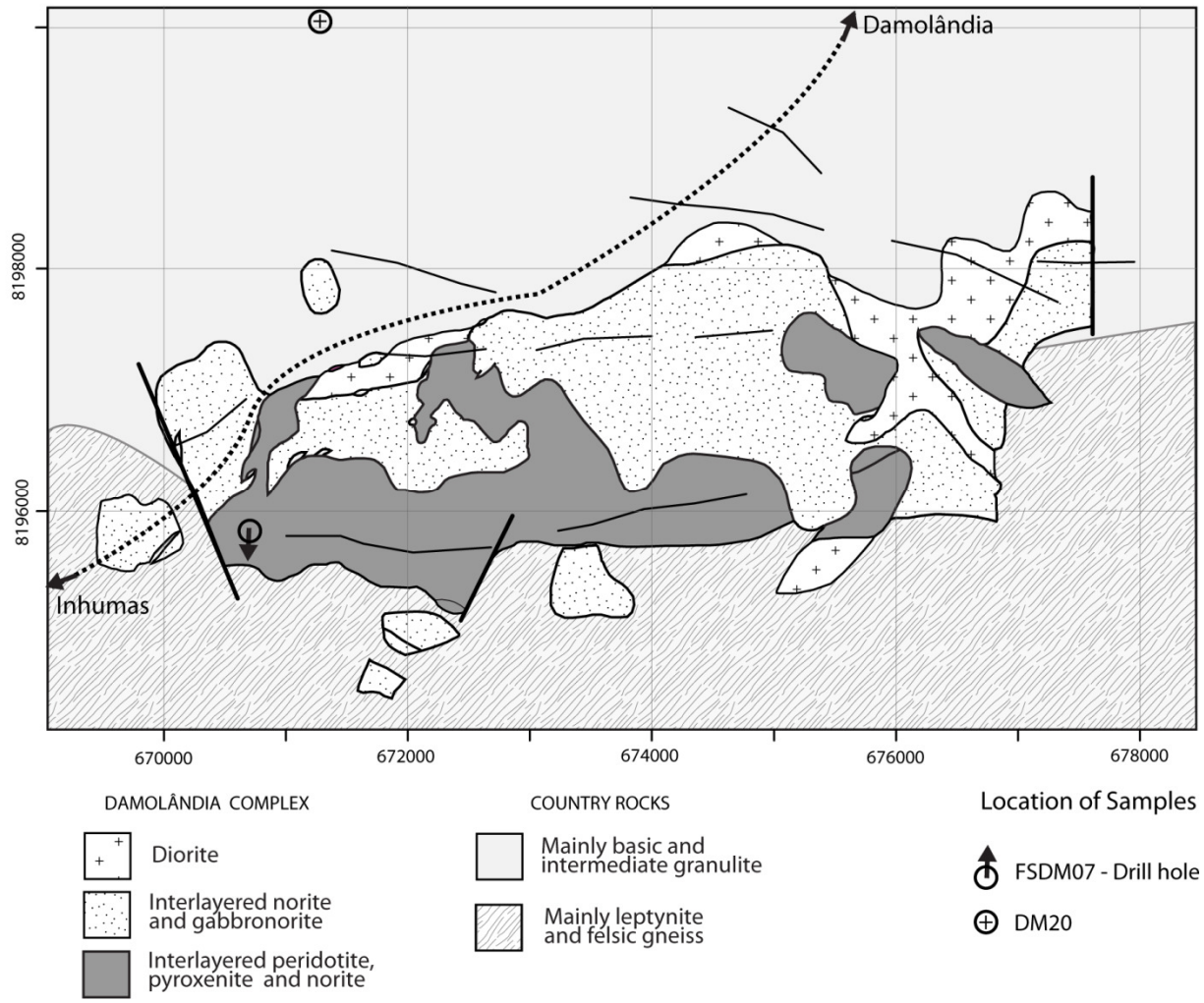

Figure 3.2 - Geology of the Damolândia Complex (from unpublished report of International Nickel Venture Ltd.).

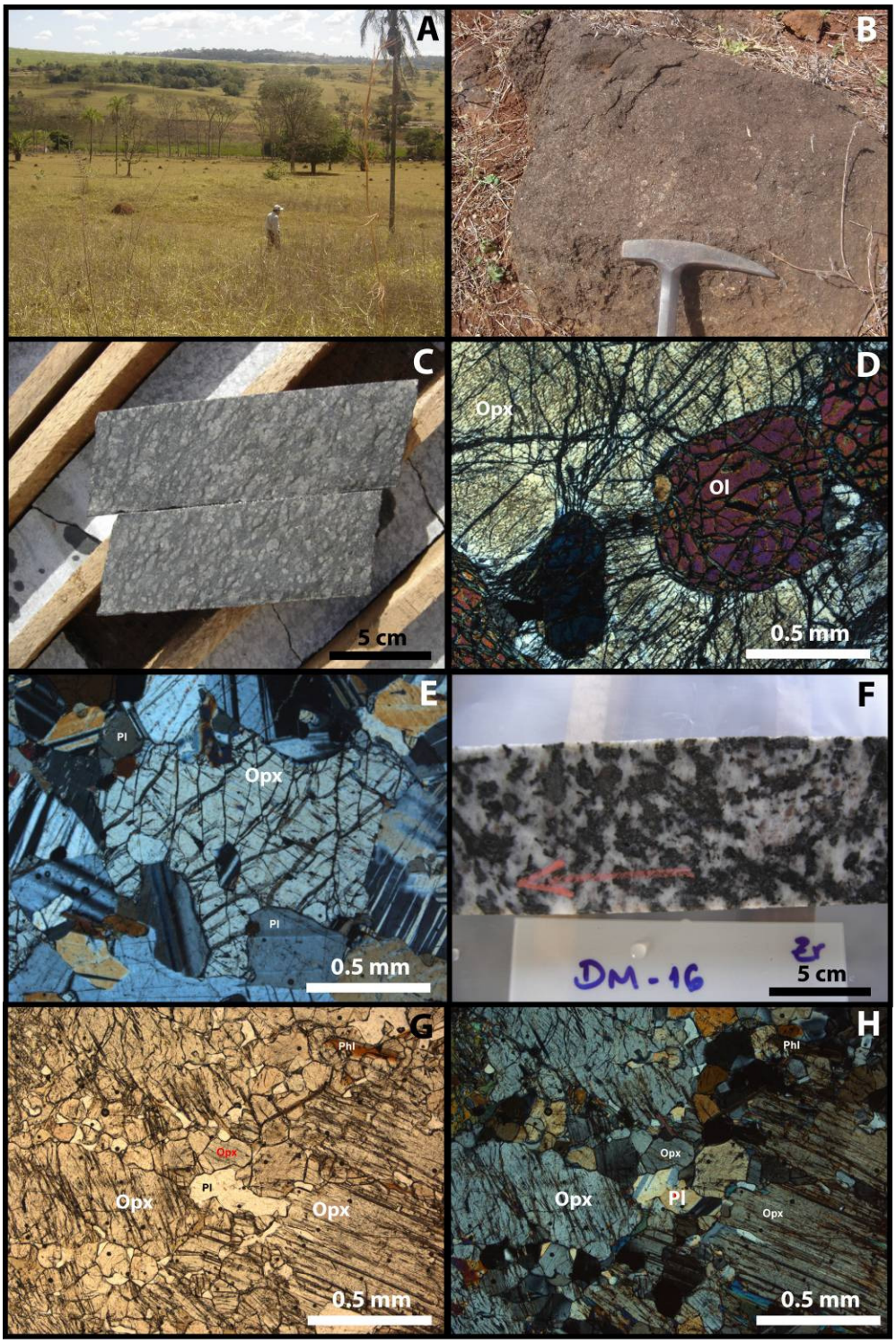

Figure 3.3 - A) View of the area close to the drill hole FSDM-07. Rare outcrops and abundant dark brownish termite mounts developed on soil from ultramafic rocks (close to drill hole FSDM-07). B) Orthopyroxenite with interstitial white plagioclase (close to drill hole FSDM-07). C) Harzburgite from drill hole FSDM-07. D) Photomicrograph of harzburgite consisting of cumulus olivine (Ol) enclosed in large orthopyroxene oikocryst (opx). E) Photomicrograph of norite consisting of cumulus orthopyroxene (opx) and plagioclase (Pl). F) Zircon-bearing hornblende gabbronorite. Sample DM-16 from drill hole FSDM-07. G) and H) Photomicrograph of partially recrystallized plagioclase-bearing orthopyroxenite. Large igneous orthopyroxene crystals are recrystallized into fine-grained granoblastic aggregates.

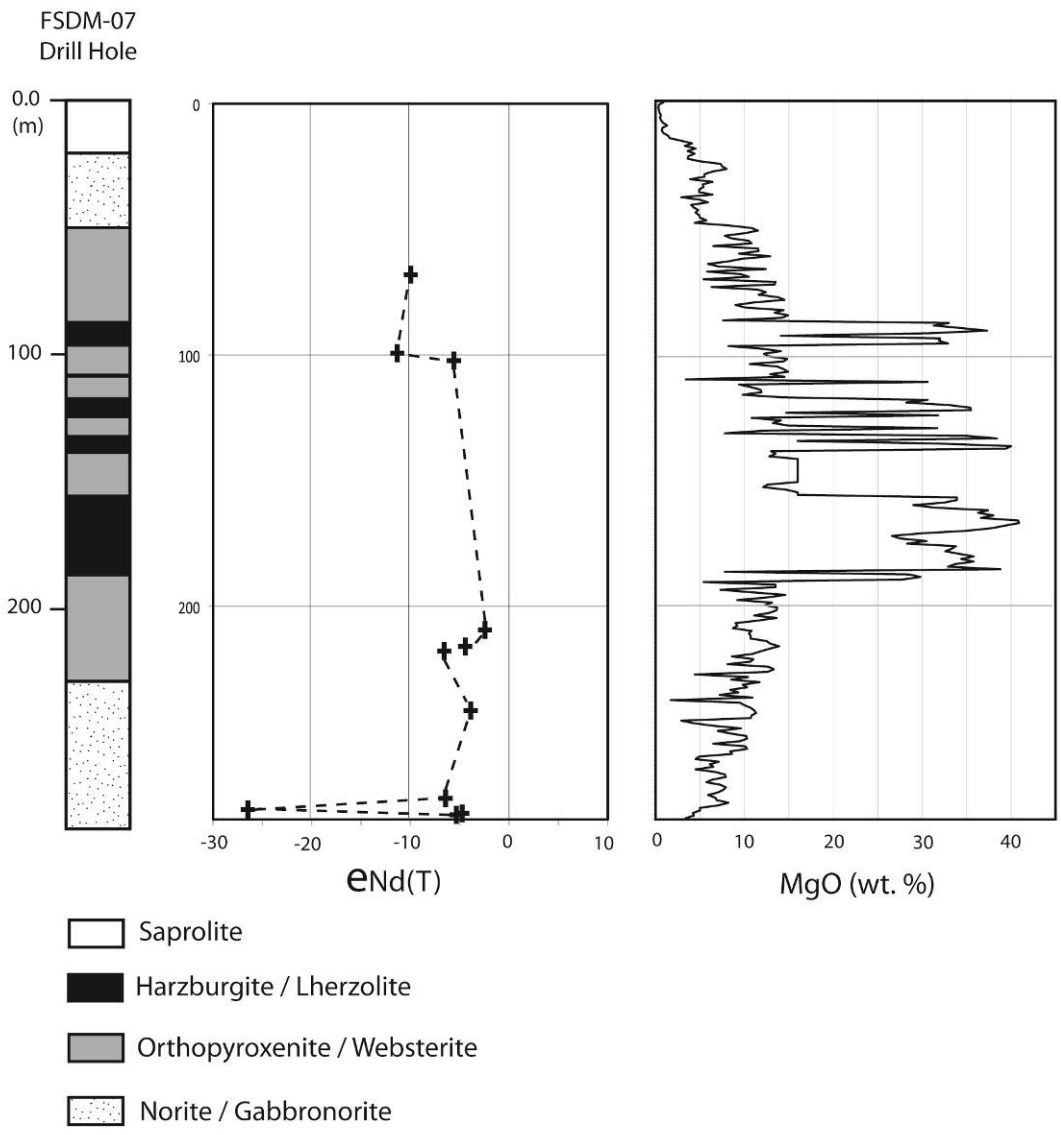

Figure 3.4 - Log, MgO content and εNd(T) for drill hole FSDM-07.

Cumulus minerals in the layered rocks suggest that the sequence of crystallization in the Damolândia Complex consists of olivine+chromite, orthopyroxene+chromite, orthopyroxene, orthopyroxene+plagioclase and orthopyroxe+plagioclase+clinopyroxene. The crystallization sequence described for the Damolândia Complex is very common (e.g. Bushveld Complex; Serra da Onça). The correlation of MgO content with CaO, TiO_2, K_2O and Cr for layered rocks of the drill hole FSDM-07 (Fig. 3.5) is consistent with this sequence of crystallization of cumulus minerals. High MgO contents of peridotite samples (up to 41 wt. %) suggests high MgO content of olivine. Low CaO and TiO_2 contents are consistent with the predominance of orthopyroxene

over clinopyroxene in the layered rocks, while high Cr contents are consistent with the presence of chromite in both peridotite and pyroxenite samples. Scattered high contents of K_2O are associated with disseminated interstitial phlogopite. High K_2O contents show no correlation with MgO content suggesting that they result from inhomogeneous assimilation of crustal rocks by the parental magma.

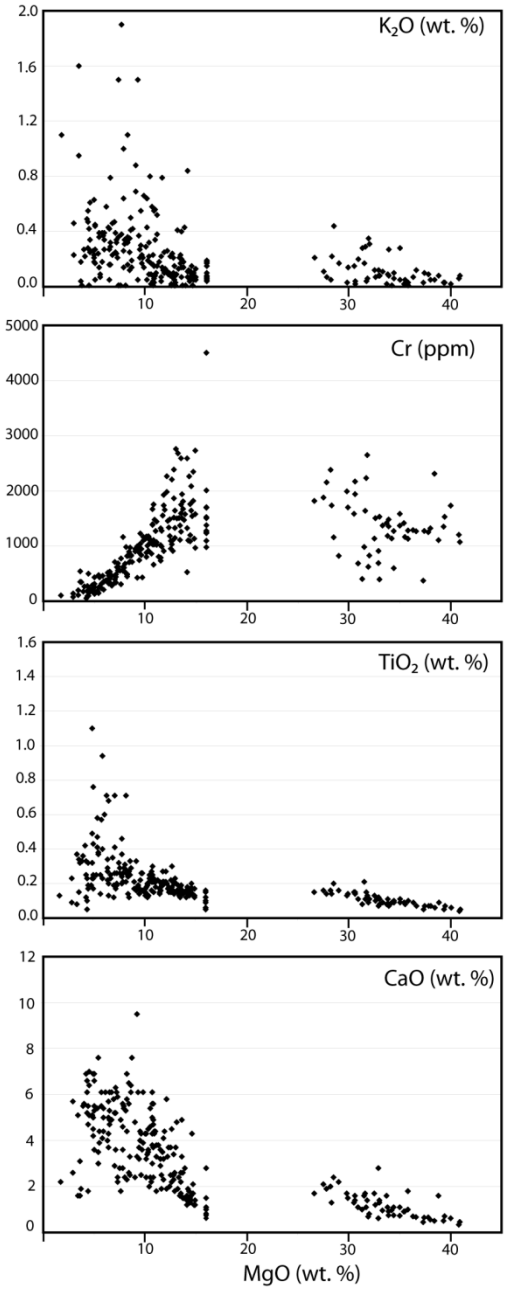

Figure 3.5 - Plot of MgO versus CaO, TiO_2, Cr and K_2O for the drill hole FSDM07.

Primary igneous texture and mineralogy prevail throughout the layered sequence of the drill hole FSDM-07. Recrystallization and ductile deformation are restricted to few-meter wide discrete zones. In these zones the primary igneous mineralogy is partially (Figure 3.3G and 3.3H) to completely recrystallized into fine-grained granoblastic assemblages of metamorphic minerals. Recrystallized norite and gabbronorite consist of fine-grained granoblastic aggregates of plagioclase, orthopyroxene, clinopyroxene and dark-brown amphibole. This assemblage indicates that recrystallization occurred under conditions of high temperature (equivalent to the granulite facies of regional metamorphism).

Taquaral

The Taquaral Complex was considered by Silva (1997) as a large (up to 50 km-long) layered mafic-ultramafic complex submitted to high-grade metamorphism and associated tectonism. Silva (1997) proposed a stratigraphic column with 5 km of inferred thickness for the Taquaral Complex. However, extensive exploration developed by mining companies in the Taquaral Complex indicates that it consists of several elongated small to medium-size (up to 15 km-long) highly tectonized mafic and mafic-ultramafic bodies. Stratigraphic correlations between different bodies are unconstrained and the complex should be considered by now as a cluster of NNW trending mafic and mafic-ultramafic bodies. Detailed mapping supported by exploration data was developed by International Nickel Venture Ltd. in 2007-2008 in the northern segment of the Taquaral Complex. Results indicate the existence of several small to medium-size mafic-ultramafic bodies (Figure 3.6) surrounded by high-grade felsic gneiss and leptynite. Mapped mafic and ultramafic rocks of the Taquaral Complex are highly tectonized and recrystallized. They have pervasive tectonic foliation (Figure 3.7A and 3.7B) parallel with the NNW (subvertical to SW dip) trend of host rocks.

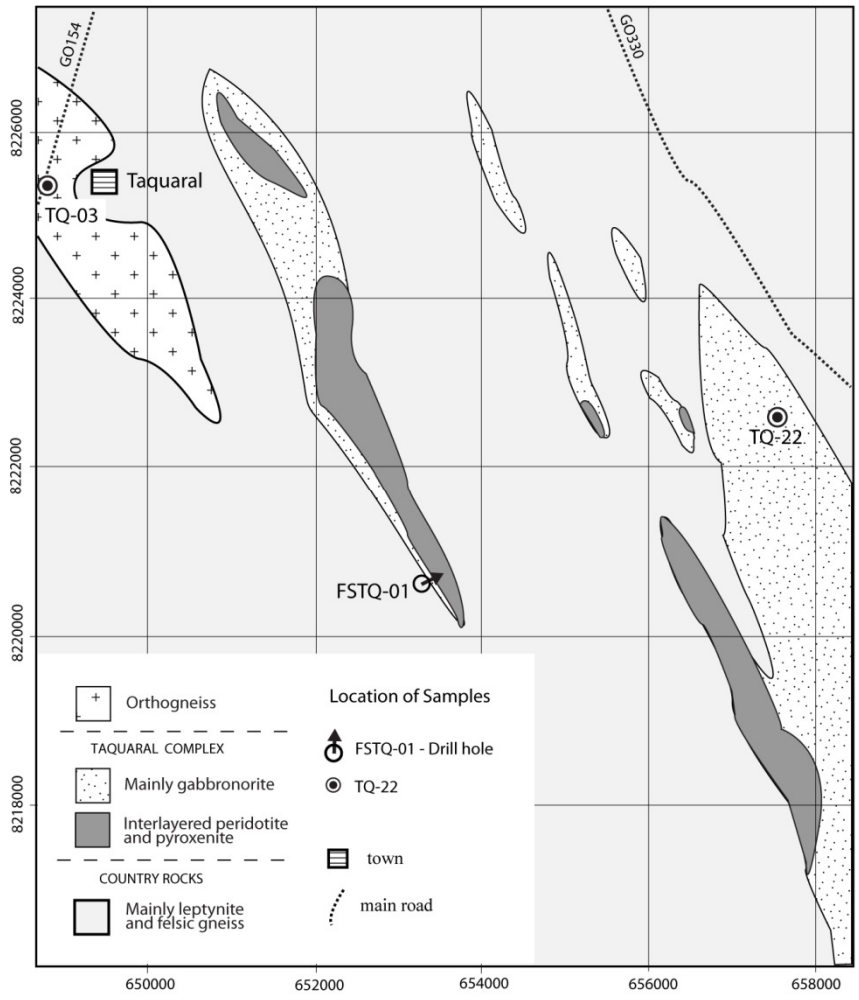

Figure 3.6 - Geology of the northern area of the Taquaral Complex (from unpublished report of International Nickel Venture Ltd.).

Cumulus minerals in the layered rocks suggest that the sequence of crystallization in the FSTQ-01 drill core consists of olivine + chromite, orthopyroxene + chromite, orthopyroxene + clinopyroxene, orthopyroxene + clinopyroxene +plagioclase and orthopyroxene + clinopyroxene + plagioclase + ilmenite. This crystallization sequence is different from the Damolândia Complex, indicating an early cristallization of clinopyroxene in the Taquaral Complex. The crystallization sequence described for the Taquaral Complex is similar to what is described in the Great Dyke and in the Niquelândia Complex (Ferreira Filho *et al.*, 1998). The correlation of MgO content with CaO, TiO_2, K_2O and Cr for layered rocks of the drill hole FSTQ-01 (Figure 3.9) is consistent with this sequence of crystallization of cumulus minerals.

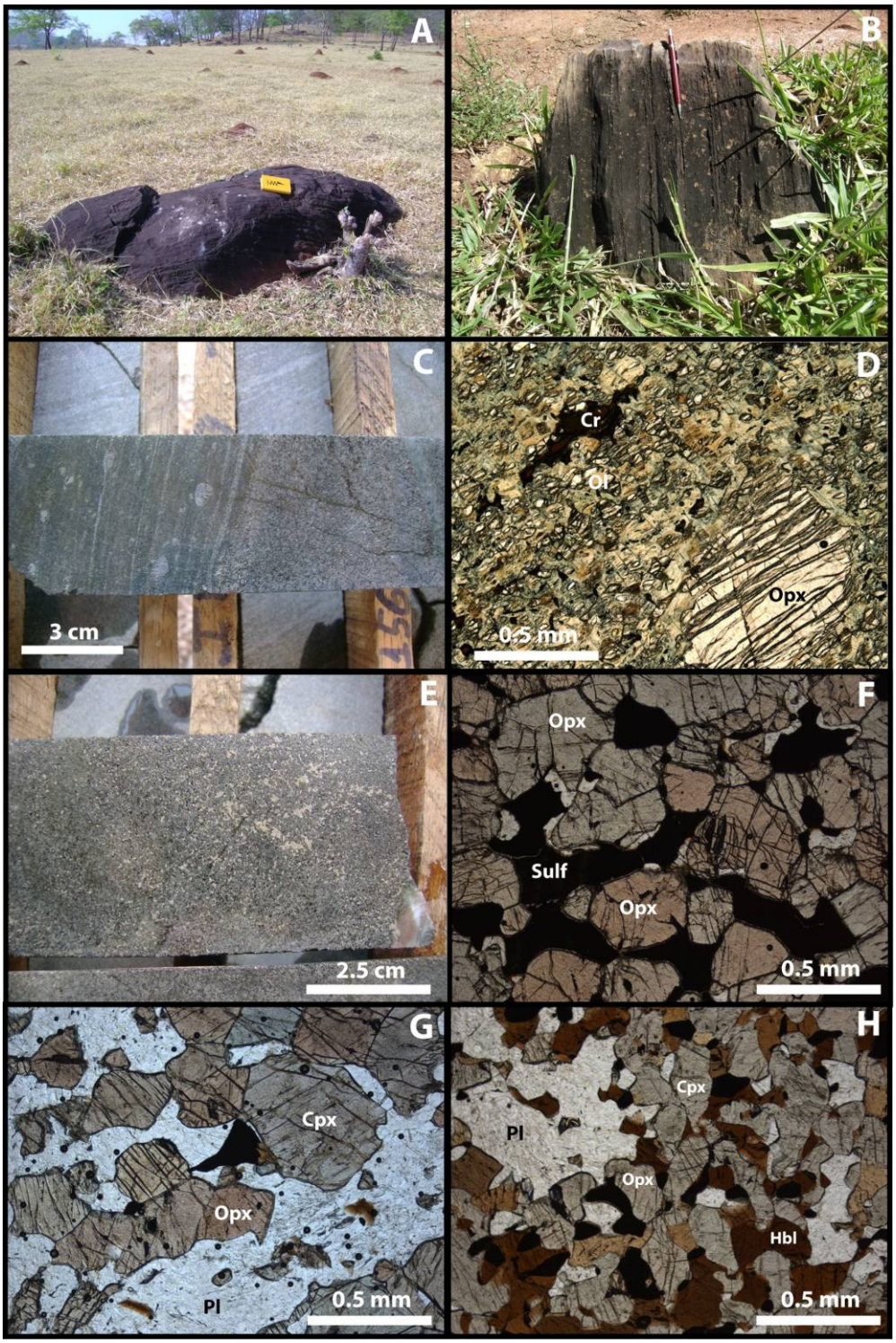

Figure 3.7 - A) Boulder of highly foliated mafic granulite. The mineral assemblage consists of orthopyroxene, clinopyroxene, plagioclase, hornblende and magnetite. Abundant reddish termite mounts are developed on soil from mafic rocks (locality of sample TQ-22). B) Outcrop of highly foliated subvertical peridotite. Elongated pyroxene crystals and pyroxene aggregates become evident in the weathered surface. C) Sharp contact between peridotite (left side) and pyroxenite (right side) from drill core FSTQ-01. Large pyroxene crystals in the peridotite show up in lighter colors. D) Photomicrograph of peridotite consisting of partially serpentinized olivine crystals (Ol) associated with large orthopyroxene (opx) and chromite (Cr). E) Orthopyroxenite with interstitial sulfides from drill core FSTQ-01.

Cont. Figure 3.7 - F) Photomicrograph of orthopyroxenite consisting of cumulus orthopyroxene (opx) and interstitial sulfides (Sulf) and plagioclase (white and low relief minerals) G) Photomicrograph of gabbronorite from FSTQ-01. Ilmenite (opaque) and phlogopite (small brownish lamellae) are accessory minerals. H) Photomicrograph of recrystallized mafic rock from drill hole FSTQ-01. This sample is a mafic granulite with fine-grained granoblastic texture. The mineral assemblage consists of orthopyroxene (Opx), clinopyroxene (Cpx), brownish hornblende (Hbl), plagioclase (Pl), ilmenite (opaques) and spinel (small greenish crystals associated with ilmenite).

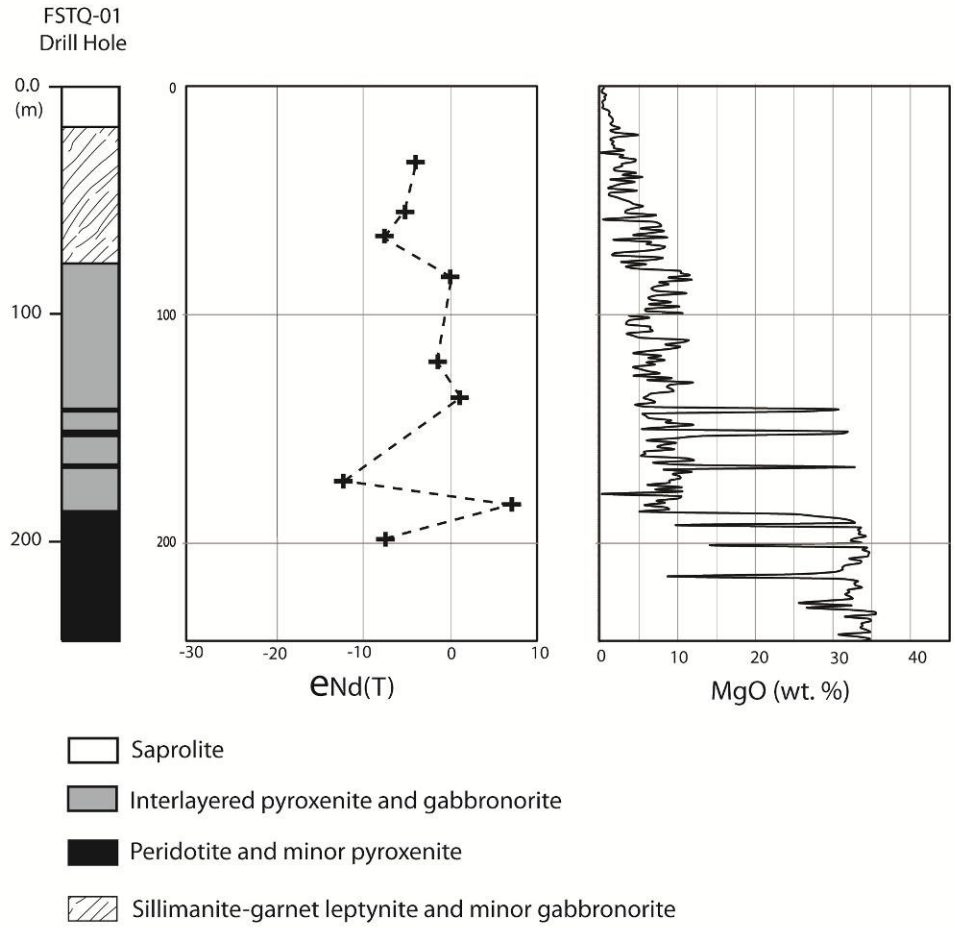

Figure 3.8 - Log, MgO content and εNd(T) for drill hole FSTQ-01 (see Fig. 6 for location).

Samples of peridotite (MgO > 24 wt.%) and pyroxenite-gabbronorite (MgO < 15 wt.%) form two distinct groups, indicating the sharp contact between olivine-rich peridotite and pyroxenite, as well as the gradational transition between pyroxenite and gabbronorite. High MgO contents of peridotite samples (up to 35 wt. %) are consistent with high MgO content of olivine from peridotite (up to Fo90) reported from Silva (1997). Higher CaO and TiO_2 contents, when compared to data from the Damolândia Complex, are consistent with the abundance of clinopyroxene in the layered rocks, while high Cr contents are consistent with the presence of

chromite in both peridotite and pyroxenite. Higher CaO contents are particularly significant in peridotites, indicating the abundance of lherzolite in the Taquaral Complex, while harzburgite predominates in the Damolândia Complex. Higher Ti contents in gabbronorite of the Taquaral Complex is associated with disseminated ilmenite. Scattered high contents of K_2O are associated with disseminated interstitial phlogopite. Similar to what was described for the Damolândia Complex, high K_2O contents show no correlation with MgO content suggesting that they result from inhomogeneous assimilation of crustal rocks by the parental magma.

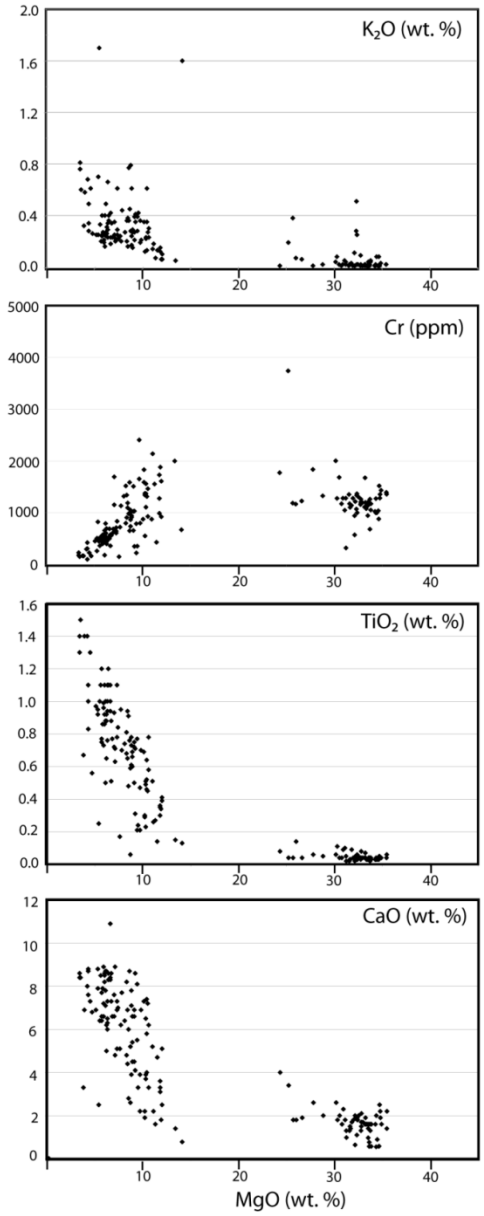

Figure 3.9 - Plot of MgO versus CaO, TiO_2, Cr and K_2O for the drill hole FSTQ-01.

Rocks with metamorphic mineralogy and tectonic texture prevail throughout the layered sequence of drill core FSTQ-01. In these zones the primary igneous mineralogy is recrystallized into fine-grained metamorphic minerals. Recrystallized mafic rocks consist of fine-grained granoblastic aggegates of plagioclase, orthopyroxene, clinopyroxene, dark-brown amphibole and minor spinel (Figure 3.7H), indicating that recrystallization occurred under conditions of high temperature (granulite facies of regional metamorphism). Mafic rocks associated with silimanite-garnet leptynite in the upper part of the drill core are similar to highly tectonized gabbronorite of the layered sequence. This feature suggests that they represent disrupted fragments of the layered sequence.

An elongated body of coarse-grained porphyritic orthogneiss occurs in the northwestern corner of the area investigated by INV (Figure 3.6). This orthogneiss has granitic composition and was sampled for isotopic studies (sample TQ-03).

3.4.Methods

***In situ* zircon analyses**

Zircon concentrates were extracted from ca. 10 kg rock samples using conventional gravimetric and magnetic techniques at the Geochronology Laboratory of the University of Brasília. Mineral fractions were hand-picked under a binocular microscope to obtain fractions of similar size, shape and color. For *in situ* U-Pb and Hf analyses, hand-picked zircon grains were mounted in epoxy blocks and polished to obtain a smooth surface. Backscattered electron and cathodoluminescence images were obtained in order to investigate the internal structures of the zircon crystals prior to analysis.

Before LA-ICP-MS analyses, mounts were cleaned with dilute (ca. 2%) HNO_3. The samples were mounted in an especially adapted laser cell and loaded into a New Wave UP213 Nd:YAG laser (λ = 213 nm), linked to a Thermo Finnigan Neptune Multi-collector ICPMS. Helium was used as the carrier gas and mixed with argon before entering the ICP. The laser was run at a frequency of 10 Hz and energy of ~100 mJ/cm^2 with a spot of 30μm for U-Pb systematics and 40μm for Hf isotopic analyses.

The U-Pb and Hf LA-ICPMS analyses followed the analytical procedure described by Buhn *et al.* (2009) and Matteini *et al.* (2009), respectively, and were performed at the Geochronology Laboratory of the University of Brasília.

Two international zircon standards were analyzed throughout the U-Pb LA-ICPMS analyses. Zircon standard GJ-1 (Jackson *et al.*, 2004) was used as the primary reference material in a standard-sample bracketing method, accounting for mass bias and drift correction. The resulting correction factor for each sample analysis considers the relative position of each analysis within the sequence of 4 samples bracketed by two standard and two blank analyses each (Albarède *et al.*, 2004). The Temora 2 standard (Black *et al.*, 2004) was run at the start and at the end of each analytical session, yielding accuracy around 2% and a precision in the range of 1% (1σ). The errors of sample analyses were propagated by quadratic addition of the external uncertainty observed for the standards to the reproducibility and within-run precision of each unknown analysis. Zircon grains with $^{206}Pb/^{204}Pb$ lower than 1000 were rejected. Plotting of U–Pb data and age calculations were performed using ISOPLOT version 3.0 (Ludwig, 2003) and errors for isotopic ratios are presented at the 1σ level.

Hf isotopic measurements were carried out on zircon grains previously investigated by U-Pb systematics. Only concordant grains (± 5%) were selected. The Hf spot analyses were located in the same CL region of zircon grains and, whenever possible, just on top of the U-Pb analytical pit. Before the laser ablation analyses, JMC 475 standard solution, doped with Yb (Yb/Hf=0.02), was run, yielding a mean $^{176}Hf/^{177}Hf$ ratio of 0.282171±20 (n=4) which is in agreement with values reported in the literature (e.g. 0.282163 +/- 09; Blichert-Toft et. al (1997)). During *in situ* analytical session, GJ-1 zircon (Jackson *et al.*, 2004) was monitored as a reference material and rendered an average $^{176}Hf/^{177}Hf$ value of 0.282001±21 (n=10) in agreement with Zeh *et al.* (2007; 0.282003 +/- 15), Morel *et al.* (2008; 0.282000 +/- 05) and Xie *et al.* (2008; 0.282028±34). The mass-bias correction considered the signal of ^{171}Yb and ^{173}Yb and, additionally, these isotopes, as well as ^{175}Lu, were applied in the isobaric interference correction of Yb and Lu on the ^{176}Hf signal. The studied zircon grains show very low Lu/Hf values (<0.0004), which reflect that the primary Hf isotopic composition is preserved and, consequently, no overcorrection is needed. Calculation of ε_{Hf} and T_{DM} model ages for each single spot analyses were based on the $^{206}Pb/^{238}U$ age, previously determined in the same grain. Errors for isotopic ratios are presented at the 2σ level.

Ion microprobe analyses were carried out in one sample using SHRIMP I at the Research School of Earth Sciences, Australian National University, Canberra, Australia. Data were collected and reduced as described by Williams & Claesson (1987) and Compston (1992). Uncertainties are given at 1σ level, and final age quoted at 95% confidence level. Reduction of raw data was carried out using Squid 1.02 (Ludwig, 2001). U/Pb isotopic ratios were referenced to the RSES standard zircon AS3 (1099 Ma, $^{*206}Pb/^{238}U = 0.1859$, Paces & Miller (1993). U and Th concentrations were determined relative to those measured in the RSES standard SL13.

ID-TIMS analyses

For the conventional U-Pb analyses, fractions were dissolved in concentrated HF and HNO_3 (HF:HNO_3 = 4:1) using microcapsules in Parr-type bombs. A mixed ^{205}Pb-^{235}U spike was used. Chemical extraction followed standard anion exchange technique, using Teflon microcolumns, following modified procedures from Krogh (1973). Pb and U were loaded together on single Re filaments with H_3PO_4 and Si gel, and isotopic analyses were carried out on a Finnigan MAT-262 multi-collector mass spectrometer equipped with secondary electron multiplier-ion counting, at the Geochronology Laboratory of the University of Brasília. Procedure blanks for Pb, at the time of analyses, were better than 20 pg. Data reduction and age calculations were performed using the PBDAT (Ludwig, 1993) and ISOPLOT version 3.0 (Ludwig, 2003) software. Errors for isotopic ratios are quoted at 2σ.

Sm-Nd isotopic analyses followed the method described by Gioia & Pimentel (2000) and were carried out at the Geochronology Laboratory of the University of Brasília. Whole rock powders (ca. 50 mg) were mixed with ^{149}Sm-^{150}Nd spike solution and dissolved in Savillex capsules. Sm and Nd extraction of whole-rock samples followed conventional cation exchange techniques. Sm and Nd samples were loaded on Re evaporation filaments of double filament assemblies and the isotopic measurements were carried out on a multi-collector Finnigan MAT 262 mass spectrometer in static mode. Uncertainties for Sm/Nd and $^{143}Nd/^{144}Nd$ ratios are better than ±0.5% (2σ) and ±0.005% (2σ), respectively, based on repeated analyses of international rock standards BHVO-1 and BCR-1. The $^{143}Nd/^{144}Nd$ ratios were normalized to $^{146}Nd/^{144}Nd$ of 0.7219 and the decay constant used was 6.54×10^{-12} a^{-1}. The T_{DM} values were calculated using the model of DePaolo (1981). Nd procedure blanks were better than 100 pg.

3.5. Samples and results

Damolândia region

Sample DM-16 is a leucogabbro corresponding to a residual, late-stage influx of magma that cut across other partially crystallized rocks. The analyzed drill-core sample from the Damolândia Layered Complex corresponds to a heterogeneous interval in terms of metamorphism, in which strongly deformed and metamorphosed areas with polygonal mineral boundaries co-exist with relict igneous pyroxene grains (see Figure 3.2 for location).

Zircon crystals occur either within adcumulate phases or within plagioclase and hornblende crystals. They are commonly bordered by intergrowths of ilmenite and magnetite. Zircon crystals are pristine, colorless to pink and show stubby to prismatic habit with varied degrees of rounding. Generally, grains are fragmented and their widths vary between 300 and 800 μm. Under cathodoluminescence, they show well defined sector zoning and are surrounded by a thin, bright outer rim with irregular boundaries (Figure 3.10A). Zircon usually contains inclusions of apatite, pyrite and ilmenite, around which recrystallization also occurs.

Eighteen U-Pb spot analyses render a chain of concordant ages spreading from 670 Ma down to 590 Ma (Figure 3.11A). There is no obvious correlation between internal structure of the crystal and U-Pb data, since there are grains with similar ages (within error) in both rim and core (Table 3.1). Lu-Hf analyses reveal $^{176}Hf/^{177}Hf_{ap}$ ratios between 0.282119 to 0.282290, and strongly negative $\varepsilon_{Hf(T)}$ signature, ranging from -3.06 to -9.83 (Table 3.2). Two-stage hafnium model ages yield $T_{(DM)}$ values from 1.60 to 1.93 Ga.

Nd isotopic data obtained for the Damolândia Layered Complex render Nd model ages between 1.78 and 2.16 Ga, with strongly negative ε_{Nd} (T=650 Ma) values (-3.9 to -26.5) (Table 3.3). The Sm-Nd data, plotted against the stratigraphy of the drill hole FSDM-07, reveals that the ε_{Nd} variation is related merely to different degrees of assimilation during the emplacement in an older continental crust (Figure 3.4).

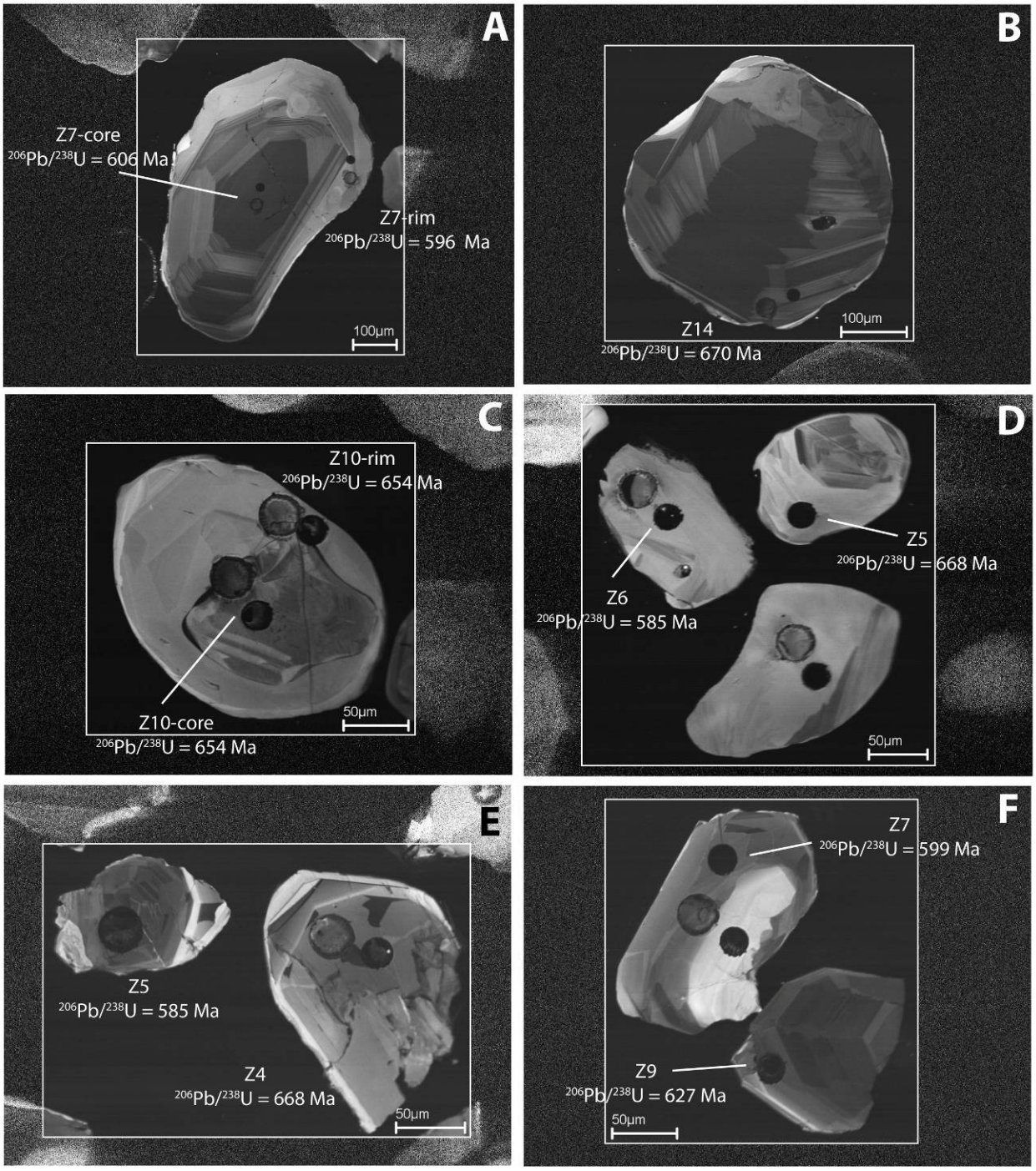

Figure 3.10 – CL images of zircon from sample DM-16 (A, B), sample DM-20 (C, D) and sample TQ-14 (E, F). Smaller spots (30 µm) represent the location of U-Pb analyses, whereas larger spots (40 µm) correspond to Hf isotopic investigation.

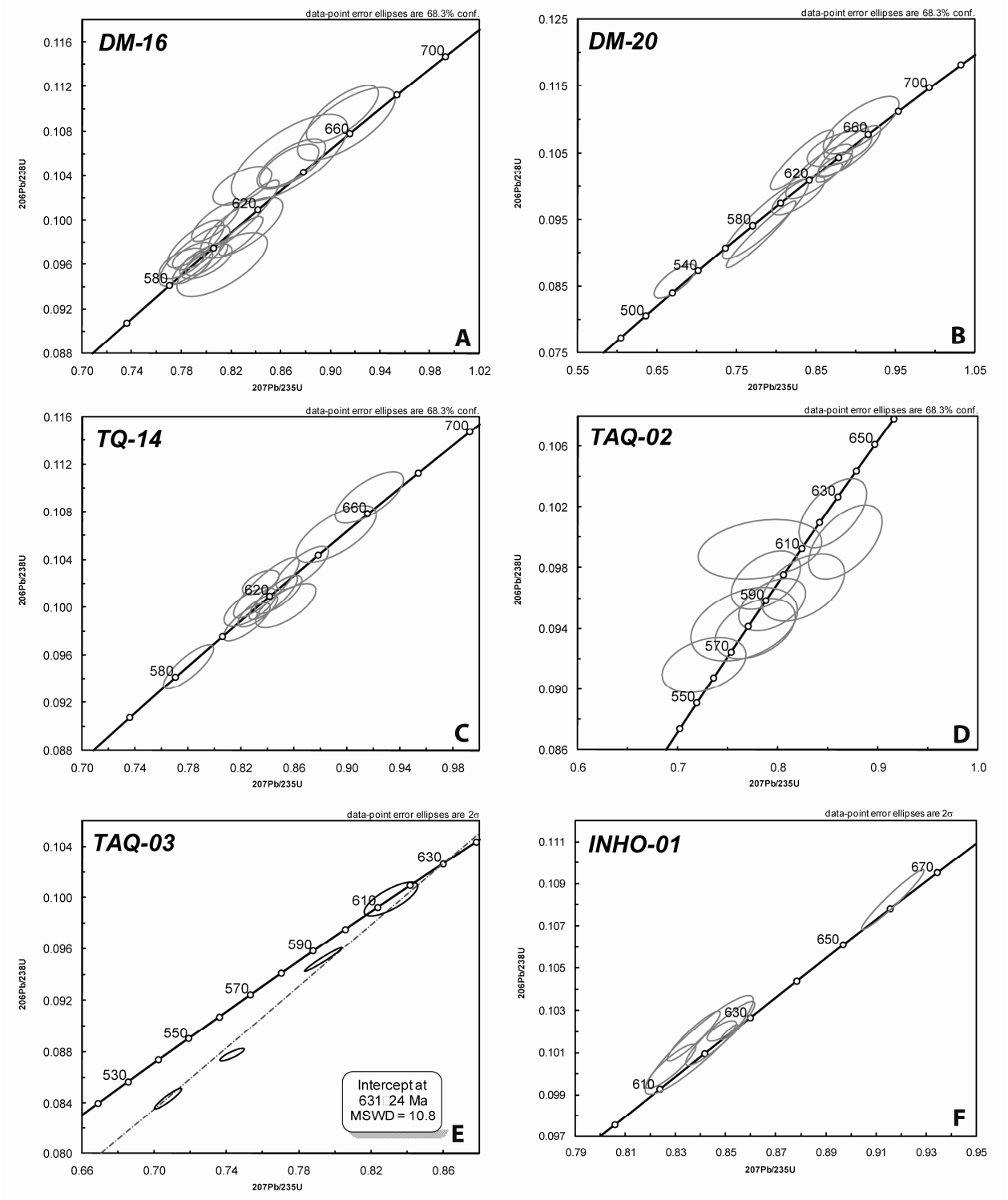

Figure 3.11 - LA-ICPMS (A-C), SHRIMP (D) and ID-TIMS (E-F) U-Pb plots for Damolândia (DM), Taquaral (TQ, TAQ) and Goianira-Trindade complexes (INHO).

Table 3.1 – U-Pb LA-ICPMS data for sample DM-16.

Sample	f(206) %	Th/ U	6/4 ratio	7/6 ratio	1s (%)	7/5 ratio	1s (%)	6/8 ratio	1s (%)	Apparent ages						Rho	Conc (%)
										7/6 age	1σ	7/5 age	1σ	6/8 age	1σ		
004-Z1	0.19	0.26	11848	0.05912	1.1	0.7891	1.4	0.09680	0.9	571.6	23.5	590.6	6.2	595.6	4.9	0.61	104
005-Z2	0.11	0.20	15807	0.06020	1.3	0.7996	1.7	0.09633	1.1	610.8	29.0	596.6	7.8	592.9	6.1	0.62	97
008-Z3	0.62	0.22	2884	0.05863	1.2	0.7915	1.9	0.09791	1.4	553.3	26.9	592.0	8.5	602.2	8.3	0.76	109
009-Z4	0.20	0.16	11349	0.05887	1.2	0.7803	1.5	0.09613	1.0	562.3	26.4	585.6	6.9	591.7	5.4	0.61	105
010-Z5	0.23	0.19	7649	0.06010	0.9	0.8000	1.4	0.09654	1.0	607.2	20.4	596.8	6.3	594.1	5.9	0.74	98
011-Z6	0.21	0.18	8499	0.06046	1.9	0.8283	2.7	0.09937	1.8	619.9	41.8	612.6	12.2	610.7	10.6	0.72	99
014-Z7RIM	0.32	0.21	5512	0.05920	1.4	0.7904	2.4	0.09683	1.9	574.5	30.7	591.4	10.6	595.8	10.7	0.80	104
015-Z7-CORE	0.12	0.27	14087	0.06089	0.8	0.8278	1.4	0.09861	1.2	635.3	17.1	612.4	6.6	606.2	6.9	0.84	95
016-Z8	0.09	0.20	18741	0.05973	0.9	0.7888	1.4	0.09578	1.0	593.8	19.9	590.5	6.1	589.6	5.7	0.75	99
017-Z9	0.14	0.18	13115	0.06138	2.2	0.8127	3.0	0.09602	2.0	652.6	47.8	604.0	13.5	591.1	11.1	0.68	91
021-Z10	0.09	0.20	19111	0.05861	1.0	0.8070	1.5	0.09986	1.2	552.7	21.9	600.8	7.0	613.6	6.8	0.76	111
022-Z11	0.14	0.20	2190	0.05993	1.5	0.8683	2.1	0.10508	1.4	601.2	33.1	634.7	9.8	644.1	8.7	0.68	107
023-Z12	0.11	0.25	16144	0.05832	1.5	0.8291	1.9	0.10311	1.1	541.6	33.4	613.1	8.7	632.6	6.7	0.58	117
024-Z13	0.12	0.18	14238	0.05951	2.6	0.8667	3.6	0.10563	2.4	585.7	56.9	633.8	16.9	647.3	15.0	0.69	111
027-Z14	0.25	0.18	7118	0.06020	1.4	0.9093	2.1	0.10955	1.5	610.8	31.3	656.7	10.2	670.1	9.8	0.73	110
028-Z15	0.18	0.20	8927	0.05989	1.4	0.8665	1.8	0.10494	1.2	599.5	29.3	633.7	8.6	643.3	7.5	0.67	107
029-Z16	0.27	0.29	6526	0.05986	1.0	0.8300	2.2	0.10056	2.0	598.5	21.0	613.6	10.4	617.7	12.0	0.91	103
030-Z17	0.20	0.32	8744	0.06093	2.1	0.9129	2.9	0.10866	2.0	636.9	44.3	658.6	13.8	665.0	12.5	0.71	104

Table 3.2 - Summary of in situ Lu–Hf analyses for sample DM-16.

Sample	176Lu/177Hf	2σ	176Hf/177Hf	2σ	Age (Ma)	(176Hf/177Hf)t	2σ	eHf(t)	1σ	$T_{(DM)}$ (Ga)
003-Z1	0.0004016	±0.000005	0.282129	0.000025	596	0.282124	0.000025	-9.83	±0.40	1.93
004-Z2	0.0004241	±0.000000	0.282198	0.000030	593	0.282193	0.000030	-7.47	±0.55	1.80
005-Z7-RIM	0.0003607	±0.000002	0.282236	0.000025	596	0.282232	0.000025	-6.03	±0.39	1.73
006-Z7-CORE	0.0006237	±0.000003	0.282159	0.000029	606	0.282152	0.000029	-8.63	±0.51	1.88
009-Z6	0.0002894	±0.000002	0.282229	0.000026	611	0.282226	0.000026	-5.92	±0.40	1.73
010-Z11	0.0003603	±0.000001	0.282290	0.000038	644	0.282285	0.000038	-3.07	±0.82	1.60
011-Z12	0.0004843	±0.000001	0.282193	0.000028	633	0.282187	0.000028	-6.79	±0.47	1.80
012-Z13	0.0003522	±0.000000	0.282156	0.000034	647	0.282151	0.000034	-7.74	±0.67	1.86
015-Z15	0.0003595	±0.000000	0.282123	0.000038	643	0.282119	0.000038	-8.98	±0.80	1.92
016-Z14	0.0004665	±0.000004	0.282195	0.000036	670	0.282189	0.000036	-5.91	±0.72	1.78
017-Z4	0.0005511	±0.000003	0.282231	0.000023	592	0.282225	0.000023	-6.36	±0.34	1.74
018-Z5	0.0003581	±0.000002	0.282220	0.000025	594	0.282216	0.000025	-6.64	±0.39	1.76

Table 3.3 - Sm-Nd data for the Damolândia Complex.

Sample	Lithotype	Prof. (m)	Sm(ppm)	Nd(ppm)	$^{147}Sm/^{144}Nd$	$^{143}Nd/^{144}Nd$	$(^{143}Nd/^{144}Nd)i$	$\varepsilon_{(0)}$	$\varepsilon_{(T)}$	T_{CHUR}(Ma)	T_{DM}(Ma)
DM 01	Gabbro	283.0	2.3296	9.4894	0.1484	0.512159	0.511527	-9.34	-5.34	1503	2046
DM 02	Gabbro	282.4	2.5896	11.0190	0.1421	0.512162	0.511557	-9.29	-4.75	1321	1857
DM 03	Norite	280.9	1.7779	7.8426	0.1370	0.511029	0.510445	-31.39	-26.48	-	-
DM 04	Norite	276.4	1.7122	7.2050	0.1437	0.512083	0.511471	-10.82	-6.43	1585	2073
DM 05	Norite	241.5	1.8431	6.5716	0.1695	0.512323	0.511601	-6.14	-3.89	-	-
DM 07	Orthopyroxenite	217.8	0.6952	2.4391	0.1723	0.512198	0.511464	-8.58	-6.56	-	-
DM 08	Orthopyroxenite	216.0	0.8166	2.8761	0.1716	0.512303	0.511572	-6.53	-4.45	-	-
DM 10	Pyroxenite	209.4	4.1570	15.6256	0.1608	0.512360	0.511675	-5.42	-2.44	1171	1947
DM 14	Ol-Orthopyroxenite	102.2	0.4490	1.7858	0.1520	0.512162	0.511514	-9.29	-5.59	1614	2162
DM 15	Orthopyroxenite	99.3	0.7883	2.5250	0.1887	0.512024	0.511220	-11.98	-11.33	-	-
DM-16	Gabbronorite	68.0	4.6482	27.7413	0.1013	0.511722	0.511290	-17.88	-9.96	1458	1778
DM 18	Mafic granulite		18.7812	105.0402	0.1081	0.512223	0.511763	-8.09	-0.72	710	1176
DM 20	Mafic granulite		3.8743	12.3038	0.1903	0.512642	0.511831	0.09	0.61	-	-

Table 3.4 - U-Pb LA-ICPMS data for sample DM-20.

Sample	f(206) %	Th/ U	6/4 ratio	7/6 ratio	1s (%)	7/5 ratio	1s (%)	6/8 ratio	1s (%)	Apparent ages 7/6 age	1σ	7/5 age	1σ	6/8 age	1σ	Rho	Conc (%)
005-Z2	0.65	0.13	2747	0.05679	1.7	0.6721	2.6	0.08583	2.0	483.4	38.5	522.0	10.7	530.8	9.9	0.75	110
013-z5	0.48	-0.02	3677	0.06019	2.3	0.9064	3.5	0.10923	2.6	610.3	49.9	655.1	16.7	668.2	16.3	0.75	110
014-z6	0.37	0.24	4609	0.05997	1.9	0.7862	4.5	0.09508	4.1	602.6	41.6	589.0	20.3	585.5	23.0	0.91	97
016-z8	0.23	0.25	7620	0.06054	1.9	0.8538	3.3	0.10229	2.6	623.0	41.3	626.8	15.3	627.8	15.8	0.82	101
021-z10-rim	0.34	0.14	5251	0.06141	1.6	0.8916	2.9	0.10530	2.4	653.7	34.7	647.2	13.9	645.4	14.8	0.83	99
022-z10-core	0.24	0.04	8689	0.06034	1.4	0.8875	2.1	0.10668	1.6	615.7	29.7	645.1	10.0	653.5	9.8	0.75	106
023-z11	0.33	0.19	5444	0.06138	2.0	0.8736	1.7	0.10322	1.2	652.7	42.9	637.5	7.8	633.2	7.1	0.72	97
028-z14	0.32	0.00	5792	0.06078	3.3	0.8270	2.7	0.09868	2.0	631.5	69.7	611.9	12.1	606.7	11.4	0.75	96
029-z15	0.12	0.03	14547	0.06154	0.8	0.8663	1.3	0.10209	1.0	658.3	17.8	633.6	6.0	626.7	5.8	0.77	95
030-z16	0.14	0.00	12996	0.06034	2.5	0.8792	3.0	0.10567	1.6	616.0	54.9	640.6	14.4	647.6	10.2	0.56	105
025-z19	0.30	0.16	5757	0.05805	1.5	0.8322	3.2	0.10397	2.8	531.7	31.9	614.8	14.6	637.6	17.1	0.89	120

Table 3.5 - Summary of in situ Lu–Hf analyses for sample DM-20.

Sample	176Lu/177Hf	2σ	176Hf/177Hf	2σ	Age (Ma)	(176Hf/177Hf)t	2σ	eHf(t)	1σ	$T_{(DM)}$ (Ga)
003-Z6	0.0003607	±0.000001	0.282587	0.000029	586	0.282583	0.000029	6.19	±0.53	1.04
005-Z8	0.0005757	±0.000001	0.282421	0.000046	628	0.282414	0.000046	1.14	±1.09	1.35
006-Z20	0.0001376	±0.000001	0.282375	0.000051	580	0.282373	0.000051	-1.36	±1.31	1.46
009-Z10-CORE	0.0000417	±0.000002	0.282447	0.000031	645	0.282447	0.000031	2.69	±0.57	1.28
010-Z10-RIM	0.0001762	±0.000004	0.282511	0.000042	654	0.282508	0.000042	5.04	±0.95	1.16
011-Z14	0.0000732	±0.000001	0.282292	0.000060	606	0.282291	0.000060	-3.70	±1.64	1.61
012-Z15	0.0001804	±0.000001	0.282519	0.000063	627	0.282517	0.000063	4.74	±1.71	1.15

Table 3.6 - U-Pb LA-ICPMS data for sample TQ-14.

Sample	f(206) %	Th/ U	6/4 ratio	7/6 ratio	1s (%)	7/5 ratio	1s (%)	6/8 ratio	1s (%)	Apparent ages						Rho	Conc (%)
										7/6 age	1σ	7/5 age	1σ	6/8 age	1σ		
005-Z2	0.14	0.02	12260	0.05993	1.1	0.8269	1.6	0.10007	1.1	600.9	24.9	611.9	7.2	614.8	6.3	0.68	102
007-Z4	0.17	0.00	10215	0.06088	1.3	0.9169	1.9	0.10922	1.3	635.1	28.4	660.7	9.0	668.2	8.3	0.70	105
010-Z5	0.11	0.05	15679	0.05954	0.9	0.7801	1.6	0.09502	1.3	587.0	20.3	585.5	7.1	585.2	7.3	0.82	100
012-Z7	0.19	0.01	9530	0.05859	1.0	0.7865	1.4	0.09737	0.9	551.8	22.2	589.2	6.0	599.0	5.1	0.65	109
016-Z9	0.10	0.07	17716	0.05928	0.9	0.8346	1.1	0.10212	0.7	577.2	18.9	616.2	5.0	626.8	3.9	0.58	109
018-Z11	0.13	0.03	14002	0.06053	0.8	0.8324	1.2	0.09973	0.9	622.7	17.2	614.9	5.5	612.8	5.2	0.75	98
022-Z13	0.12	0.03	15039	0.06085	0.9	0.8482	1.4	0.10110	1.0	633.9	19.6	623.7	6.4	620.9	6.2	0.76	98
023-Z14	0.11	0.00	21400	0.06051	0.9	0.8243	1.4	0.09880	1.1	621.8	19.4	610.4	6.5	607.4	6.3	0.78	98
024-Z15	0.08	0.03	23582	0.06070	0.8	0.8442	1.5	0.10087	1.2	628.6	17.1	621.5	6.7	619.5	7.2	0.85	99
025-Z16	0.08	0.07	22193	0.06092	1.7	0.8917	2.2	0.10616	1.5	636.4	35.6	647.3	10.6	650.4	9.2	0.68	102
028-Z17	0.12	0.00	14569	0.05986	1.0	0.8390	1.9	0.10165	1.6	598.5	22.5	618.6	9.0	624.1	9.8	0.85	104
029-Z18	0.13	0.04	13054	0.06080	1.0	0.8661	1.5	0.10332	1.1	632.1	21.3	633.4	7.1	633.8	6.9	0.76	100
030-Z19	0.25	0.00	7064	0.06181	1.3	0.8536	1.7	0.10016	1.2	667.4	26.9	626.6	8.2	615.4	7.1	0.69	92

Table 3.7 - Summary of in situ Lu–Hf analyses for sample TQ-14.

Sample	176Lu/177Hf	2σ	176Hf/177Hf	2σ	Age	(176Hf/177Hf)t	2σ	eHf(t)	1σ	T(DM) Ga
004-Z2	0.0001583	±0.000003	0.282301	0.000065	615	0.282299	0.000065	-3.19	±1.80	1.59
005-Z4	0.0000923	±0.000001	0.282287	0.000040	668	0.282286	0.000040	-2.47	±0.85	1.59
006-Z5	0.0002344	±0.000004	0.282343	0.000064	585	0.282341	0.000064	-2.34	±1.78	1.52
009-Z7	0.0002078	±0.000001	0.282200	0.000073	599	0.282197	0.000073	-7.03	±2.08	1.79
011-Z11	0.0002111	±0.000012	0.282267	0.000057	612	0.282265	0.000057	-4.51	±1.50	1.65
012-Z14	0.0002436	±0.000005	0.282249	0.000039	607	0.282247	0.000039	-5.25	±0.87	1.69
013-Z15	0.0002784	±0.000006	0.282338	0.000049	619	0.282335	0.000049	-1.86	±1.21	1.51
014-Z16	0.0001586	±0.000002	0.282255	0.000048	650	0.282252	0.000048	-4.09	±1.15	1.66

Table 3.8 - U-Pb SHRIMP data for sample TAQ-02.

Grain spot	% 206 Pb	U ppm	Th ppm	232Th/ 238U	ppm 206Pb*	6/8 age	7/6 age	Conc (%)	207/206 ratio	±%	207/235 ratio	±%	206/238 ratio	±%	err corr
1.1	0.00	96	55	0.59	7.03	525.0 ±6.3	633 ± 39	17	0.0608	1.8	0.712	2.2	0.0848	1.3	0.57
2.1	0.50	65	30	0.48	5.15	565.3 ±7.3	510 ± 77	-11	0.0575	3.5	0.726	3.8	0.0916	1.3	0.36
3.1	0.42	32	16	0.52	2.60	581.1 ±9.4	564 ± 94	-3	0.0589	4.3	0.766	4.6	0.0943	1.7	0.76
4.1	0.00	38	17	0.47	3.26	612.9 ±9.1	709 ± 51	14	0.0630	2.4	0.867	2.8	0.0997	1.6	0.55
5.1	0.56	62	27	0.45	5.31	609.8 ±7.7	498 ± 110	-22	0.0572	5.1	0.782	5.2	0.0992	1.3	0.25
6.1	0.00	47	30	0.65	4.07	623.6 ±8.7	640 ± 47	3	0.0610	2.2	0.855	2.6	0.1016	1.5	0.56
7.1	0.32	55	25	0.47	4.47	579.4 ±7.5	600 ± 68	3	0.0599	3.1	0.777	3.4	0.0940	1.4	0.40
8.1	0.27	46	22	0.51	3.81	594.8 ±8.4	671 ± 64	11	0.0619	3.0	0.925	3.3	0.0967	1.5	0.44
9.1	0.25	68	36	0.55	5.72	598.1 ±7.3	559 ± 56	-7	0.0588	2.6	0.788	2.9	0.0972	1.3	0.44
10.1	0.27	71	59	0.87	5.81	588.4 ±7.0	612 ± 55	4	0.0602	2.5	0.794	2.8	0.0956	1.2	0.44

Table 3.9 – U-Pb ID-TIMS data for sample TAQ-03.

								Radiogenic Ratios							Age			
Sample	# grains	Size (mg)	U ppm	Th ppm	Pb ppm	U/ Th	206/ 204	207*/ 235		206* /238		rho	207*/ 206*		206*/ 238	207*/ 235	207*/ 206*	Ma
TAQ03R	1	0.019	416.29	57.27	38.216	7.27	635	0.7073	0.89	0.0844	0.78	0.932	0.0608	0.23	522	543	632	9
TAQ03S	1	0.02	186.31	54.41	36.839	3.42	76	0.8305	1.45	0.0999	1.09	0.757	0.0609	0.8	608	614	636	36
TAQ03T	2	0.034	303.7	32.01	30.012	9.49	668	0.7428	0.74	0.0878	0.43	0.854	0.0614	0.21	542	564	653	11
TAQ03U	3	0.025	199.65	43.53	20.996	4.59	555	0.7932	1.09	0.0952	0.8	0.976	0.0604	0.21	586	593	620	7

Table 3.10 – Sm-Nd data for the Taquaral Complex.

Sample	Lithotype	Prof. (m)	Sm(ppm)	Nd(ppm)	$^{147}Sm/^{144}Nd$	$^{143}Nd/^{144}Nd$	$(^{143}Nd/^{144}Nd)i$	$\varepsilon_{(0)}$	$\varepsilon_{(T)}$	T_{CHUR}(Ma)	T_{DM}(Ma)
TQ 03	Gabbronorite	33.4	2.144	7.858	0.1649	0.512306	0.511603	-6.48	-3.85	1581	2293
TQ 05	Gabbronorite	55.2	7.981	29.540	0.1633	0.512238	0.511542	-7.81	-5.05	1814	2432
TQ 06	Orthopyroxenite	65.7	1.324	3.050	0.2624	0.512538	0.511420	-1.95	-7.42	-	-
TQ 08	Orthopyroxenite	83.6	2.121	8.847	0.1449	0.512424	0.511806	-4.18	0.12	626	1358
TQ 10	Gabbronorite	120.7	3.646	13.196	0.1670	0.512445	0.511733	-3.77	-1.31	982	1930
TQ 12	Gabbronorite	136.5	4.155	13.688	0.1835	0.512643	0.511862	0.11	1.21	-	-
TQ 15	Orthopyroxenite	173.0	0.638	1.200	0.3212	0.512547	0.511179	-1.78	-12.14	-	-
TQ 16	Gabbronorite	183.2	3.136	7.586	0.2499	0.513232	0.512168	11.59	7.18	-	-
TQ 18	Peridotite	198.4	0.099	0.189	0.3162	0.512773	0.511426	2.64	-7.31	-	-
TQ 22	Mafic granulite		5.893	22.327	0.1596	0.512354	0.511674	-5.54	-2.46	1157	1919

Table 3.11 – U-Pb ID-TIMS data for sample INHO-01.

									Radiogenic Ratios					Age			
Sample	# grains	Size (mg)	U ppm	Th ppm	Pb ppm	U/ Th	206/ 204	207*/ 235	206* /238			rho	207*/ 206*		206*/ 238	207*/ 235	207*/ 206*	Ma
INHO7	3	0.022	566.71	57.345	49.46	0.09	3573	0.8484	0.56	0.1020	0.383	0.73	0.0603	0.386	626	624	614	8.3
INHO10	1	0.012	993.29	102.08	90.68	0.09	3536	0.8513	0.32	0.1020	0.296	0.91	0.0605	0.132	626	625	623	2.8
INHO8	5	0.017	94.138	11.537	64.01	0.68	483	0.9168	1.11	0.1083	1.07	0.96	0.0614	0.289	663	661	654	6.2
INHO2	4	0.026	140.52	15.063	41.85	0.30	928	0.8477	1.33	0.1019	1.22	0.92	0.0603	0.516	625	623	616	11
INHO5	4	0.026	147.74	16.077	41.85	0.28	880	0.8371	1.04	0.1018	0.949	0.93	0.0596	0.386	635	618	591	8.4
INHO13	3	0.015	601.99	65.572	72.55	0.12	851	0.8281	0.98	0.1003	0.85	0.88	0.0598	0.465	616	613	598	10
INHO14	2	0.019	201.34	22.302	57.27	0.28	368	0.8395	2.11	0.1014	1.9	0.91	0.0600	0.864	622	619	606	19

Table 3.12 - Sm-Nd data for the Goianira-Trindade Complex.

Sample	Sm(ppm)	Nd(ppm)	$^{147}Sm/^{144}Nd$	$^{143}Nd/^{144}Nd$	$(^{143}Nd/^{144}Nd)i$	$\varepsilon_{(0)}$	$\varepsilon_{(T)}$	T_{CHUR}(Ma)	T_{DM}(Ma)
GT-4	1.517	4.121	0.223	0.512772	0.511822	2.61	0.43	789	-
GT-6B	3.91	10.68	0.221	0.512748	0.511807	2.15	0.13	703	-
GT-6C	1.663	4.988	0.202	0.512711	0.511850	1.42	0.99	2149	-
GT-9A	2.705	8.329	0.196	0.512648	0.511813	0.20	0.25	-	-
GT-9B	0.881	4.785	0.111	0.5123	0.511827	-6.59	0.53	-	1098
GT-9D	4.833	13.7	0.213	0.512719	0.511812	1.58	0.23	777	-
GT-10B	4.349	12.54	0.21	0.512647	0.511752	0.18	-0.93	-	-
GT-41	0.133	0.463	0.174	0.512704	0.511963	1.29	3.18	-	1281

Sample DM-20 corresponds to a strongly foliated mafic granulite with dioritic composition, exposed near (~2.5 km) an occurrence of sapphirine+quartz bearing granulites (sample PT-62; Moraes *et al.*, 2002; Baldwin *et al.*, 2005). In sample DM 20, zircon is included in plagioclase crystals and also occurs close to hornblende corona. Zircon grains are approximately 150 μm long and are pristine and colorless. Commonly, these crystals show a "soccer-ball" habit, with rounded terminations, typical of zircon grown under granulite facies conditions (Vavra *et al.*, 1999; Schaltegger *et al.*, 1999). Primary internal texture in igneous crystals is represented by sector zoning, which is partially preserved in some grains, while featureless zircon is the main metamorphic texture. Some grains also show bright, luminescent rims with lobate, curved inward boundaries (Figure 3.10B). Generally, these luminescent domains render highly discordant U-Pb ages.

Ten spot analyses yield a spread of concordant ages from 670 to 530 Ma (Figure 3.11B; Table 3.4) and identical ages in rims and cores are identified, similarly to the previously described results for sample DM-16. $^{176}Hf/^{177}Hf_{ap}$ ratios range from 0.282291 to 0.282583 and $\varepsilon_{Hf(T)}$ vary in the interval of 5.73 to -3.65. Two-stage hafnium model ages reveal values from 1.05 to 1.60 Ga (Table 3.5).

Regional granulites, contrary to the mafic-ultramafic complex, show younger Nd model ages (1.2 Ga) and only slightly negative ε_{Nd} (T=650 Ma) values (-0.72; Table 3.3). This might indicate either a different degree of assimilation of older continental crust or even that these rocks were generated from a distinct, more depleted magma source.

Taquaral area

TQ-14 is an amphibolite drill-core sample from the Taquaral Layered Complex. Zircon grains occur included in plagioclase and hornblende. They are pristine, colorless and commonly show stubby to prismatic habit, with sharp to rounded surfaces. The crystals vary in size from 200 μm to 500 μm. Bright, luminescent cores with weak sector zoning usually present very low Pb contents and reveal highly discordant and occasionally younger U-Pb ages than that observed in the correspondent rim. These nucleii are surrounded by a dark domain and some grains also have a very thin and brilliant external rim (Figure 3.10C). In addition, featureless zircon is recurrent.

Thirteen spot analyses reveal concordant ages varying from 670 to 585 Ma (Figure 3.11C, Table 3.6). As observed in the Damolândia Complex, the scatter of ages cannot be linked to internal features in zircon grains. Hf isotopic ratios of these crystals range from 0.282197 to 0.282341, with strongly negative $\varepsilon_{Hf(T)}$ values (from -1.86 to -7.03). Two-stage Hf model ages vary between 1.51 and 1.69 Ga (Table 3.7).

Sample TAQ-02 corresponds to a medium-grained gabbronorite with granoblastic texture. Zircon crystals are pristine and occur as stubby to prismatic grains, smaller than 300 μm, that usually are fragmented. BSE imaging reveals the existence of cores with relict sector zoning, which are surrounded by a bright, outer domain with curved, irregular boundaries (Figure 3.10D). Featureless crystals are also commonly observed. Ten SHRIMP spot analyses yield variable discordant results, with $^{206}Pb/^{238}U$ ages ranging from 623 Ma to 525 Ma (Figure 3.11 D; Table 3.8).

In the Taquaral Complex, Nd model ages are slightly younger (1.36 to 1.92 Ga) and ε_{Nd} (T=650Ma) varies from +0.1 to -7.8 (Table 3.9). The deviation in the ε_{Nd} value reflects varied degrees of crustal contamination, similarly to that described for the Damolândia Complex (Figure 3.8).

Sample TAQ-03 corresponds to a porphyritic biotite orthogneiss exposed in the western margin of the mafic complex. It consists of pink, clear elongated and prismatic (4:1) zircon grains. Inclusions or fractures are rare. Four zircon fractions were investigated by conventional ID-TIMS and yielded highly discordant compositions. However, the upper intercept age of 631 ± 24 Ma (MSWD=8.1, Figure 3.11E, Table 3.9) is interpreted as being representative of the igneous crystallization.

Goianira-Trindade Complex

The Goianira-Trindade Complex is an additional mafic-ultramafic complex that occurs within the AIC, to the south of the Damolândia layered body (see Figure 3.1B for location). It is composed of peridotite, pyroxenite and gabbronorite, with varied degrees of deformation and high-grade metamorphic imprint, similarly to that described in the Damolândia and Taquaral complexes.

Sample INHO-01 is a coarse-grained leucogabbro in which two zircon populations can be distinguished. Small, prismatic grains characterize the first group, whereas the second is

composed of colorless, rounded crystals with stubby habit, typical of metamorphic growth. However, there is no correlation among the data obtained and zircon population. ID-TIMS analyses of seven fractions reveal variably discordant results with a cluster of $^{206}Pb/^{238}U$ ages around 620 Ma, whereas one fraction yield a value of 662 Ma (Figure 3.11F, Table 3.11).

Nd isotopic data obtained for seven cogenetic rocks from the Goianira-Trindade Complex reveal positive to slightly negative ε_{Nd} values (-0.93 to +3.18) and T_{DM} Nd model ages between 1.10 and 1.28 Ga (Table 3.12). The results suggest derivation from a depleted mantle, with restricted crustal contribution.

3.6.Discussion

"Metamorphic" zircon and the meaning of the spread of concordant U-Pb ages

Zircon is a common mineral in almost all rock types and occurs in a wide range of environments, ranging from the Earth's surface to deeper crustal levels. Owing to its resilience, even in such extreme conditions, zircon allows the link between P-T paths and geological time. However, recent studies have shown that processes taking place during high-grade metamorphism affect the U-Pb isotopic signature of zircon.

In granulite facies, zircon may display two distinct behaviors as a response to the extraordinary pressure and temperature conditions. New zircon may grow either in the subsolidus state, due to the breakdown of Zr-bearing minerals in metamorphic reactions, or from a melt/fluid phase (Roberts & Fringers, 1997; Fraser *et al.*, 1997; Schaltegger *et al.*, 1999; Vavra *et al.*, 1999; Degeling *et al.*, 2001; Bingen *et al.*, 201; Rubatto, 2002; Ayers *et al.*, 2003; Whitehouse & Platt, 2003; Möller *et al.*, 2003; Rubatto & Hermann, 2007). Growth of new zircon results in the overgrowth of older grains or in the crystallization of a new population of individual crystals. In general, minerals generated under such conditions are pristine and small. Their external and internal patterns are variable, as they might form prisms with oscillatory zoning (Nÿstrom & Kriegsman, 2003), as well as equant, granoblastic crystals with "soccer ball" habit (Vavra *et al.*, 1999; Schaltegger *et al.*, 1999).

However, the new zircon commonly shows different geochemical signature compared to the protolith igneous grain, since it crystallizes in (i) a chemically distinct environment, or (ii) in equilibrium with other minerals, such as garnet and monazite, which can influence the partition

coefficient of important constituents of zircon (Bingen *et al.*, 2001; Rubatto, 2002; Rubatto & Hermann, 2007). Besides that, because of the complete opening of the isotopic system, their ages and isotope ratios are distinguishable from older crystals and, hence, newly grown zircon records younger geological events.

In a second hypothesis, zircon can ***re-equilibrate*** in the presence of a fluid or a melt phase (Schaltegger *et al.*, 1999; Vavra *et al.*, 1999; Ashwal *et al.*, 1999; Hoskin & Black, 2000; Corfu *et al.*, 2003; Martin *et al.*, 2008). Under CL images, crystals that have experienced such alteration show an irregular and diffuse, curved inward boundary, typical of consumption (Hoskin & Black, 2000; Corfu *et al.*, 2003; Geisler *et al.*, 2007). Occasionally, primary structures are partially preserved, rendering a "ghost" feature in the altered zone (Hoskin & Black, 2000).

In this scenario, if the crystal is radiation-damaged, the defects may enhance the diffusion of elements in zircon, promoting both the gain of common Pb and unusual cations (Ca, Al, Fe) and the loss of essential components, such as Zr, Si, Pb, Hf, REE and U (Schaltegger *et al.*, 1999; Vavra *et al.*, 1999; Geisler *et al.*, 2007). Consequently, the diffusion reaction usually yields discordant U-Pb analyses.

However, if zircon is crystalline, re-equilibrium occurs dynamically in a coupled dissolution-reprecipitation process, in which the system remains closed (or partially closed) for the main components (Ashwal *et al.*, 1999; Putnis, 2002; Tomaschek *et al.*, 2003; Geisler *et al.*, 2007; Martin *et al.*, 2008). If the equilibrium is not complete, the crystal retains part of the isotopic and geochemical information of the protolith grain. Accordingly to that, such zones shall yield intermediate ages between primary, igneous ages, and secondary, metamorphic or hydrothermal alteration and, therefore, their geological meaning may not be real (Mezger & Krogstad, 1997; Hoskin & Black, 2000; Möller *et al.*, 2002; Geisler *et al.*, 2007).

Since the Lu-Hf isotopic system is decoupled from U-Pb systematics during alteration, it has been used to solve geological events related to such recrystallization processes (Gerdes & Zeh, 2009). In contrast to CL imaging and chemical analysis, Hf isotopes allow verifying the number of zircon forming episodes, based on the fact that individuals formed within an isotopically homogeneous magmatic suite and/or in the same geological event shall yield similar initial Hf isotopic ratios (Nebel *et al.*, 2007; Gerdes & Zeh, 2009).

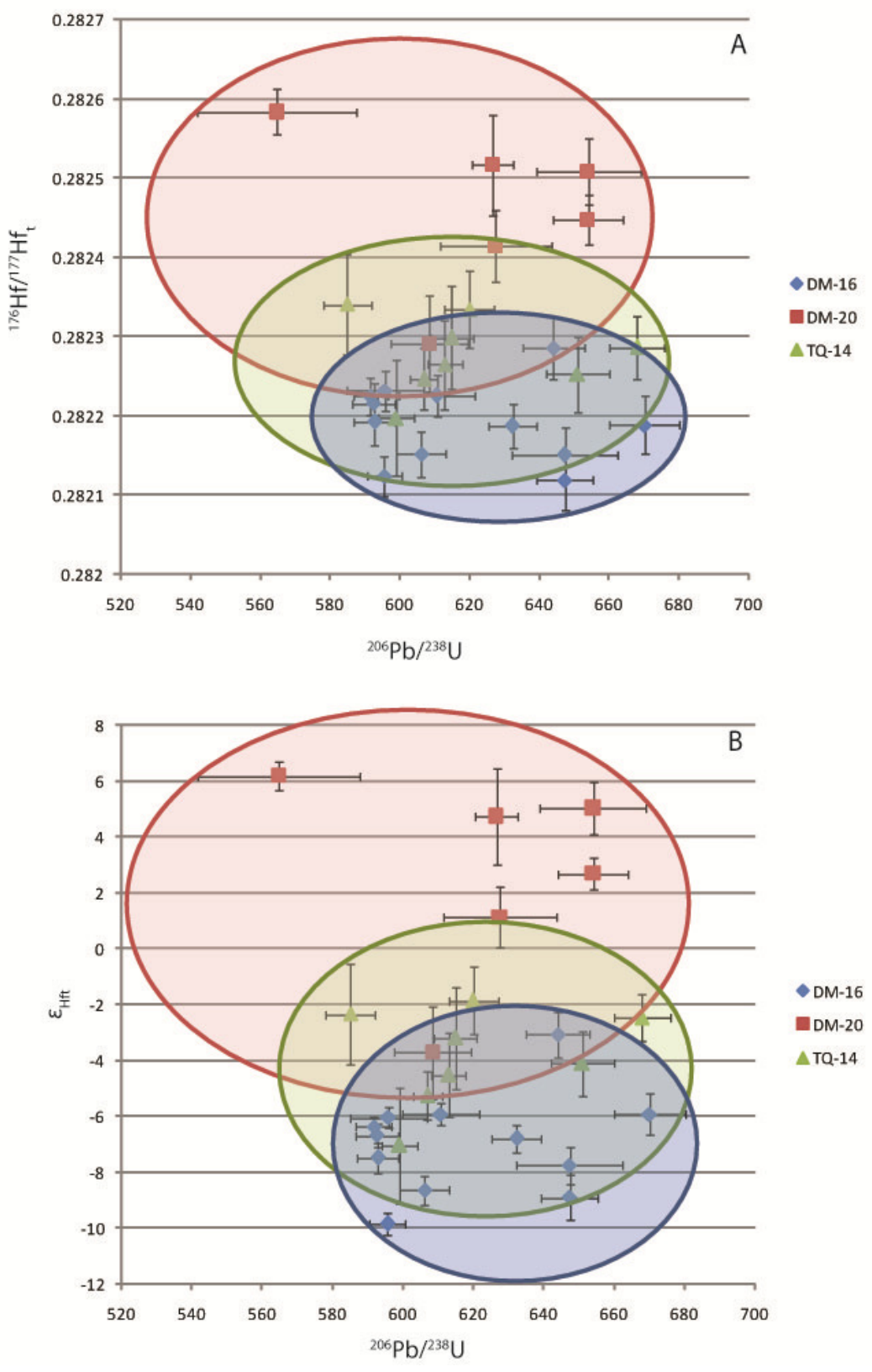

Figure 3.12 - Zircon i*n situ* Hf isotopic data (A, $^{176}Hf/^{177}Hf_t$; B, ε_{Hft}) versus U-Pb age plots.

As discussed in the previous section, there is a variation in the Hf isotopic signature of Damolândia and Taquaral zircon grains (Tables 3.2, 3.5 and 3.7). This behavior may be attributed to different degrees of interaction between mantle-derived melts and older crustal components, which is also corroborated by the Nd whole-rock data (Tables 3.3 and 3.10). However, neither the Hf isotopic ratios nor the $\varepsilon_{Hf}(t)$ can be linked to any specific zircon age domain. As shown in Figure 3.12, the Hf data scatter randomly along the $^{206}Pb/^{238}U$ axis, revealing no correlation with the large spread of concordant U-Pb ages, which suggests that the oscillation of Hf isotopic signature is related merely to crustal contamination and, therefore, all zircon crystals (within individual samples) were grown in a single geological episode.

As previously stated, since high-grade metamorphism does not disturb the Lu-Hf systematic in zircon grains, the Hf isotopic ratios should evidence primary, igneous conditions and, hence, the older ages, around 670 Ma, may be interpreted as representative of the emplacement of the Damolândia and Taquaral mafic-ultramafic complexes.

Furthermore, the Hf isotopic signature supports that, during metamorphism, in these complexes zircon ***re-equilibrated*** rather than ***re-grew***. This is also justified by the CL characteristics of the crystals, in which curved, inward-moving boundaries are frequent. The fact that all individuals reveal concordant ages and that there is no evidence of a radiation-damage effect in the analyzed grains suggests that crystals might have experienced a concomitant dissolution-reprecipitation process. In view of this, the observed chain of ages in the Concordia diagram probably corresponds to intermediate values between igneous crystallization and the final closure of the U-Pb isotopic system, following the high-grade metamorphism.

Nonetheless, it is still not possible to distinguish a clear peak metamorphic age for the studied rocks based only on zircon analyses. Further research on rutile and other metamorphic minerals is in progress and might help to elucidate this question in the future.

The geochronological framework here described is similar to that of the Napier Complex, Antarctica (Kelly & Harley, 2005) and, likewise, suggests that the studied rocks were kept in high temperatures for a long time. This unusually hot condition might be achieved in deep levels in the crust, where igneous crystallization and metamorphic overprint are concomitant. Moreover, it may promote the partial opening of the U-Pb system in zircon and, consequently, produce the large spread of ages observed in the AIC.

Comparison between dating methods

Another essential aspect when interpreting U-Pb data is the method used for dating. ID-TIMS ages are obtained from the dissolution of a randomly, optically selected grain and, occasionally, from more than one crystal. As stated in the previous section, zircon that undergoes re-equilibration during metamorphism might preserve a component of the original isotopic information. Therefore, the main issue remains on whether ID-TIMS ages of zircon crystals from metamorphic terranes have a geological meaning or are only a geochronological artifact enhanced by a memory effect. Moreover, obtaining the correct crystallization age might also depend on "luck" when picking the grains.

Such peculiarities may be shown in the sample INHO-01, in which U-Pb ID-TIMS analyses revealed a cluster of concordant to nearly concordant ages around 620 Ma, whereas only one fraction yielded a $^{206}Pb/^{238}U$ of 662 Ma (Table 3.11). The younger group of ages is analogous to other mafic-ultramafic complexes identified to the west of the AIC, in the domain of the Goiás Magmatic Arc (Laux *et al.*, 2004). Additionally, titanite grains of a wollastonite-scapolite marble that occurs nearby the Goianira-Trindade Complex rendered an age of 632 Ma (Moraes *et al.*, 2007).

Conversely, considering that re-equilibration of zircon grains during high-grade metamorphism was noteworthy in some of the mafic-ultramafic intrusions within the AIC and that the older value obtained in sample INHO-01 is similar to that interpreted as the crystallization age for both Damolândia and Taquaral rocks, it suggests an analogous geochronological framework for the three layered complexes.

However, it is not possible to confirm neither of the interpretations above based only in the available U-Pb ID-TIMS data and, therefore, this method has shown to be inadequate for dating high-grade metamorphic terranes such as the AIC.

In-situ dating methods such as SIMS and LA-ICPMS, for instance, have proven to be the more efficient technique in determining distinct geological events within one single grain, since it allows the analysis of all zircon domains, altered or not during metamorphism. Yet, the control of internal textures with CL or BSE imaging is a crucial condition for an accurate analysis and a correct interpretation of the ages obtained with these methods.

Tectonic implications for the evolution of the Brasília Belt

U-Pb zircon analyses of both Damolândia and Taquaral complexes revealed crystallization ages of ~ 670 Ma. Such values have been already reported in previous studies on the felsic high-grade rocks of the AIC (Piuzana *et al.*, 2003; Möller *et al.*, 2006). However, in such examples, older values were discarded as inheritance, rendering concordia ages of ca. 645 Ma, which are accepted as representative of the timing of high-grade metamorphism in the AIC (Piuzana *et al.*, 2003).

Nevertheless, Möller *et al.* (2006) also reported 680 Ma zircon cores in UHT paragranulites, which were interpreted as grown in a prograde path, in equilibrium with garnet. In addition, similar ages were obtained in rutile grains shielded in garnet, with Zr content that corresponds to peak temperatures (Möller *et al.*, 2006; Zack et.al., 2006). Therefore, the prograde metamorphism attested by the paragranulites suggests that the prograde-to-peak UHT stage in the AIC may have occurred around 680-670 Ma, earlier than previously suggested. If so, at least part of the widespread mafic magmatism is coeval with the high-grade metamorphic episode and most likely represents the additional heat source required to the development of the UHT assemblages.

The post-peak cooling age of the AIC is marked by the growth of euhedral individual zircon crystals in opx-bearing leucossome at ca. 630 Ma, as well as by the crystallization of titanite grains in wollastonite-scapolite marble (Möller *et al.*, 2006; Moraes *et al.*, 2007). Coeval to this stage are a number of mafic-ultramafic intrusions in the domain of the Goiás Magmatic Arc, with crystallization ages of ~630 Ma (Laux *et al.*, 2004).

Hence, there may have been two distinct episodes of mafic magmatism in the southern Brasília Belt; the older around 670 Ma and related to the development of the UHT assemblages and the latter, near 630 Ma, associated with the cooling history of the orogen.

The geological context here described, with voluminous mafic and felsic magmatism spatially and temporally associated with high-grade metamorphism, might correspond to extensional episodes within the collisional setting, during which the upwelling of the hot asthenosphere results in partial melting of both the mantle and continental crust generating extensive mafic and felsic magmatism.

3.7. Conclusions

Combined geological and new geochronological data on mafic rocks within the Anápolis-Itauçu Complex allow the following conclusions:

- The Damolândia and Taquaral intrusions correspond to layered mafic-ultramafic complexes, which partially preserve igneous textures, even with the pervasive, although heterogeneous, high-grade metamorphic overprint.
- Whole-rock Sm-Nd isotopic data attest the strongly contaminated signature of these mafic rocks, which indicates that they were emplaced into older continental crust.
- CL zircon images reveal internal textures typical of consumption, such as irregular, inward-moving boundaries, implying that these crystals were submitted to a varied degree of alteration during high-grade metamorphism.
- Hf-in-zircon analyses yield homogeneous isotopic ratios and ε_{Hf} values (within population) which cannot be linked to U-Pb ages, suggesting that the grains were crystallized in one single episode.
- In the studied rocks, during high-grade metamorphism zircon crystals have re-equilibrated rather than re-grew. Hence, the spread of ages between 670 and ~580 Ma illustrates that in such grains the U-Pb isotopic system was partially reset.
- From the statements above, it is concluded that the older ages, around 670 Ma, are representative of the igneous crystallization of the Damolândia and Taquaral complexes. Therefore, the studied rocks represent an older episode of mafic magmatism in the Brasília Belt than that recorded in the domain of the Goiás Magmatic Arc, to the west. However, the U-Pb data do not allow the discrimination of the peak metamorphic age.
- The mafic magmatism in the Brasília Belt is coeval to the prograde path of high-grade metamorphism and characterizes the additional heat source required for the development of UHT paragenesis in the paragranulites of the AIC.

3.8.Acknowledgments

Support from CNPq research grant (477347/2007-0) is thankfully acknowledged. M.M.P. and C.F.F.F. are CNPq research fellows. M.E.S.D.G. thanks CNPq fellowship. The authors are grateful to International Nickel Venture-INV and Amazônia Mineração for providing access to exploration data and support during field work. Horizonte Minerals and BCV Consultoria, which currently hold the mining rights for the Damolândia area, are also acknowledged. Sérgio Junges, Jeanne Grasyelle and Bárbara Lima are appreciated for providing laboratory assistance.

4. HIGH-GRADE METAMORPHIC ALTERATION OF ZIRCON: A COMBINED LA-ICPMS ISOTOPIC AND TRACE ELEMENT STUDY OF A COMPOSITE MAFIC-ULTRAMAFIC LAYERED COMPLEX IN CENTRAL BRAZIL

Maria Emilia Schutesky Della Giustina[1]*

Márcio Martins Pimentel[1a]

Cesar F. Ferreira Filho[1]

Reinhardt A. Fuck[1]

Sandra Andrade[2]

1 Universidade de Brasilia, Instituto de Geociências, 70910-900, Brasilia-DF-Brazil

*Corresponding author: maria_emilia@unb.br;

Phone: +55-61-3307-1113; Fax: +55-61-3272-4286

2 Universidade de São Paulo, Instituto de Geociências, Rua do Lago, 562, Cidade Universitária, 05508-900, São Paulo-SP-Brazil.

Abstract

Zircon recrystallization is a common process during high-grade metamorphism and promotes partial or complete resetting of the original isotopic and chemical characteristics of the mineral, which may lead to the misunderstanding of U-Pb isotopic/geochronological data. In Central Brazil, this may be illustrated by three composite mafic-ultramafic intrusions metamorphosed under amphibolite-to-granulite conditions. Their emplacement and metamorphism ages have been a matter of controversy for the last thirty years. The Serra da Malacacheta and Barro Alto complexes compose the southernmost of these layered bodies and four samples from distinct rock types were investigated in order to verify the consequences of metamorphic alteration of zircon for U-Pb dating. Cathodoluminescence imaging reveals internal features which are typical of concomitant dissolution-reprecipitation processes, such as convolute zoning and inward-moving recrystallization fronts, even in samples in which partially preserved igneous textures are observed. Due to this extensive alteration, LA-ICPMS U-Pb dating rendered inconclusive

[a] Present address: Universidade Federal do Rio Grande do Sul, Instituto de Geociências, 91501-970, Porto Alegre-RS-Brazil.

data. However, in situ Hf isotopic and trace-element analyses help clarifying the real meaning of the geochronological data. Low Lu/Hf (<0.004) and homogeneous $^{176}Hf/^{177}Hf_t$ values imply that the zircon populations within individual samples have crystallized in a single episode, despite the observed variations in age values. Trace element signature of zircon grains from garnet-bearing samples reveals that they were unreactive to the development of the peak metamorphism mineral assemblage and, thus, the main chemical feature in such grains is attributed to a coupled dissolution-reprecipitation process. However, in the Cafelândia amphibolite an additional alteration process is identified, probably related to the influx of late-stage fluids. Ti-in-zircon thermometer renders constant values at ca. 700°C which cannot be interpreted as representative of igneous or metamorphic conditions. Combined isotopic and geochemical investigation on zircon grains allowed the distinction of two magmatic events. The first corresponds to the crystallization of the Serra da Malacacheta Complex and characterizes a juvenile magmatism at ~1.3 Ga. The younger episode, recognized in the Barro Alto Complex, is dated at ca. 800 Ma and is represented by mafic and ultramafic rocks showing intense contamination with continental crust, implying that the emplacement took place, most likely, in a continental back-arc setting. Altered domains of zircon grains as well as titanite grains date the metamorphic event at ca. 760-750 Ma.

Key-words: Metamorphic zircon; LA-ICPMS; Hf isotopes; Ti-in-zircon; Serra da Malacacheta Complex; Barro Alto Complex

4.1.Introduction

High-grade metamorphism produces modifications in rocks in consequence of the adjustment to elevated pressure and temperature conditions. Despite the changes in mineral assemblage and rock structure, zircon was always believed to be a robust mineral, even in such severe conditions, owing to the high closure temperature of the U-Pb system. However, in the last decade, a number of studies have shown that zircon is not as resilient as previously thought (Schaltegger *et al.*, 1999; Ashwal *et al.*, 1999; Hoskin & Black, 2000; Bingen *et al.*, 2001; Möller *et al.*, 2003; Hoskin & Schaltegger, 2003; Harley *et al.*, 2007; Rubatto *et al.*, 2007; Geisler *et al.*, 2007; Martin *et al.*, 2008; among others). Cathodoluminescence imaging and in-situ isotopic and trace-element investigations, allied with the development of more accurate and precise analytical techniques, have revealed that zircon might be extensively recrystallized during high-grade metamorphism and that, during this process, primary characteristics, such as the U-Pb signature, are partially to totally obliterated. Consequently, U-Pb zircon ages of high-

grade rocks may not have geological meaning, leading to misinterpretation and controversy in the literature.

In Central Brazil, the age of three composite mafic-ultramafic complexes has been a matter of debate for the last 30 years. They constitute a ~300 km long NNE belt and are formed of two distinct igneous associations, metamorphosed under amphibolite to granulite facies conditions (Figure 4.1). Although robust geochronological data is available for the central composite intrusion (Niquelândia Complex; Pimentel *et al.*, 2004; 2006), U-Pb zircon ages ranging from 2.0 Ga to 0.8 Ga have been attributed to these magmatic systems, which resulted in controversial interpretation of their tectonic setting. In recent studies (Pimentel *et al.*, 2004; 2006; Ferreira Filho *et al.*, 2010) the intrusions are described as composite bodies formed by a Mesoproterozoic (ca. 1.26 Ga) intrusion and a Neoproterozoic (ca. 800 Ma) mafic-ultramafic layered association.

The present study focuses on the geochronology of the southernmost composite layered intrusion, comprising the Serra da Malacacheta and Barro Alto complexes (Figure 1). LA-ICPMS investigation of U-Pb and Hf isotopes and trace-element signature of zircon grains were carried out in order to evaluate the influence of high-grade metamorphism on the U-Pb systematic. The new data provide a background that helps to elucidate the geological framework of the Serra da Malacacheta and Barro Alto complexes. Additionally, this investigation contributes to a better understanding of zircon alteration processes in high-grade terranes.

4.2.Regional Geological Setting

The Brasília Belt is a Neoproterozoic orogen in central Brazil. Its evolution involved island arc accretion and continental collision between the São Francisco-Congo and the Paranapanema continent to the south, covered by the Paraná Basin (Figure 4.1; Pimentel et al., 2000; Valeriano et al., 2008). It is part of a global network of Neoproterozoic orogenic belts which resulted in the final amalgamation of Gondwana. It may be divided into four domains: (i) in the easternmost part is a thrust-and-fold belt consisting of various Neoproterozoic metasedimentary sequences formed along the western margin of the São Francisco Craton; (ii) in the central part of the belt is the metamorphic core, comprising high-grade rocks and, locally, ultra-high temperature granulites – the Anápolis-Itauçu Complex; (iii) the Goiás Magmatic Arc, which represents a juvenile terrane forming the westernmost part of the belt; and (iv) the Goiás

Massif, interpreted as a microcontinent/exotic terrane accreted to the orogen at the end of the Neoproterozoic (Brito Neves & Cordani, 1991; Pimentel & Fuck, 1992; Fuck *et al.*, 1994; Pimentel *et al.* 2000; Figure 4.1).

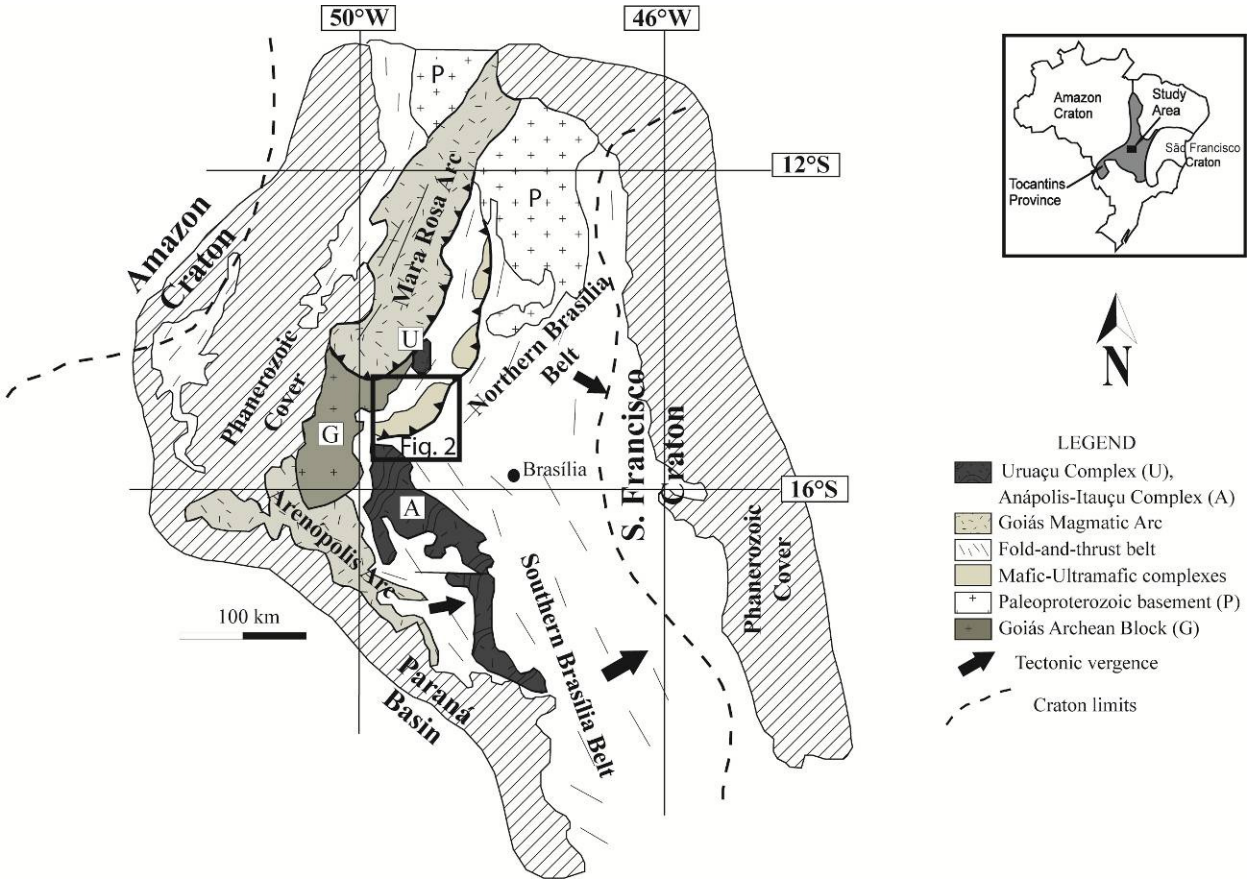

Figure 4.1 - Regional geotectonic setting of the Brasilia Belt, in the eastern part of the Tocantins Province (modified after Pimentel *et al.*, 2006; Giustina *et al.*, 2009).

Three composite Meso-Neoproterozoic layered complexes define the eastern boundary of the Goiás Massif (Figure 4.1). Due to their geological and geochronological similarities, they have been interpreted as representative of an originally single regional-scale structure, which was disrupted during the Brasiliano event forming three individual bodies (Wernick & Almeida, 1979; Danni *et al* 1982; Ferreira Filho, 1998). The three complexes consist of two magmatic systems, which are individualized owing to distinct petrological aspects and igneous crystallization ages (Danni *et al.*, 1982; Suita, 1996; Ferreira Filho *et al.*, 1994; Ferreira Filho & Pimentel, 2000).

The composite intrusions were formerly known as the Cana Brava, Niquelândia and Barro Alto complexes, from north to south, but their nomenclature was recently reviewed and

these terms are presently assigned only to the Neoproterozoic sections of the complexes (Ferreira Filho *et al.*, 2010; Figure 4.1). In addition, previous denominations for the Mesoproterozoic layered units, exposed in the southern and central intrusions, were revisited and, accordingly, they were re-named Serra da Malacacheta and Serra dos Borges complexes, respectively (Ferreira Filho *et al.*, 2010; Figure 4.1).

The Mesoproterozoic intrusions (~1.3 Ga) are composed of interlayered leucotroctolite, leucogabbro, anorthosite and occasional pyroxenite, whereas the Neoproterozoic complexes (~0.8 Ga) consist of several cyclic units of dunite, pyroxenite and gabbronorite, within which slices of supracrustal rocks and granite intrusions metamorphosed under high grade conditions are widespread. Trace element composition and Sm-Nd isotopic data reveal divergent geochemical signature for both units; in the older unit, analyses attest to a depleted-mantle source for the original magmas (Ferreira Filho & Pimentel, 2000; Moraes *et al.*, 2003), whereas the younger association shows a large degree of crustal contamination with older sialic crust (Suita, 1996; Pimentel *et al.*, 2004; 2006).

To the west, the three composite bodies are in contact with Mesoproterozoic bi-modal volcano-sedimentary sequences, namely the Palmeirópolis, Indaianópolis and Juscelândia sequences, from north to south. The sequences display similar stratigraphy and consist of metapelite, calc-silicate rocks and metachert interbedded with metavolcanic rocks, consisting of fine-to-medium grained amphibolite and felsic gneiss (Brod and Jost, 1991; Araújo, 1996; Moraes & Fuck, 1994, 1999; Ferreira Filho, 1998; Moraes *et al.*, 2003). Amphibolites of the Juscelândia and Palmeirópolis sequences show positive ε_{Nd} values and trace element signatures typical of MORB-like magmas, suggesting that the volcano-sedimentary sequences represent a continental rift that evolved towards an oceanic basin (Araújo, 1996; Moraes *et al.*, 2003, 2006).

The composite mafic-ultramafic complexes, together with their respective volcano-sedimentary sequences, underwent amphibolite to granulite facies metamorphism, with P and T conditions increasing progressively from west to east. Locally, ultrahigh-temperature mineral assemblages are observed (Moraes & Fuck, 1994, 2000; Ferreira Filho *et al.*, 1998). SHRIMP U-Pb zircon analyses performed on metamorphic overgrowths constrain the age of the high-grade metamorphism in the composite layered intrusions at approximately 760-750 Ma (Pimentel *et al.*, 2004; 2006; Moraes *et al.* 2006). Additionally, rutile U-Pb ages reveal a younger metamorphic event around 610 Ma, which is interpreted as related to the uplift of the complexes

at the end of the Brasiliano orogeny (Ferreira Filho *et al.*, 1994). The current structural configuration of the three composite layered complexes (Figure 4.1) is ascribed to this final tectono-metamorphic episode.

4.3. The Serra da Malacacheta and Barro Alto complexes

The Serra da Malacacheta (SMC) and the Barro Alto (BAC) complexes compose the southernmost and the largest of the three composite layered mafic-ultramafic intrusions (Figure 4.1). Resembling the shape of a boomerang, it may be subdivided in a southern segment, which shows a W-E structural trend, and a northern section, with NNE-SSW structures and original igneous layering (Figure 4.2).

The Serra da Malacacheta complex (SMC) comprises a Mesoproterozoic gabbro-anorthosite sequence heterogeneously metamorphosed under amphibolite-to-granulite facies (Fuck *et al.*, 1981). In the NNE-SSW segment, it consists of two different lithological successions (Figure 4.2). The meridional exposures comprise clinopyroxenite, gabbro, leucogabbro and anorthosite, whereas to the north of the city of Barro Alto, leucogabbro, olivine leucogabbro and leucotroctolite prevail (Figure 4.2). The crystallization sequence of the latter series, involving olivine+plagioclase, is distinct from the former, which includes clinopyroxene+plagioclase, and, thus, it characterizes a distinct layered body within the SMC (Ferreira Filho *et al.*, 2010). Additionally, partially preserved primary features, such as diopside oikocrysts and subophitic textures, are locally identified (Ferreira Filho *et al.*, 2010).

The SMC mafic-ultramafic rocks display LREE depleted patterns and low incompatible trace element contents (Suita, 1996) which, allied to a positive ε_{Nd} values, point toward a depleted mantle source for the original magmas.

U-Pb zircon ages obtained in a hornblende leucogabbro result in a discordia line with an upper intercept around 1.3 Ga, interpreted as representative of the igneous crystallization of the SMC (Suita *et al.*, 1994). The lower intercept (~0.77 Ga), on the other hand, reflects the timing of the metamorphic overprint. However, recent SHRIMP U-Pb zircon dating suggests Neoproterozoic crystallization ages for the amphibolite-facies meta-anorthosites of the SMC, with concordant to nearly concordant dates ranging from 799 to 726Ma (Correia *et al.*, 2007).

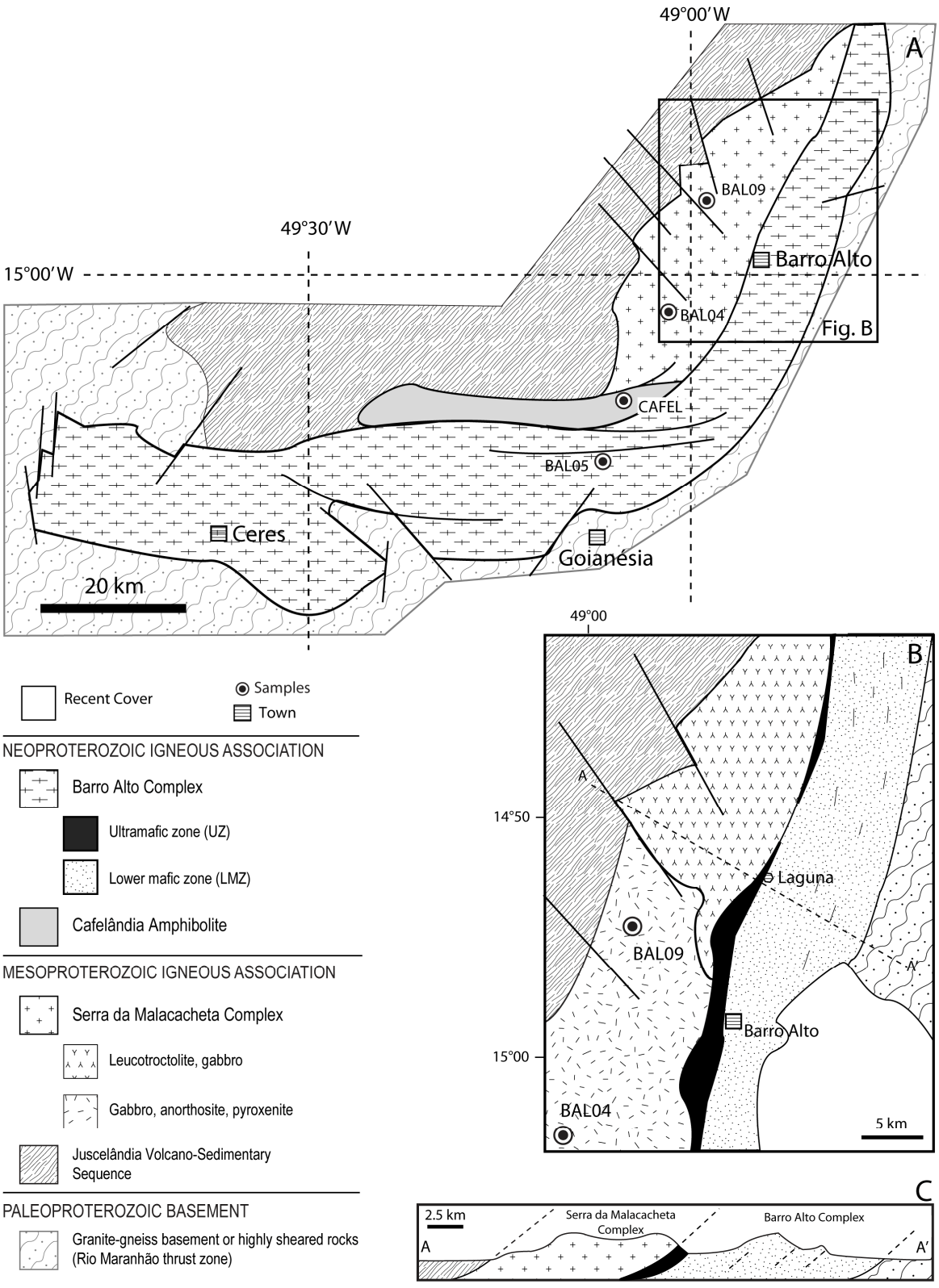

Figure 4.2 – A) Geological sketch map of the Barro Alto and Serra da Malacacheta complexes showing sample locations. Geological sketch map (B) and geological section (A-A'; C) of the NNE-section of the Barro Alto and Serra da Malacacheta complexes in the Laguna-Barro Alto region (modified after Ferreira Filho *et al.*, 2010).

In the W-E section of the SMC, intense deformation and high-grade metamorphism obliterated almost completely the original igneous characteristics. The main rock type of this segment is a medium-grained banded mafic plutonic rock, known as the Cafelândia amphibolite which, due to its depleted Nd isotopic signature (ε_{Nd} = +4.2, Moraes *et al.*, 2003), was formerly ascribed to the SMC. It is composed of hornblende and plagioclase, with variable amounts of quartz, clinopyroxene and garnet (Moraes & Fuck 1994). Typically metamorphic, granoblastic orthopyroxene grains are uncommon but, in conjunction with assemblages involving clinopyroxene+orthopyroxene+plagioclase±hornblende indicate that these rocks attained granulite facies conditions, calculated at ca. 870°C and 10.9 kbar (Moraes & Fuck 1994; Moraes *et al.*, 1994; Lima *et al.*, 2008). New U-Pb data reveal a Neoproterozoic crystallization age for the amphibolite protolith, as will be discussed below.

The Barro Alto Complex (BAC) represents the Neoproterozoic part of the southernmost composite layered intrusion and, similarly to the SMC, it is divided into two distinct segments. In the NNE-SSW section of the BAC, rocks were partially preserved from the tectono-metamorphic imprint. As a result, the original igneous stratigraphy is preserved and reveals a transitional contact between a lower mafic zone (LMZ), characterized by gabbronorite and minor pyroxenite and dunite, and an ultramafic zone (UZ), which comprises serpentinized dunite, harzburgite, pyroxenite and gabbronorite (Ferreira Filho *et al.*, 2010).

The southern segment is characterized by several parallel tectonic slices of mafic-ultramafic rocks following a W-E structural trend. The main rock type is a medium-grained diopside-hypersthene granulite, corresponding to norite and gabbronorite, with subordinate serpentinite derived from harzburgite, websterite and dunite (Fuck *et al.*, 1981; Danni *et al.*, 1984; Ferreira Filho, 1998). Quartz-dioritic granulites with abundant xenoliths of supracrustal rocks and enclaves of gabbronorites are widespread in this section and are interpreted as late-stage products derived by strong contamination with sialic country rocks (Fuck *et al.*, 1981; Danni *et al.*, 1984; Ferreira Filho, 1998; Ferreira Filho *et al.*, 2010). Additionaly, lenses of felsic aluminous granulites comprising both metagranitic rocks and supracrustal rocks are restricted to the W-E section (Fuck *et al.*, 1981; Moraes & Fuck, 2000) and, locally, these rocks present UHT parageneses that indicate peak metamorphic conditions around 980°C and 7.9 kbar (Moraes & Fuck, 2000).

Primary pyroxene composition and whole-rock trace element signature of mafic and ultramafic rocks of the BAC are analogous to similar rocks from the Niquelândia Complex and, likewise, reveal intense crustal contamination of the primitive parental magma (Suita, 1994; Oliveira, 1993; Ferreira Filho *et al.*, 2010).

U-Pb conventional (Suita *et al.*, 1994) and SHRIMP (Correia *et al.*, 1999) zircon data reveal lower intercept ages at ca. 790 Ma, which are interpreted as representative of the igneous crystallization of the BAC (Ferreira Filho *et al.*, 2010).

4.4.Methods

Zircon concentrates were extracted from ca. 10 kg rock samples using conventional gravimetric and magnetic techniques at the Geochronology Laboratory of the University of Brasília. Mineral fractions were hand-picked under a binocular microscope to obtain fractions of similar size, shape and color. For in situ U-Pb and Hf analyses, hand-picked zircon grains were mounted in epoxy blocks and polished to obtain a smooth surface. Before every micro-analytical procedure, mounts were cleaned with dilute (ca. 2%) HNO3. Cathodoluminescence images were obtained using a LEO-1430 electronic microscope at the UFPA working at 10 kV.

For U-Pb and Hf isotopic LA-ICPMS analyses, the samples were mounted in an especially adapted laser cell and loaded into a New Wave UP213 Nd:YAG laser (λ = 213 nm), linked to a Thermo Finnigan Neptune Multi-collector ICPMS. Helium was used as the carrier gas and mixed with argon before entering the ICP. The laser was run at a frequency of 10 Hz and energy of ~100 mJ/cm2 with a spot of 30μm for U-Pb systematic and 40μm for Hf isotopic analyses. The U-Pb and Hf LA-ICPMS analyses followed the analytical procedure described by Buhn *et al.* (2009) and Matteini *et al.* (2009), respectively, and were carried out at the Geochronology Laboratory of the University of Brasília.

For the U-Pb LA-ICPMS analyses two international zircon standards were used. Zircon standard GJ-1 (Jackson *et al.*, 2004) was used as the primary reference material in a standard-sample bracketing method, accounting for mass bias and drift correction. The resulting correction factor for each sample analysis considers the relative position of each analysis within the sequence of 4 samples bracketed by two standard and two blank analyses each (Albarède *et al.*, 2004). The Temora 2 standard (Black *et al.*, 2004) was run at the start and at the end of each analytical session, yielding accuracy around 2% and a precision in the range of 1% (1σ).

Uncertainties in sample analyses were propagated by quadratic addition of the external uncertainty observed for the standards to the reproducibility and within-run precision of each unknown analysis. Zircon grains with $^{206}Pb/^{204}Pb$ lower than 1000 were rejected. Plotting of U–Pb data was performed using ISOPLOT v.3 (Ludwig, 2003) and errors for isotopic ratios are presented at the 1σ level.

Hf isotopic measurements were carried out on zircon grains previously investigated by U-Pb systematics. The Hf spot analyses were located in the same CL domain of zircon. During *in situ* analytical session and every ca. 6 samples, GJ-1 zircon (Jackson *et al.*, 2004) was monitored as a reference material and rendered an average measured $^{176}Hf/^{177}Hf$ value of 0.281994±25 (n=11), in agreement with Zeh *et al.* (2007; 0.282003 +/- 15), Morel *et al.* (2008; 0.282000 +/- 05) and Xie *et al.* (2008; 0.282028±34). Mass-bias correction considered the signal of ^{171}Yb and ^{173}Yb and, additionally, these isotopes, as well as ^{175}Lu, were applied for the isobaric interference correction of Yb and Lu on the ^{176}Hf signal. The studied zircon grains show very low Lu/Hf values (<0.001), which indicates that the primary Hf isotopic composition is preserved and, consequently, no further correction is needed. Calculation of initial $^{176}Hf/^{177}Hf$, ε_{Hf} and T_{DM} model ages for each single spot analyses was based on the $^{206}Pb/^{238}U$ age, previously determined in the same grain. When both discordant and concordant zircon grains from the same sample revealed similar Lu-Hf isotopic signature, the upper intercept dates were used in the calculation of the Hf parameters when a concordia age could not be established. Errors for isotopic ratios are presented at the 2σ level.

Zircon trace element composition was obtained in the LA-ICPMS facility at the University of São Paulo. Time-resolved analyses were performed on an ELAN 6100 quadrupole ICPMS coupled to a NewWave Research UP213 Nd:YAG laser. Instrumental parameters and operation conditions are given in Table 4.1. Data were reduced using GEMOQ Glitter reduction software and element concentrations were referenced against the yield of the isotope 29Si, which was selected as the internal standard since SiO_2 is stoichometric in zircon with a concentration of 32.8%. NIST 612 standard glass was applied as external standard and considered the recommended values of Jochum *et al.* (2005) for calibration, rendering an accuracy of ca. 2%. The precision based in repeated measurements of the standard varies from 1.3 to 7.5% and the detection limits for heavy elements (amu >139) ranges from 0.02 to 0.22μg/g. For graphic

presentation, rare-earth elements were normalized with CI chondrite values of Sun & McDonough (1989).

Table 4.1 - Instrumental and analytical parameters for LA-ICPMS trace-element analyses.

Instrumental parameters		
ICPMS:	ELAN 6100DRC ICPMS	
RF Power		1300
Gas flow		
	Plasma	16 L/min
	Auxiliary	1 L/min
	Carrier (sample)	0.55 L/min
Laser:	NewWave Research UP213 Nd:YAG	
Wavelenght		213 nm
He gas flow		0.5 L/min
Spot size		30 μm
Repetition rate		15 Hz
Pulse Energy		aprox. 0.1 mJ
Laser warm-up		10s
Aquisition Conditions		
Data acquisition protocol		Time-resolved analyses in a fast peak-jumping mode
Integration Time		
	Background	60s
	Sample ablation	60s
Total aquisiton time		120 s
ThO+/Th+		<0.5%
Ce2+/Ce		<0.5%

Ti concentrations in zircon were obtained within the same analytical session and spot location of other trace elements. The temperatures were calculated using the Ti-in-zircon thermometer of Watson *et al.* (2006), considering the activities of SiO_2 and TiO_2 equal to unit since all the samples have Ti-rich phases (rutile or titanite) and quartz.

4.5. Samples and Results

Three selected samples representative of key units from the Serra da Malacacheta Complex and one from the Barro Alto Complex were investigated.

Leucogabbro BAL-09

Sample BAL-09 is a leucogabbro from the Serra da Malacacheta complex. Primary igneous textures, such as relict pyroxene crystals in a subophitic arrangement, are occasionally observed. Zircon crystals are pristine, colorless to pink, and show stubby habit with rounded terminations, which render oval morphologies to some grains. Generally, crystals are fragmented and their widths vary between 100 and 250 μm. Cathodoluminescence images of zircon grains reveal textures indicating metamorphic recrystallization. The most distinctive feature is the irregular sector/chaotic zoning that evolve to a featureless pattern, as well as lobate, inward-moving alteration fronts with smooth boundaries (Figure 4.3A, B). Low-luminescence cores are enclosed by brighter rims and some grains are even surrounded by an outer, porous and inclusion-rich rim (Figure 4.3A, B). Ghost zoning is also commonly observed.

Eighteen U-Pb spot analyses yield concordant to slightly discordant dates that reveal a poorly constrained discordia upper intercept around 1.3 Ga (Figure 4.4; Table 4.2). Five concordant grains yield a mean $^{206}Pb/^{238}U$ age of 1288 ± 14Ma (MSWD 0.33; Figure 4.4), which is interpreted as the best estimate of the igneous crystallization. Neither U-Pb ages nor Th/U ratios (0.28-0.62) evidence correlation with any specific CL domain (Table 4.2). Crystals comprise homogeneous HfO_2 contents (1.1 to 1.2%) and Lu-Hf isotopic analyses reveal a mean $^{176}Hf/^{177}Hf_t$ ratio of 0.282133 ± 20 (Table 4.3). $\varepsilon_{Hf(1288)}$ values are positive and range from 5.8 to 7.9 and two-stage hafnium model ages yield T_{DM} values between 1.62 and 1.50 Ga. Similarly to the U-Pb systematics, there is no difference in the Hf isotopic composition between the distinct CL domains.

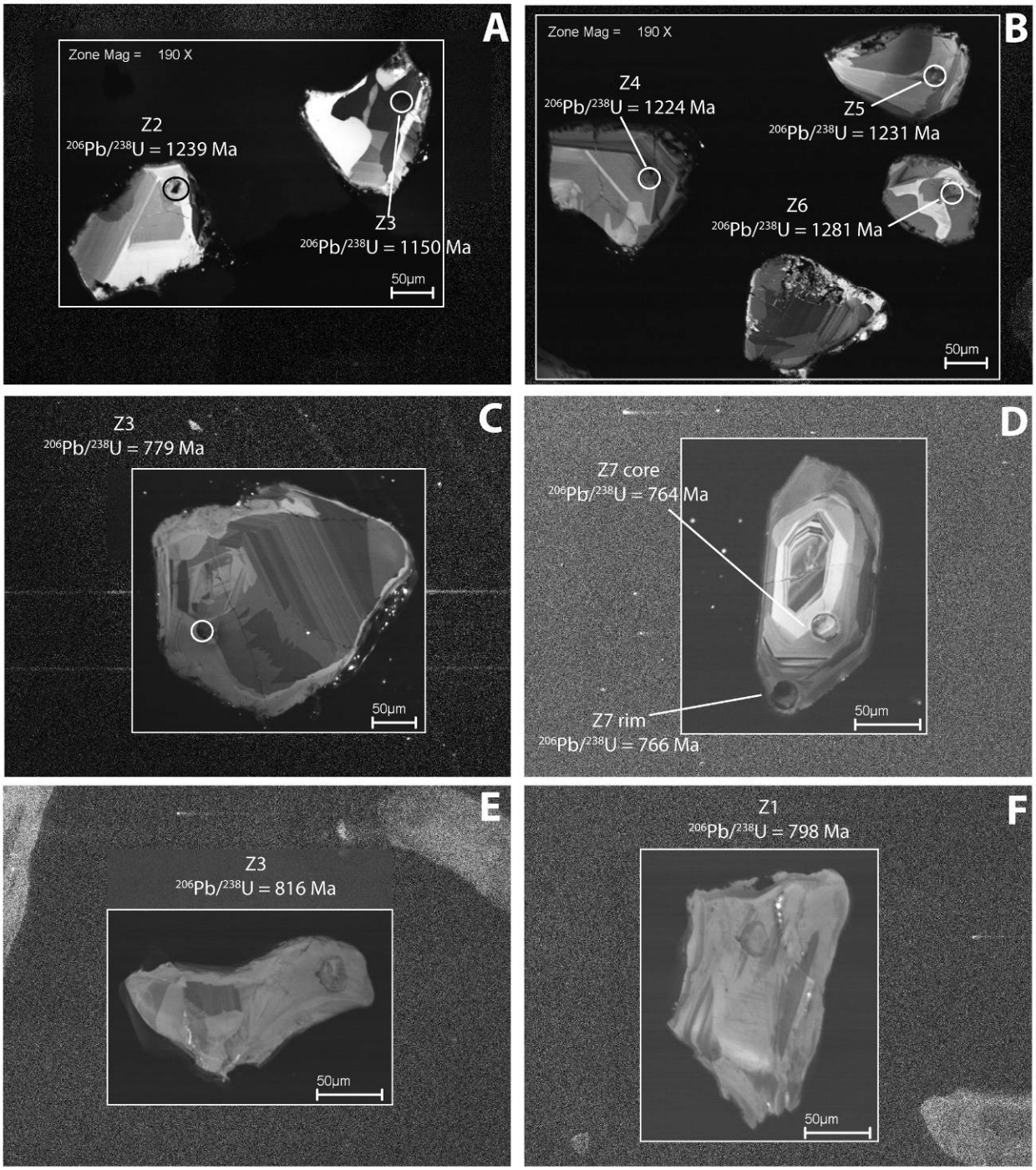

Figure 4.3 - CL images of zircon from the SMC and BAC. A, B) Sample BAL-09. (C-F) Sample CAFEL. G, H) Sample BAL-05. Smaller spots (30 µm) represent the location of U-Pb analyses, whereas larger spots (40 µm) correspond to Hf isotopic investigation.

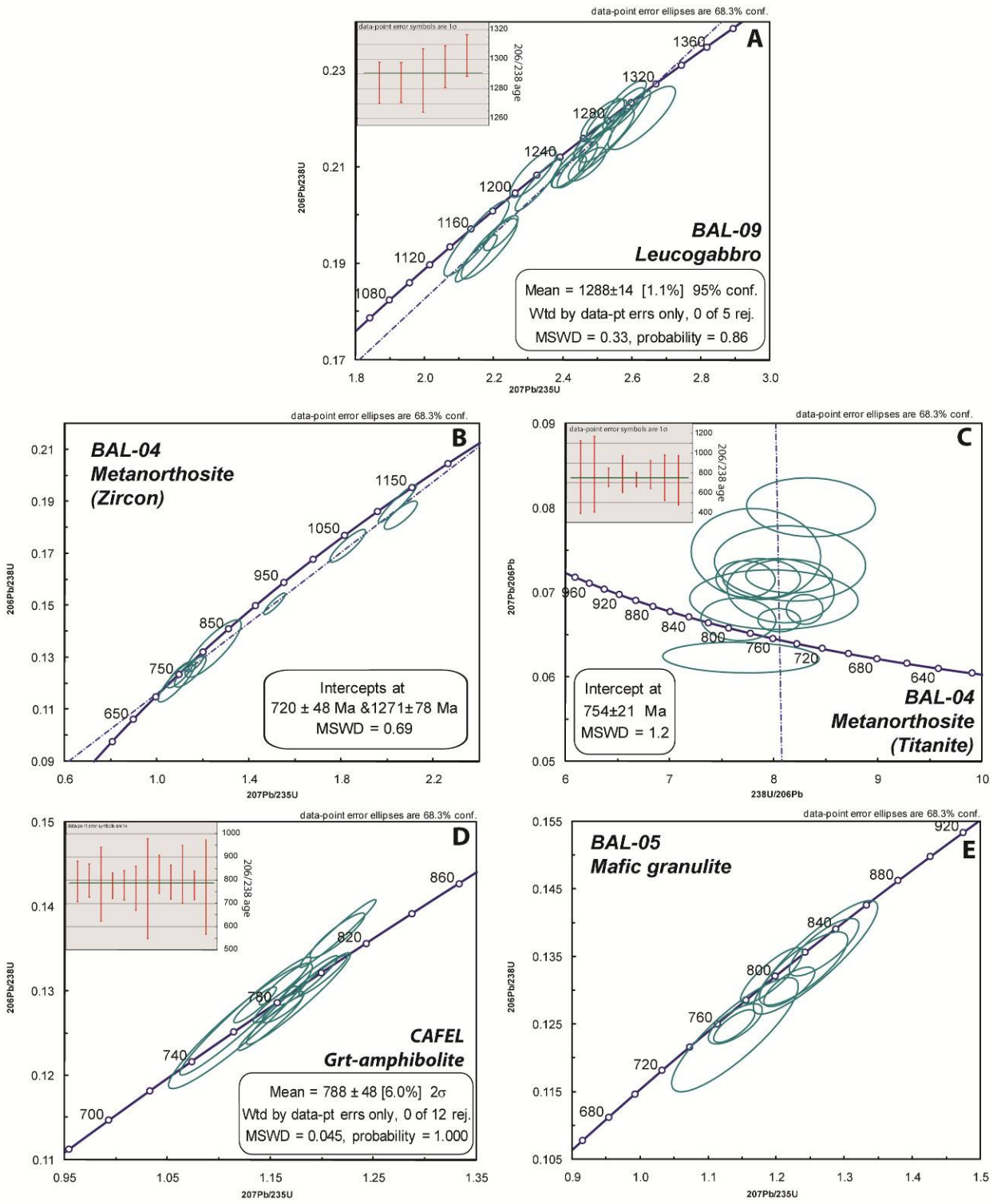

Figure 4.4 - LA-ICPMS U-Pb diagrams for sample BAL-09 (A); sample BAL-04 (zircon, B; titanite, C); sample CAFEL (D); sample BAL-05 (E).

Table 4.2- Pb LA-ICPMS data for sample BAL-09.

										Apparent ages (Ma)							
Sample	f(206)%	Th/U	6/4 ratio	7/6 ratio	1s (%)	7/5 ratio	1s (%)	6/8 ratio	1s (%)	7/6 Age	1σ	7/5 Age	1σ	6/8 age	1σ	Rho	Conc (%)
004-Z1	0.13	0.35	9354	0.08215	3.2	2.1868	2.5	0.19307	2.1	1249.0	62.2	1176.8	17.0	1138.0	22.1	0.87	91
005-Z2	0.27	0.39	6154	0.08431	2.9	2.4624	2.1	0.21181	1.9	1299.8	54.5	1261.1	15.3	1238.5	21.3	0.90	95
006-Z3	0.05	0.55	34258	0.07985	1.1	2.1493	2.9	0.19521	2.6	1193.4	22.3	1164.8	19.9	1149.5	27.8	0.91	96
009-Z4	0.14	0.51	11512	0.08391	0.9	2.4182	1.4	0.20900	1.1	1290.5	16.6	1248.0	9.8	1223.5	11.8	0.79	95
010-Z5	0.15	0.31	8928	0.08380	1.0	2.4323	1.8	0.21051	1.5	1288.0	20.1	1252.2	13.1	1231.5	16.9	0.83	96
011-Z6	0.20	0.47	8359	0.08296	1.1	2.5146	1.7	0.21984	1.3	1268.2	20.5	1276.3	12.1	1281.0	15.0	0.78	101
012-Z7	0.09	0.32	18881	0.08043	1.1	2.3132	1.9	0.20860	1.6	1207.5	21.2	1216.3	13.5	1221.3	17.5	0.83	101
017-Z8	0.14	0.33	11787	0.08502	1.0	2.4688	1.4	0.21061	1.1	1316.0	18.5	1262.9	10.4	1232.1	12.2	0.75	94
018-Z9	0.07	0.28	21554	0.08156	0.8	2.1487	1.8	0.19107	1.7	1235.0	14.9	1164.6	12.8	1127.2	17.4	0.92	91
019-Z10	0.14	0.50	12225	0.08198	0.8	2.2198	1.5	0.19639	1.2	1245.0	16.6	1187.3	10.4	1155.9	12.9	0.83	93
020-Z11	0.14	0.31	11748	0.08657	1.4	2.6279	2.4	0.22016	2.0	1351.0	27.7	1308.5	18.0	1282.7	23.1	0.82	95
023-Z12	0.10	0.53	16698	0.08330	0.9	2.5255	1.5	0.21988	1.2	1276.3	17.4	1279.4	11.2	1281.2	14.5	0.82	100
024-Z13	0.08	0.62	18124	0.08339	0.7	2.4790	1.3	0.21560	1.1	1278.5	12.8	1265.9	9.3	1258.6	12.6	0.88	98
025-Z14	0.12	0.37	14130	0.08368	0.9	2.5798	1.6	0.22360	1.3	1285.1	17.3	1294.9	11.4	1300.9	15.1	0.83	101
026-Z15	0.07	0.44	24346	0.08460	1.2	2.5258	2.1	0.21653	1.7	1306.5	23.9	1279.5	15.2	1263.5	19.4	0.84	97
029-Z16	0.10	0.34	17050	0.08187	0.8	2.3293	1.9	0.20634	1.7	1242.5	15.6	1221.3	13.6	1209.3	19.1	0.92	97
030-Z17	0.20	0.30	6968	0.08502	0.9	2.5490	2.7	0.21746	2.5	1315.9	18.2	1286.2	19.7	1268.4	29.1	0.94	96
031-Z18	0.09	0.47	18157	0.08415	0.9	2.5765	1.6	0.22206	1.3	1296.0	16.6	1294.0	11.3	1292.8	15.2	0.85	100

Table 4.3 - Summary of in situ Lu–Hf analyses for sample BAL-09.

Sample	176Lu/177Hf	2σ	176Hf/177Hf	2σ	Age (Ga)	(176Hf/177Hf)t	2σ	eHf(t)	1σ	T(DM) Ga
Z1	0.000542	0.000013	0.282125	0.000059	1.29	0.282112	0.000059	5.13	0.99	1.63
Z2	0.000537	0.000014	0.282151	0.000020	1.29	0.282137	0.000020	6.03	0.37	1.58
Z3	0.000910	0.000003	0.282139	0.000022	1.29	0.282116	0.000022	5.30	0.32	1.62
Z5	0.000437	0.000002	0.282136	0.000021	1.29	0.282125	0.000021	5.62	0.34	1.61
Z7	0.000622	0.000010	0.282186	0.000024	1.29	0.282171	0.000024	7.22	0.23	1.52
Z8	0.000379	0.000002	0.282156	0.000019	1.29	0.282147	0.000019	6.37	0.43	1.56
Z13	0.000784	0.000004	0.282147	0.000024	1.29	0.282128	0.000024	5.69	0.25	1.60

Table 4.4 - Trace element composition of zircon crystals from sample BAL-09.

Sample	BAL-09-Z1		BAL-09-Z2-a		BAL-09-Z2-b		BAL-09-Z3-a		BAL-09-Z5-a		BAL-09-Z13	
	µg/g	1σ (%)	µg/g	1σ (%)	µg/g	1σ (%)	µg/g	1σ (%)	µg/g	1σ (%)	µg/g	1σ (%)
P	129.60	19.4	133.62	14.7	112.92	15.2	105.47	16.7	152.38	16.5	113.92	17.2
Sc	191.21	6.2	210.57	5.3	210.20	5.4	183.64	5.6	218.07	5.8	202.60	6.0
Ti	8.29	26.7	9.63	12.3	7.33	14.1	3.89	25.2	9.75	13.2	10.16	13.2
Mn	0.77	28.6	<d.l.		<d.l.		<d.l.		<d.l.		<d.l.	
Sr	0.16	25.8	0.16	12.3	0.14	13.9	0.14	18.7	0.15	13.7	0.12	14.5
Y	439.79	9.0	475.65	7.9	475.44	8.0	367.10	8.3	501.94	8.6	382.20	8.8
Nb	10.28	10.3	11.16	8.6	11.40	8.7	8.90	9.2	11.32	9.3	10.95	9.5
Mo	10.57	15.1	11.30	11.4	11.75	11.6	8.98	12.9	12.38	12.2	12.02	12.4
Ba	<d.l.		0.06	46.4	<d.l.		0.10	49.5	<d.l.		<0.054	
La	0.052	40.4	0.015	35.4	0.004	69.0	0.017	47.4	<d.l.		0.007	41.5
Ce	2.13	10.8	1.54	7.8	1.33	8.3	2.52	8.3	1.85	8.1	1.17	8.5
Pr	0.025	64.0	0.016	29.6	<d.l.		0.013	56.9	<d.l.		0.007	45.5
Nd	0.310	51.6	0.107	38.3	0.084	41.7	0.159	45.9	0.17	30.4	0.209	27.3
Sm	0.37	45.9	0.54	16.4	0.41	19.2	0.62	22.6	0.55	16.4	0.62	15.5
Eu	0.15	39.7	0.18	15.9	0.11	20.6	0.16	25.2	0.20	15.9	0.11	19.3
Gd	3.87	18.1	5.20	9.8	5.91	10.0	4.90	12.4	5.92	10.5	4.77	10.9
Tb	1.85	11.4	1.97	7.6	2.26	7.5	1.90	8.9	2.22	8.1	1.81	8.3
Dy	28.03	10.2	30.95	8.3	32.93	8.4	26.99	9.0	33.71	9.1	26.00	9.3
Ho	10.64	8.5	13.24	7.0	13.22	7.1	11.60	7.5	14.52	7.6	11.15	7.8
Er	63.92	8.5	69.41	7.2	68.96	7.3	60.23	7.7	74.33	7.9	57.17	8.0
Tm	15.33	9.1	16.32	7.7	15.94	7.8	12.91	8.2	17.45	8.4	13.82	8.6
Yb	145.81	7.8	152.86	6.7	149.48	6.8	134.36	7.1	168.50	7.2	133.03	7.4
Lu	32.56	8.5	31.64	7.4	31.57	7.5	26.99	7.8	34.95	8.0	26.53	8.2
Hf	9463	10.1	10417	8.8	10065	8.9	9268	9.2	10088	9.6	9294	9.8
Ta	0.22	26.3	0.18	13.1	0.16	14.1	0.21	18.0	0.27	11.9	0.11	15.7
Pb	7.6	8.7	3.9	7.0	4.3	7.2	9.3	7.5	6.6	7.4	4.9	7.7
Th	67.59	8.0	36.65	7.0	41.88	7.1	79.46	7.3	57.60	7.6	40.84	7.7
U	103.49	9.4	45.95	8.3	49.44	8.4	102.21	8.6	72.34	9.0	56.09	9.1
Nb/Ta	46		61		70		42		42		101	
HfO_2	1.11		1.23		1.18		1.09		1.19		1.09	

Cont. Table 4.4 - Trace element composition of zircon crystals from sample BAL-09.

Sample	BAL-09-Z1		BAL-09-Z2-a		BAL-09-Z2-b		BAL-09-Z3-a		BAL-09-Z5-a		BAL-09-Z13	
	µg/g	1σ (%)	µg/g	1σ (%)	µg/g	1σ (%)	µg/g	1σ (%)	µg/g	1σ (%)	µg/g	1σ (%)
ΣREE	305		324		322		283		354		276	
Ce/Ce*	14		24		>59.59		41		>43.62		44	
Eu/Eu*	0.39		0.32		0.21		0.28		0.34		0.19	
$(Sm/La)_N$	11		57		150		56		>80.23		148	
$(Yb/Gd)_N$	46		36		31		33		34		34	
Ti-in-zircon Temperature (°C)	729		742		718		664		744		747	

Table 4.5 - U-Pb LA-ICPMS data for sample BAL-04.

										Apparent ages (Ma)							
Sample	f(206)%	Th/U	6/4 ratio	7/6 ratio	1s (%)	7/5 ratio	1s (%)	6/8 ratio	1s (%)	7/6 age	1σ	7/5 age	1σ	6/8 age	1σ	Rho	Conc (%)
Zircon																	
004-Z1	0.18	0.17	8202	0.08072	3.0	2.0565	2.3	0.18478	1.9	1214.7	57.9	1134.5	15.7	1093.0	19.1	0.83	90
005-Z2	0.30	0.17	5666	0.07658	3.7	1.8259	2.8	0.17292	2.4	1110.3	72.6	1054.8	18.2	1028.2	23.3	0.88	93
006-Z3	0.35	0.29	4948	0.06524	2.5	1.0868	5.0	0.12082	4.3	782.2	52.1	747.0	26.2	735.3	29.8	0.87	94
009-Z4	0.33	0.17	5084	0.07830	0.9	2.0421	2.7	0.18915	2.5	1154.5	18.3	1129.6	18.4	1116.8	26.0	0.95	97
010-Z5	1.25	0.25	1255	0.06758	3.4	1.2439	6.4	0.13349	5.5	855.9	71.4	820.7	36.3	807.7	41.4	0.85	94
011-Z6	0.70	0.23	2484	0.06465	1.8	1.0986	3.2	0.12325	2.7	762.9	38.5	752.7	17.2	749.2	19.0	0.83	98
028-Z17	0.13	0.18	11967	0.07271	0.9	1.5105	2.0	0.15066	1.8	1006.0	18.5	934.6	12.5	904.7	15.5	0.90	90
029-Z18	0.15	0.17	11910	0.06638	1.0	1.1673	2.0	0.12754	1.7	818.3	20.9	785.4	10.7	773.8	12.3	0.87	95
033-Z20	0.65	0.21	2711	0.06657	2.3	1.1438	3.9	0.12462	3.1	824.3	47.9	774.3	21.1	757.1	22.4	0.81	92
Titanite																	
012-T7	0.79	1.61	2217	0.06916	10.1	1.1920	7.6	0.12500	6.7	903.6	196.3	796.9	41.2	759.3	48.0	0.89	84
015-T8	1.39	2.14	1256	0.06232	9.5	1.1181	6.9	0.13013	6.4	685.0	190.5	762.1	36.2	788.6	48.3	0.96	115
016-T9	0.46	1.56	3805	0.06671	2.8	1.1430	2.2	0.12426	1.7	828.9	56.6	773.9	11.8	755.0	12.1	0.79	91
017-T10	1.01	2.50	1732	0.06684	5.2	1.2034	4.1	0.13059	3.1	832.7	103.9	802.2	22.4	791.2	23.4	0.80	95
022-T13	0.04	1.15	241403	0.06803	1.7	1.1307	2.2	0.12054	1.4	869.5	35.1	768.1	11.9	733.7	9.8	0.64	84
023-T14	0.72	1.97	2438	0.07158	4.0	1.2774	3.2	0.12943	2.4	974.0	80.3	835.7	18.2	784.6	18.1	0.78	81
024-T15	0.53	1.68	3270	0.07025	7.1	1.2009	5.7	0.12397	4.2	935.7	139.8	801.0	31.3	753.4	30.1	0.78	81
027-T16	1.03	1.59	1694	0.08008	7.6	1.3210	5.8	0.11964	4.9	1198.9	143.2	854.9	33.0	728.5	33.9	0.87	61
030-T19	0.95	1.58	1831	0.07454	9.0	1.3130	7.3	0.12775	5.2	1056.1	171.3	851.4	41.1	775.0	38.4	0.76	73
034-T21	0.91	2.71	1533	0.07169	5.0	1.2541	3.9	0.12687	3.1	977.3	98.7	825.3	21.7	770.0	22.9	0.83	79
035-T22	0.93	1.29	1888	0.07194	5.2	1.2177	3.9	0.12276	3.4	984.2	102.2	808.7	21.6	746.4	23.9	0.88	76
036-T23	1.10	1.24	1587	0.07345	9.4	1.2418	7.3	0.12262	5.9	1026.4	180.1	819.7	40.4	745.6	41.8	0.83	73

Table 4.6 - Summary of in situ Lu–Hf analyses for sample BAL-04.

Sample	176Lu/177Hf	2σ	176Hf/177Hf	2σ	Age (Ga)	(176Hf/177Hf)t	2σ	eHf(t)	1σ	T(DM) Ga
Z3	0.0005667	0.000002	0.282189	0.000017	1.27	0.282175	0.000017	7.00	0.49	1.52
Z4	0.0007465	0.000001	0.282259	0.000014	1.27	0.282240	0.000014	9.30	0.57	1.39
Z5	0.0002716	0.000003	0.282263	0.000022	1.27	0.282256	0.000022	9.88	0.29	1.36
Z6	0.0002490	0.000001	0.282261	0.000016	1.27	0.282255	0.000016	9.84	0.51	1.36
Z17	0.0005524	0.000003	0.282218	0.000017	1.27	0.282204	0.000017	8.02	0.48	1.46
Z18	0.0005330	0.000003	0.282240	0.000013	1.27	0.282227	0.000013	8.83	0.62	1.41

Table 4.7 - Trace element composition of zircon crystals from sample BAL-04.

Sample	Bal-04-1-Z4		Bal-04-2-Z3		BAL-04-a-Z4		BAL-04-a-Z4b		Bal-04-8-Z5		Bal-04-7-Z6		Bal-04-5-Z17	
	µg/g	1σ (%)	µg/g	1σ (%)	µg/g	1σ (%)	µg/g	1σ (%)	µg/g	1σ (%)	µg/g	1σ (%)	µg/g	1σ (%)
P	225.88	22.2	256.06	22.5	252.92	14.0	249.96	14.2	206.52	24.4	95.83	24.5	187.65	23.3
Sc	243.81	10.1	246.28	10.4	170.16	5.2	176.99	5.3	291.82	11.8	271.44	11.5	287.11	10.9
Ti	1.88	35.1	7.78	21.3	4.04	19.1	2.27	25.6	11.26	22.0	5.93	23.9	8.34	21.9
Mn	<d.l.		<d.l.		<0.200		<0.201		<d.l.		<d.l.		<d.l.	
Sr	0.34	12.7	0.29	11.6	0.42	10.3	0.53	9.5	0.22	13.0	0.21	13.6	0.30	11.3
Y	1188.61	12.0	870.66	12.3	766.99	7.8	1074.50	7.9	785.92	13.9	343.04	13.6	799.90	12.9
Nb	23.95	5.5	22.13	5.6	14.88	8.5	14.65	8.5	20.93	6.1	21.84	6.0	25.76	5.8
Mo	20.25	7.2	18.62	7.4	11.70	11.5	11.95	11.3	20.93	7.9	22.03	7.8	22.95	7.5
Ba	<d.l.		<d.l.		0.12	34.1	0.24	20.5	<d.l.		<d.l.		<d.l.	
La	<d.l.		0.013	49.2	0.088	15.9	0.050	18.8	0.020	30.0	0.030	26.1	0.008	48.8
Ce	8.26	4.6	3.93	5.1	16.29	7.1	9.55	7.2	1.57	6.0	9.55	4.9	5.24	5.0
Pr	<d.l.		<d.l.		0.03	26.3	0.01	57.1	0.02	31.4	0.06	19.7	0.02	34.7
Nd	0.31	29.8	0.28	27.0	0.70	17.1	0.34	23.0	0.74	20.3	0.79	19.0	0.38	24.1
Sm	1.36	14.0	0.86	16.3	1.17	13.7	1.19	12.6	1.56	14.7	1.24	15.3	0.83	16.9
Eu	0.16	23.6	0.33	13.0	0.29	14.4	0.18	16.6	0.32	13.7	0.58	11.1	0.14	18.2
Gd	13.46	17.1	10.02	17.7	7.88	9.5	10.03	9.2	11.91	19.9	7.28	19.8	7.47	18.7
Tb	5.30	10.4	3.97	10.8	3.24	7.4	4.56	7.2	4.60	12.2	1.98	12.1	3.42	11.4
Dy	93.29	14.1	60.05	14.6	51.62	8.1	75.14	8.1	69.34	16.6	25.90	16.2	47.42	15.4
Ho	40.19	13.2	27.58	13.5	23.13	6.8	33.84	6.9	25.25	15.3	9.36	15.0	23.68	14.2

Cont. Table 4.7 - Trace element composition of zircon crystals from sample BAL-04.

Sample	Bal-04-1-Z4		Bal-04-2-Z3		BAL-04-a-Z4		BAL-04-a-Z4b		Bal-04-8-Z5		Bal-04-7-Z6		Bal-04-5-Z17	
	µg/g	1σ (%)	µg/g	1σ (%)	µg/g	1σ (%)	µg/g	1σ (%)	µg/g	1σ (%)	µg/g	1σ (%)	µg/g	1σ (%)
Er	205.00	11.3	142.73	11.6	131.13	7.1	180.25	7.1	125.00	13.1	47.34	12.8	136.34	12.2
Tm	49.35	11.4	35.02	11.7	31.80	7.5	44.24	7.6	26.98	13.3	12.22	13.0	31.46	12.3
Yb	467.66	12.9	347.06	13.3	326.12	6.5	441.47	6.6	249.85	15.0	123.72	14.6	328.28	13.9
Lu	103.27	13.7	70.91	14.1	70.54	7.2	90.72	7.3	52.72	16.0	28.35	15.6	73.22	14.8
Hf	15745	15.4	15359	15.8	12685	8.6	13008	8.7	13788	17.9	20241	17.5	19366	16.6
Ta	3.53	8.5	1.23	9.8	1.79	7.8	1.92	7.8	1.33	10.5	1.21	9.9	2.77	9.0
Pb	3.92	6.4	2.58	7.0	7.38	6.9	5.34	6.9	1.11	8.3	2.85	7.4	3.37	6.8
Th	64.45	9.0	41.51	9.3	97.81	6.8	72.75	6.9	16.04	10.4	55.79	10.1	51.86	9.7
U	111.67	6.3	56.33	6.44	126.50	8.13	134.64	8.18	22.31	7.1	57.77	6.9	113.28	6.7
Nb/Ta	7		18		8		8		16		18		9	
HfO_2	1.85		1.81		1.49		1.53		1.62		2.38		2.28	
ΣREE	988		703		664		892		570		268		658	
Ce/Ce*	>55.35		>62.51		73.2		106.2		19.5		54.5		115.8	
Eu/Eu*	0.12		0.34		0.29		0.15		0.22		0.59		0.17	
$(Sm/La)_N$	>63.26		100.9		20.6		37.2		119.0		63.4		156.8	
$(Yb/Gd)_N$	42		42		50		53		25		21		53	
Ti-in-zircon Temperature (°C)	610		723		667		623		757		699		729	

Table 4.8 - U-Pb LA-ICPMS data for sample CAFEL.

Sample	f(206)%	6/4 ratio	7/6 ratio	1s (%)	7/5 ratio	1s (%)	6/8 ratio	1s (%)	Apparent Ages (Ma) 7/6 age	1σ	7/5 age	1σ	6/8 age	1σ	Rho	Conc (%)
004-z1	0.04	64529	0.06556	0.6	1.1868	1.6	0.13130	1.5	792.3	12.4	794.5	8.7	795.3	11.0	0.94	100
005-z2	0.04	39425	0.06604	0.5	1.2007	1.3	0.13186	1.2	807.6	10.8	800.9	7.2	798.5	9.0	0.94	99
006-z3	0.02	76598	0.06612	0.7	1.1770	2.8	0.12911	2.8	810.1	15.1	789.9	15.6	782.8	20.3	0.96	97
012-z5	0.04	44120	0.06580	0.6	1.1620	1.2	0.12808	1.0	799.9	13.2	782.9	6.3	776.9	7.1	0.86	97
013-z6	0.07	30628	0.06521	0.6	1.1548	1.2	0.12843	1.1	781.2	12.1	779.5	6.8	778.9	8.1	0.91	100
014-z7-R	0.04	48526	0.06609	0.6	1.1499	1.8	0.12619	1.7	809.2	12.3	777.2	9.8	766.1	12.3	0.96	95
015-z7-C	0.13	13330	0.06456	1.3	1.1205	4.1	0.12588	3.9	760.0	27.9	763.2	22.1	764.3	28.1	0.94	101
019-z8	0.06	27227	0.06453	0.7	1.2150	1.4	0.13656	1.3	759.0	14.0	807.5	8.0	825.2	9.9	0.91	109
020-Z9-R	0.04	46684	0.06445	0.5	1.1628	1.4	0.13085	1.2	756.5	11.3	783.3	7.4	792.7	9.3	0.94	105
026-z12	0.04	41700	0.06443	0.6	1.2153	2.0	0.13679	1.9	755.9	11.6	807.6	11.2	826.5	15.0	0.97	109
027-z13	0.05	34044	0.06413	0.5	1.1350	1.2	0.12835	1.1	746.0	11.4	770.1	6.5	778.5	7.9	0.92	104
028-z14	0.05	33773	0.06424	0.9	1.1253	3.7	0.12705	3.6	749.5	19.5	765.5	20.0	771.0	26.3	0.97	103

Table 4.9 - Summary of in situ Lu–Hf analyses for sample CAFEL.

Sample	176Lu/177Hf	2σ	176Hf/177Hf	2σ	Age (Ma)	(176Hf/177Hf)t	2σ	eHf(t)	1σ	T(DM) Ga
Z13	0.0002882	0.000002	0.282450	0.000024	779	0.282446	0.000024	5.61	0.20	1.22
Z14	0.0002988	0.000005	0.282472	0.000022	771	0.282467	0.000022	6.19	0.12	1.18
Z1	0.0003113	0.000003	0.282411	0.000017	795	0.282406	0.000017	4.55	0.05	1.29
Z7	0.0003733	0.000005	0.282462	0.000022	766	0.282456	0.000022	5.69	0.15	1.21
Z8	0.0002626	0.000002	0.282418	0.000063	825	0.282413	0.000063	5.49	1.53	1.26
Z9	0.0002100	0.000003	0.282434	0.000027	793	0.282431	0.000027	5.39	0.30	1.25
Z2	0.0004084	0.000006	0.282449	0.000036	799	0.282442	0.000036	5.93	0.61	1.22
Z12	0.0002590	0.000002	0.282414	0.000024	826	0.282410	0.000024	5.37	0.15	1.27

Table 4.10 - Trace element composition of zircon crystals from sample CAFEL.

Sample	CAFEL-Z14-a		CAFEL-Z2-a		CAFEL-Z2-b		CAFEL-I-117		CAFEL-I-105-a		CAFEL-I-105-b		CAFEL-I-121	
Zircon Domain	Core		Core		Rim		Core		Core		Rim		Rim	
	µg/g	1σ (%)	µg/g	1σ (%)	µg/g	1σ (%)	µg/g	1σ (%)	µg/g	1σ (%)	µg/g	1σ (%)	µg/g	1σ (%)
P	76.24	19.3	59.89	22.2	76.19	22.3	76.61	22.9	45.81	24.8	68.06	24.3	73.14	25.0
Sc	224.87	6.4	219.16	7.0	196.13	7.2	209.22	7.3	207.28	7.5	178.97	7.7	205.62	7.9
Ti	4.53	18.1	4.86	19.8	5.29	18.0	6.02	17.6	5.82	17.5	7.33	16.8	4.78	19.9
Mn	<d.l.		<d.l.		<d.l.		<d.l.		<d.l.		0.23	43.5	2.95	10.5
Sr	0.16	13.6	0.12	16.0	0.09	17.0	0.12	16.0	0.13	15.1	0.09	17.8	0.11	16.7
Y	435.7	9.4	312.26	10.3	170.65	10.5	389.98	10.7	242.12	10.9	106.45	11.2	181.94	11.4
Nb	11.43	10.1	10.94	11.1	11.23	11.3	11.53	11.5	10.16	11.7	10.25	12.0	11.21	12.2
Mo	13.02	13.1	13.03	14.2	11.95	14.5	12.22	14.7	11.58	15.0	10.9	15.3	11.18	15.7
Ba	<d.l.		0.0088	100.0	<d.l.		<d.l.		0.076	35.5	<d.l.		0.086	32.6
La	<d.l.		<d.l.		0.013	43.5	<d.l.		0.133	15.0	0.034	22.7	0.063	19.0
Ce	1.91	8.9	1.16	9.5	1.11	9.9	1.6	10.0	1.72	9.9	1.01	10.9	1.25	10.4
Pr	0.0154	39.0	0.0124	54.8	0.0088	48.9	0.0178	33.7	0.121	14.9	0.0218	31.2	0.0239	28.5
Nd	0.198	30.3	0.242	28.5	0.143	37.8	0.245	25.7	0.92	17.4	0.292	25.0	0.225	27.6
Sm	0.72	15.3	0.65	16.9	0.253	24.1	0.56	17.9	0.81	16.0	0.185	27.6	0.304	23.7
Eu	0.435	13.3	0.258	15.9	0.173	17.9	0.409	14.4	0.538	13.9	0.181	17.7	0.232	17.7
Gd	5.23	11.5	3.68	13.0	1.88	14.9	5.18	12.9	3.16	13.9	1.12	17.0	2.22	15.3
Tb	2.3	8.7	1.36	9.6	0.69	10.7	1.87	10.2	1.07	10.3	0.406	11.8	0.816	11.3
Dy	30.96	10.0	21.27	11.0	10.72	11.5	27.75	11.5	14.79	11.8	6.75	12.3	11.57	12.4
Ho	12.56	8.3	9.39	9.1	4.45	9.4	11.51	9.5	6.62	9.7	2.72	10.3	4.7	10.2
Er	65.31	8.6	50.84	9.4	24.21	9.7	58.63	9.8	36.81	10.1	15.09	10.4	26.32	10.6
Tm	16.2	9.2	13.55	10.1	6.57	10.4	14.58	10.6	9.91	10.8	4.2	11.2	6.77	11.4
Yb	172.07	7.8	148.95	8.6	76.18	8.8	152.46	8.9	115.5	9.1	45.41	9.4	77.77	9.6
Lu	35.74	8.7	34.29	9.6	16.35	9.8	31.61	10.0	29.19	10.2	10.17	10.5	16.84	10.7
Hf	9995.02	10.5	9900.24	11.6	9405.41	11.9	9746.67	12.2	8930.63	12.4	9708.38	12.7	9869.58	13.0
Ta	0.519	10.6	0.249	13.3	0.328	12.5	0.416	12.0	0.118	16.1	0.282	13.1	0.431	12.5
Pb	13.13	7.9	4.35	8.7	4.49	8.9	11.5	8.9	2.64	9.5	2.67	9.7	4.94	9.5
Th	178.67	8.2	59.93	9.0	62.88	9.2	159.72	9.3	34.76	9.6	35.22	9.8	69.39	10.0
U	345.22	9.7	147.03	10.6	199.99	10.8	314.36	11.1	78.22	11.3	126.35	11.5	211.21	11.8
Nb/Ta	22		44		34		28		86		36		26	
HfO_2	1.18		1.16		1.11		1.15		1.05		1.14		1.16	
ΣREE	344		286		143		306		221		88		149	

Cont. Table 4.10 - Trace element composition of zircon crystals from sample CAFEL.

Sample	CAFEL-Z14-a		CAFEL-Z2-a		CAFEL-Z2-b		CAFEL-I-117		CAFEL-I-105-a		CAFEL-I-105-b		CAFEL-I-121	
Zircon Domain	Core		Core		Rim		Core		Core		Rim		Rim	
	µg/g	1σ (%)	µg/g	1σ (%)	µg/g	1σ (%)	µg/g	1σ (%)	µg/g	1σ (%)	µg/g	1σ (%)	µg/g	1σ (%)
Ce/Ce*	>46.17		>27.45		25.35		>36.08		3.32		9.06		7.90	
Eu/Eu*	0.7		0.5		0.8		0.7		1.0		1.2		0.9	
(Sm/La)N	>166.96		>116.27		29.92		>130.64		9.43		8.35		7.47	
(Sm/Nd)N	11.1		8.2		5.4		7.0		2.7		1.9		4.1	
(Yb/Gd)N	40.0		49.0		49.0		35.6		44.2		49.0		42.3	
Ti-in-zircon Temperature (°C)	677.00		682		689		700		697		718		681	

Table 4.11 - U-Pb LA-ICPMS data for sample BAL-05.

Sample	f (206)%	Th/U	6/4 ratio	7/6 ratio	1s (%)	7/5 ratio	1s (%)	6/8 ratio	1s (%)	Apparent Ages						Rho	Conc (%)
										7/6 age	1σ	7/5 age	1σ	6/8 age	1σ		
004-Z1	0.14	0.18	11862	0.06760	1.1	1.2279	1.9	0.13174	1.5	856.3	23.1	813.4	10.6	797.8	11.4	0.81	93
005-Z2	0.39	0.18	4415	0.06546	3.3	1.1933	2.5	0.13222	2.1	789.1	67.3	797.5	13.8	800.5	15.7	0.84	101
006-Z3	0.31	0.16	5544	0.06760	6.3	1.2579	4.8	0.13495	4.1	856.4	126.1	827.0	26.8	816.1	31.6	0.88	95
009-Z4-C	1.14	0.50	1437	0.08518	18.0	2.7911	12.9	0.23766	12.5	1319.6	314.3	1353.2	91.8	1374.5	154.5	0.99	104
010-Z4-R	0.34	0.37	5160	0.08375	4.9	2.4138	3.6	0.20903	3.3	1286.8	92.1	1246.7	25.4	1223.7	36.7	0.93	95
011-Z6	0.23	0.22	7396	0.06756	3.4	1.2703	2.7	0.13637	2.1	855.2	68.2	832.5	14.9	824.1	15.9	0.78	96
012-Z7	0.28	0.22	6238	0.06748	4.4	1.2400	3.4	0.13327	2.7	852.7	88.3	818.9	19.2	806.5	20.3	0.79	95
015-Z8	0.39	0.16	4506	0.06610	2.8	1.1394	2.3	0.12502	1.6	809.5	57.3	772.2	12.4	759.4	11.3	0.70	94
016-Z9	0.22	0.16	5479	0.06775	2.5	1.2192	2.0	0.13051	1.5	861.0	51.5	809.4	11.3	790.8	11.0	0.74	92
017-Z10	0.33	0.16	5312	0.06618	2.2	1.1381	1.8	0.12472	1.3	812.1	45.2	771.6	9.5	757.7	9.3	0.75	93
018-Z11	0.53	0.15	3306	0.06690	7.1	1.1387	5.4	0.12345	4.5	834.7	140.6	771.9	28.7	750.4	32.2	0.85	90
018-Z12	0.06	0.16	30282	0.06753	1.3	1.0912	2.3	0.11720	1.9	854.1	26.4	749.1	11.9	714.4	12.6	0.83	84

Table 4.12 - Summary of in situ Lu–Hf analyses for sample BAL-05.

Sample	176Lu/177Hf	2σ	176Hf/177Hf	2σ	Age (Ma)	(176Hf/177Hf)t	2σ	eHf(t)	1σ	T(DM) Ga
Z1	0.0003994	0.000002	0.281991	0.000031	798	0.281985	0.000031	-10.31	0.44	2.11
Z3	0.0004356	0.000003	0.282044	0.000029	816	0.282037	0.000029	-8.05	0.34	2.00
Z12	0.0003379	0.000005	0.282025	0.000022	854	0.282019	0.000022	-7.84	0.08	2.02
Z7	0.0005564	0.000017	0.281919	0.000106	806	0.281910	0.000106	-12.76	3.07	2.25

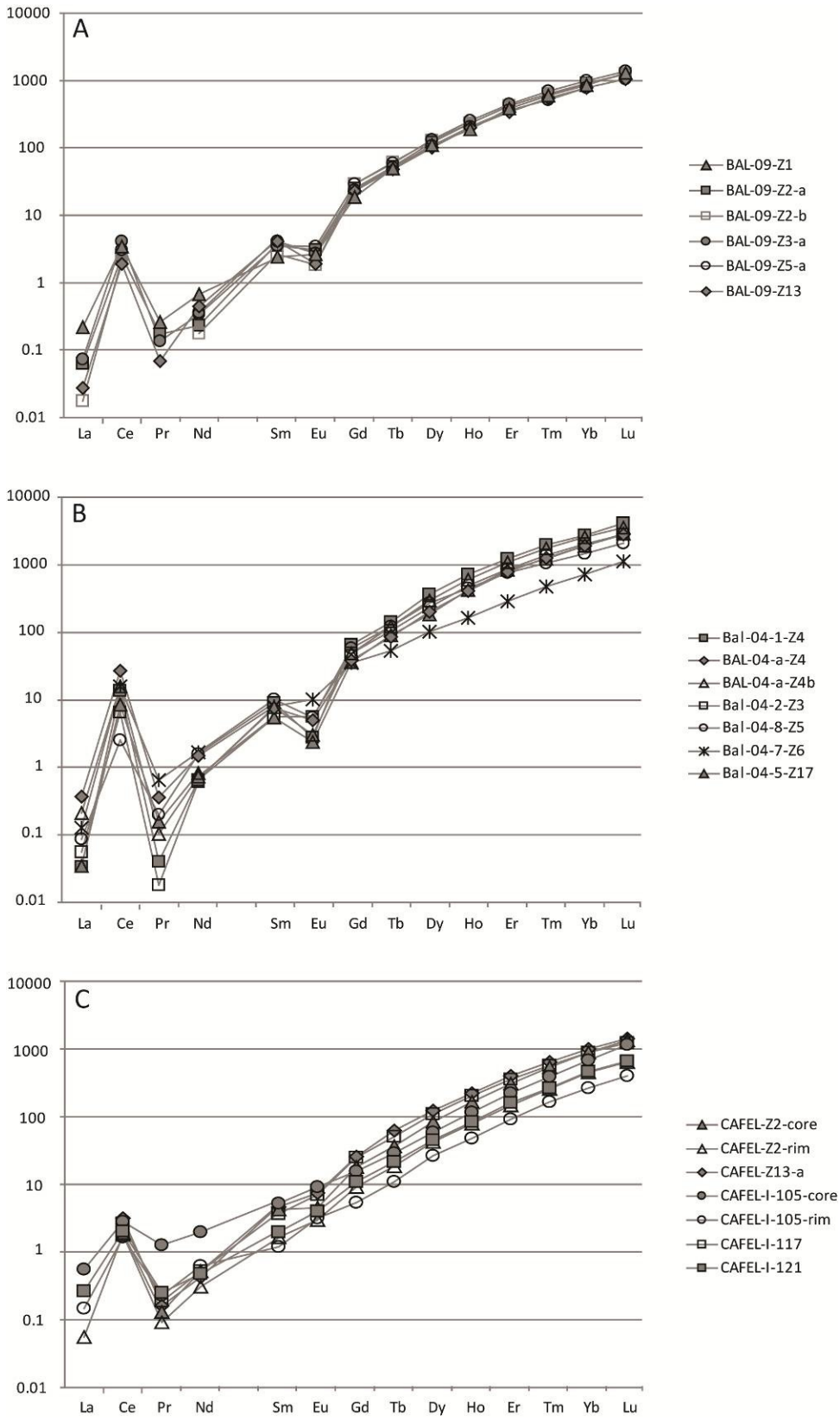

Figure 4.5 – Zircon REE normalized plots from samples BAL-09 (A), BAL-04 (B) and CAFEL (C).

Zircon grains display low contents of trace elements (Table 4.4), as illustrated by Th (37-79 μg/g), U (46-104 μg/g), Pb (3-9 μg/g), P (113-152 μg/g) and Y (382-502 μg/g; Table 4.4). REE contents fluctuate within zircon population (ΣREE between 276 and 354 μg/g; Table 4.4), but this deviation results in no difference in the degree of fractionation of HREE and, as a result, the slope in normalized plots is uniform (Figure 4.5). Zircon grains exhibit a steep HREE normalized pattern, with Yb_N/Gd_N ratios between 37 and 45, and moderate positive Ce anomalies (Ce/Ce* 14-60) and negative Eu anomalies (Eu/Eu* 0.19-0.39; Figure 4.5, Table 4.4). The large variation observed in $(Sm/La)_N$ ratios (11-157) may be credited to the reduced overall content of LREE, specially La, which is commonly below the detection limit. Also, such low values result in large individual uncertainties in the analyses (Table 4.4).

Ti contents vary between 3.89 and 10.16 μg/g and provide Ti-in-zircon temperatures ranging from 644 to 747 °C (Table 4.4).

Metanorthosite BAL-04

Sample BAL-04 corresponds to an amphibolite facies recrystallized garnet metanorthosite, characterized by granoblastic pyroxenes and garnet, as well as plagioclase aggregates substituting relict blue-gray labradorite. Zircon crystals are pristine and colorless and exhibit prismatic habit. Grains are generally fragmented and range from 200 to ca. 400 μm. They show weak CL, except for two crystals that reveal structureless, low-luminescent cores which are surrounded by a very thin bright outer rim with curved boundaries.

U-Pb analyses performed in nine zircon grains reveal concordant to slightly discordant dates indicating an upper intercept age of 1271 ± 78 Ma (MSWD=0.69; Figure 4.4B; Table 4.5). The lower intercept is characterized by a spread of ages between 800 and 735 Ma, which are in agreement with the values obtained by Correia *et al.* (2007) in a sample from the same locality. Th/U ratios vary between 0.17 and 0.29 and do not present correlation with U-Pb ages. Pristine and inclusion-free titanite grains were also investigated by the U-Pb systematics. Twelve spot analyses yield concordant to highly discordant compositions in the Tera-Wasseburg diagram, indicating the age of 754 ± 21 Ma (MSWD=1.2, Figure 4.4C, Table 4.5), which is interpreted as representative of cooling after peak metamorphism.

HfO_2 contents in zircon grains from sample BAL-04 vary in the range between 1.5 and 2.4% (Table 4.6). Hf-enriched zircon is commonly associated with evolved rocks and, therefore,

the elevated HfO_2 values observed in this sample are coherent with the higher degree of differentiation of the original magma when compared to other rock samples investigated. Initial Hf isotopic ratios range from 0.282175 to 0.282256, with strongly positive $\varepsilon_{Hf(1271)}$ values (7.0 to 9.9) and two-stage hafnium model ages between 1.52 and 1.36 Ga (Table 4.6).

U, Th and Pb contents in zircon from sample BAL-04 are low and comparable to sample BAL-09, with values in the range of 22-135 µg/g, 16-98 µg/g and 1-7 µg/g, respectively (Table 4.7). However, these crystals display the highest concentrations of other trace elements among the studied samples, such as P (96-253 µg/g), Y (343-1189 µg/g), Nb (15 to 26 µg/g) and Ta (1.2-3.5 µg/g; Table 4.7). Total REE content varies between 658 and 988 µg/g and $(Yb/Gd)_N$ is in the range of 45-50, resulting in steep HREE patterns in chondrite-normalized plots, with pronounced positive Ce anomalies (Ce/Ce* 19-116) and negative Eu anomalies (Eu/Eu* 0.12-0.59; Figure 4.5, Table 4.7). $(Sm/La)_N$ values are highly variable, ranging from 21 to 157. Grains #5 and #6, conversely, are slightly HREE-depleted and show lower ΣREE (570 and 268 µg/g, respectively) and $(Yb/Gd)_N$ values (< 26; Table 4.7). These crystals present the highest ε_{Hf} values (+9.8) and the lowest T_{DM} ages (1.36 Ga; Table 4.6). In addition, U-Pb isotopic analyses reveal that both grains have incorporated a larger degree of common lead, resulting in $^{206}Pb/^{204}Pb$ lower than 2500 (Table 4.5). However, due to the inexistence of luminescence response, it is not possible to correlate any isotopic or chemical composition to a particular CL domain.

Ti contents in zircon grains vary from 1.88 to 11.26 µg/g and reveal temperatures ranging from 610 to 757 °C (Table 4.7).

Garnet-amphibolite CAFEL

Sample CAFEL is representative of the type-locality of the Cafelândia garnet-amphibolite (Moraes & Fuck, 1994; Moraes *et al.*, 2003; Lima *et al.*, 2008). Zircon grains are pristine, colorless and show a varied morphology with sizes ranging from 100 µm to 250 µm. Stubby and ovoid habits characterize the most frequent zircon-type, but elongated prisms with aspect ratios of 4:1 and rounded terminations are also observed. In the CL images, these crystals reveal the most varied internal features, such as: i) diverse zoning aspects (convolute, sector, fir-tree and ghost zoning); ii) inward-moving alteration fronts, with irregularly curved boundaries, that characterize a bright outer rim in which porous domains and mineral inclusions are common; and iii) featureless and chaotic textures (Figure 4.3C-F).

Twelve U-Pb spot analyses render a chain of concordant to slightly discordant ages spreading from 826 Ma down to 766 Ma (Figure 4.4, Table 4.8). As exemplified by grain #7, there is no obvious correlation between internal crystal structure and U-Pb data, since both rim and core yield similar ages (Table 4.8). The HfO_2 content is homogeneous and varies between 1.1 and 1.2%. Hf isotopic analyses reveal $^{176}Hf/^{177}Hf_t$ ratios ranging from 0.282406 to 0.282467, with positive $\varepsilon_{Hf(780)}$ values (4.5 to 6.2) and two-stage Hf model ages between 1.2 and 1.3 Ga (Table 4.9).

Zircon grains from sample CAFEL are trace-element poor, similarly to sample BAL-09. Usually, the cores are richer in MREE and HREE than the rims, in a proportion of ca. 2:1, and this is reproduced in the $(Sm/Nd)_N$ values and also in Eu/Eu* ratios, which reveal a modest negative anomaly in cores that is absent in the borders (Figure 4.5; Table 4.10). Sc and Sr are also slightly enriched in the innermost parts of the grain. Albeit Th (35-179 μg/g) and Pb (3-13 μg/g) contents remain constant in the different grain domains, U contents are enhanced from cores to altered rims, in a proportion of ca. 50 μg/g, and result in lower Th/U ratios in the rims (Table 4.10). Zircon core #I-105, although having overall lower trace-element content when compared to other investigated grains, also reveals a depletion of the rim relative to the core (Table 4.10). Nevertheless, $(Yb/Gd)_N$ values are uniform within the population (0.36 to 0.49) and result in virtually parallel and steeply rising HREE slopes in a chondrite-normalized plot (Figure 4.5).

Regardless of this general behavior of trace elements, Ti contents do not present correspondence with core-rim domains and the Ti-in zircon thermometer provides temperatures ranging from 677 to 718 °C (Table 4.10).

Basic granulite BAL-05

Sample BAL-05 is a typical medium-grained 2-pyroxene mafic granulite from the Barro Alto Complex (Fuck *et al.*, 1981; Ferreira Filho, 1998). Zircon grains from sample BAL-05 are pristine and colorless and show stubby habit with varied degrees of rounding. Generally, crystals are fragmented and their widths vary between 100 and 200μm. In the CL images, the grains present weak luminescence and encompass chaotic to structureless internal features, as well as ghost zoning (Figure 4.3G, H).

Nine spot analyses yield a spread of concordant ages of ~100 Ma, with $^{206}Pb/^{238}U$ dates varying from 824 to 714 Ma (Figure 4.4; Table 4.11). Additionally, an inherited zircon grain reveals concordant Mesoproterozoic ages in both core and rim (Table 4.4).

Hf isotopic analyses render a mean $^{176}Hf/^{177}Hf_t$ of 0.281988±56 and strongly negative $\varepsilon_{Hf(T)}$ values, between -7.8 to -12.8. Two-stage hafnium model ages range from 2.0 to 2.25 Ga (Table 4.12).

4.6. Discussion

High-grade metamorphic imprint and the interpretation of zircon U-Pb ages

In this study, zircon Hf isotopic and trace element composition were investigated in order to better constrain the U-Pb data and, consequently, to solve the geological-geochronological impasse which has been a matter of debate for the last 10 years (Ferreira Filho *et al.*, 1994, 2010; Suita *et al.*, 1994; Correia *et al.*, 1999, 2007; Ferreira Filho & Pimentel, 2000; Pimentel *et al.*, 2004, 2006; Rivalenti *et al.*, 2008).

Hf isotopic signature of zircon grains: key for distinguishing crystallization events

In the last decade, zircon Hf isotopic signature has been widely used in addition to U-Pb geochronology, particularly with aim at addressing the characteristics of sedimentary source in provenance investigations, as well as to unravel the crustal evolution of Precambrian terranes (Griffin *et al.*, 2000; Kinny & Maas, 2003; Scherer *et al.*, 2007; among others). Nevertheless, few articles have focused on poli-metamorphosed regions (Zheng *et al.*, 2005; Gerdes & Zeh, 2009) and these studies have demonstrated that Hf-in-zircon is also efficient in solving distinct geological events that could not be characterized based merely on U-Pb ages.

Since Hf^{4+} enters the structure of zircon in a simple substitution for Zr^{4+}, it is generally an important constituent of this mineral, with HfO_2 values reaching even 12% (Uher *et al.*, 1998), and this crystalochemical aspect limits the mobility/diffusion of Hf in zircon throughout high-grade metamorphism (Cherniack *et al.*, 1997; Cherniak & Watson, 2003). Hence, the primary isotopic signature, reflecting the isotopically homogeneous conditions operating in the melt during the crystallization, is preserved even after partial melt and granulite/eclogite-facies metamorphic imprint (Zheng *et al.*, 2005; Gerdes & Zeh, 2009; Xia *et al.*, 2009). Consequently, zircon retains the Lu-Hf information of each episode of crystal growth in which it was involved,

in opposition to the U-Pb systematic, commonly disturbed or even totally reset under the same P-T-fluid circumstances.

As exposed in the last section, zircon grains from both the SMC and BAC were submitted to a pervasive metamorphic alteration that promoted varied degrees of loss of the U-Pb information in the analyzed samples. For instance, leucogabbro is the least recrystallized sample and, regardless of the internal features typical of a coupled dissolution-reprecipitation process, crystals still retain the primary U-Pb crystallization ages (Figure 4.4). Conversely, zircon from the amphibolite-facies metanorthosite (BAL-04) is predominantly concentrated near the discordia lower intercept (Figure 4.4), with few discordant individuals distributed along a Pb-loss line that points toward 1.3 Ga. Considering only the U-Pb data, these older grains could be interpreted as inherited crystals, but the homogeneous $^{176}Hf/^{177}Hf_t$ ratios within the population, allied to strongly positive $\varepsilon_{Hf(1270)}$ values, advocates against this interpretation and suggests that these zircon grains still record the primary U-Pb signature, albeit only partially. Therefore, the Hf isotopic data indicate that, in sample BAL-04, the Mesoproterozoic upper intercept most likely corresponds to the real crystallization age. Thus, samples BAL-09 and BAL-04 characterize the same crystallization episode and, moreover, they might share the same depleted mantle source.

In opposition, the garnet amphibolite (CAFEL) shows a spread of concordant ages between 800 and 760 Ma (Figure 4D). Since this rock was subjected to partial melting, it is expected that new zircon overgrowths retain a different $^{176}Hf/^{177}Hf_t$ in consequence of mixing with the more radiogenic matrix hafnium. Nevertheless, despite the U-Pb system behavior and the variation of zircon chemistry observed between core and rims, the Hf signature of sample CAFEL is very homogeneous (mean $^{176}Hf/^{177}Hf_t = 0.282434\pm0.000023$) and does not correlate with any CL or chemical domains (Figure 4.6). Thus, the primary Hf composition was preserved. Furthermore, since Lu-Hf and U-Pb systematics are decoupled in zircon grains, the constant Hf ratios also support that the older concordant ages (~800 Ma) are representative of the igneous magmatic episode, whereas the spread of $^{206}Pb/^{238}U$ dates illustrates the partial loss of the U-Pb information due to the granulite-facies metamorphic imprint.

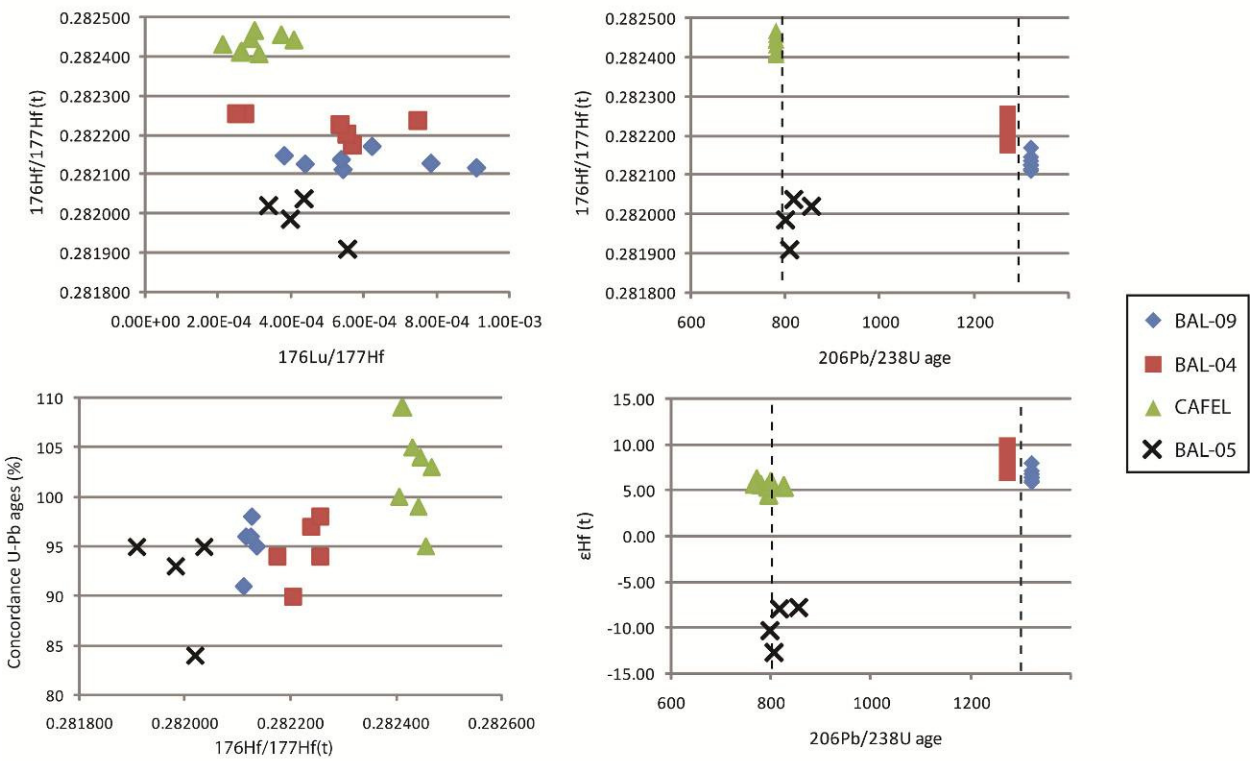

Figure 4.6 - Zircon i*n situ* Hf isotopic data plotted against U-Pb systematics. Hf signature is homogeneous within individual samples and do not correlate with neither Lu-Hf ratios nor U-Pb ages, regardless of the concordance level. Additionally, Hf isotopic data reveal two distinct zircon crystallization events, the first at ca. 1.3 Ga and the second near 0.8 Ga. See text for discussion

Lu/Hf ratios in zircon from sample CAFEL, however, are lower in the borders (<0.00017) than in the core (<0.0032; Table 4.10). According to Gerdes & Zeh (2009), such feature might illustrate that either i) Lu was fractionated into other co-crystallizing mineral or ii) the rims crystallized from lower temperature melts, which diminishes the trace element melt-crystal partitioning. Considering that there is no new zircon growth during metamorphism, as revealed by the uniform $^{176}Hf/^{177}Hf_t$ ratios, none of the above premises is applicable to this sample. Moreover, potential modifications in the Lu/Hf ratios could reflect a process operating during igneous crystallization but, in layered mafic-ultramafic complexes, fractional crystallization is frequent and, therefore, as soon as zircon started to nucleate, other minerals which might fractionate Lu, such as pyroxenes, were already formed. Besides, during high-grade metamorphism, the co-crystallization of garnet in a closed-system could also promote the observed lower Lu/Hf ratios (Rubatto, 2002), but the trace-element signature suggests that zircon was unreactive to the formation of garnet, as will be explored further.

Therefore, the combination of CL images, which reveal internal features typical of recrystallization process (Figure 4.3C-F), with the low U-Th-Pb contents and consistent Hf ratios within core and rims indicate that grains from sample CAFEL were subjected to a concomitant dissolution and reprecipitation process. Through this alteration, inward-moving fronts promote the structural recover of the grain due to the progressive removal of ions with different ionic-radii, resulting in reacted borders in which trace element contents are lower than in unreacted crystalline domains (Geisler *et al.*, 2007). Hence, the metamorphic recrystallization is most likely the factor that promotes the disparity in Lu/Hf ratios among cores and rims in sample CAFEL.

Mafic granulite (BAL-05), lastly, shows an extensive spread of concordant ages of c.a. 100 Ma. Also, the Hf isotopic composition is distinct from the other analyzed samples, given that the strongly negative ε_{Hf} reveals a strong crustal contamination process, which is in agreement with whole-rock Sm-Nd and geochemical data previously published (Suita, 1996; Ferreira Filho & Pimentel, 2000; Pimentel *et al.*, 2004). However, similarly to sample CAFEL, the homogeneous $^{176}Hf/^{177}Hf$ data suggest that the primary isotopic signature was preserved and, consequently, the older concordant dates shall represent the age of emplacement and crystallization. In view of that, the mafic granulite, in conjunction with the garnet-amphibolite, typify a second episode of mafic magmatism in the composite layered mafic-ultramafic complex.

Zircon chemistry and the concomitant crystallization of garnet

The study of zircon chemistry in high-grade metamorphic rocks is applied in order to set the timing of zircon growth during the metamorphic evolution of an orogen. Since zircon might form in a pre-peak, peak or post-peak stage (see Harley *et al.*, 2007 for a discussion over this topic), the investigation of the zircon REE signature helps to constrain the metamorphic reactions in which it might have been involved.

As previously stated, in the course of the high-grade reactions, metamorphic zircon might form by two mechanisms: i) new growth due to the breakdown of Zr-bearing minerals in metamorphic reactions or from a melt/fluid phase (Roberts & Fringers, 1997; Fraser *et al.*, 1997; Schaltegger *et al.*, 1999; Vavra *et al.*, 1999; Degeling *et al.*, 2001; Bingen *et al.*, 2001; Rubatto, 2002; Ayers *et al.*, 2003; Whitehouse & Platt, 2003; Möller *et al.*, 2003; Rubatto & Hermann,

2007); or ii) the recrystallization of the protocryst (Schaltegger *et al.*, 1999; Vavra *et al.*, 1999; Ashwal *et al.*, 1999; Hoskin & Black, 2000; Corfu *et al.*, 2003; Martin *et al.*, 2008).

Nevertheless, Hf isotopes have already revealed that, in the SMC and BAC, zircon has re-equilibrated during the granulite-facies metamorphism through a coupled dissolution-reprecipitation process, rather than re-grew. Accordingly, the dynamic break of bonds allied to the contemporaneous nucleation and growth result in a closed or partially closed system for trace-element exchange, resulting in very low REE mobility at the crystal scale (Ashwal *et al.*, 1999; Putnis, 2002; Tomaschek *et al.*, 2003; Geisler *et al.*, 2007; Martin *et al.*, 2008). However, crystals in chemical communication with metamorphic garnet might be affected by its growth and, as a result, REE partition would evolve to equilibrium and promote the depletion of HREE in zircon grains (Harley & Kelly, 2007).

In this study, two garnet bearing samples were investigated. In the garnet metanorthosite (BAL-04), despite of the steep HREE patterns in chondrite-normalized plots shown by majority of grains, zircon #5 and 6 encompass a depletion in HREE that results in lower $(Yb/Gd)_N$ ratios, suggesting that at least part of the crystals attained equilibrium with garnet during recrystallization. In conformity, these grains have completely reset U-Pb dates that point toward the age of metamorphism (Figure 4.4).

Zircon from garnet amphibolite CAFEL, in opposition, has different core-rim compositions with lower HREE contents but constant $(Yb/Gd)_N$ ratios, which produces a parallel and steeply rising distribution of HREE in chondrite-normalized diagrams (Figure 4.5). The concomitant dissolution-reprecipitation process, previously identified in these grains, may generate such trace-element depletion, since the recrystallization tends to make zircon pure through the removal of non-formulae elements toward the end-points of the solid-solution (Geisler *et al.*, 2007; Martin *et al.*, 2008). Therefore, the homogeneous $(Yb/Gd)_N$ values observed in different grain domains imply that zircon was chemically unresponsive to garnet formation and, hence, it suggests that the recrystallization occurred in a closed-system at the crystal scale. Consequently, the peak metamorphic episode was not chemically registered by the zircon grains from the garnet-amphibolite.

Nonetheless, zircon from sample CAFEL also comprises some geochemical characteristics that advocate against a closed-system during the alteration process. The most prominent aspect is the reduction of MREE contents in the rims that is spatially coincident with

recrystallized domains, as revealed by CL images. It is characterized by $(Sm/Nd)_N$ ratios, which are lower in outer borders and correlates positively with Lu contents and, consequently, Lu/Hf ratios. However, there is no correspondence with $(Yb/Gd)_N$ values. Since REE have identical valence state (except for Ce and Eu), they are incorporated at the same crystallographic site in zircon lattice by reason of a coupled substitution along with P, Nb and Ta (Hoskin & Schaltegger, 2003). Thus, recrystallization during high-grade metamorphism would promote the purging of all REE spectrums from the crystal structure, reducing absolute contents without noticeably changing the normalizing ratios. Therefore, the MREE and HREE depletion was promoted by distinct mechanisms, operating in different moments during the evolution of the orogen. In addition, the lack of a pronounced Eu negative anomaly in borders (Figure 4.5C, Table 4.10) implies that zircon has grown in the absence of plagioclase (Rubatto, 2002; Hoskin & Schaltegger, 2003). Lastly, zircon grains also reveal an increase of the U content in the rims, that is typified by U-Pb dates plotting above the Concordia curve (Figure 4.4D), as well as by lower Th/U ratios in the borders.

The geochemical features described in zircon from sample CAFEL are very similar to those observed by Harley & Kelly (2007) in grains from the Rauer Islands, Antarctica. Based on REE partition coefficients between zircon, garnet and orthopyroxene, along with $\delta^{18}O$ values, the MREE mobility and the U gain was attributed to a later fluid infiltration due to the emplacement of pegmatites (Harley & Kelly, 2007). In the BAC, a number of late-stage granites and pegmatites are mapped, but no geochronological information is available for these rocks. Nevertheless, in the Niquelândia Complex (NC), similar lithotypes have rendered a Sm-Nd isochronic age of 759±65 Ma (Pimentel *et al.*, 2006). Therefore, considering the whole geological and geochronological similarity among the BAC and the NC, these granitic rocks might have provided the abundant late-stage fluids that promoted the second alteration in zircon grains from the garnet-amphibolite.

Ti-in-zircon Thermometry and the role of high-grade metamorphism

Ti-in-zircon thermometry (Watson *et al.*, 2006; Ferry & Watson, 2007) is widely used in investigations of high-grade terranes, in conjunction with geochemistry of other trace-elements, aiming at constraining the time of metamorphic reactions involving zircon growth and/or recrystallization.

In both the SMC and BAC, zircon grains yield homogeneous temperatures for all analyzed samples, with a mean value of 700±40°C (RSD, n=20), despite of the geological evidence that reveal progressive decrease in the metamorphic grade westward, from granulite to amphibolite facies (Figure 4.7). There is no correlation among Ti concentrations and U-Pb ages or Hf isotopic signature and identical temperatures were obtained for both cores and rims (Figure 4.7). Furthermore, THERMOCALC calculations in the peak-metamorphic parageneses for the Cafelândia amphibolite reveal temperatures of ~870°C (Lima *et al.*, 2008), which is almost 200°C higher than the values obtained in the Ti-in-zircon investigation.

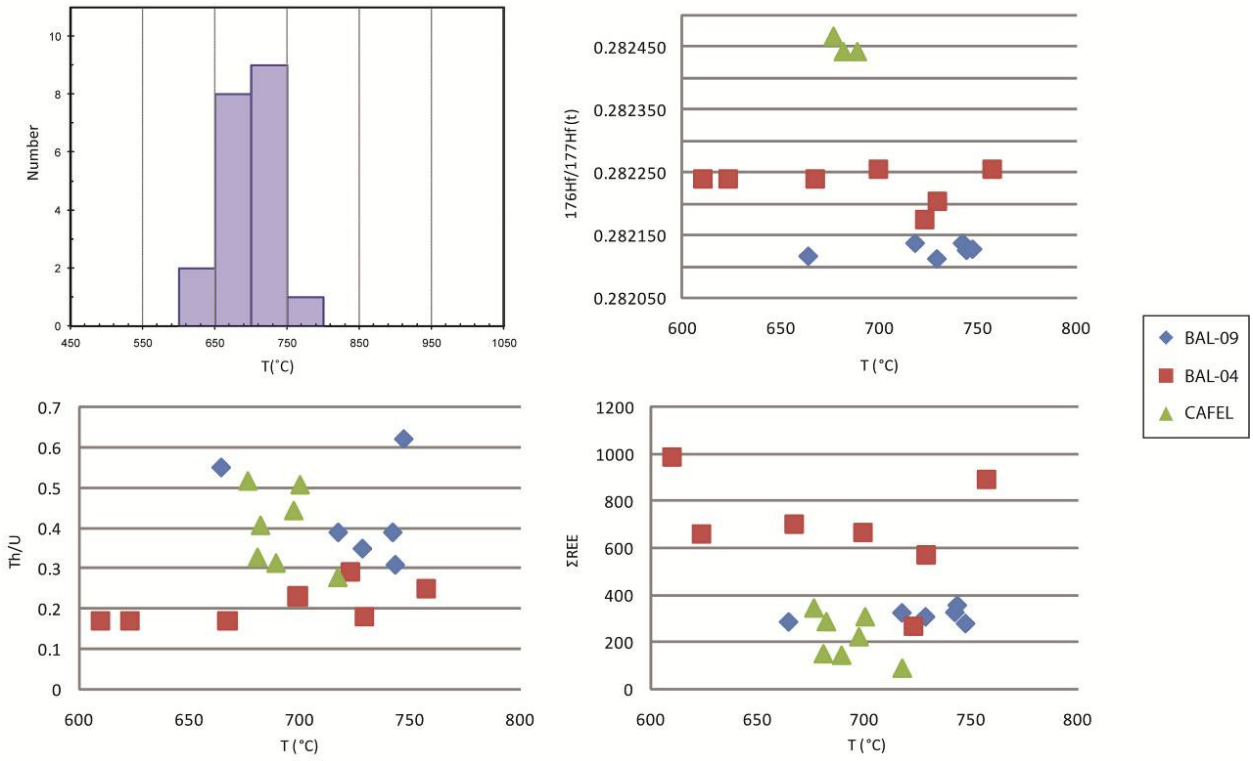

Figure 4.7 - Ti-in-zircon temperatures plotted against U-Pb, Lu-Hf systematics and trace element contents. There is no correlation among Ti-in-zircon data and Th/U ratios, Hf isotopes or total REE contents. Additionally, the regular distribution of temperatures near 700°C is noteworthy.

Similarly to the SMC and BAC, low Ti-in-zircon temperatures in mafic rocks were also obtained elsewhere (Bea *et al.*, 2006; Harrison *et al.*, 2007; Fu *et al.*, 2008). Particularly, data on crystals of non-metamorphosed gabbros and anorthosites of distinct intrusions in North America reveal no difference in zircon temperatures when compared to their high-grade metamorphic equivalents (Fu *et al.*, 2008). The consistent overlap of values from different rock types suggest that temperature calculation by the Ti-in-zircon thermometer might also depend upon variables other than the activities of SiO_2 and TiO_2 (Fu *et al.*, 2008), such as Si^{4+} and Zr^{4+} coupled substitution for REE and P (Fu *et al.*, 2008; Hoffman *et al.*, 2009).

The isotopic and chemical composition of zircon from the SMC and BAC, as discussed in the last topic, indicates that the primary signature is only partially preserved in such crystals due to the coupled dissolution-reprecipitation process operating during high-grade metamorphism. Thus, the homogeneous Ti-in-zircon data observed in zircon crystals from the SMC and BAC reproduces neither igneous crystallization temperatures for mafic-ultramafic magmas nor metamorphic conditions, since the equilibrium with the peak assemblage was not completely achieved. Moreover, the lack of correlation with REE contents reveals that, throughout the recrystallization process, Ti might have been more efficiently removed from the crystallographic lattice than other minor and trace elements. The recrystallization process seems to occur until a "lower boundary" is reached, in which the Ti concentration is proportional to a temperature of 650-700°C. Accordingly, the simple substitution mechanism of Ti in zircon structure, allied to the larger ionic radius of Ti^{4+} (0.42Å) in comparison with Si^{4+} (0.26Å; Ferry & Watson, 2007), might ease such removal toward an equilibrium condition, both in composition and in total lattice strain.

Therefore, it is suggested that Ti-in-zircon temperatures on recrystallized grains from high-grade terranes, comparable to the SMC and BAC, should be evaluated with caution when applied in investigations of peak metamorphic conditions.

Geological Implications

The geochronological and geochemical features described above allow the identification of two distinct episodes of voluminous mafic magmatism in the composite layered intrusion, similarly to that described in the Niquelândia and Serra dos Borges complexes, to the north (Pimentel *et al.*, 2004; Ferreira Filho *et al.*, 2010).

The first magmatic event occurred in the Mesoproterozoic and is ascribed to rocks of the Serra da Malacacheta Complex which, in this study, are typified by leucogabbro (BAL-09) and metanorthosite (BAL-04). In these rocks, despite of the partial to complete reset of the U-Pb system, the igneous crystallization is dated around 1.3 Ga. Moreover, the highly positive εHf obtained in zircon grains advocate for a depleted mantle source for the original magma, as well as for restricted contribution of an older Mesoproterozoic crust, probably of mafic to intermediate composition. This is coherent with whole-rock Sm-Nd signature of basic metavolcanic rocks from the Juscelândia Sequence, interpreted as the extrusive counterpart of the SMC (Moraes *et al.*, 2003; 2006) and, accordingly, new zircon data reveal the juvenile signature of this extensional event and corroborate the hypothesis that the initially bi-modal volcanic succession evolved toward the opening of an oceanic basin (Moraes *et al.*, 2003; 2006; Pimentel *et al.*, 2004; 2006). Such ages, however, are not common within the Brasília Belt and correspond more likely to a global rifting event recorded in Laurentia and Baltica (for this discussion see Ferreira Filho *et al.*, 2010), corroborating the allochthonous nature of this terranes which might have been accreted to the Brasília Belt at the final stages of the Brasiliano orogeny.

The second episode of mafic magmatism took place at ~0.8 Ga and is represented by rocks of the Barro Alto Complex. Hf isotopic data obtained on zircon from mafic granulite (BAL-05) evidences that this magma has assimilated older crust and, moreover, two-stage model ages yield Paleoproterozoic values which are coherent with the SHRIMP U-Pb age of orthogneisses adjacent to the BAC (Correia *et al.*, 1997). Additionally, an inherited zircon crystal identified in the mafic granulite suggests that the Mesoproterozoic layered complex also compose the basement of the Neoproterozoic intrusion. Therefore, the new geochronological and isotopic data indicate that the intrusion of the Barro Alto Complex took place in an extensional environment within older continental crust. In addition, this episode is similarly recorded by rocks of the Goiás Magmatic Arc, which shows voluminous magmatism at ~790 Ma, and, therefore, the subduction environment associated with the formation of the arc is most likely the same promoting crustal extension and the emplacement of the BAC, as formerly suggested (Moraes *et al.*, 2006; Pimentel *et al.*, 2006).

In contrast, the Cafelândia amphibolite, although coeval to the mafic granulite protolith, rendered a depleted Hf signature, with highly positive ε_{Hf} zircon values, in agreement with whole-rock Sm-Nd investigation (Moraes *et al.*, 2003). Due to its Nd isotopic composition,

comparable to MORB-type volcanic rocks of the Juscelândia Sequence, the amphibolite protolith was interpreted as the intrusive equivalent of these rocks (Moraes *et al.*, 2003; 2006). However, the new geochronological data reveal that the Cafelândia amphibolite is, in fact, related with the Neoproterozoic magmatic episode and, therefore, it characterizes a distinct intrusion within the BAC.

Additionally, considering the isotopic signature of the Cafelândia amphibolite, it is feasible that this second extensional event has also constituted a volcanic pile, similarly to that described for the Mesoproterozoic rifting episode, but such lithotypes have not been recognized yet. Therefore, further geological and geochronological research is necessary to confirm this hypothesis.

Neoproterozoic high-grade metamorphic imprint

The timing of high-grade metamorphism in the SMC and BAC is poorly constrained by recrystallized zircon domains that converge to dates as low as 745 Ma, in accord with data obtained in metamorphic overgrowths in felsic metavolcanic rocks of the Juscelândia Sequence (Moraes *et al.*, 2006). This suggests that the Neoproterozoic metamorphism was pervasive in both the SMC and BAC and, consequently, the complexes must have been already joined by the time of the high-grade imprint.

Throughout this high-grade episode, peak metamorphic conditions attained temperatures as high as 980°C in lenses of quartz-bearing rock within the BAC mafic granulites (Moraes & Fuck, 2000). Such extremely hot crustal conditions could not be achieved in modern collisional orogens and an additional heat source would be fundamental to explain the ultra-high temperature parageneses (Jamieson *et al.*, 1998, 2004; Beaumont *et al.*, 2001, 2006; Collins, 2002; Hyndman *et al.*, 2005). Recent review articles on the UHT paradox (Harley, 2004, 2008; Brown, 2007; Kelsey, 2008) attempted to envisage potential geotectonic environments in which such conditions could be attained, but a thermal gap among the geological record and the available numerical models is still recognized (Jamieson *et al.*, 1998, 2004; Beaumont *et al.*, 2001, 2006; Harley, 2008). Nevertheless, the actual best-fit hypothesis to explain UHT conditions is that of large-scale hot accretionary orogen, in which tectonic switching promotes episodes of extension within the overall lithospheric contractional system (Collins, 2002). In

such scenario, the development of a backarc setting results in crustal thinning and upwelling of the hot asthenosphere which, consequently, promotes granulite-facies metamorphism in the root of the weakened crust, extensive decompressional melting and granite generation, as well as ductile deformation (Jamieson *et al.*, 1998; Thompson *et al.*, 2001; Collins, 2002; Hyndman *et al.*, 2005).

The geological and geochronological characteristics favors a backarc setting for the BAC emplacement, but an orogenic deformational process is claimed to explain the high-grade metamorphism described in both the SMC and the BAC. However, the roughly coeval magmatism and high-grade metamorphism in the BAC requires a supplementary heat source, either to keep the rocks hot for almost 40 Ma or to promote the widespread development of UHT parageneses and late granite generation. Hence, this scenario is coherent with the hypothesis of a hot orogen, as discussed above, and, consequently, the development of high-T-low-P granulites is probably a consequence of the heat coming from the backarc, not from an orogenic deformation process (Hyndman *et al.*, 2005). Moreover, UHT rocks of the BAC show an isobaric cooling P-T path (Moraes & Fuck, 2000), revealing that no considerable thickening occurred after peak metamorphic conditions were attained and, hence, the compressional event was weak.

Therefore, considering that the ~750Ma metamorphic event is also recognized in rocks of the Goiás Magmatic Arc (Junges *et al.*, 2002), the high-grade episode shall be representative of the accretion of the magmatic arc to a Paleoproterozoic continental block, in which the SMC and BAC were formerly emplaced. Another evidence of the accretionary nature of this collage is the occurrence of paragneisses of the Uruaçu Complex in which the maximum depositional age of the protolith is defined by 720 Ma zircon grains (Giustina *et al.*, 2009), thus suggesting that the restricted basin was not closed during the convergent process.

4.7. Conclusions

Combined geological and new geochronological data for the Serra da Malacacheta and Barro Alto complexes allow the following conclusions:

- Zircon data obtained by this study imply that the SMC and the BAC represent different layered intrusions, both in petrological and geochronological features.
- CL images of zircon grains reveal internal features typical of solid-state recrystallization process. This alteration has shown to be pervasive through the

composite layered complex, since such modifications are observed even on zircon grains from rocks that still preserve igneous textures.

- U-Pb in zircon is inconclusive in dating the metanorthosite and the garnet-amphibolite. In these samples, the geochronological data could only be correctly interpreted with additional information engendered by the Hf isotopic and geochemical signature of zircon crystals.
- Hf isotopes allow the undoubtedly individualization of two events of zircon growth. The first occurred at ~1.3 Ga and corresponds to the Serra da Malacacheta Complex, whereas the latter is dated around 800 Ma and is recognized in the Barro Alto Complex.
- U-Pb in titanite yields an age of 754±21 Ma, which is interpreted as representative of cooling after peak metamorphism. This age is also roughly attained in zircon altered domains but, due to the recrystallization process, U-Pb dates probably retain a memory of the parent isotopic composition and, hence, the peak metamorphic age could not be achieved. Therefore, the pervasive nature of the high-grade metamorphic imprint in the Neoproterozoic implies that both the SMC and BAC were already joined before 750 Ma.
- The Cafelândia amphibolite, although ascribed to the same magmatic episode as the mafic granulite, has a distinct Hf isotopic signature. The highly positive ε_{Hf} values obtained in zircon from the amphibolite contrasts with the strongly contaminated data from the granulite. Therefore, the Cafelândia amphibolite characterizes a distinct unit within the composite layered complex and, therefore, is not included in the Barro Alto Complex.
- Mineral chemistry reveals that a small number of zircon grains from the metanorthosite have recrystallized in equilibrium with garnet, whereas those of the amphibolite were unreactive to the formation of the peak metamorphic parageneses.
- The Cafelândia amphibolite has undergone a second process of zircon alteration that yields the depletion of MREE, as noticed by $(Sm/Nd)_N$ ratios, and the gain of U in the rims. Evidence suggests that this process might have been promoted by a later influx due to the emplacement of late-stage granites and pegmatites.

- Ti-in-zircon thermometer is not efficient for the investigation of high-grade metamorphic terranes in which zircon grains were affected by recrystallization processes.
- Igneous and metamorphic ages obtained in this study are in agreement with previously published data from the Niquelândia Complex, to the north, and reinforce that both complexes were part of a huge structure, disrupted during the final stages of the Brasiliano orogeny.

4.8.Acknowledgments

Support from CNPq research grant (477347/2007-0) is thankfully acknowledged. M.M.P., C.F.F.F. and R.A.F. are CNPq research fellows. M.E.S.D.G. thanks CNPq fellowship. Thanks to Sergio Junges, Barbara Alcântara and Massimo Matteini for laboratorial support and to Prof. Claudio Lamarão (UFPA) for cathodoluminescence images.

5. DISCUSSÃO

Neste capítulo são discutidos os processos de recristalização mineral no metamorfismo de alto-grau e as implicações para a datação pelo sistema U-Pb em zircão, a fim de caracterizar o processo responsável pelas alterações texturais, isotópicas e químicas observadas em cristais dos complexos Anápolis-Itauçu e Serra da Malacacheta-Barro Alto.

5.1. Processos de recristalização mineral no metamorfismo

A correta interpretação dos dados isotópicos obtidos em zircão metamórfico requer a compreensão do mecanismo de recristalização deste mineral. No metamorfismo de alto grau, fatores como pressão, temperatura, intensidade de deformação e composição de fluido são determinantes no processo de substituição mineral, visto que a modificação de qualquer um destas variáveis promove aumento na energia livre de Gibbs do sistema (G). Com isso, reações de recristalização são estimuladas para atingir novamente a condição de equilíbrio (Spry, 1969; Yardley, 1988).

O fato de não se observarem mudanças significativas na morfologia de minerais recristalizados no metamorfismo de alto grau é geralmente interpretado como decorrente de alteração via difusão intragranular (Putnis & Putnis, 2007). O processo de difusão envolve o transporte de átomos, íons ou moléculas, no estado sólido através do retículo cristalino, a fim de minimizar gradientes de potencial químico (Yardley, 1988). Assim, promove-se mudança composicional das fases envolvidas, tornando-as homogêneas, porém sem episódios de dissolução ou de novo crescimento. Visto que a maioria das ligações químicas nos minerais é forte, este processo é extremamente lento. No entanto, com o aumento da temperatura no metamorfismo, as taxas de difusão elevam-se de forma exponencial e, dessa forma, torna-se possível a realização de trocas catiônicas entre as fases minerais (Yardley, 1988; Figura 5.1A). Tais reações ocorrem devido aos diferentes coeficientes de distribuição (K_D) dos elementos em questão entre o par de minerais coexistentes. Como o valor de K_D é dependente da temperatura, sob condições metamórficas de alto-grau há o re-equilíbrio entre as fases por meio da difusão intragranular (Figura 5.1A). Este processo de recristalização perdura até que seja atingida a temperatura de fechamento do sistema, a partir da qual a difusão é novamente muito lenta.

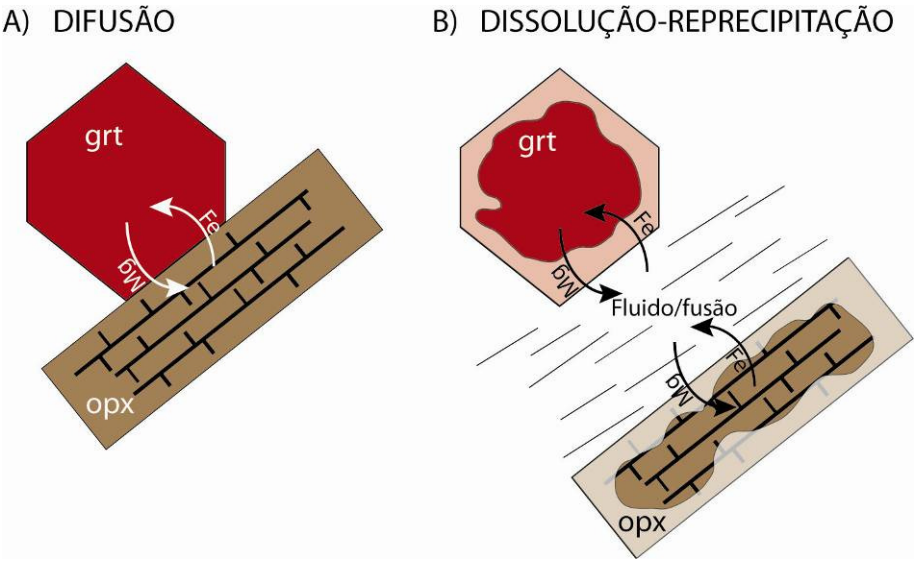

Figura 5.1 - Ilustração esquemática dos processos de difusão (A) e dissolução-reprecipitação concomitante (B). No caso de difusão, a troca de elementos químicos se dá em estado sólido (A), enquanto que na dissolução-reprecipitação o fluido ou o magma facilitam a troca (B). Neste último caso, desenvolve-se uma borda de recristalização em ambos os minerais envolvidos, na qual se mantém preservada a orientação cristalográfica. O desenho não está em escala.

Entretanto, estudos recentes demonstraram que, na presença de fluidos, a recristalização por dissolução-reprecipitação concomitante é mais provável (Putnis & Putnis, 2007; Putnis, 2009). Fluidos são comuns durante o metamorfismo e podem advir tanto das reações de desidratação como também de fusões parciais e magmas graníticos gerados concomitantemente ao episódio metamórfico (Yardley, 1988). Os fluidos funcionam como um solvente/catalisador da reação de recristalização, podendo adicionar ou remover elementos do sistema, e ainda influenciam o estilo de deformação da rocha (Yardley, 1988).

O processo de dissolução-reprecipitação concomitante envolve a quebra das ligações atômicas e subsequente nucleação, em etapas acopladas no espaço e no tempo (Putnis, 2002; 2009; Figura 5.2B). As reações são, portanto, rápidas e são incitadas por mínimas variações na energia livre de Gibbs oriundas de desequilíbrio químico ou textural no sistema rocha-fluido (Putnis, 2002). Adicionalmente, a aplicação de tensão localizada também pode desencadear o processo de dissolução.

O principal fator que governa a dissolução-reprecipitação concomitante é a solubilidade relativa entre as fases minerais envolvidas, visto que a recristalização ocorre na interface entre as mesmas (Putnis, 2009). A presença de impurezas no retículo cristalino reduz a estabilidade do mineral e, além disso, amplia a reatividade da superfície do grão devido à tensão estrutural elevada resultante da incorporação de íons durante a cristalização. Destarte, a solubilidade do

termo metaestável pode persistir reduzida, porém esta ainda será superior aos valores para o seu equivalente puro. Suscita-se então a dissolução da fase mineral em desequilíbrio, o que torna o fluido supersaturado no componente dissolvido. Devido à solubilidade inferior do produto, ocorre instantaneamente a precipitação do mesmo (Putnis, 2009). Logo, vê-se que o balanço termodinâmico entre as taxas de dissolução e precipitação não reside na dissolução de grandes quantidades de material, mas depende fundamentalmente na supersaturação interfacial do fluido. O processo de dissolução-recristalização concomitante ocorre, portanto, em curtas distâncias (poucos μm) e envolve transporte restrito de elementos (Putnis, 2009). Consequentemente, enquanto o sistema rocha-fluido pode permanecer fechado, em uma escala espacial reduzida o ambiente pode ser considerado aberto (Putnis 2009).

Conforme Putnis (2009), o processo de dissolução-reprecipitação concomitante desenvolve características particulares nas fases envolvidas:

- A recristalização é pseudomórfica, o que implica em dissolução e reprecipitação intimamente associadas no tempo-espaço. Ainda, se a estrutura cristalina de ambos os minerais for similar, a orientação cristalográfica é mantida (epitaxia).
- Desenvolve-se porosidade, pois há redução do volume molar devido à reorganização do retículo cristalino, com perda de constituintes para o fluido. Isso promove maior permeabilidade na frente de alteração, permitindo que o fluido mantenha contato com a região não recristalizada do mineral e que, desta forma, o processo seja continuado (Putnis, 2002; 2009; Putnis & Putnis, 2007). Ainda, caso haja grande variação no volume molar, pode ocorrer fraturamento.
- Os gradientes composicionais na frente de reação constituem limites bem definidos, o que indica que houve limitada difusão dos íons entre as fases envolvidas (Erambert & Austrheim, 1993).

Na literatura existem numerosos exemplos de substituição mineral pelo processo de dissolução-reprecipitação concomitante, os quais são descritos em diversos minerais e em ambiente ígneo, metamórfico, hidrotermal e mesmo diagenético. Na Figura 5.2A observa-se uma imagem de elétrons retro-espalhados de um grão de granada recristalizado durante retrometamorfismo em fácies eclogito. Nesta rocha, a eclogitização é promovida pela re-hidratação de granulitos ao longo de zonas de cisalhamento e encontra-se restrita pelo grau de penetração lateral do fluido a partir do plano de falha (Pollock *et al.*, 2008). Nos domínios

escuros do cristal há a preservação da composição referente ao metamorfismo em fácies granulito, enquanto que nas zonas claras a assinatura geoquímica é referente ao episódio de retrometamorfismo em fácies eclogito e, portanto, reflete o equilíbrio com o fluido (Pollock *et al.*, 2008). Ainda, a transição entre estes dois domínios composicionais não é difusa e constitui uma frente bem definida (Figura 5.2A). Tais evidências, aliadas à preservação da orientação cristalográfica, sugerem que a recristalização ocorreu via dissolução-reprecipitação concomitante (Pollock *et al.*, 2008).

Comportamento análogo é observado em cristais de monazita de granulito básico da Zona do Rio Ivrea, Itália, os quais apresentam texturas internas típicas de recristalização, como reentrâncias curvilíneas e obliteração da zonação primária por um domínio homogêneo, mais claro (Figura 5.3B). Feições similares foram também obtidas experimentalmente em cristais de monazita originalmente homogêneos em composição e textura, após serem submetidos à ação de fluidos alcalinos sob diferentes condições de pressão (500-1000 MPa) e temperatura (600-900°C; Harlov, 2009). O experimento resultou na substituição parcial da monazita por zonas irregulares, ricas em Th, desenvolvidas a partir da borda do cristal rumo ao centro (Figura 5.2C). Ainda, houve perda significativa de Pb nos domínios alterados. Após o experimento os grãos apresentavam o mesmo hábito original, o que implica que a substituição foi pseudomórfica (Harlov, 2009).

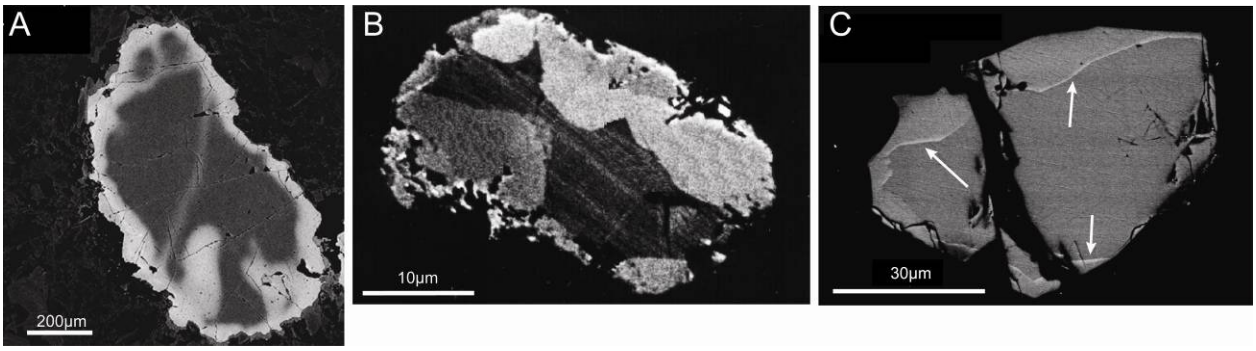

Figura 5.2 - Exemplos do processo de dissolução-reprecipitação concomitantes. A) Imagem de elétrons retro-espalhados em granada alterada pelo reequilíbrio com fluido hidrotermal (Pollock *et al.*, 2008). As porções escuras preservam a assinatura de facies granulito, enquanto que as bordas claras apresentam composição de granada eclogítica. B) Monazita de granulito básico da Zona Ivrea, Itália (Förster & Harlov, 1999). C) Cristal de monazita, inicialmente homogêneo, submetido àalteração por fluidos alcalinos (Harlov, 2009). As setas indicam as frentes de recristalização desenvolvidas sob condições de 900°C e 1000 MPa, após 25 dias de experimento.

Portanto, os resultados experimentais bem como as observações em cristais naturais revelam que, na presença de fluidos, a recristalização de minerais dá-se preferencialmente a partir da dissolução-reprecipitação concomitante. Além disso, verifica-se que este processo pode ser mais comum do que anteriormente suposto (Tomaschek *et al.*, 2003).

5.2. Dissolução-reprecipitação concomitante em zircão

No caso do zircão, não há dados experimentais que comprovem que o processo de dissolução-reprecipitação concomitante seja responsável pela recristalização de zircão no metamorfismo de alto grau, apesar de vários estudos recentes sugerirem tal processo frente às evidências texturais, isotópicas e geoquímicas (Vavra *et al.*, 1999., Schaltegger *et al.*, 1999; Tomaschek *et al.*, 2003; Rubatto & Hermann, 2007; Geisler *et al.*, 2007; entre outros).

O zircão constitui um dos componentes da solução sólida do sistema Th-Y-Zr-U (Förster, 2006) e, deste modo, durante a cristalização ígnea há a incorporação destes elementos na estrutura do zircão (Geisler *et al.*, 2007). A teoria de soluções sólidas preconiza que as composições intermediárias entre os membros finais são metaestáveis, o que resulta na tendência de exsolução das fases via difusão para atingir o equilíbrio (Prieto, 2009). Entretanto, em cristais de zircão a difusão é descrita somente em grãos metamíticos, amorfos, nos quais a estrutura danificada pela emissão de radiação é gradualmente recristalizada na presença de fluidos hidrotermais (Geisler *et al.*, 2007). Adicionalmente, as taxas de difusão de cátions em zircão cristalino, definidas experimentalmente, são extremamente baixas, mesmo sob temperaturas elevadas e, portanto, não são favoráveis à difusão (Cherniak & Watson, 2003). Portanto, o processo de dissolução-reprecipitação revela-se o mais provável para a recristalização da solução sólida envolvendo zircão (Prieto, 2009; Putnis, 2009).

Destarte, a incorporação de elementos traço à estrutura do zircão deforma o retículo cristalino e promove, assim, a força motriz para a reação de recristalização (Tomaschek *et al.*, 2003). O zircão impuro ($ZrMSiO_4$) é mais solúvel em fluidos do que o seu equivalente puro e, portanto, é dissolvido, o que torna o fluido interfacial supersaturado tanto em $ZrSiO_4$ como no outro termo final da solução sólida, representado por $MSiO_4$ (Figura 5.3; Lippmann, 1980). O fluido, então, evolui para uma composição eutética, no qual os produtos puros são estáveis e, devido à menor solubilidade relativa, ambos são contemporaneamente precipitados ao longo da frente de alteração, conforme a Equação 5.1:

$$(ZrMSiO_4)_{SS} \rightarrow (Zircão\ pobre\ em\ M) \pm (MSiO_4\ pobre\ em\ Zr) \pm Zr_{aq} \pm M_{aq}$$

(Equação 5.1)

No caso do zircão, como a estrutura cristalina do reagente e do produto é idêntica, há a preservação da forma externa e das dimensões do cristal.

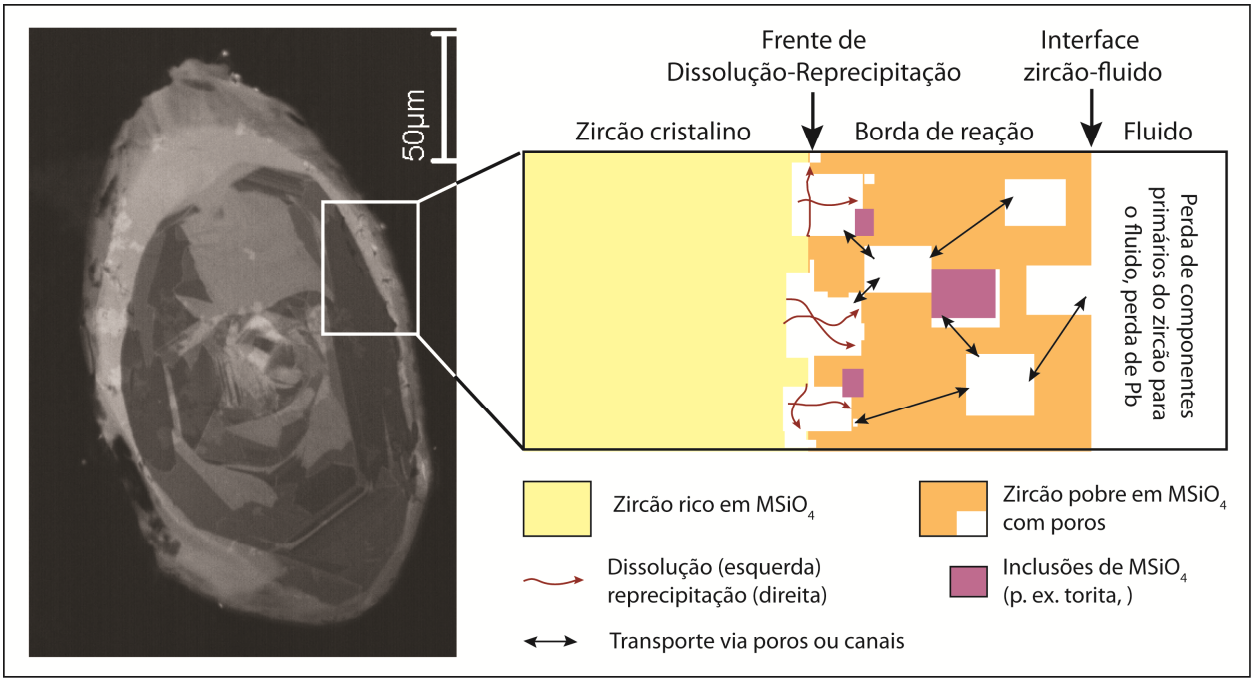

Figura 5.3 - Processo de dissolução-reprecipitação concomitante (modificado de Geisler *et al.*, 2007). O processo envolve a dissolução de zircão rico em $MSiO_4$ e a concomitante precipitação de zircão puro e inclusões de $MSiO_4$. O zircão (amostra CAFEL) apresenta inclusões representadas por zonas com catodoluminescência mais elevada, feição característica deste tipo de recristalização. Ressalta-se que a recristalização se dá localmente (em escala de µm) e envolve transporte restrito.

Esse mecanismo é, ainda, responsável pela geração de porosidade, visto que componentes como elementos terras-raras e Pb são perdidos para o fluido (Equação 5.1; Figura 5.3). Com isso, o meio torna-se permeável, o que permite que a reação prossiga rumo ao núcleo do cristal, enquanto houver fluido disponível na interface entre as fases envolvidas.

Conclui-se, portanto, que a recristalização de zircão por dissolução-reprecipitação concomitante promove importantes mudanças texturais e composicionais no zircão. Tal fato traz conseqüências principalmente para a datação, uma vez que há perda dos componentes essenciais do sistema U-Pb e, portanto, da informação isotópica original. Dessa forma, idades individuais

obtidas em grãos recristalizados devem ser interpretadas com cautela, pois estas podem não representar episódios geológicos reais.

5.3. Evidências dos complexos Anápolis-Itauçu e Serra da Malacacheta-Barro Alto

A aplicação de diversos métodos analíticos em zircão de rochas máfico-ultramáficas acamadadas dos complexos Anápolis-Itauçu e Serra da Malacacheta-Barro Alto revelaram a ocorrência de domínios recristalizados em todos os grãos, cujo desenvolvimento foi atribuído ao episódio metamórfico de alto grau. Conforme discutido no item anterior, o mecanismo de difusão intragranular não é eficiente em zircão, mesmo sob temperaturas elevadas, e, destarte, a recristalização pelo processo de dissolução-reprecipitação é mais provável em tais condições.

Além disso, as características texturais e químicas dos cristais analisados são também favoráveis a esta interpretação. Inicialmente, o imageamento por catodoluminescência revela feições internas complexas, mesmo em amostras que ainda preservam parcialmente as texturas primárias (DM-16 e BAL-09). Observa-se o desenvolvimento de zonas externas irregulares e reentrâncias, com limites agudos, que migram da borda para o núcleo do cristal (vide Figuras 3.10 e 4.3). Nas porções recristalizadas, zonações tipicamente magmáticas são interrompidas e sobrepostas por um domínio de textura homogênea, no qual é comum a presença de poros de poucos μm de dimensão, além de inclusões minerais variadas.

Os resultados de datação U-Pb em zircão, por outro lado, não permitem a distinção geocronológica dos domínios preservados ou alterados dos cristais, independente da amostra em questão. Nas duas áreas de estudo, há um espalhamento de idades na concórdia que geralmente supera o intervalo de 80 Ma (Figuras 3.11 e 4.4) e, no caso de dados discordantes, como nas amostras do Complexo Serra da Malacacheta (BAL-09 e BAL-04; Figura 4.4), os mesmos tendem para o intercepto inferior da discordia.

Entretanto, análises de Hf em zircão têm sido aplicadas com sucesso na distinção de idades ígneas e metamórficas em situações geológicas similares às descritas neste estudo (Gerdes & Zeh, 2009; Xia *et al.*, 2009). Tal fato decorre da independência entre os sistemas Lu-Hf e U-Pb, decorrente do intenso controle cristaloquímico nas substituições iônicas no zircão (Hoskin & Schaltegger, 2003). Consequentemente, o metamorfismo de alto grau não altera a informação do sistema Lu-Hf (Gerdes & Zeh, 2009). Deste modo, a assinatura isotópica de Hf em zircão reflete

as condições operantes no magma quando da cristalização do mesmo e, portanto, é possível individualizar cada evento de novo crescimento de zircão.

Nas amostras analisadas a assinatura isotópica de Hf é homogênea, mesmo frente à ampla variação das idades U-Pb (vide Figuras 3.12 e 4.6). Além disso, domínios texturais distintos, revelados por catodoluminescência, apresentam razões $^{176}Hf/^{177}Hf_t$ idênticas dentro do erro analítico, o que indica que o zircão cristalizou-se em um único episódio e a partir de um magma de composição isotópica homogênea. Assim, os dados de Hf evidenciam que o "rejuvenescimento" progressivo observado nas idades não está relacionado a novas etapas de cristalização, porém reflete que houve recristalização dos grãos durante o metamorfismo de alto grau, o qual promoveu o reequilíbrio do sistema U-Pb. Portanto, a assinatura Lu-Hf sugere que as idades mais antigas de cada população sejam representativas do episódio de magmatismo. Contudo, este preceito somente será verdadeiro caso as datações tenham representatividade estatística no grupo de amostras em questão. Todavia, essa premissa é satisfeita nas duas áreas de estudo (Complexo Anápolis-Itauçu: 670 Ma, n=4; C. Serra da Malacacheta: 1300 Ma, n=5; C. Barro Alto: 800 Ma, n=8).

Finalmente, a composição de elementos traço em zircão, disponível apenas para os complexos Serra da Malacacheta e Barro Alto, revela que, entre os domínios preservados e zonas recristalizadas, não há variação das razões elementares, somente uma diminuição no conteúdo absoluto de cada elemento. Ainda, a distribuição dos elementos terras-raras pesados no zircão é incoerente com o equilíbrio químico com a assembléia mineral do pico metamórfico, em especial a granada, e, por conseguinte, verifica-se que o quimismo original permaneceu parcialmente preservado na maioria dos cristais. A exceção é a amostra do anfibolito Cafelândia, na qual se identifica um segundo evento de recristalização de zircão, provavelmente resultante da percolação de fluidos hidrotermais relacionados a granitos e pegmatitos tardi-tectônicos (Fuck *et al*., 1981). Deste modo, a preservação mesmo que parcial da assinatura geoquímica primária indica que os mecanismos responsáveis pela recristalização não foram isolados no espaço e no tempo e, portanto, corroboram a interpretação de que a alteração se deu por meio de dissolução-reprecipitação concomitante. Neste processo as impurezas incorporadas no retículo cristalino foram progressivamente expulsas, o que deu origem a zircão mais puro, conforme explicitado no item anterior.

Dessa forma, interpreta-se que o processo de dissolução-reprecipitação concomitante seja o responsável pelo desenvolvimento das feições físicas, químicas e isotópicas descritas em zircão dos complexos Anápolis-Itauçu e Serra da Malacacheta-Barro Alto.

6. CONCLUSÕES

A partir do estudo de cristais de zircão dos complexos Anápolis-Itauçu e Serra da Malacacheta-Barro Alto verificou-se que o problema geocronológico identificado em ambas as unidades é reflexo do processo de metamorfismo de alto grau, o qual alterou o sistema isotópico U-Pb deste mineral e promoveu, consequentemente, a perda parcial da informação isotópica. Por este motivo, as idades obtidas não permitiram a individualização dos eventos de cristalização magmática e da alteração metamórfica, visto que os valores distribuíram-se progressivamente por intervalos superiores a 80 Ma. Além disso, apesar de as razões Th/U mostrarem-se amplamente variáveis nas populações investigadas, estas não apresentaram qualquer correlação com idades U-Pb e, portanto, foram inconclusivas na determinação de domínios metamórficos em zircão em ambas as áreas de estudo.

Dessa forma, investigações complementares revelaram-se fundamentais para a distinção da *real-idade* geológica contida nos cristais de zircão.

Inicialmente, o imageamento por catodoluminescência ou por elétrons retro-espalhados revelou, em ambas as áreas de estudo, a presença de bordas irregulares, luminescentes e de aspecto homogêneo, que migram da borda rumo ao centro do cristal, bem como reentrâncias que obliteraram a zonação primária do cristal. Além disso, identificaram-se possível porosidade e inclusões minerais relacionadas aos domínios alterados.

A assinatura isotópica de Hf em zircão, por outro lado, resultou em razões $^{176}Hf/^{177}Hf_t$ e valores de ε_{Hft} homogêneos, independente do domínio analisado de cada grão, implicando que, em cada amostra analisada, os cristais formaram-se durante um único episódio de cristalização. Dessa forma, a composição isotópica primária de Hf manteve-se preservada, apesar do metamorfismo de alto grau superimposto e, com base nesta evidência, sugeriu-se que o grupo de idades mais antigas obtidas seria representativo do magmatismo máfico em cada área.

Adicionalmente, nos complexos Serra da Malacacheta-Barro Alto, análises pontuais de química de zircão evidenciaram que as bordas alteradas apresentam concentrações de elementos traço inferiores a zonas preservadas do grão. Porém, as razões elementares mantiveram-se preservadas, indicando que não se atingiu o equilíbrio químico com as demais fases minerais ou com o magma/fluido durante o metamorfismo.

Destarte, evidências texturais, isotópicas e geoquímicas indicam que, durante o metamorfismo de alto grau, o processo de dissolução-reprecipitação concomitante promoveu a alteração dos cristais de zircão. Por meio deste mecanismo, elementos traço incorporados ao retículo cristalino no momento de cristalização, como Th, U e elementos terras raras, bem como Pb, oriundo do decaimento radioativo, foram progressivamente suprimidos a fim de reduzir a energia livre dos grãos. Como este processo não foi completo, perdeu-se parcialmente a informação isotópica e química primária. Portanto, este estudo revelou que as idades intermediárias, distribuídas ao longo de cerca de 80 Ma, constituem uma situação intermediária entre a cristalização ígnea e a recristalização metamórfica e, por conseguinte, não representam um episódio geológico particular.

6.1.Implicações analíticas

A observação de que o zircão pode ser recristalizado durante o metamorfismo de alto grau influencia consequentemente a escolha do procedimento analítico utilizado para a datação.

O método de diluição isotópica (ID-TIMS) constitui a técnica mais difundida na geocronologia devido à elevada precisão das análises. Entretanto, este procedimento baseia-se na dissolução completa da amostra e, por vezes, mais de um grão é utilizado para compor a fração analítica. Com isso, além de impedir a caracterização de texturas internas por catodoluminescência, este método promove a homogeneização isotópica do cristal analisado e, no caso de zircão recristalizado, a informação dos domínios alterados e preservados do grão é combinada, gerando idades mistas e sem significado geológico. Ainda, visto que é uma técnica destrutiva, não é possível realizar análises suplementares na mesma amostra. Logo, estas particularidades restringem a utilização do método de diluição isotópica para a datação em situações de recristalização por dissolução-reprecipitação concomitante.

Por outro lado, análises U-Pb *in situ* obtidas por LA-ICPMS e SHRIMP resultam em elevada resolução espacial e, quando aliadas ao imageamento por catodoluminescência, permitem a seleção das áreas de especial interesse para a datação, distinguindo domínios alterados e preservados do cristal. Entretanto, observa-se que mesmo em setores cuja textura interna é interpretada como primária obtêm-se resultados intermediários, sugestivos do processo de recristalização. Por conseguinte, o cálculo de idades concórdia a partir destes grãos resulta em

um valor que representa apenas a condição estatística mais provável para o grupo de pontos selecionados, e não um episódio geológico.

Assim, evidencia-se a necessidade da aplicação de técnicas adicionais para a correta interpretação das idades U-Pb, mesmo com a utilização de métodos de datação pontuais como LA-ICPMS e SHRIMP.

6.2. Implicações geotectônicas

A reinterpretação dos dados U-Pb em zircão frente aos processos de recristalização operantes durante o metamorfismo de alto-grau resultou, ainda, em importantes implicações geológicas para a Faixa Brasília.

Complexo Anápolis-Itauçu

Datações do volumoso magmatismo máfico presente no Complexo Anápolis-Itauçu eram inexistentes e, assim sendo, utilizavam-se idades obtidas em intrusões similares do Arco Magmático de Goiás, em torno de 630 Ma, como uma aproximação para este episódio magmático. Entretanto, os novos dados U-Pb em zircão obtidos nas intrusões acamadadas de Damolândia e Taquaral revelaram idades de cristalização mais antigas, próximas a 670 Ma. Valores análogos já haviam sido reportados para a intrusão máfico-ultramáfica acamadada Córrego Lageado, nos terrenos do Arco de Goiás (672 ± 6 Ma; Hollanda *et al.*, 2003) e, dessa forma, a conexão dos resultados sugere que é possível que um evento prévio de magmatismo máfico tenha ocorrido na Faixa Brasília.

Adicionalmente, datações realizadas em cristais de zircão de paragranulitos de temperatura ultra-alta aproximam-se deste episódio magmático mais antigo. Nestes cristais, a assinatura geoquímica revela que a cristalização deu-se em equilíbrio com as demais fases minerais metamórficas, em especial granada, em uma etapa progressiva da trajetória P-T (Möller *et al.*, 2006; Zack *et al.*, 2006). Por conseguinte, este fato sugere que o pico do metamorfismo também seja anterior ao atualmente aceito, em torno de 645 Ma (Piuzana *et al.*, 2003a).

Destarte, frente aos novos dados U-Pb em zircão de intrusões máficas do Complexo Anápolis-Itauçu, surgem duas implicações geológicas significativas para o entendimento da evolução geotectônica da Faixa Brasília. Primeiro, os dados indicam que pelo menos parte do magmatismo máfico observado no Complexo Anápolis-Itauçu ocorreu concomitantemente ao

metamorfismo de alto grau e, portanto, estas intrusões revelam-se como promissoras fontes adicionais de calor, necessárias para a formação de assembléias minerais de temperatura ultra-alta nos paragranulitos contíguos. Assim, corrobora-se a interpretação de que a Faixa Brasília representa um orógeno acrescionário quente, no qual episódios de extensão intercalam-se ao movimento dominantemente colisional e resultam na ascensão da astenosfera (Pimentel *et al.*, 2003), proporcionando volumoso magmatismo máfico e metamorfismo de alto grau concomitante (Collins, 2002; Hyndmann *et al.* 2005).

Em segundo lugar, a conjunção dos resultados reflete que possam ter ocorrido etapas distintas de magmatismo-metamorfismo na evolução da Faixa Brasília, sobretudo se considerada a "alternância tectônica"[1] descrita em orógenos quentes (Collins, 2002; Hyndmann *et al.*, 2005). Porém, uma investigação mais profunda, que envolva o refinamento do mapeamento geológico-estrutural, além da datação sistemática e fundamentada em métodos suplementares, vê-se necessária para corroborar esta hipótese.

Complexos Serra da Malacacheta e Barro Alto

As informações geocronológicas obtidas em amostras dos complexos Serra da Malacacheta e Barro Alto confirmaram em parte as interpretações de investigações anteriores (Pimentel *et al.*, 2004; Pimentel *et al.*, 2006; Ferreira Filho *et al.*, 2010). Assim, reafirmou-se que duas intrusões distintas compõem este corpo acamadado, o Complexo Serra da Malacacheta, cristalizado em torno de 1300 Ma, e o Complexo de Barro Alto, cujo magmatismo é datado em 800 Ma. Estas rochas foram metamorfisadas em aproximadamente 750 Ma, conforme revelado por titanita do Complexo Serra da Malacacheta e domínios recristalizados de zircão das duas unidades, o que confirma a sugestão de que os complexos já se encontravam justapostos quando do metamorfismo de alto grau. Confirmou-se, dessa forma, que o contexto geológico e geocronológico é análogo ao descrito no complexo Serra dos Borges-Niquelândia, exposto ao norte, o que implica que ambos os corpos compunham o mesmo cinturão máfico-ultramáfico acamadado, desmembrado durante a orogenia Brasiliana.

[1] Do inglês *tectonic switching* (Collins, 2002).

Entretanto, os dados U-Pb foram inconclusivos em duas das amostras investigadas e somente a aplicação de métodos suplementares permitiu a correta identificação das idades de cristalização.

Metanortositos, apesar de sempre descritos na unidade Mesoproterozóica, haviam sido datados no Neoproterozóico (Correia *et al.*, 2007). Porém, os dados espalhavam-se entre 800 Ma e 730 Ma, revelando, portanto, um problema geocronológico. Deste modo, selecionou-se uma amostra de afloramento equivalente ao previamente datado que rendeu idades dispersas ao longo de uma linha de perda de Pb entre 1200 Ma e 750 Ma. Contudo, a assinatura isotópica de Hf e a composição química de zircão mostraram-se homogêneas, independente do resultado U-Pb obtido no grão, o que indica que estes cristais estiveram envolvidos em um único episódio de cristalização. Portanto, durante o metamorfismo houve apenas a recristalização do zircão, a qual promoveu a destruição parcial da informação geocronológica. Assim, os novos dados permitiram o reposicionamento do metanortosito no Complexo Serra da Malacacheta, formado no primeiro evento magmático.

Por outro lado, a inserção do anfibolito Cafelândia no Complexo Serra da Malacacheta era advogada em função da similaridade da assinatura isotópica de Nd com os anfibolitos da Sequência Juscelândia (Moraes *et al.*, 2003). Todavia, os resultados apresentados neste estudo revelaram apenas idades neoproterozóicas, distribuídas entre 800 Ma e 740 Ma. As razões isotópicas de Hf mostraram-se novamente homogêneas, apesar do espalhamento dos dados U-Pb, e forneceram ainda valores extremamente positivos de ε_{Hf} (+8 a +10) e idades modelo T_{DM} de ~ 1300 Ma. Logo, estes dados confirmaram que o protolito máfico formou-se a partir de um magma depletado, conforme previamente estabelecido (Moraes *et al.*, 2003), porém atestaram idade de cristalização neoproterozóica, relacionada ao segundo episódio de magmatismo máfico, para o protolito do anfibolito Cafelândia.

Deste modo, os aspectos isotópicos e geocronológicos do Complexo Barro Alto favorecem um contexto de retro-arco para o episódio magmático Neoproterozóico. Assim, a hipótese do orógeno quente revela-se novamente coerente com a geração concomitante de volumoso magmatismo máfico e metamorfismo de temperatura ultra-alta.

7. BIBLIOGRAFIA CONSULTADA

Albarède, F., Telouk, P., Blichert-Toft, J., Boyet, M., Agranier, A., Nelson, B. 2004. Precise and accurate isotopic measurements using multiple collector ICPMS. Geochimica et Cosmochimica Acta, 68: 2725-2744.

Araújo, S.M. 1996. Geochemical and isotopic characteristics of alteration zones in highly metamorphosed volcanogenic massive sulfide deposits and their potential application to mineral exploration. Unpublised Ph.D. Thesis, Department of Geology, University of Toronto, Canada, 210 pp.

Ashwal, L.D., Tucker, R.D. & Zinner, E.K., 1999. Slow cooling of deep crustal granulites and Pb-loss in zircon. Geochimica et Cosmochimica Acta, 63(18), 2839 -2851.

Ayers, J.C., DelaCruz, K., Miller, C., Switzer, O. 2003. Experimental study of zircon coarsening in quartzite +- H2O at 1.0 GPa and 1000C, with implications for geochronological studies of high-grade metamorphism. American Mineralogist, 88, 365-376.

Baldwin, J.A. & Brown, M., 2008. Age and duration of ultrahigh-temperature metamorphism in the Anápolis–Itauçu Complex, Southern Brasília Belt, central Brazil - constraints from U-Pb geochronology, mineral rare earth element chemistry and trace element thermometry. Journal of Metamorphic Geology, 26, 213-233.

Baldwin, J.A., Powell, R., Brown, M., Moraes, R., Fuck, R.A. 2005. Modelling of mineral equilibra in ultrahigh-temperature metamorphic rocks from the Anápolis-Itauçu Complex, central Brazil. Journal of Metamorphic Geology, 23, 511-531.

Bea, F., Montero, P., Ortega, M. 2006. A LA–ICP–MS evaluation of Zr reservoirs in common crustal rocks: implications for Zr and Hf geochemistry, and zircon-forming processes. The Canadian Mineralogist, 44: 693-714.

Beaumont, C., Jamieson, R A., Nguyen, M H., Lee, B. 2001. Himalayan tectonics explained by extrusion of a low-viscosity channel coupled to focused surface denudation. Nature, 414, 738-742.

Beaumont, C., Ngugen, M H., Jamieson, R A., Ellis, S 2006. Crustal flow modes in large hot orogens. In: Channel Flow, Ductile Extrusion and Exhumation in Continental Collision Zones. Geological Society of London Special Publication, 268, 91-145.

Belousova, E.A., Griffin, W.L., O´Reilly, S.Y. 2006. Zircon crystal morphology, trace element signatures and Hf isotope composition as a tool for petrogenetic modelling: examples from Eastern Australian Granitoids. Journal ou Petrology, 47 (2): 329-353.

Bingen, B., Austrheim, H. & Whitehouse, M., 2001. Ilmenite as a Source for Zirconium during High-grade Metamorphism? Textural Evidence from the Caledonides of Western Norway and Implications for Zircon Geochronology. Journal of

Black, L.P., Kamo, S. L., Allen, C. M., Davis, D. W., Aleinikoff, J. N., Valley, J. W., Mundil, R., Campbell, I. H., Korsch, R. J., Williams, I. S., Foudoulis, C. 2004. Improved 206 Pb/ 238 U microprobe geochronology by the monitoring of a trace-element-related matrix effect; SHRIMP, ID–TIMS, ELA–ICP–MS and oxygen isotope documentation for a series of zircon standards. Chemical Geology, 205, 115 - 140.

Blichert-Toft, J., Chauvel, C. & Albarède, F., 1997. Separation of Hf and Lu for high-precision isotope analysis of rock samples by magnetic sector-multiple collector ICPMS. Contrib. Mineral. Petrol., 127(3), 248-260.

Brito Neves, B.B. & Cordani, U.G., 1991. Tectonic evolution of South America during the late Proterozoic. Precambrian Research, 53: 23-40.

Brod, J.A., Jost, H., 1991. Características estruturais, litológicas e magmáticas da zona de cisalhamento dúctil do Rio Traíras, bloco do Complexo Niquelândia, Goiás. Revista Brasileira de Geociências 21, 205–217 (in Portuguese with abstract in English).

Brown, M. 2007. Metamorphic conditions in orogenic belts: a record of secular change. International Geology Review, 49: 193-234.

Bühn, B., Pimentel, M. M., Matteini, M., Dantas, E. L. 2009. High spatial resolution analysis of Pb and U isotopes for geochronology by laser ablation multi-collector inductively coupled plasma mass spectrometry (LA-MC-ICP-MS). Anais Da Academia Brasileira De Ciencias, 81, 1-16.

Cherniak, D.J. & Watson, E.B. 2003. Diffusion in zircon. Zircon. Reviews in Mineralogy and Geochemistry, 53, 113-143.

Cherniak, D.J.; Hanchar, J.M.; Watson, E.B. 1997. Diffusion of tetravalent cations in zircon. Contributions to Mineralogy and Petrology, 127: 383-390

Collins, W.J., 2002. Hot orogens, tectonic switching, and creation of continental crust. Geology, 30, 535-538.

Compston, W.,Williams, I.S., Kirschvink, J.L., Zhang, Z.C., Ma, G.G. 1992. Zircon U-Pb ages for the Early Cambrian time-scale. Journal of the Geological Society of London, 149, 171–184.

Corfu, F., Hanchar, J. M., Hoskin, P. W. O., Kinny, P. 2003. Atlas of Zircon Textures. Reviews in Mineralogy and Geochemistry, 53, 469-500.

Correia, C.T., Girardi, V.A.V., Basei, M.A.S., Nutman, A., 2007. Cryogenian UPb (SHRIMP I) zircon ages of anorthosites from the upper sequences of Niquelândia and Barro Alto complexes, central Brazil. Rev. Bras. Geociências 37, 70-75.

Correia, C.T., Jost, H., Tassinari, C.C.G., Girardi, V.A.V., Kinny, P., 1999. Ectasian Mesoproterozoic U–Pb ages (SHRIMP-II) for the metavolcanosedimentary sequences of Juscelândia and Indaianópolis and for high-grade metamorphosed rocks of Barro Alto stratiform igneous complex, Goiás State, central Brazil. In: SAAGI—South American Symposium on Isotopic Geology, v. 2. Actas SEGEMAR, Córdoba, p. 31–33.

Correia, C.T.; Tassinari, C.C.G.; Lambert, D.D.; Kinny, P.; Girardi, V.A.V. 1997. U-Pb (SHRIMP-II), Sm-Nd and Re-Os systematic of the Cana Brava, Niquelândia and Barro Alto layered intrusions in Central Brazil and constraints on the tectonic evolution. In: I SSAGI, Extended Abstracts, Campos do Jordão, pp. 88-89.

Danni, J.C.M., Fuck, R.A., Kuyumjian, R.M., Leonardos, O.H., Winge, M., 1984. O Complexo de Barro Alto na região de Ceres-Rubiataba, Goiás. Rev. Bras. Geociências 14, 128–136.

Danni, J.C.M., Fuck, R.A., Leonardos Jr., O.H., 1982. Archean and lower Proterozoic Units in Central Brazil. Geol. Rundsch. 71, 291–317.

Degeling, H., Eggins, S. & Ellis, D.J., 2001. Zr budgets for metamorphic reactions, and the formation of zircon from garnet breakdown. Mineralogical Magazine, 65(6), 749-758.

DePaolo, D.J., 1981. A neodymium and strontium isotopic study of the Mesozoic calc-alkaline granitic batholiths of the Sierra Nevada and Peninsular Ranges, California. J. Geophysical Research, 86, 10470-10488.

Erambert, M. & Austrheim, H. 1993. The effect of fluid and deformation on zoning and inclusion patterns in poly-metamorphic garnet. Contributions to Mineralogy and Petrology, 115: 204-214.

Ferreira Filho, C. F. 1998. Geology and Petrology of the large layered intrusions of Central Brazil, implications for PGE mineralization. VIII Platinum Symposium, Extended Abstracts, pp. 107-110.

Ferreira Filho, C.F. & Pimentel, M.M., 2000. Sm–Nd isotope systematics and REE–Hf–Ta–Th data of troctolites and their amphibolitized equivalents of the Niquelândia Complex upper layered series, central Brazil: further constraints for the timing of magmatism and high-grade metamorphism. J. South Am. Earth Sci. 13, 647–659.

Ferreira Filho, C.F., Kamo, S., Fuck, R.A., Krogh, T.E., Naldret, A.J., 1994. Zircon and rutile geochronology of the Niquelândia layered mafic and ultramafic intrusion, Brazil: constraints for the timing of magmatism and high grade metamorphism. Precambrian Res. 68, 241–255.

Ferreira Filho, C.F., Moraes, R., Fawcett, J.J., Naldrett, A.J., 1998. Amphibolite to granulite progressive metamorphism in the Niquelândia Complex, Central Brazil: regional tectonic implications. Journal of South American Earth Science, 11 (1): 35-50.

Ferreira Filho, C.F.; Pimentel, M.M.; Araújo, S.M.; Laux, J.H. 2010. Layered Intrusions and Volcanic Sequences in Central Brazil: Geological and Geochronological Constraints for Mesoproterozoic (1.25 Ga) and Neoproterozoic (0.79 Ga) Igneous Associations. Precambrian Research, in press.

Ferry, J.M. & Watson, E.B., 2007. New thermodynamic models and revised calibrations for the Ti-in-zircon and Zr-in-rutile thermometers. Contrib. Mineral. Petrol., 154, 429-437.

Förster, H.J. 2006. Composition and origin of intermadiate solid solutions in the system thorite-xenotime-zircon-coffinite. Lithos, 88: 35-55.

Förster, H.J. & Harlov, D. 2009. Monazite (Ce)-huttonite solid solutions in granulite facies metabasites from the Ivrea-Verbano Zone, Italy. Mineralogical Magazine, 63: 587-594.

Fraser, G., Ellis, D. & Eggins, S., 1997. Zirconium abundance in granulite-facies minerals, with implications for zircon geochronology in high-grade rocks. Geology, 25, 607-610.

Fu, B.; Page, F.Z.; Cavosie, A.J.; Fournelle, J.; Kita, N.T.; Lackey, J.S.; Wilde, S.A.; Valley, J.W. 2008. Ti-in-zircon thermometry: applications and limitations. Contributions to Mineralogy and Petrology, 156: 197-215.

Fuck R.A., Pimentel M.M., Silva L.J.H.D., 1994. Compartimentação tectônica da porção oriental da Província Tocantins. In: 38th Cong. Bras. Geologia, v. 1, p. 215–216.

Fuck, R.A., Danni, J.C.M., Winge, M., Andrade, G.F., Barreira, C.F., Leonardos, O.H., Kuyumjian, R.M., 1981. Geologia da Região de Goianésia. In: 1st Simp. Geologia do Centro-Oeste, p. 447–467.

Geisler, T., Schaltegger, U. & Tomaschek, F., 2007. Re-equilibration of Zircon in Aqueous Fluids and Melts. Elements, 3, 43-50.

Geisler, T., Trachenki, K., Rios, S., Dove, M.T., Salje, E.K.H. 2003. Experimental hydrothermal alteration of partially metamict zircon. American Mineralogist, 88, 1496-1513.

Gerdes, A. & Zeh, A., 2009. Zircon formation versus zircon alteration — New insights from combined U–Pb and Lu–Hf in-situ LA-ICP-MS analyses, and consequences for the interpretation of Archean zircon from the Central Zone of the Limpopo Belt. Chemical Geology, 261, 230-243.

Gioia, S.M. & Pimentel, M.M., 2000. The Sm-Nd isotopic method in the Geochronology Laboratory of the University of Brasília. Anais da Academia Brasileira de Ciências, 72(2), 219-254.

Girardi, V.A.V., Rivalenti, G., Sinigoi, S., 1986. The petrogenesis of the Niquelândia layered basic-ultrabasic complex, Central Goiás, Brazil. J. Petrol. 27, 715–744.

Giustina, M.E.S.D., Oliveira, C.G., Pimentel, M.M., Buhn, B. 2009. Neoproterozoic magmatism and high-grade metamorphism in the Goiás Massif: NewLA-MC-ICMPS U–Pb and Sm–Nd data and implications for collisional history of the Brasília Belt. Precambrian Research, 172, 67-79.

Griffin, W. L., Pearson, N. J., Belousova, E., Jackson, S. E., Van Achterbergh, E., O'reilly, S., Shee, S. R. 2000. The Hf isotope composition of cratonic mantle: LAM-MC-ICPMS analysis of zircon megacrysts in kimberlites. Geochimica et Cosmochimica Acta, 64: 133-147

Harley, S.L., 1998. On the occurrence and characterization of ultrahigh-temperature crustal metamorphism. Geological Society of London Special Publication, 138, 81-107.

Harley, S.L., 2004. Extending our understanding of Ultrahigh temperature crustal metamorphism. Journal of Mineralogical and Petrological Sciences, 99, 140-158.

Harley, S.L., 2008. Refining the P–T records of UHT crustal metamorphism. Journal of Metamorphic Geology, 26, 125-154.

Harley, S.L & Kelly, N.M. 2007. The impact of zircon-garnet REE distribution data on the interpretation of zircon U-Pb ages in complex high-grade terranes: an example from the Rauer Islands, East Antarctica. Chemical Geology, 241: 62-87.

Harley, S.L.; Kelly, N.M.; Möller, A. 2007. Zircon behavior and the thermal histories of mountain chains. Elements, 3(1): 25-30.

Harlov, D.E. 2009. Metasomatic alteration of monazite and xenotime in fluids: the role of coupled dissolution-reprecipitation versus volume diffusion. In: Programme and Abstracts, Micro-Analysis, Processes and Time, Edinburgh, p. 91-92.

Harrison, T. M., Watson, E. B., Aikman, A. B., 2007. Temperature spectra of zircon crystallization in plutonic rocks. Geology, 35 (7): 635-638.

Hoffman, A.E., Valley, J.W., Watson, E.B., Cavosie, A.J., Eiler, J.M. 2009. Sub-micron scale distributions of trace elements in zircon. Contributions to Mineralogy and Petrology, 158: 317-335.

Hollanda, M.H.B.M., Pimentel, M.M., Armstrong, R. 2003. Isotopic and geochronological constraints for the origin of syn- to post-Brasiliano mafic magmatism and crustal re-melting in the Brasília Belt, Central Brazil. In: Extended abstracts, IV SSAGI, Salvador, p. 194-197.

Hoskin, P.W. & Black, L.P., 2000. Metamorphic zircon formation by solid-state recrystallization of protolith igneous zircon. Journal of Metamorphic Geology, 18, 423-439.

Hoskin, P.W. & Schaltegger, U., 2003. The Composition of Zircon and Igneous and Metamorphic Petrogenesis. Reviews in Mineralogy and Geochemistry, 53, 28-62.

Hyndman, R.D.; Currie, C.A.; Mazzotti, S.P. 2005. Subduction zone backarcs, mobile belts and orogenic heat. GSA Today, 15 (2): 4-10.

Jackson, S.E., Pearson, N. J.; Griffin, W. L.; Belousova, E. A. 2004. The application of laser ablation-inductively coupled plasma-mass spectrometry to in situ U–Pb zircon geochronology. Chemical Geology, 211, 47 - 69.

Jamieson, R.A., Beaumont, C.; Medvedev, S., Nguyen, M.H. 2004. Crustal channel flows. 2. Numerical models with implications for metamorphism in the Himalayan–Tibetan orogen. Journal of Geophysical Research, 109.

Jamieson, R.A., Fullsack, P.; Lee, B. 1998. Barrovian regional metamorphism: where's the heat? Geological Society of London Special Publication, 138, 23-51.

Jochum, K.P., Nohl, U., Herwig, K., Lammel, E., Stoll, B., Hofmann, A.W. 2005. GeoREM: A new geochemical database for Reference Materials and Isotopic Standards. Geostandards and Geoanalytical Research, 29 (3): 333-338.

Junges, S.L. Pimentel, M.M.; Moraes, R. 2002. Nd isotopic study of the Neoproterozoic Mara Rosa Arc, Central Brazil: implications for the evolution of the Brasília Belt. Precambrian Research, 117: 101-118.

Kelly, N.M. & Harley, S.L., 2005. An integrated microtextural and chemical approach to zircon geochronology: refining the Archaean history of the Napier Complex, east Antarctica. Contrib. Mineral. Petrol., 149, 57-84.

Kelsey, D.E. 2008. On ultrahigh-temperature crustal metamorphism. Gondwana Research, 13: 1-29.

Kinny, P.D. & Maas, R. 2003. Lu-Hf and Sm-Nd isotope system in zircon. Reviews in Mineralogy and Geochemistry, 53: 327-341.

Krogh T E, 1973. A low-contamination method for hydrothermal decomposition of zircon and extraction of U and Pb for isotopic age determinations. Geochimica et Cosmochimica Acta, 37, 485-494.

Laux, J.H., Pimentel, M.M., Dantas, E.L., Armstrong, R. Armele, A., Nilson, A.A. 2004. Mafic magmatism associated with the Goiás magmatic arc in the Anicuns region, Goiás, central Brazil central Brazil: Sm–Nd isotopes and new ID-TIMS and SHIMP U–Pb data. Journal of South American Earth Sciences, 16, 599-614.

Laux, J.H., Pimentel, M.M., Dantas, E.L., Armstrong, R., Armele, A. 2003. Mafic magmatism associated with the Goiás Magmatic Arc in Anicuns-GO, Central Brazil: new ID-TIMS and SHRIMP U-Pb data. In: Extended abstracts, IV SSAGI, Salvador, p. 575-578.

Lima, R.P., Moraes, R., Fuck, R.A. 2008. A Influência do quartzo nas reações de fusão de rochas máficas com hornblenda: exemplo do anfibolito Cafelândia, Complexo Barro Alto, Goiás. In: Anais, 44º Congresso Brasileiro de Geologia, Curitiba.

Lippmann, F. 1980 Phase diagrams depicting the aqueous solubility of mineral systems. Neues Jahrb Mineral Abh 139:1-25.

Ludwig, K.R. 1993. PBDAT. A computer program for processing Pb-U-Th isotope data. *USGS Open File Report*, **88-542**, p. 34.

Ludwig, K.R. 2001a. Squid 1.02. A User's Manual. BGC Special Publication 2, Berkeley, 19 pp.

Ludwig, K.R. 2003 User's Manual for Isoplot/Ex v. 3.00. A Geochronological Toolkit for Microsoft Excel. BGC Special Publication 4, Berkeley, 71 pp.

Martin, L.A., Duchene, S., Deloule, E., Vanderhaeghe, O. 2008. Mobility of trace elements and oxygen in zircon during metamorphism: Consequences for geochemical tracing. Earth and Planetary Science Letters, 267, 161 - 174.

Matteini, M., Junges, S.L., Dantas, E.L., Pimentel, M.M., Buhn, B. 2009. In situ zircon U–Pb and Lu–Hf isotope systematic on magmatic rocks: Insights on the crustal evolution of the Neoproterozoic Goiás Magmatic Arc, Brasília belt, Central Brazil. Gondwana Research.

Mezger, K. & Krogstad, E.J., 1997. Interpretation of discordant U-Pb ages. An evaluation. Journal of Metamorphic Geology, 15, 127-140.

Möller, A., Moraes, R., Hellebrand, E., Kennedy, A., Fuck, R.A. 2006. Age and duration of the UHT Event in the Brasilia Fold Belt: in-situ dating of zircon and rutile and equilibrium REE distribution between zircon and orthopyroxene. In Granulites & Granulites 2006. Brasilia, p. 54.

Möller, A., O'Brien, P.J., Kennedy, A., Kroner, A. 2002. Polyphase zircon in ultrahigh-temperature granulites (Rogaland, SW Norway): constraints for Pb diffusion in zircon. Journal of Metamorphic Geology, 20, 727-740.

Möller, A., O'Brien, P.J., Kennedy, A., Kröner, A. 2003. Linking growth episodes of zircon and metamorphic textures to zircon chemistry: an example from the ultrahigh-temperature granulites of Rogaland (SW Norway). Geological Society of London Special Publication, 220, 65-81.

Moraes, R., Brown, M., Fuck, R.A., Camargo, M.A., Lima, T.M., 2002. Characterization and P–T Evolution of Melt- bearing Ultrahigh-temperature Granulites: an Example from the Anápolis–Itauçu Complex of the Brasília Fold Belt, Brazil. Journal of Petrology, 43(9), 1673-1705.

Moraes, R., Fuck, R.A., 1994. Deformação e metamorfismo das sequências Juscelândia e Serra da Malacacheta, Complexo Barro Alto, Goiás. Rev. Bras. Geociêcias 24, 189–197.

Moraes, R., Fuck, R.A., 1999. Trajetória P-T Horária para o Metamorfismo da Sequência Juscelândia, Goiás: Condições do Metamorfismo e Implicações Tectônicas. Rev. Bras. Geociências 29, 603–612.

Moraes, R.D. & Fuck, R.A., 2000. Ultra-high-temperature metamorphism in Central Brazil: the Barro Alto complex. Journal of Metamorphic Geology, 18, 345-358.

Moraes, R., Fuck, R.A., Brown, M., Piccoli, P., Baldwin, J., Dantas, E.L., Laux, J.H., Junges, S. 2007. Wollastonite–scapolite–clinopyroxene marble of the Anápolis-Itauçu Complex, Goiás: more evidence of ultrahigh-temperature metamorphism. Revista Brasileira de Geociências, 37(4), 11-17.

Moraes, R., Fuck, R.A., Pimentel, M.M., Gioia, S.M.C.L., Figueiredo, A.M.G., 2003. Geochemistry and Sm–Nd isotope characteristics of bimodal volcanic rocks of Juscelândia, Goiás, Brazil: Mesoproterozoic transition from continental rift to ocean basin. Precambrian Res. 125, 317–336.

Moraes, R., Fuck, A.R., Pimentel, M.M., Gioia, S.M.C.L., Hollanda, M.H.B.M., Armstrong, R., 2006. The bimodal rift-related volcanosedimentary sequence in Central Brazil: Mesoproterozoic extension and Neoproterozoic metamorphism. J. South Amer. Earth Sci. 20, 287–301.

Morel, M.L., Nebel, O., Nebel-Jacobsen, Y.J., Miller, J.S., Vroon, P.Z. 2008. Hf isotope characterization of the GJ-1 zircon reference material by solution and laser-ablation MC-ICPMS. Chemical Geology, 255, 231-235.

Nebel, O., Nebel-Jacobsen, Y., Mezger, K., Berndt, J. 2007. Initial Hf isotope compositions in magmatic zircon from early Proterozoic rocks from the Gawler Craton, Australia: A test for zircon model ages. Chemical Geology, 241, 23 - 37.

Nilson, A.A., 1992. Geologia e aspectos petrológicos do complexo máfico-ultramáfico de Águas Claras, Araçu, Goiás. In XXXVII Congresso Brasileiro de Geologia. São Paulo, p. 457.

Nilson, A.A. & Motta, F., 1969. Geologia da área de Goianira-Trindade. DNPM, Bol. Div. Fom. Da Produção Mineral (133): 108 p.

Nystrom, A. I. & Kriegsman, L. M. 2003. Prograde and retrograde reactions, garnet zoning patterns, and accessory phase behaviour in SW Finland migmatites, with implications for geochronology. *In:* VANCE, D., MOLLER, W. & VILLA, I. M. (eds) *Geochronology: Linking the Isotopic Record with Petrology and Textures.* Geological Society London, Special Publications, 220, 213-230.

Oliveira, 1993. Petrografia, estratigrafia, petroquímica e potencialidade para Elementos do Grupo da Platina (EGP) do Complexo de Barro Alto, na região de Goianésia, Goiás. Unpublised M.Sc. dissertation, Universidade de Brasília, Brazil, 86 pp.

Oliver, N. H., Bodorkos, S., Nemchin, A. A., Kinny, P.D., Watt, G.R. 1999. Relationships between Zircon U–Pb SHRIMP Ages and Leucosome Type in Migmatites of the Halls Creek Orogen, Western Australia. Journal of Petrology, 40(10), 1553-1575.

Paces, J.B. & Miller, J.D., 1993. Precise U-Pb ages of Duluth Complex and related mafic intrusions, northeastern Minnesota: geochronological insights to physical, petrogenetic, paleomagnetic and tectonomagmatic processes associated with the 1.1 Ga mid-continent rift system. J. Geophys. Research, 98, 13997-14013.

Pearce, J.A. & Parkinson, I.J., 1993. Trace element models for mantle melting: application to volcanic arc petrogenesis. Geological Society Special Publication, 76, 373-403.

Pimentel, M.M., Ferreira Filho, C.F., Amstrong, R.A., 2004. Shrimp U–Pb and Sm-Nd ages of the Niquelândia Layered Complex: Meso (1.25 Ga) and Neoproterozoic (0.79 Ga) extensional events in Central Brazil. Precambrian Res. 132, 132–135.

Pimentel, M.M., Ferreira Filho, C.F., Armele, A., 2006. Neoproterozoic age of the Niquelândia complex, Central Brazil: Further ID-TIMS and Sm-Nd isotopic evidence. J. South Amer. Earth Sci. 21, 228–238.

Pimentel, M.M., Fuck, R.A., Jost, H., Ferreira Filho, C.F., Araújo, S.M., 2000. The basement of the Brasília Fold Belt and the Goiás Magmatic Arc. In: Cordani, U.G., Milani, E.J., Thomaz Filho, A., Campos, D.A. (Eds.), The Tectonic Evolution of South America, Rio de Janeiro. Proceedings of the 31st International Geological Congress, p. 195–229.

Pimentel, M.M., Laux, J.H., Hollanda, M.H.B.M., Gioia, S.M.C.L. 2003. The Brasília Belt as a "Hot Orogen": new SHRIMP and conventional U-Pb data and Sm-Nd isotopic constraints from terminal mafic magmatism in central-western Goiás. In III International Symp. on Tectonics. Búzios, pp. 21-23.

Piuzana, D., Pimentel, M.M., Fuck, R.A., Armstrong, R. 2003a. Neoproterozoic granulite facies metamorphism and coeval granitic magmatism in the Brasilia Belt, Central Brazil: regional implications of new SHRIMP U–Pb and Sm–Nd data. Precambrian Research, 125, 245-273.

Piuzana, D., Pimentel, M.M., Fuck, R.A., Armstrong, R. 2003b. SHRIMP U–Pb and Sm–Nd data for the Araxá Group and associated magmatic rocks: constraints for the age of sedimentation and geodynamic context of the southern Brasília Belt, central Brazil. Precambrian Research, 125, 139-160.

Pollock, K., Lloyd, G.E., Austrheim, H., Putnis, A. 2008. Complex replacement patterns in garnets from Bergen Arcs eclogites: A combined EBSD and analytical TEM study. Chemie der Erde 68:177-191

Prieto, M. 2009. Thermodynamics of solid solution-aqueous solution systems. Reviews in Mineralogy and Geochemistry 70 (1):47‑85

Putnis, A. 2002. Mineral replacement reactions: from macroscopic observations to microscopic mechanisms. Mineralogical Magazine, 66(5), 689-708.

Putnis, A. 2009. Mineral replacement reactions. Reviews in Mineralogy and Geochemistry, 70 (1): 87-124.

Putnis, A. & Putnis, C. V. 2007. The mechanism of reequilibration of solids in the presence of a fluid phase. Journal of Solid State Chemistry, 180 (5): 1783-1786.

Rivalenti, G., Correia, C.T., Girardi, V.A.V., Mazzicchelli, M., Tassinari, C.C.G., Bertotto, G.W., 2008. Sr–Nd isotopic evidence for crustal contamination in the Niquelândia complex, Goiás, Central Brazil. J. South Amer. Earth Sci. 25, 298– 312.

Roberts, M.P. & Finger, F., 1997. Do U-Pb zircon ages from granulites reflect peak metamorphic conditions? Geology, (25), 319-322.

Rubatto, D. 2002. Zircon trace element geochemistry: partitioning with garnet and the link between U-Pb ages and metamorphism. Chem. Geol, 184, 123-138.

Rubatto, D. & Hermann, J. 2003. Zircon formation during fluid circulation in eclogites (Monviso, Western Alps): Implications for Zr and Hf budget in subduction zones. Geochimica et Cosmochimica Acta, 67: 2173-2187.

Rubatto, D. & Hermann, J., 2007. Experimental zircon / melt and zircon / garnet trace element partitioning and implications for the geochronology of crustal rocks. Chemical Geology, 241, 38-61.

Rubatto, D., Müntener, O., Barnhoorn, A., Gregory, C. 2008. Dissolution-reprecipitation of zircon at low-temperature, high-pressure conditions (Lanzo Massif, Italy). American Mineralogist, Volume 93: 1519–1529

Sandiford, M. & Powell, R., 1986. Deep crustal metamorphism during continental extension: modern and ancient examples. Earth and Planetary Science Letters, 79, 151-158.

Schaltegger, U., Fanning, M., Günther, D., Maurin, J.C., Schulmann, K., Gebauer, D. 1999. Growth, annealing and recrystallization of zircon and preservation of monazite in high-grade metamorphism: conventional and in-

situ U-Pb isotope, cathodoluminescence and microchemical evidence. Contributions to Mineralogy and Petrology, 134, 186-201.

Scherer, E.E.; Whitehouse, M.J.; Münker, C. 2007. Zircon as a monitor of crustal growth. Elements, 3(1): 19-24.

Schott, B. & Schmeling, H., 1998. Delamination and detachment of a lithospheric root. Tectonophysics, 296, 225-247.

Silva, F.O., 1991. Geologia, estrutura, petrologia e mineralização de Fe, Ti e V associadas ao complexo gabro-anortosítico acamadado de Santa Bárbara (Goiás). Dissertação de Mestrado, Universidade de Brasília, 190p.

Silva, F.O., 1997. Geologia e petrologia do extremo noroeste do Complexo máfico-ultramáfico de Taquaral, GO. Tese de Doutorado, Universidade de Brasília, 171p.

Spry, A. 1969. Metamorphic textures. Pergamon Press, Oxford, 350pp.

Suita, M.T.F., 1996. Geoquímica e Metalogenia de Elementos do Grupo da Platina (EGP + Au) em Complexos Máfico-Ultramáficos do Brasil: Critérios e Guias com Ênfase no complexo Máfico-Ultramáfico Acamadado de Alto Grau de Barro Alto (CBA, Goiás). Unpublished PhD thesis. Universidade Federal do Rio Grande do Sul, Porto Alegre RS, Brazil, 600 pp.

Suita, M.T.F., Kamo, S., Kroght, T.E., Fyfe, W.S., Hartmann, L.A., 1994. U–Pb ages from the high-grade Barro Alto mafic–ultramafic complex (Goiás, central Brazil): middle Proterozoic continental mafic magmatism and upper Proterozoic continental collision. In: International Conference on Geochron. Cosmochr. Isot. Geol., ICOG, Abstracts, v. 8, Berkeley, USGS, p. 309.

Sun, S.S. & McDonough, W. F. 1989. Chemical and isotopic characteristics of oceanic basalts: implications for mantle composition and processes. In: Saunders, A.D. & Norry, M.J. (eds.): Magmatism in oceanic basins. Geological Society of London Special Publication, 42, pp. 313-345.

Thompson, A.B.; Sculmann, K.; Jezek, J.; Tolar, V. 2001. Thermally softened continental extensional zones (arcs and rifts) as precursors to thickened orogenic belts. Tectonophysics, 332: 115-141.

Tomaschek, F., Kennedy, A.K., Villa, I.M., Lagos, M., Ballhaus, C. 2003. Zircons from Syros, Cyclades, Greece: Recrystallization and Mobilization of Zircon during High-Pressure Metamorphism. Journal of Petrology, 44(11), 1977-2002.

Uher, P., Breiter, K., Kleèka, M., Pivec, E. 1998. Zircon in highly evolved Hercynian Homolka Granite, Moldanubian Zone, Czech Republic: indicator of magma source and petrogenesis. Geologica Carphatica, 49: 151-160.

Valeriano, C. M., Pimentel, M. M., Heilbron, M., Almeida, J. C. H., Trouw, R. A. J. 2008. Tectonic evolution of the Brasília Belt, Central Brazil, and early assembly of Gondwana. In: Pankhurst, R.J., Trouw, R.A.J., Brito Neves, B.B., de Wit, MJ. (eds) *West Gondwana: Prec-Cenozoic correlations acrossthe South Atlantic region.* Geological Society of London, Special Publications, 294: 197-210.

Valley, J. W 2003. Oxygen isotopes in zircon. Reviews in Mineralogy and Geochemistry, 53: 343-386.

Vavra, G., Gebauer, D., Schim, R., Compostons, W. 1996. Multiple zircon growth and recrystallization during polyphase Late Carboniferous to Triassic metamorphism in granulites of the Ivrea Zone (Southern Alps): and ion microprobe (SHRIMP) study. Contribution to Mineralogy and Petrology, 122: 337-358.

Vavra, G., Schmid, R. & Gebauer, D., 1999. Internal morphology, habit and U-Th-Pb microanalysis of amphibolite-to-granulite facies zircons: geochronology of the Ivrea Zone (Southern Alps). Contrib. Mineral. Petrol., 134, 380-404.

Watson, E.B., Wark, D.A. & Thomas, J.B., 2006. Crystallization thermometers for zircon and rutile. Contrib. Mineral. Petrol., 151, 413-433.

Wernick, E., Almeida, F.F.M., 1979. The geotectonic environments of Early Precambrian granulites in Brazil. Precambrian Res. 8, 1-17.

Whitehouse, M.J. & Platt, J.P., 2003. Dating high-grade metamorphism-constraints from rare-earth elements in zircon and garnet. Contrib. Mineral. Petrol., 145, 61-74.

Williams, I.S. & Claesson, S., 1987. Isotopic evidence for the Pre-Cambrian provenance and Caledonian metamorphism of high grade paragneisses from the Svecoffenian Nappes, Scandinavia Caledonides: II Ion microprobe zircon U-Th-Pb. Contrib. Mineral. Petrol., 97, 205-217.

Winge, M., 1995. Evolução dos terrenos granulíticos da Província Tocantins, Brasil Central. Tese de Doutorado, Universidade de Brasília, 550 p.

Winge, M & Danni, J.C.M. 1994. Gênese de sillimanita granada leptinitos no Complexo Anápolis-Itauçu,Goiás. In: Congresso Brasileiro de Geologia, 38, Camboriú-SC, 1994, SBG. Boletim de Resumos Expandidos, 2:76-77.

Xia, Q.X.; Zheng, Y.F.; Yuan, H.; Wu, F.Y. 2009. Contrasting Lu-Hf and U-Th-Pb isotope systematic between metamorphic growth and recrystallization of zircon from eclogite-facies metagranites in the Dabie orogen, China. Lithos, 112: 477-496

Xie, L.W., Zhang, Y.B., Zhang, H.H., Sun, J.F., Wu, F.Y. 2008. In situ simultaneous determination of trace elements, U-Pb and Lu-Hf isotopesin zircon and baddeleyite. Chinese Science Bulletin, 53(10), 1565-1573.

Yardley, B.W.D. 1988. Introdução à Petrologia Metamórfica. Editora Universidade de Brasília, Brasília, 340 pp, (Tradução de Reinhardt A. Fuck).

Zack, T., Luvizotto, G.L., Moraes, R., Möller, A., Kronz, A. 2006. Rutile and zircon thermometry of granulites: premetamorphic relicts, prograde growth, disequilibrium and diffusional resetting. In Granulites & Granulites 2006. Brasilia, p. 98.

Zeh, A., Gerdes, A., Klemd, R., Barton Jr., J.M. 2007. Archaean to Proterozoic Crustal Evolution in the Central Zone of the Limpopo Belt (South Africa-Botswana): Constraints from Combined U-Pb and Lu-Hf.

Zheng, Y.F.; Wu, Y.B.; Zhao, Z.F.; Zhang, S.B.; Xu, P.; Wu, F.Y. 2005. Metamorphic effect on zircon Lu-Hf and U-Pb isotope systems in ultrahigh-pressure eclogite-facies metagranites and metabasite. Earth and Planetary Science Letters, 240: 378-400.

ANEXO

IMAGENS DE CATODOLUMINESCÊNCIA

COMPLEXOS MÁFICO-ULTRAMÁFICOS DE DAMOLÂNDIA E TAQUARAL

Amostra DM-16

Z1

206Pb/238U = 596 Ma

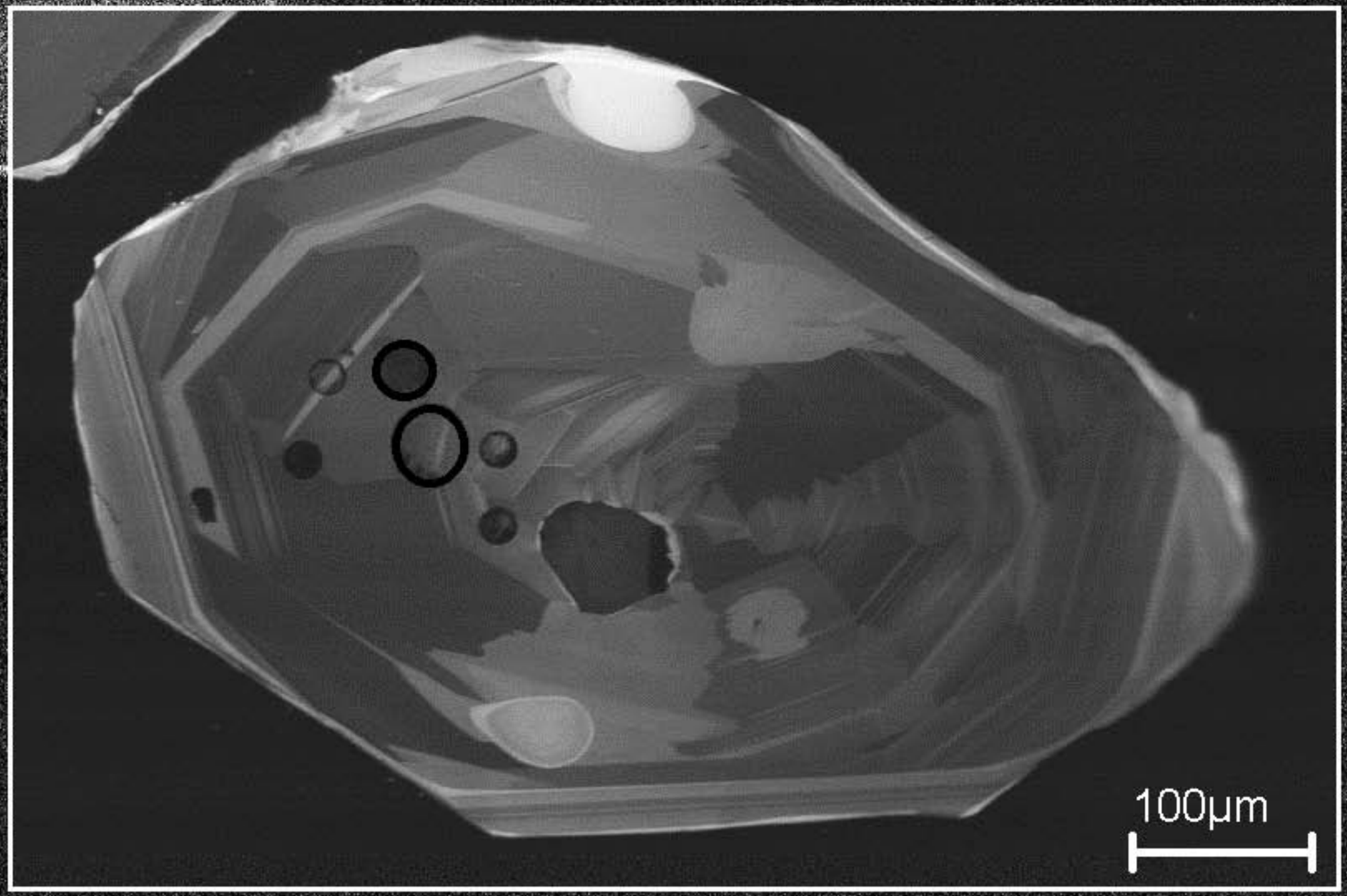

Amostra DM-16

Z2

206Pb/238U = 593 Ma

Amostra DM-16

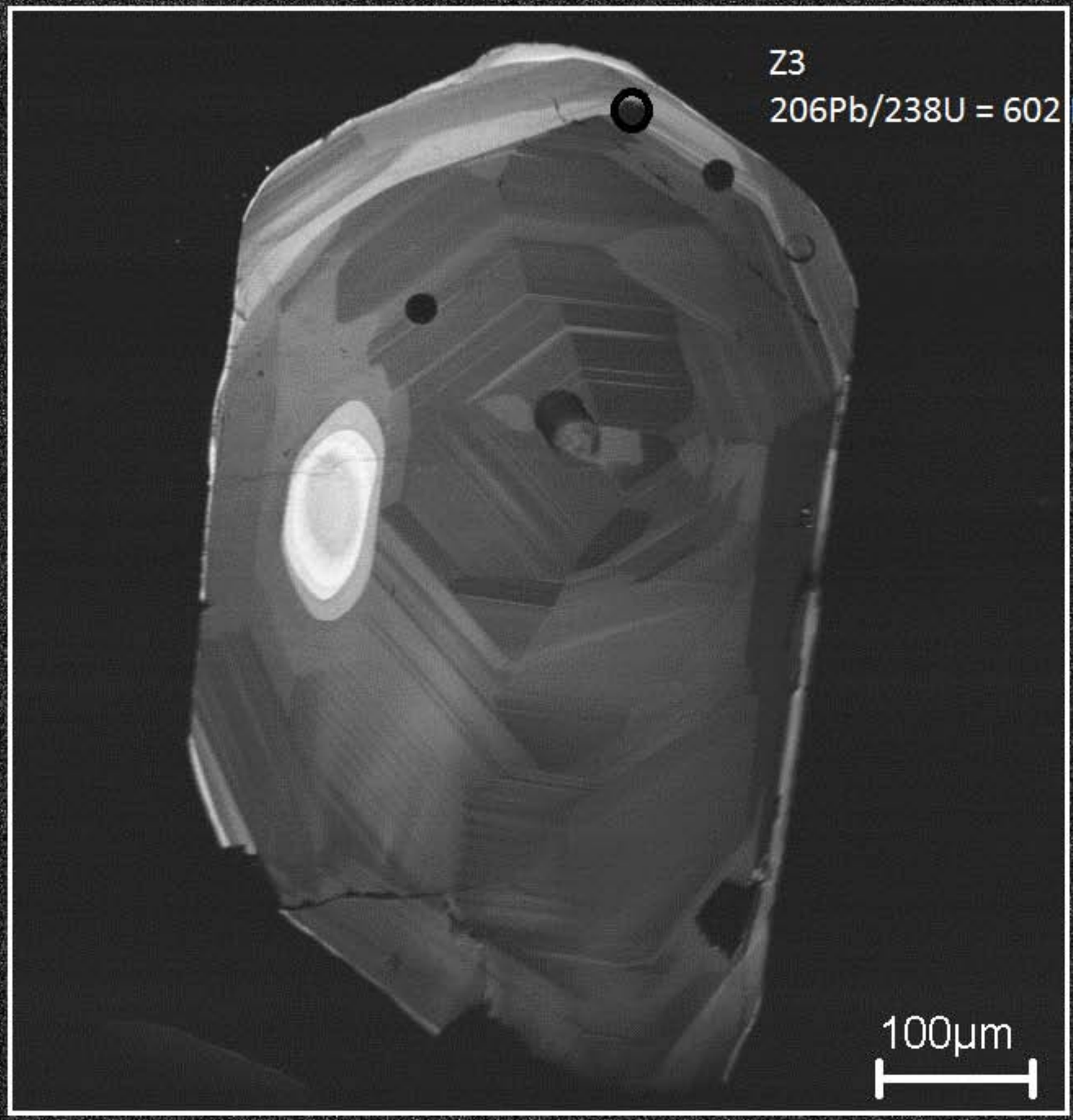

Amostra DM-16

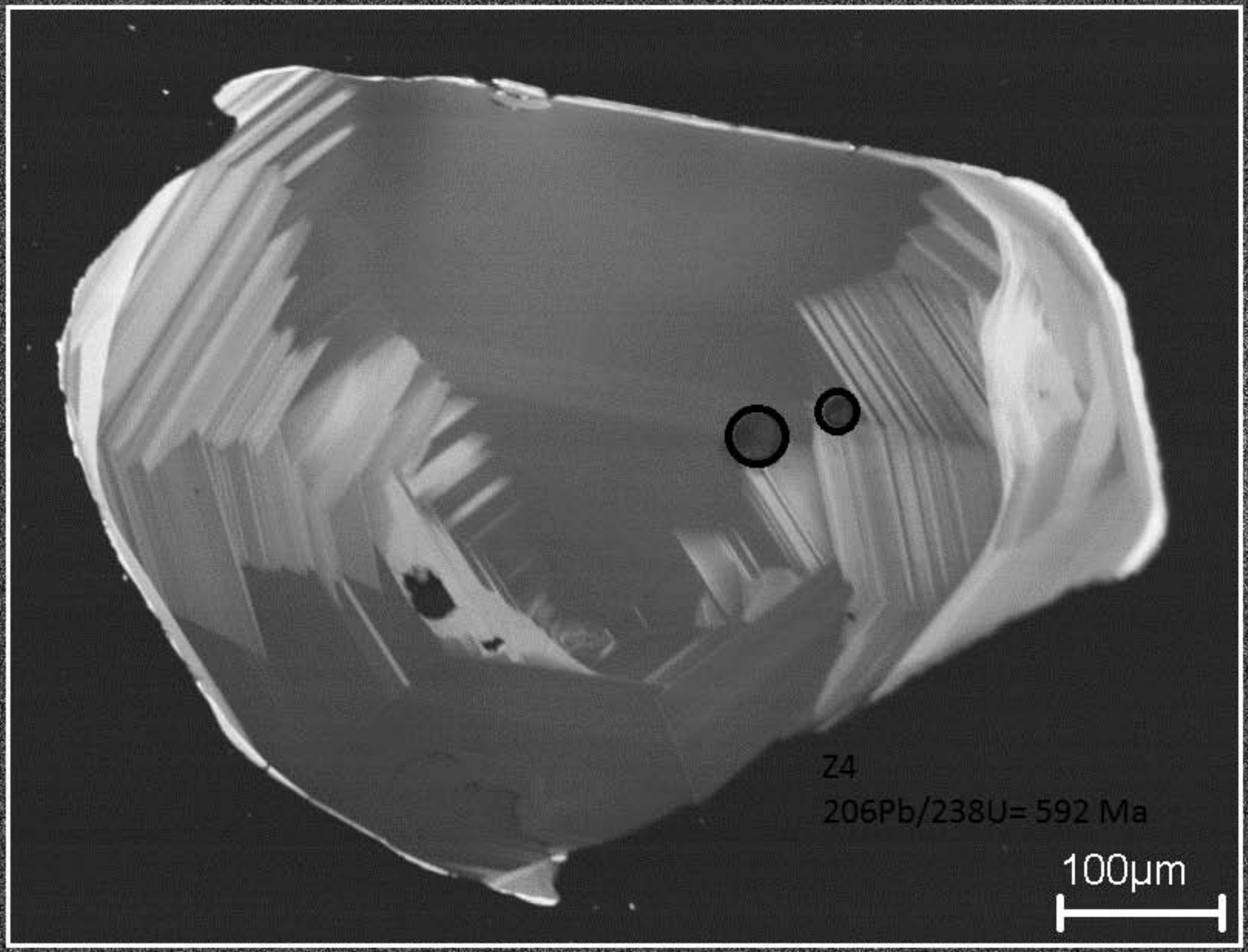

Amostra DM-16

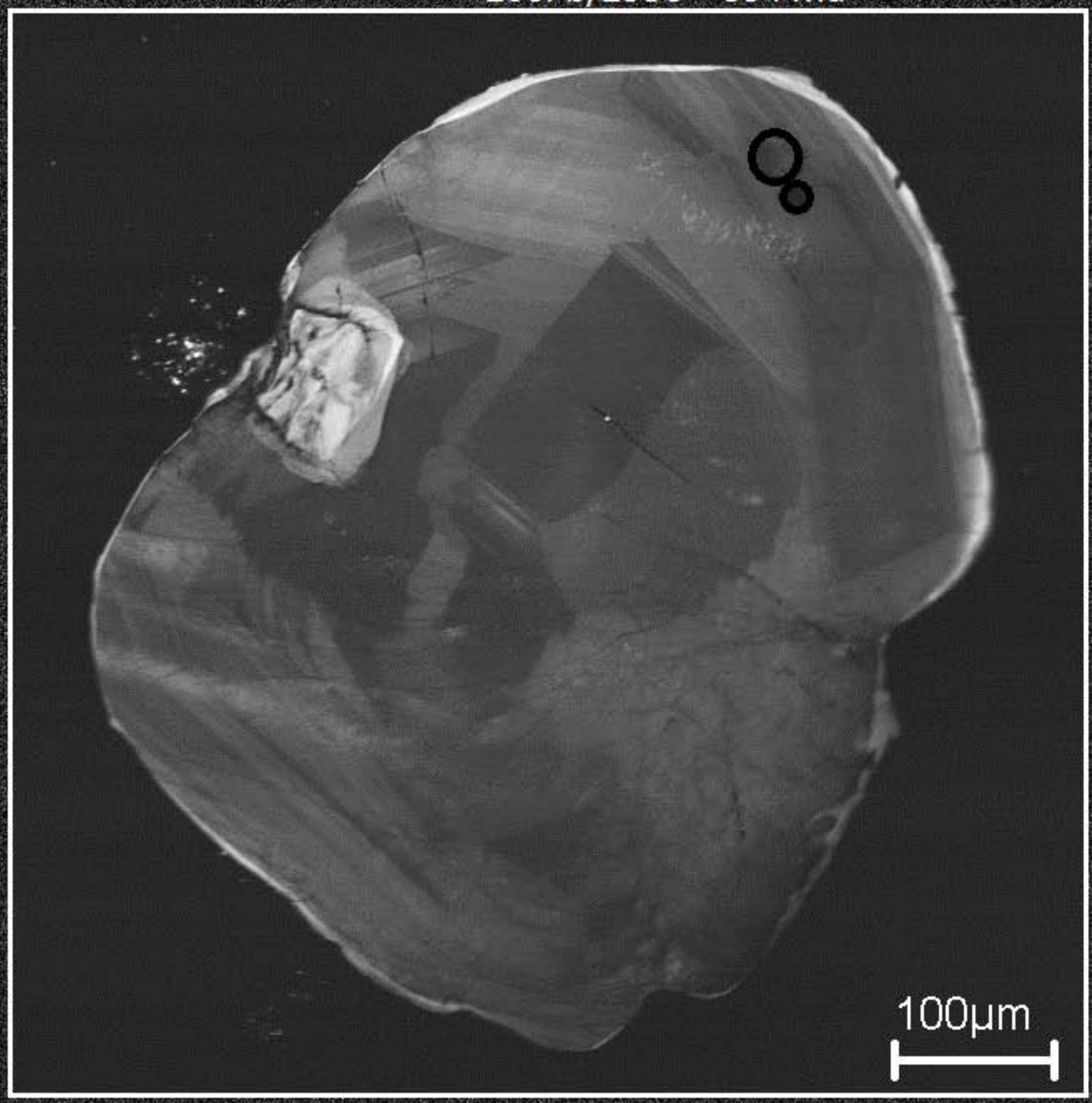

Amostra DM-16

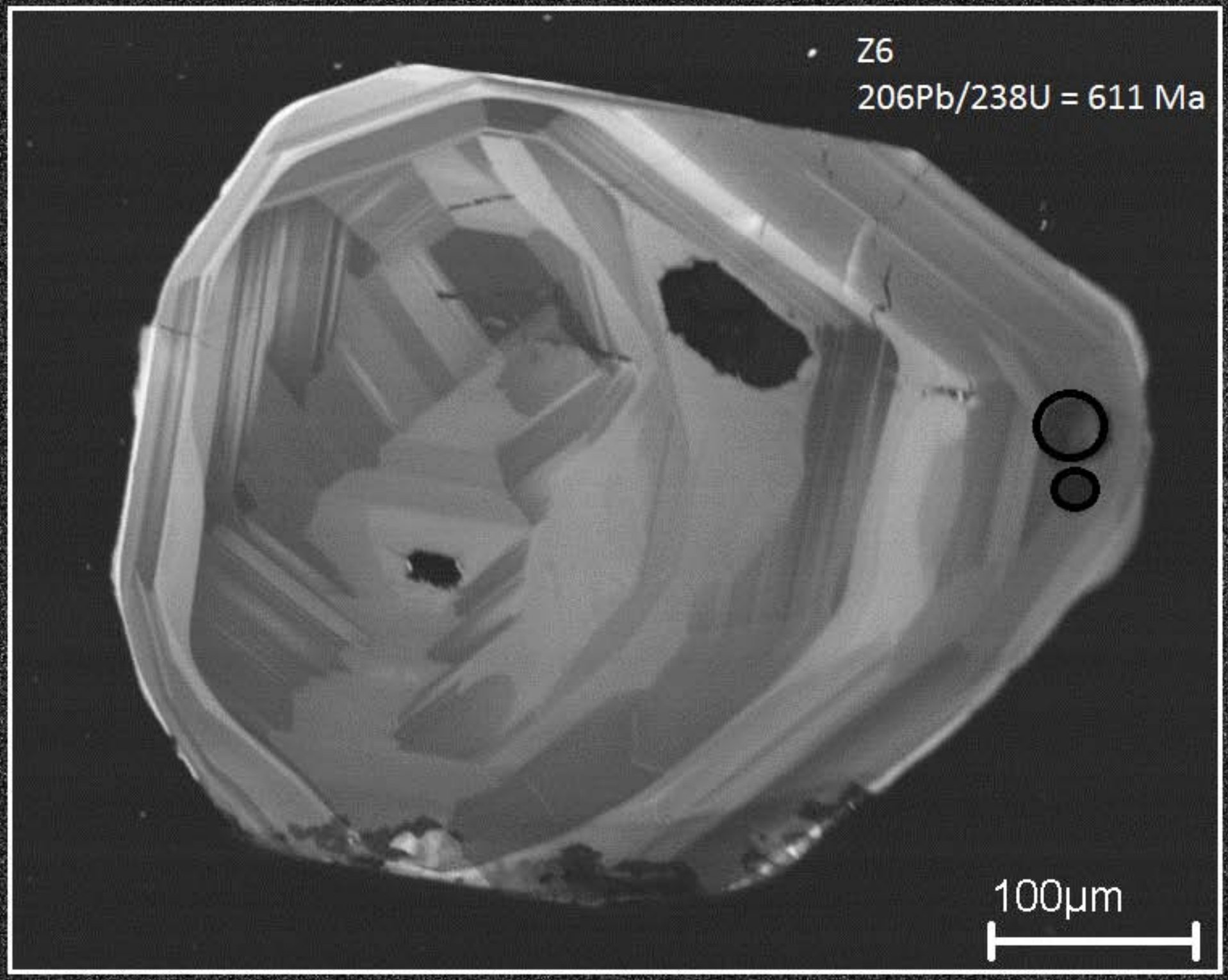

Amostra DM-16

Z7-rim
206Pb/238U = 596 Ma

Z7-core
206Pb/238U = 606 Ma

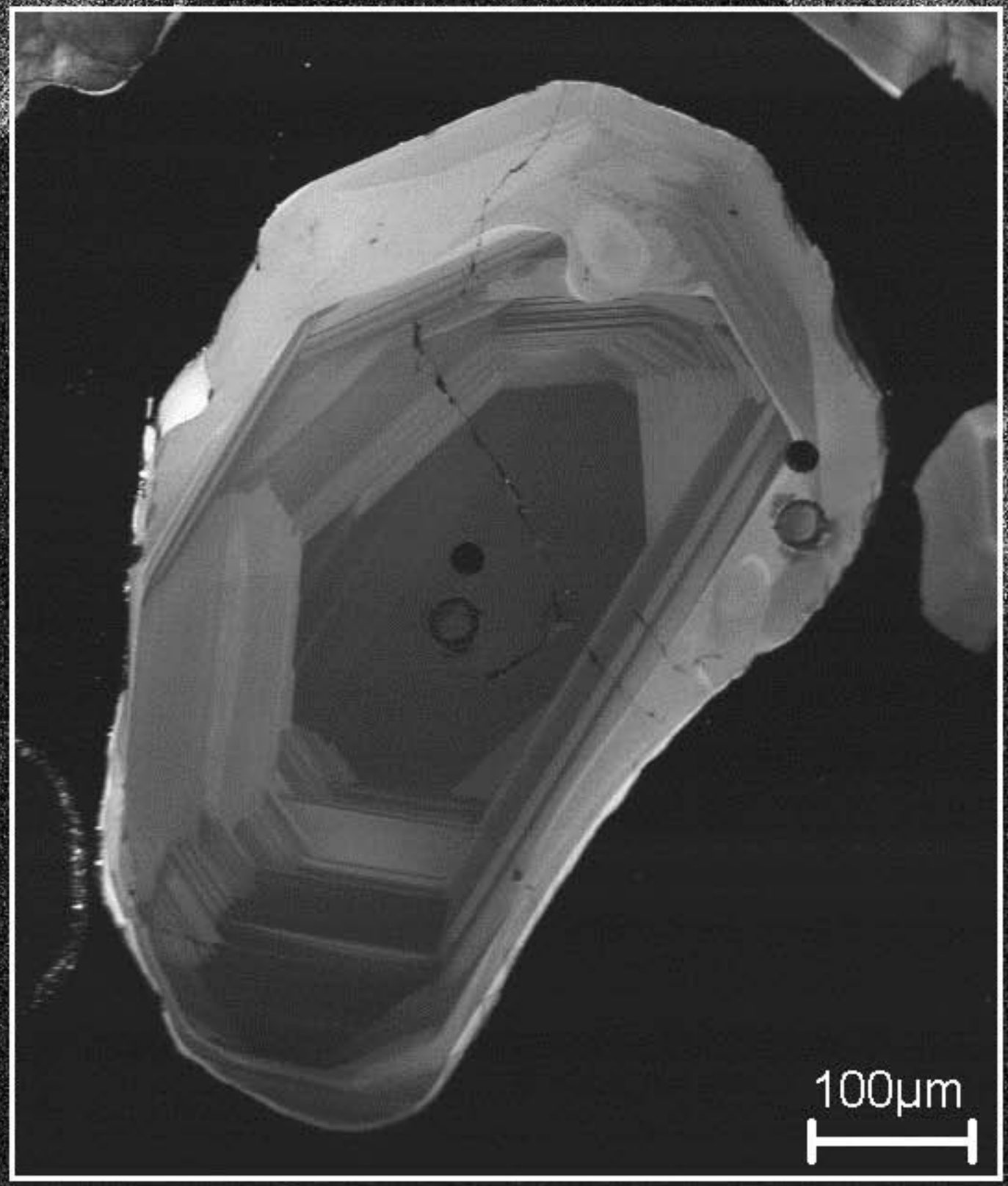

Amostra DM-16

Z8

206Pb/238U = 590 Ma

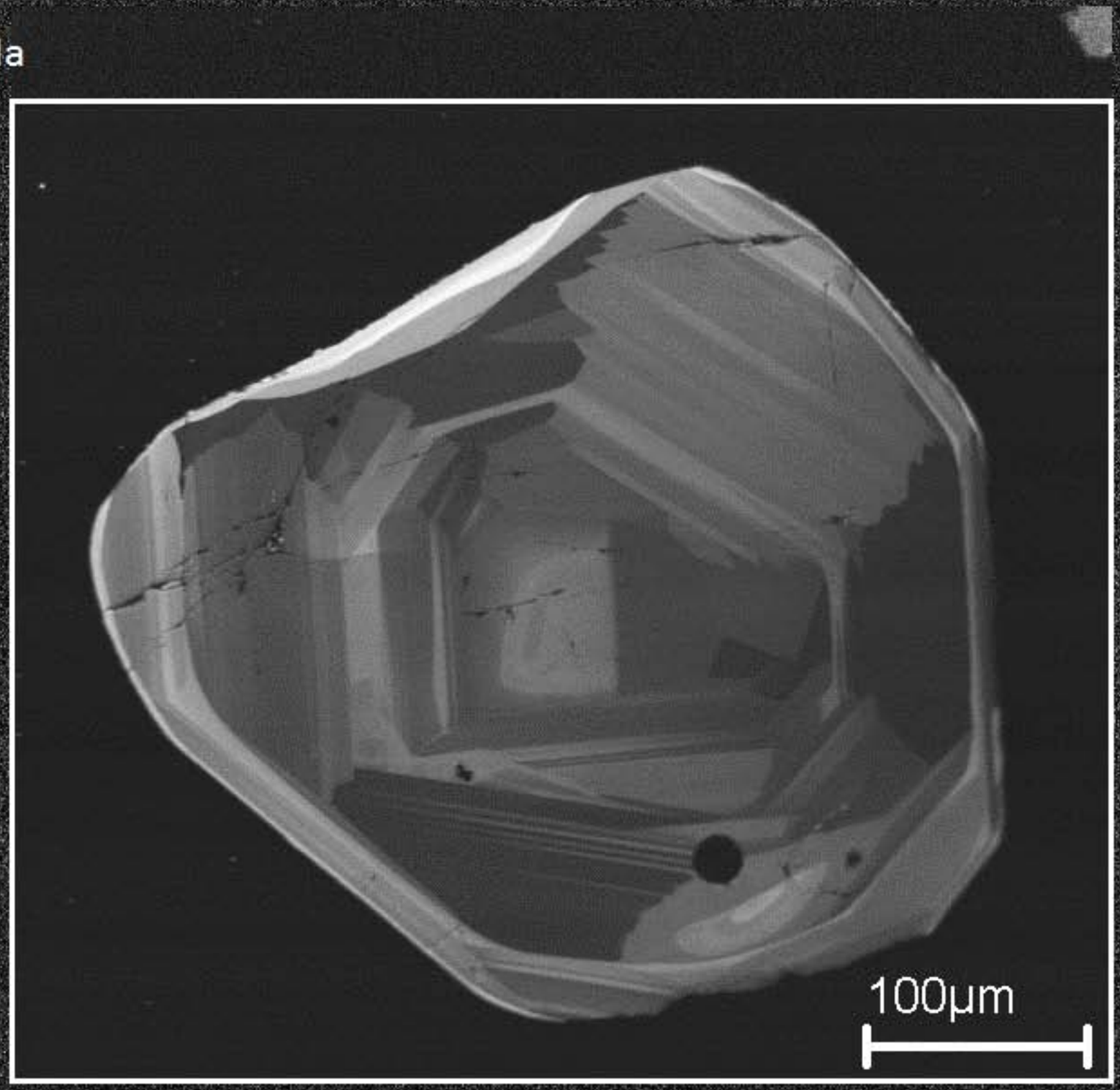

Amostra DM-16

Z9

206Pb/238U = 591 Ma

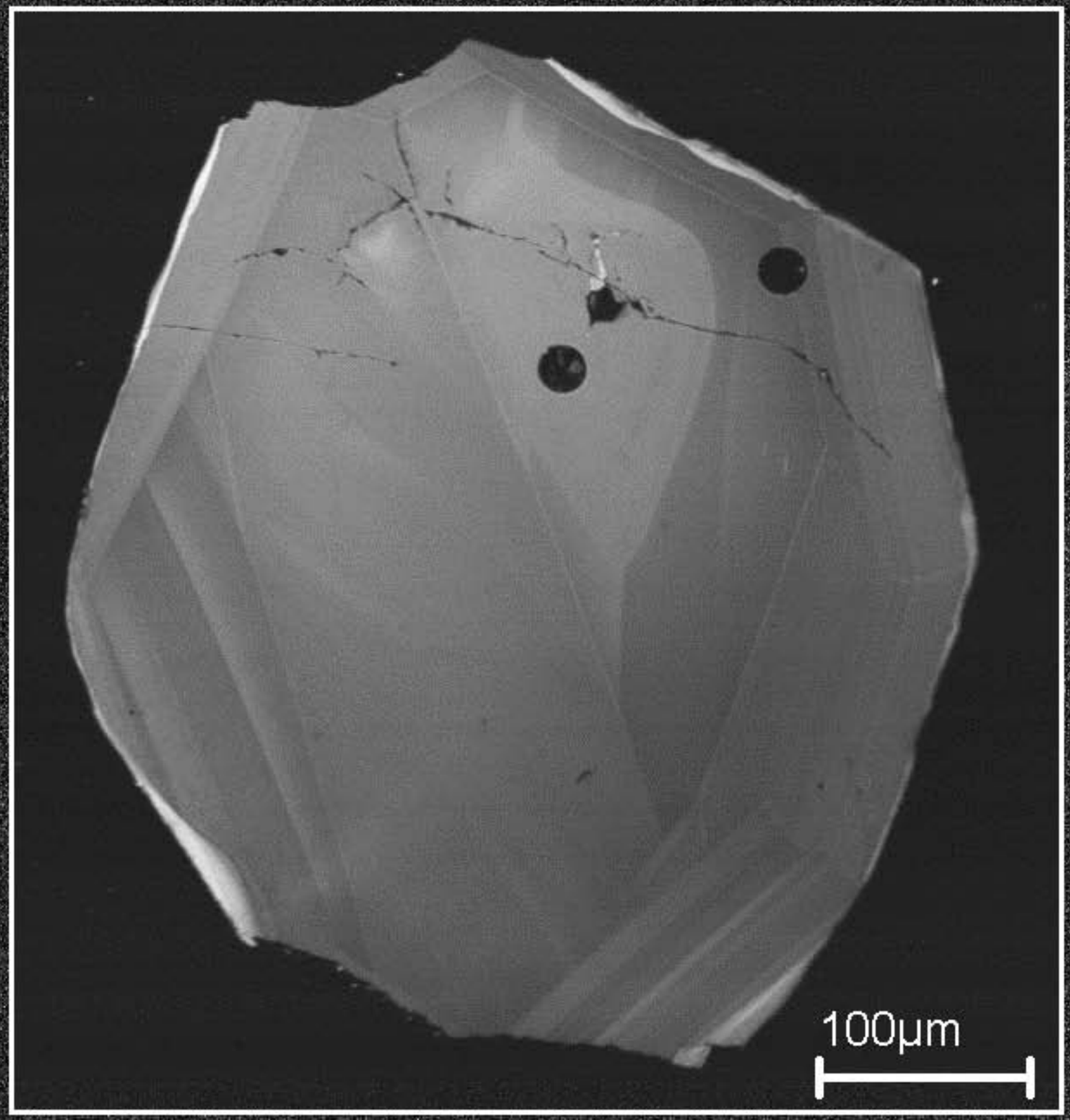

Amostra DM-16

Z10
206Pb/238U = 614 Ma

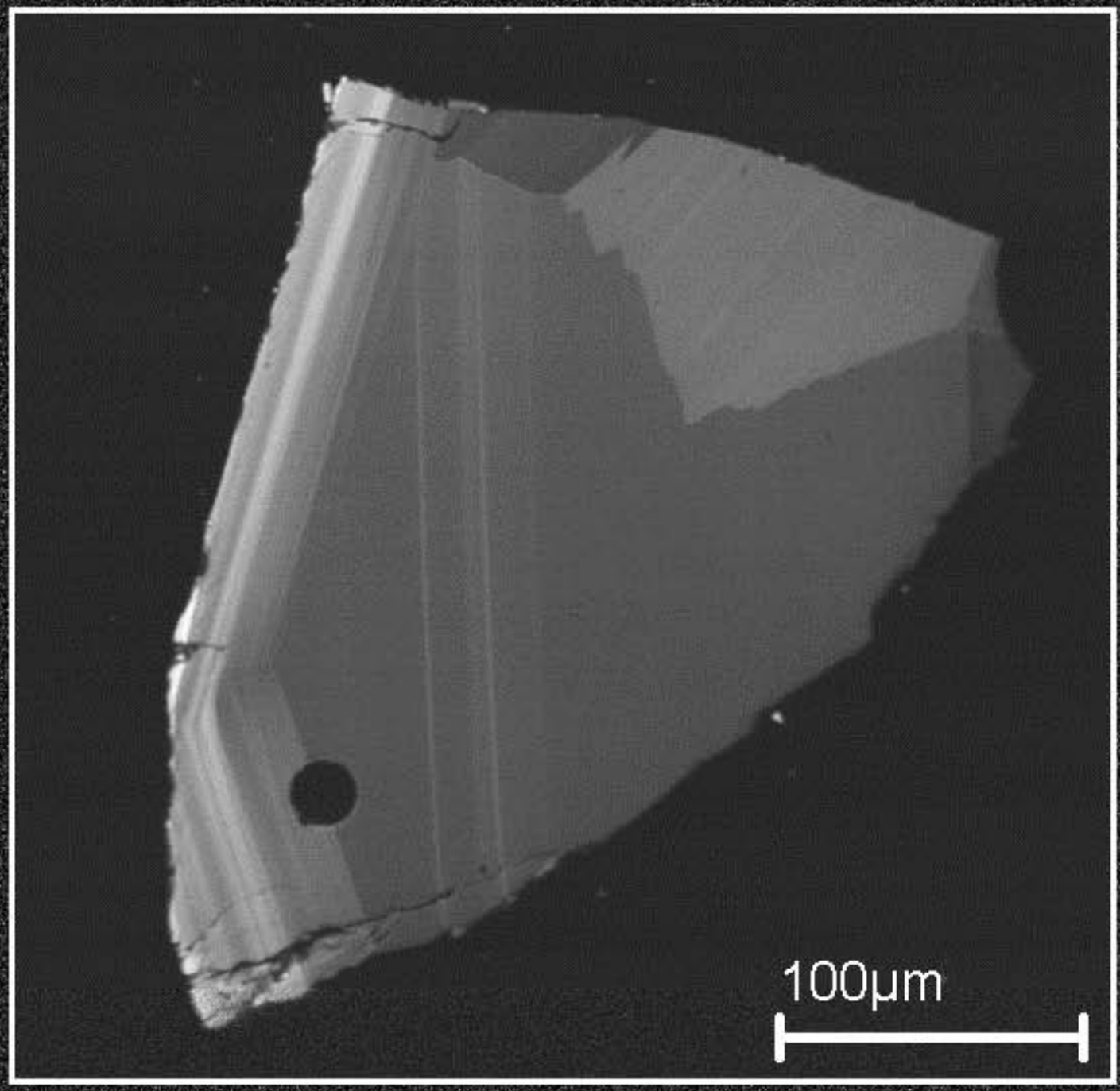

Amostra DM-16

Z11
206Pb/238U = 644 Ma

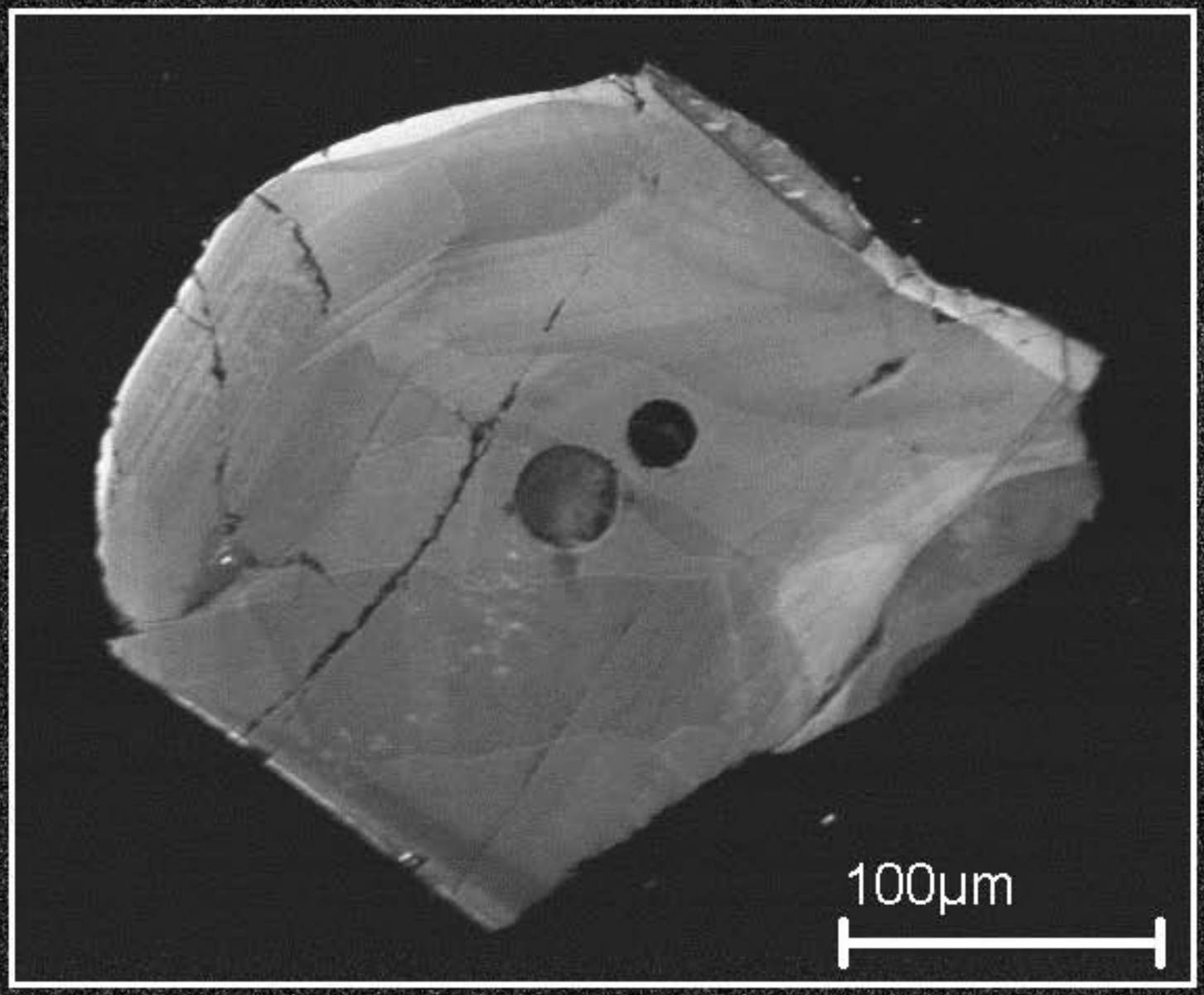

Amostra DM-16

Z12

206Pb/238U = 633 Ma

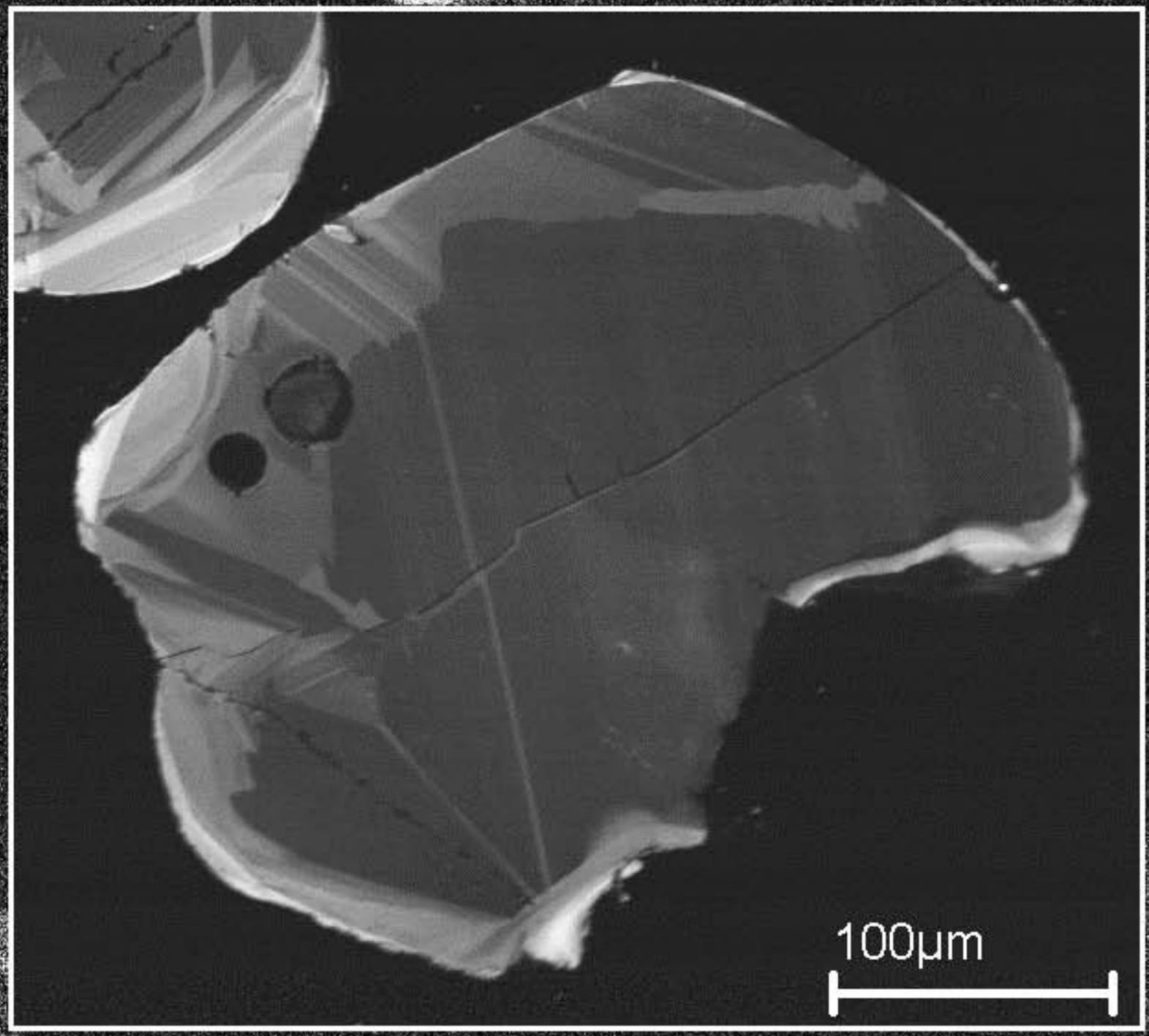

Amostra DM-16

Z13
206Pb/238U = 647 Ma

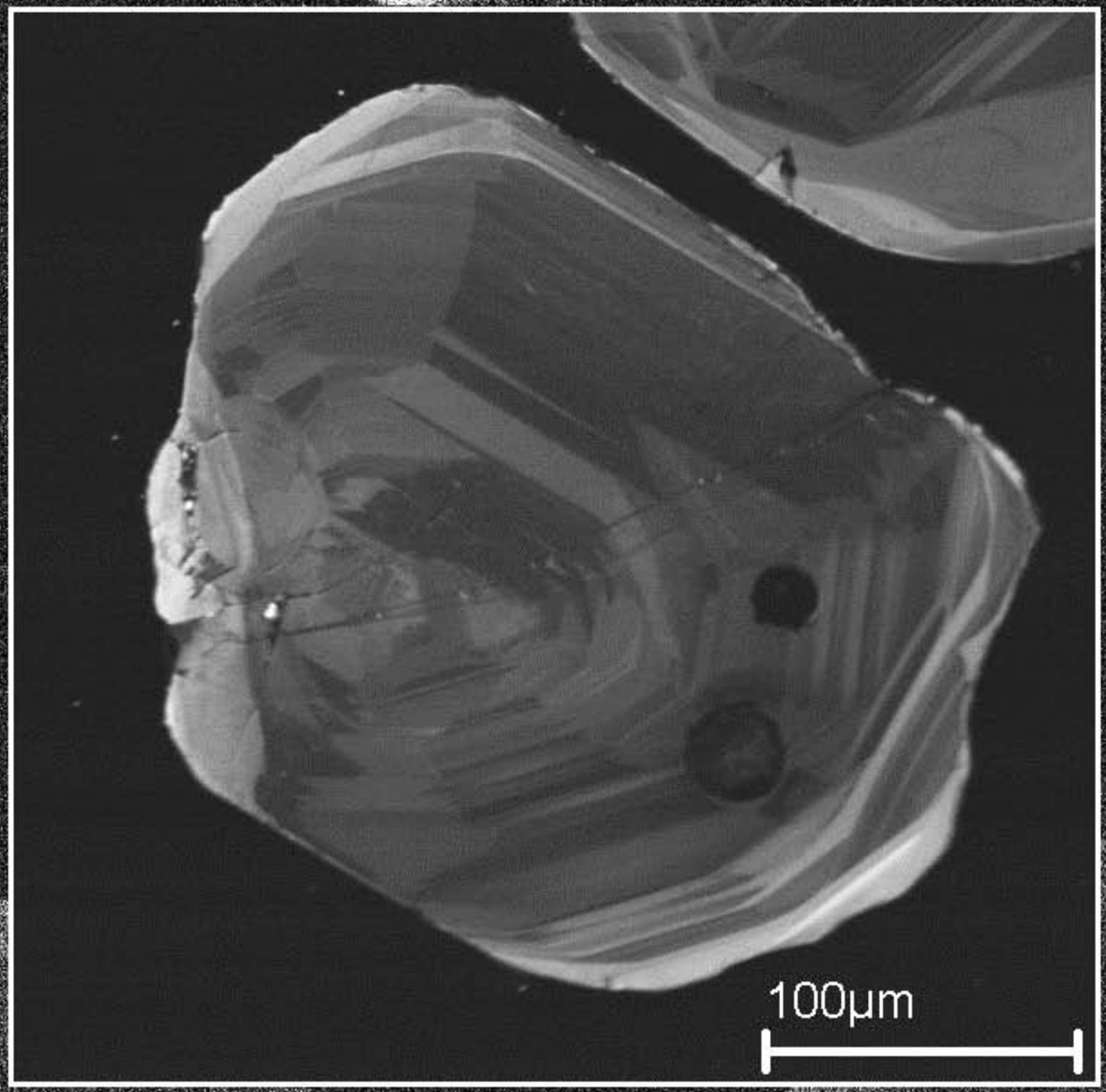

Amostra DM-16

Z14
206Pb/238U = 670 Ma

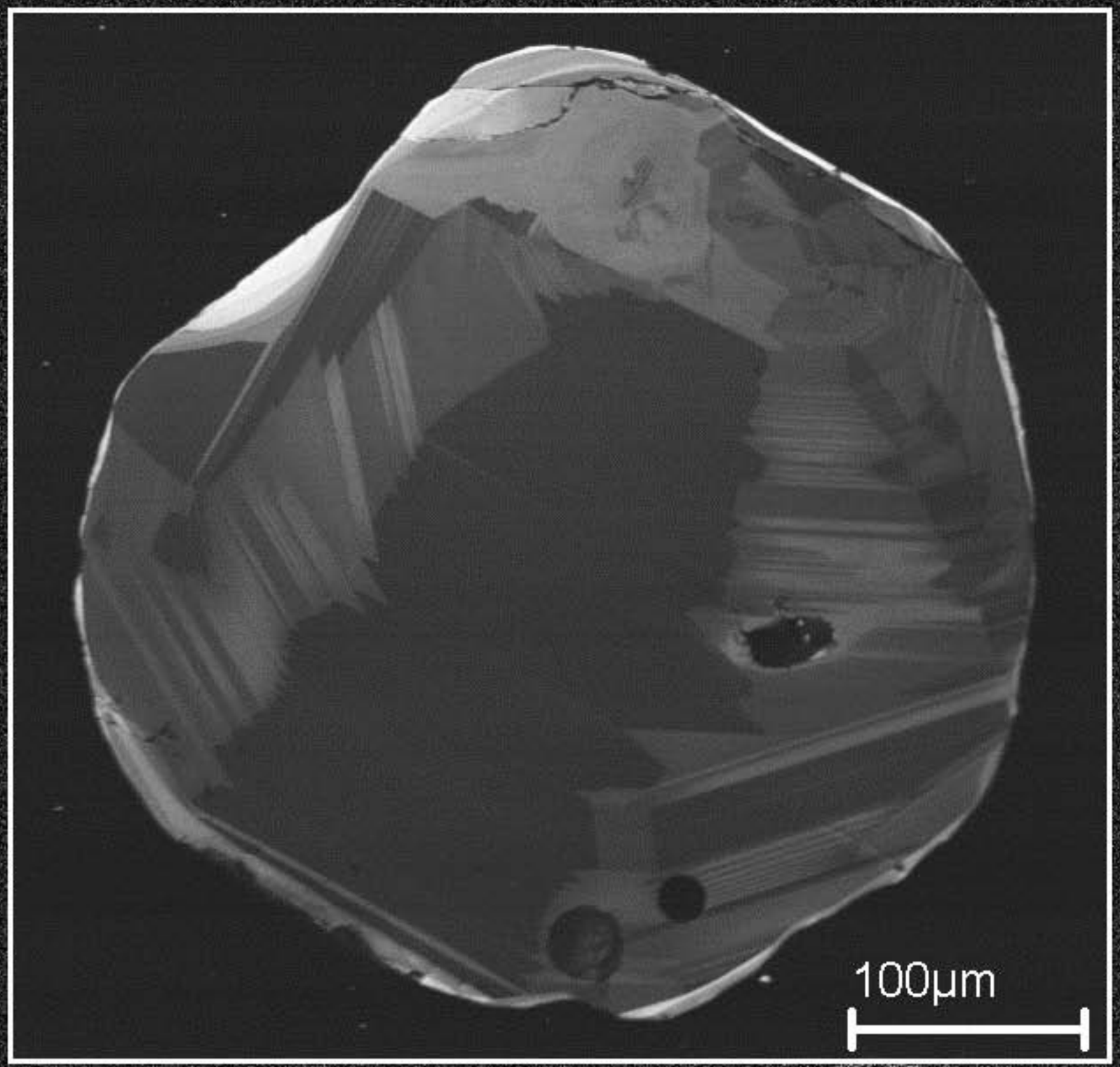

Amostra DM-16

Z15
206Pb/238U = 643 Ma

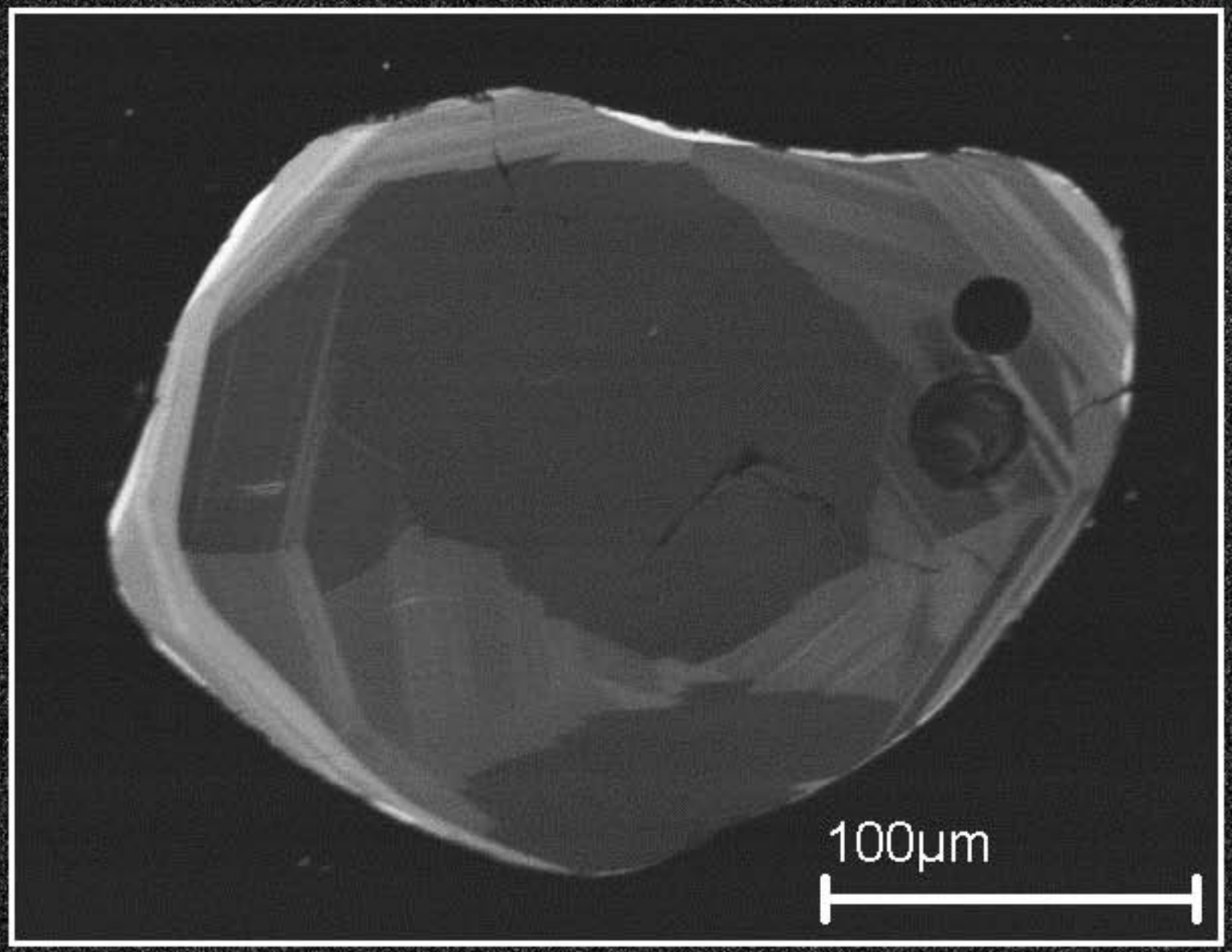

Amostra DM-20

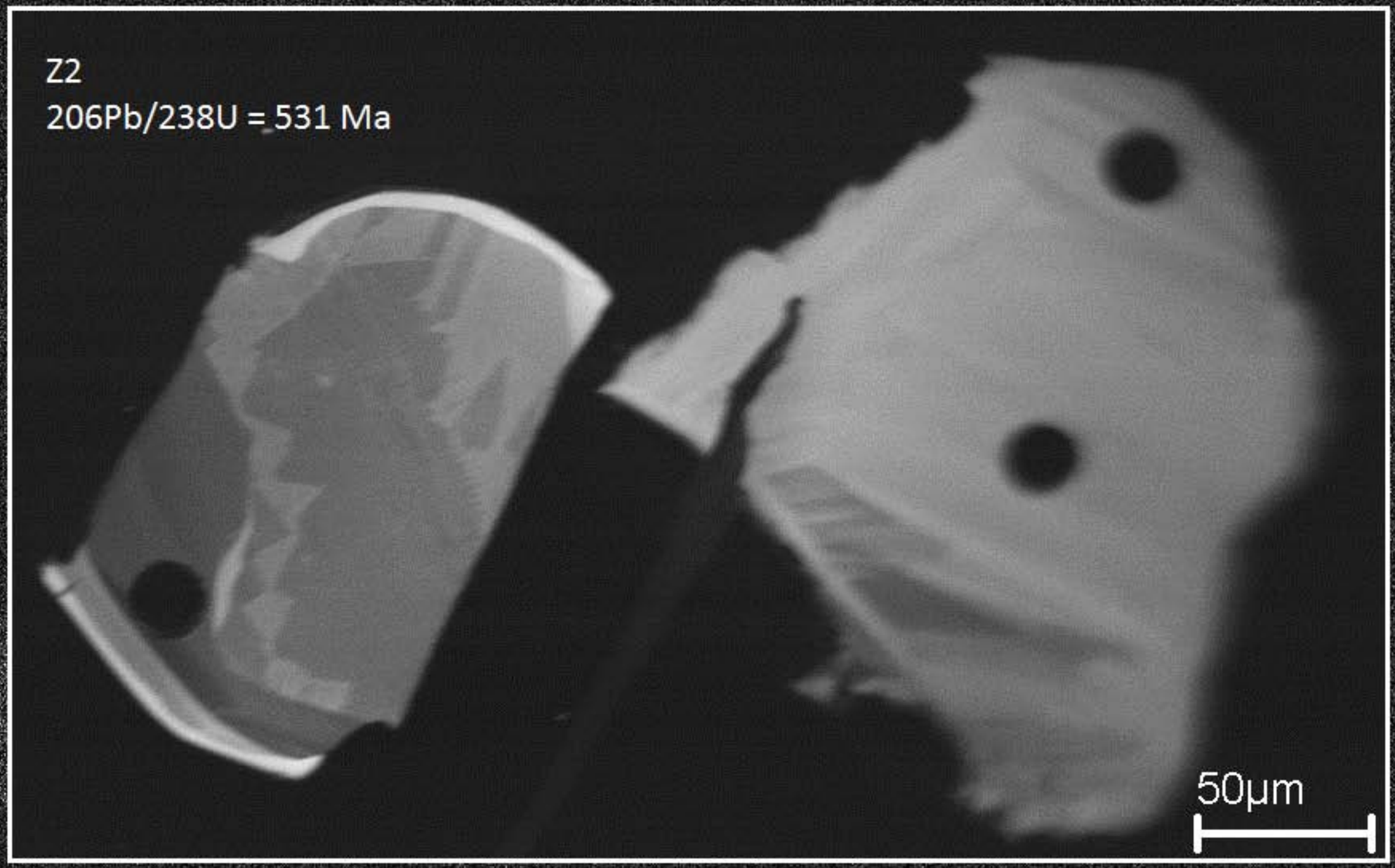

Amostra DM-20

Amostra DM-20

Z8

206Pb/238U = 628 Ma

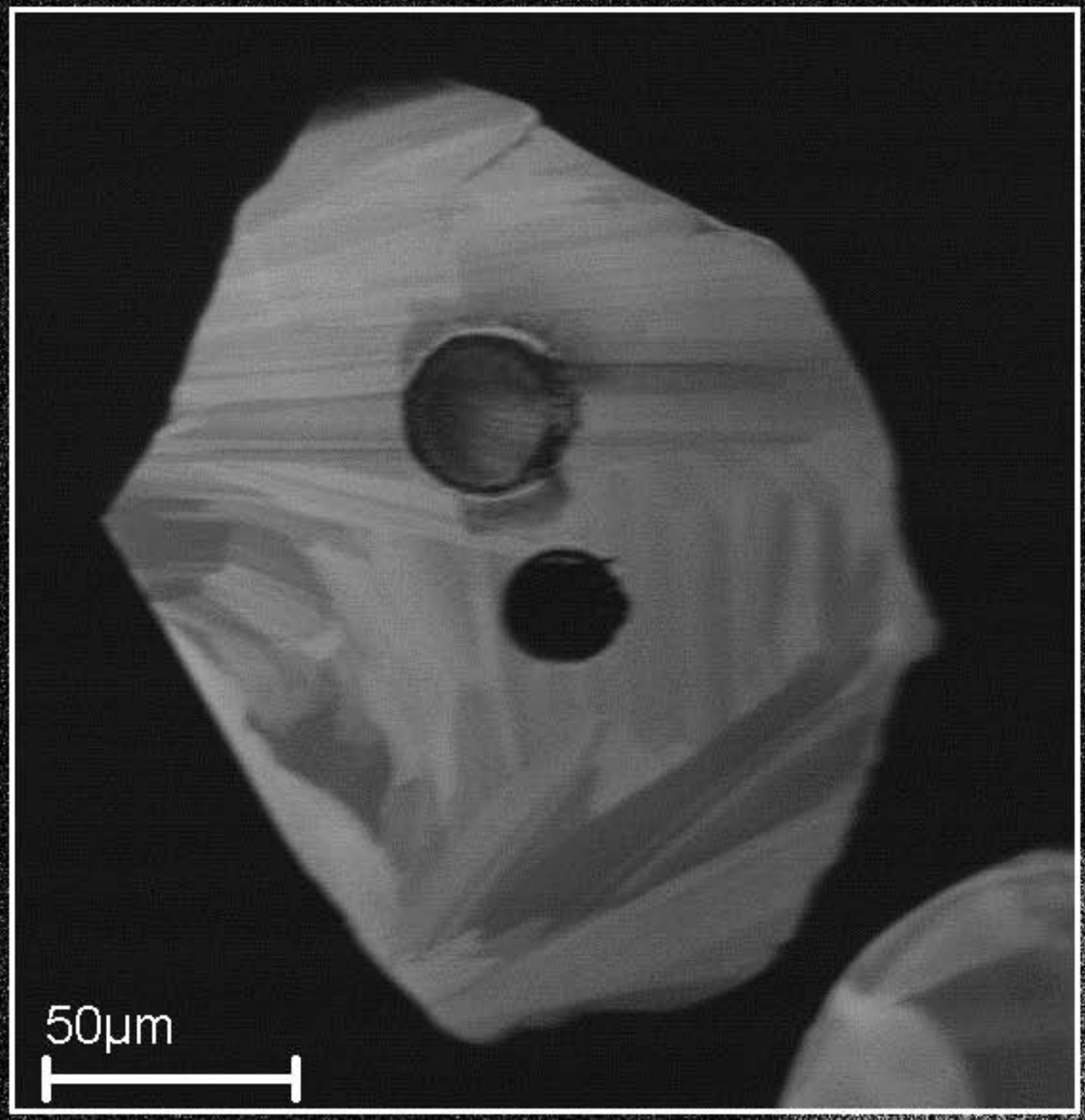

Amostra DM-20

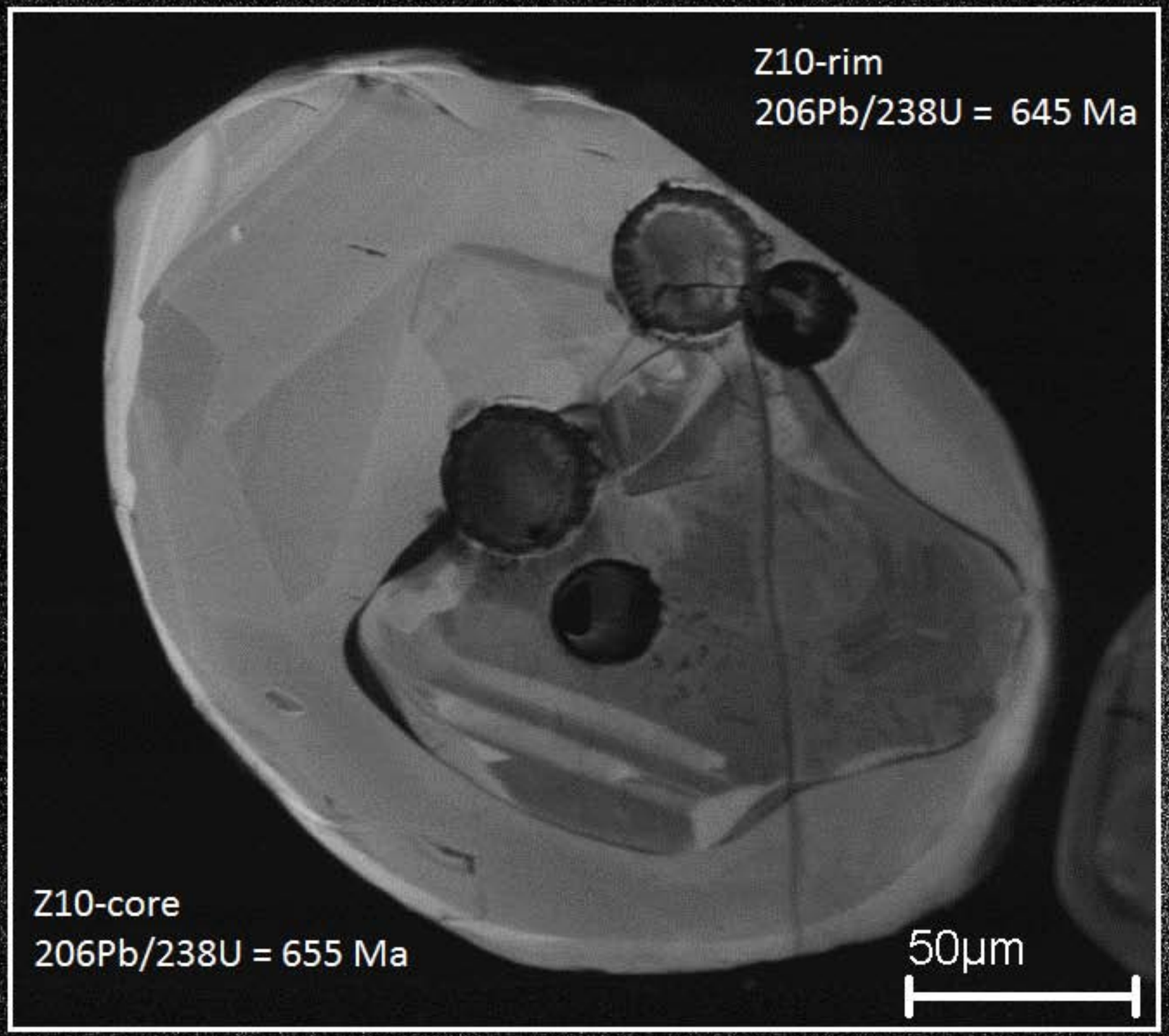

Amostra DM-20

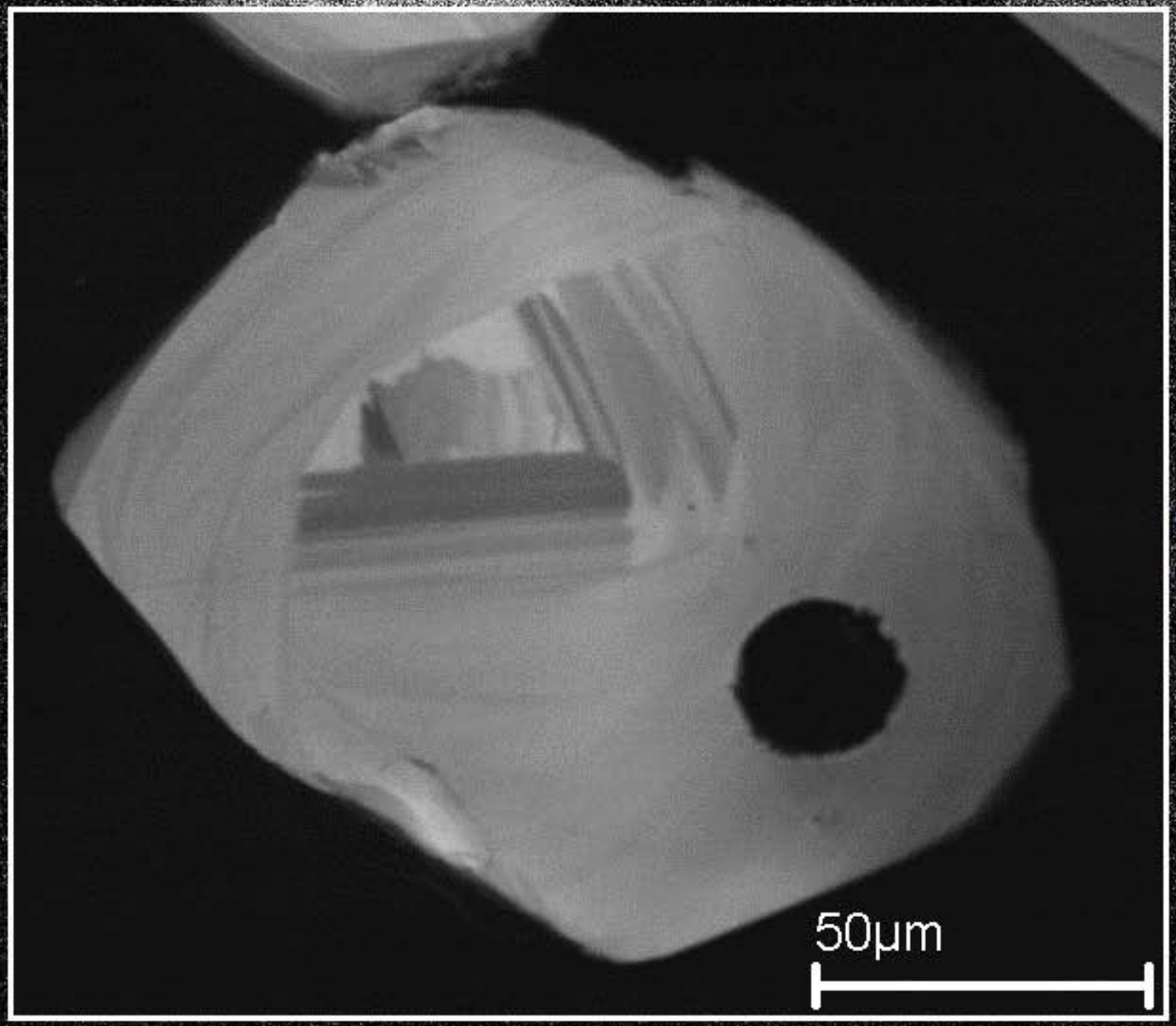

Z11
206Pb/238U = 633 Ma

Amostra DM-20

Z14
206Pb/238U = 607 Ma

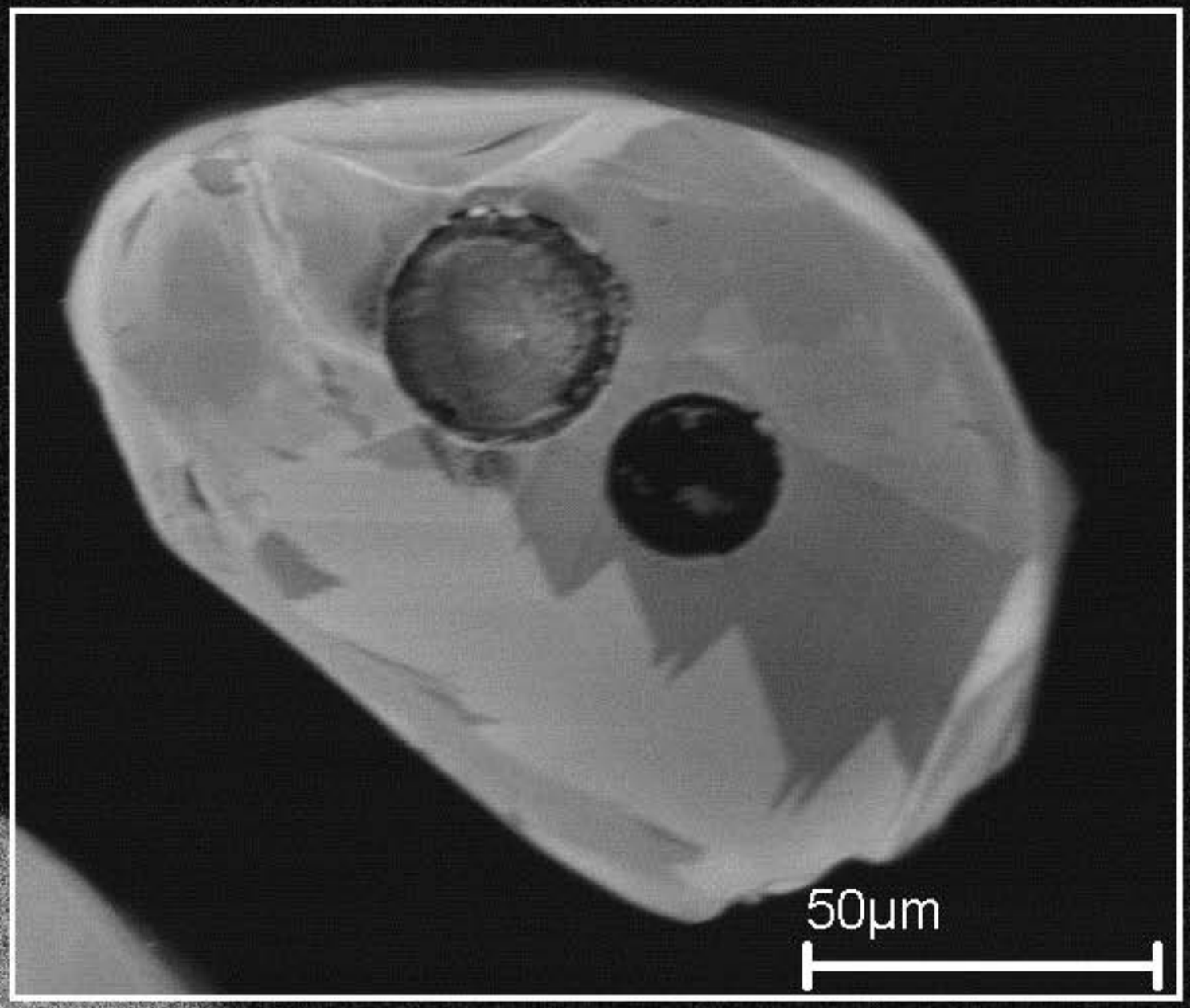

Amostra DM-20

Z15

206Pb/238U = 627 Ma

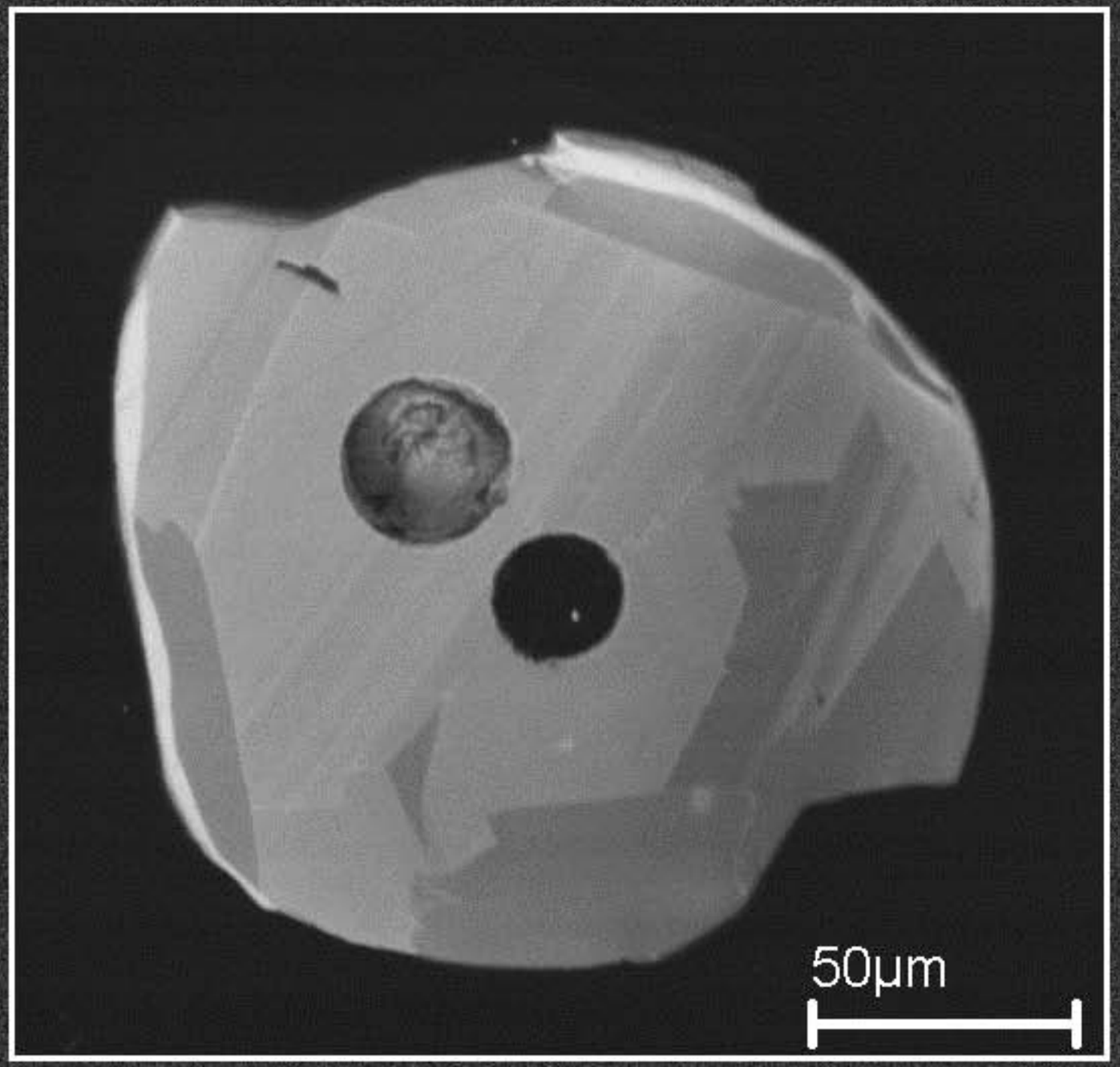

Amostra DM-20

Z16

206Pb/238U = 648 Ma

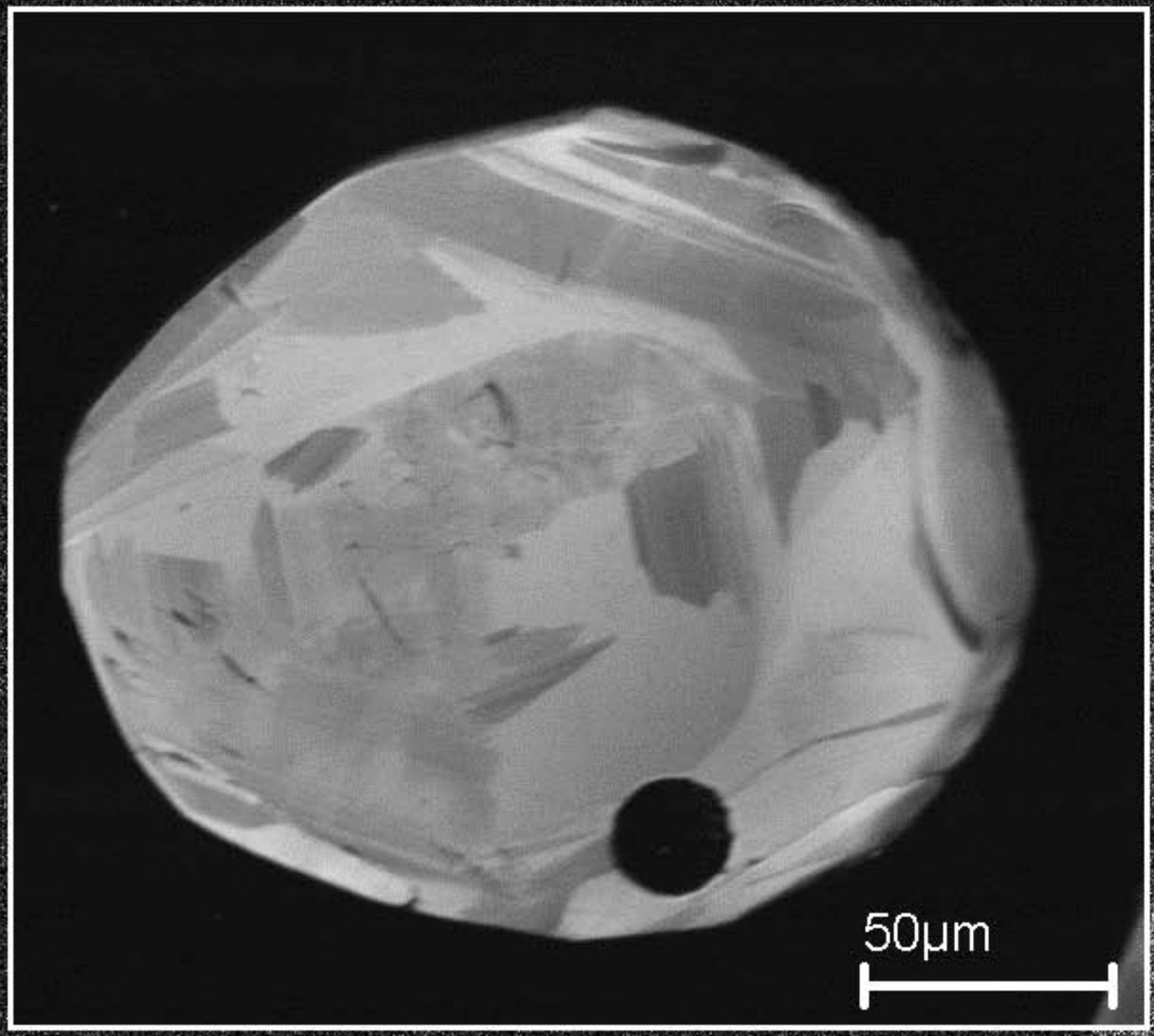

Amostra DM-20

Z19
206Pb/238U = 638 Ma

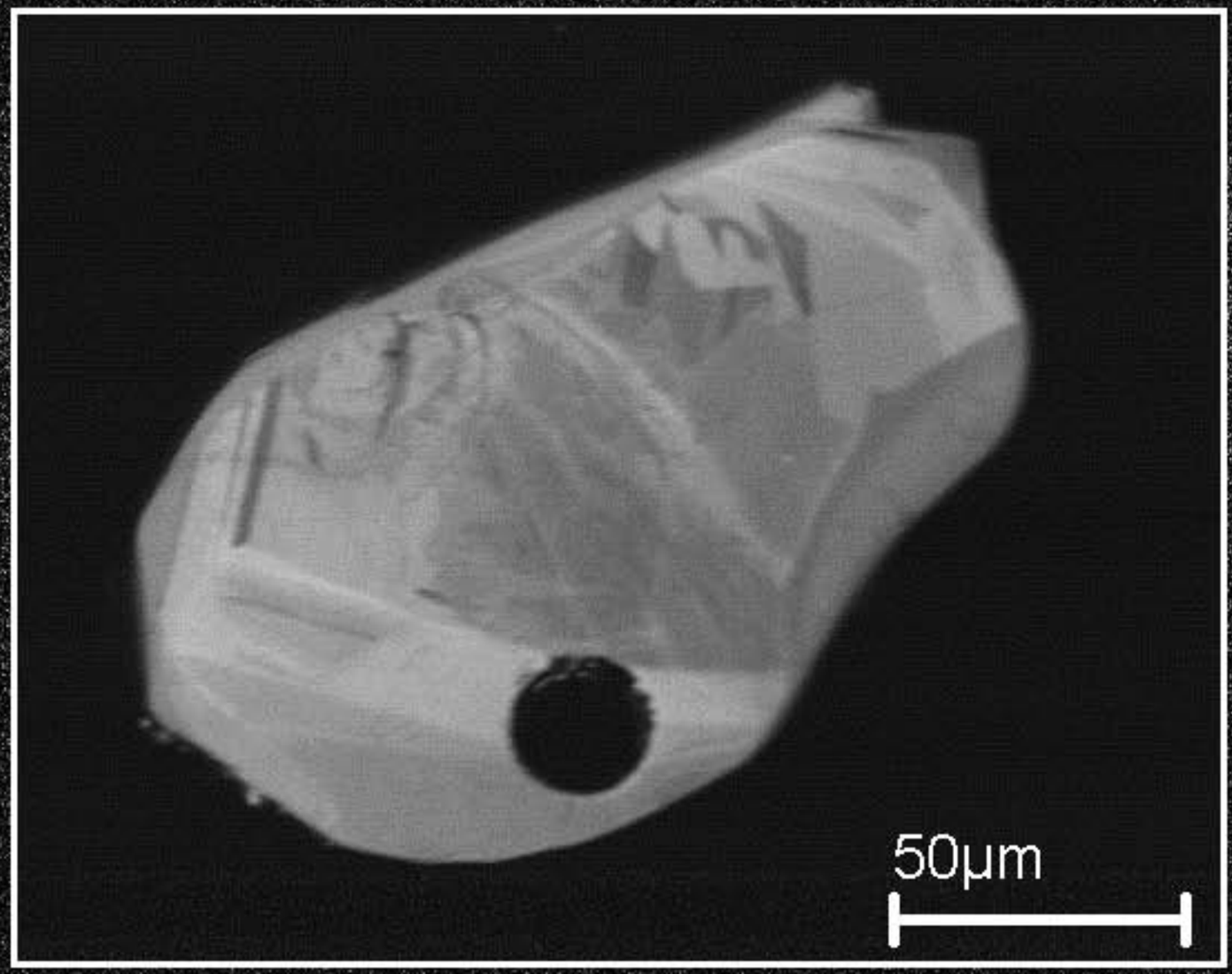

Amostra TQ-14

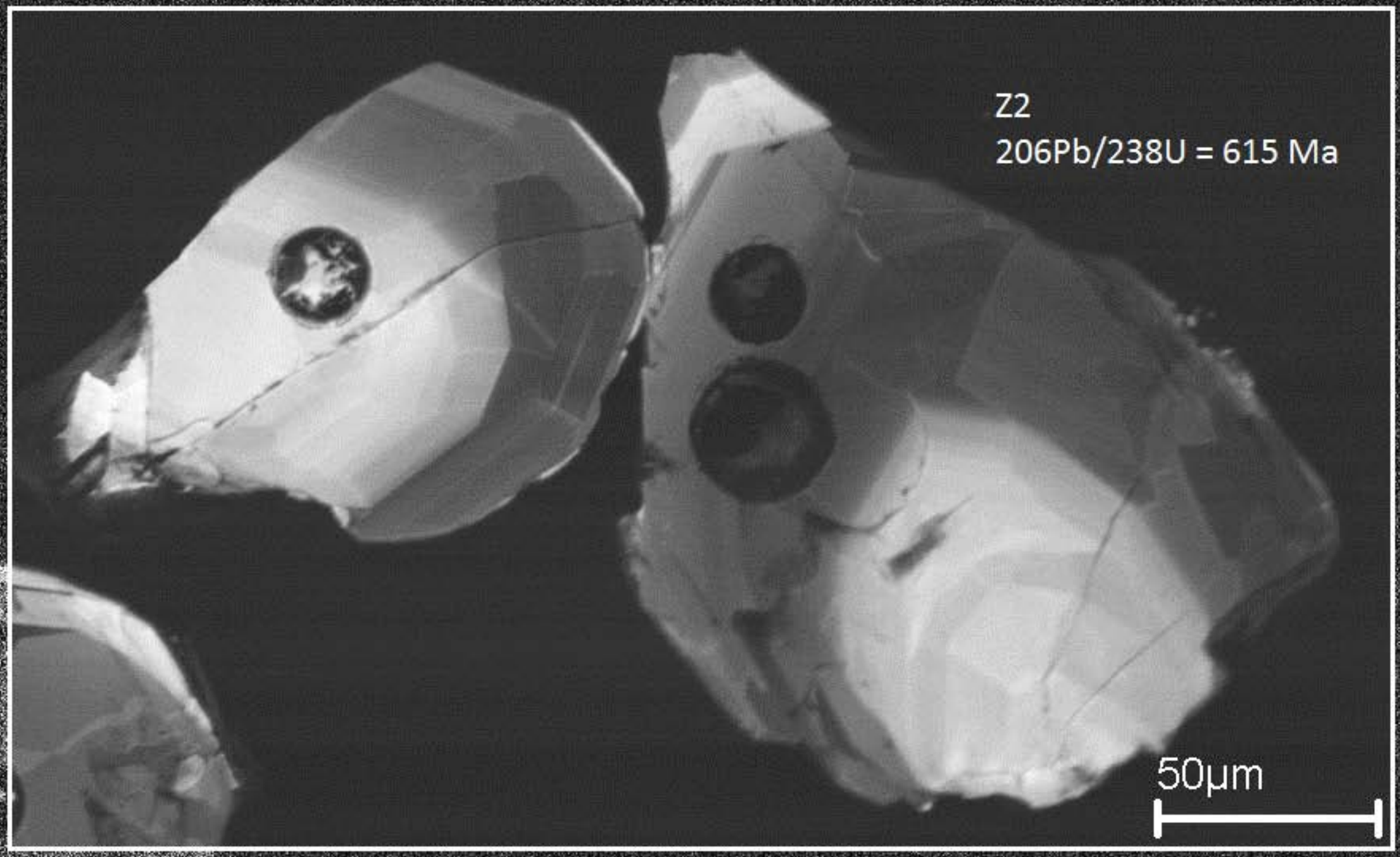

Amostra TQ-14

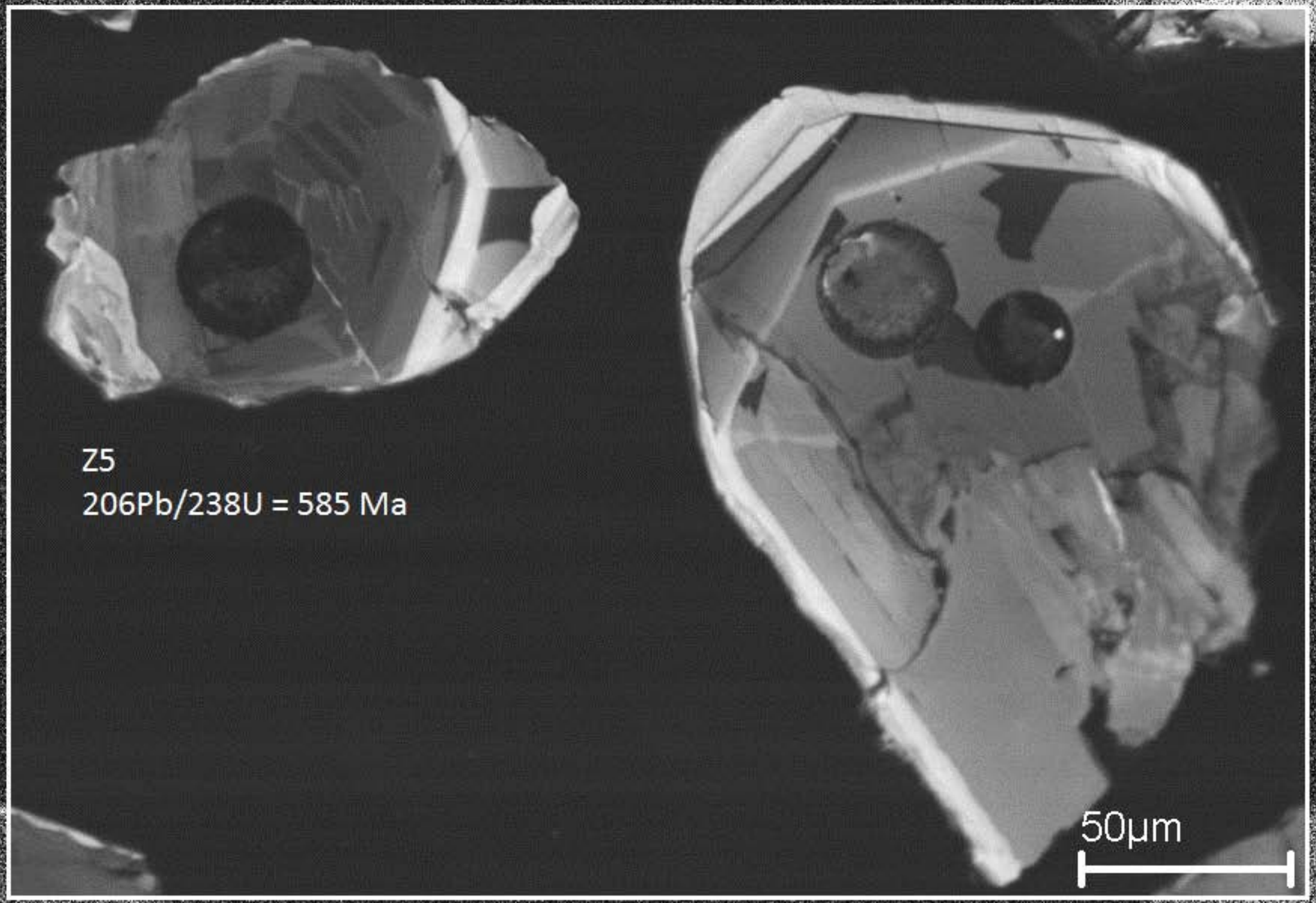

Amostra TQ-14

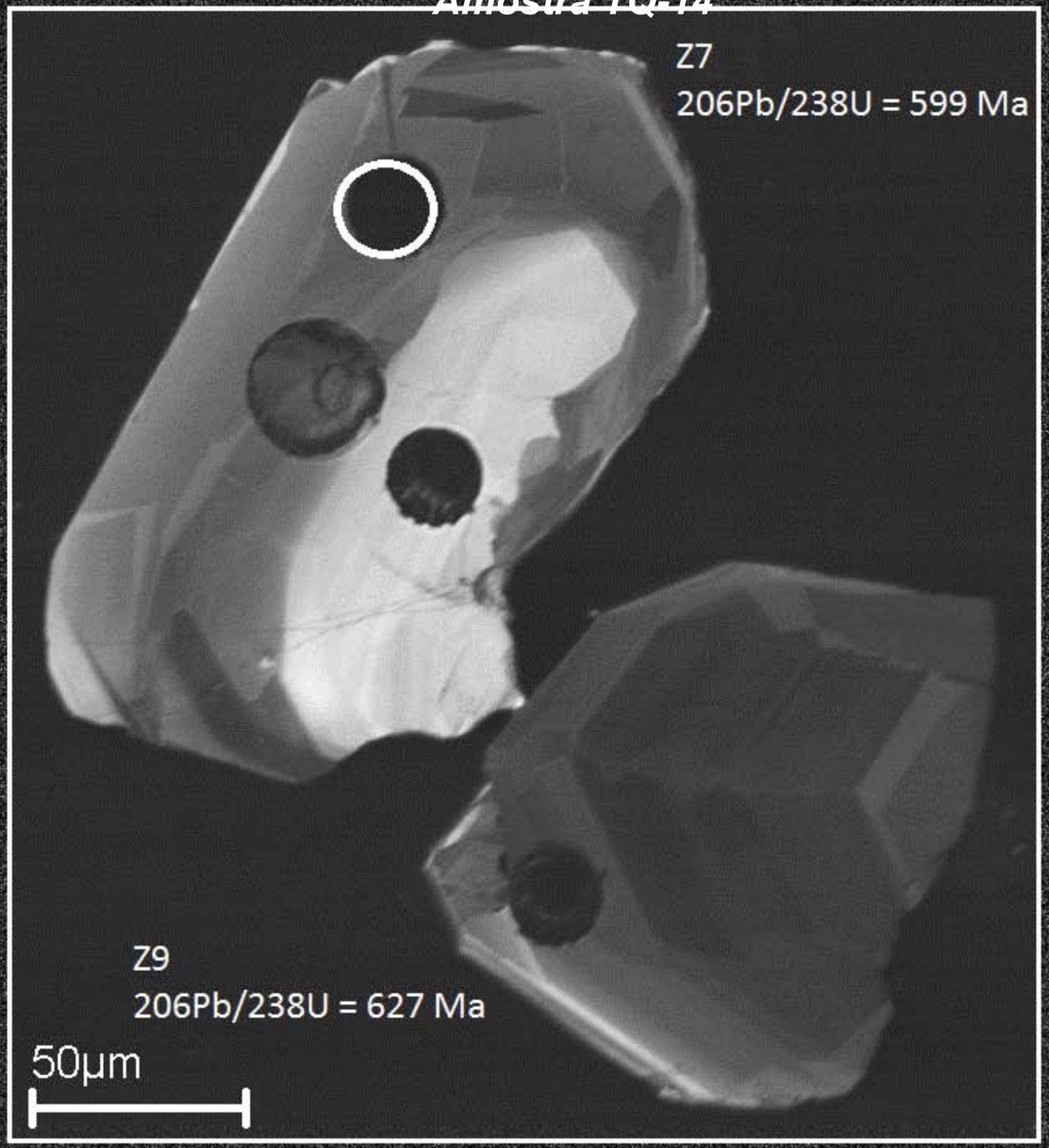

Amostra TQ-14

Z11
206Pb/238U = 613 Ma

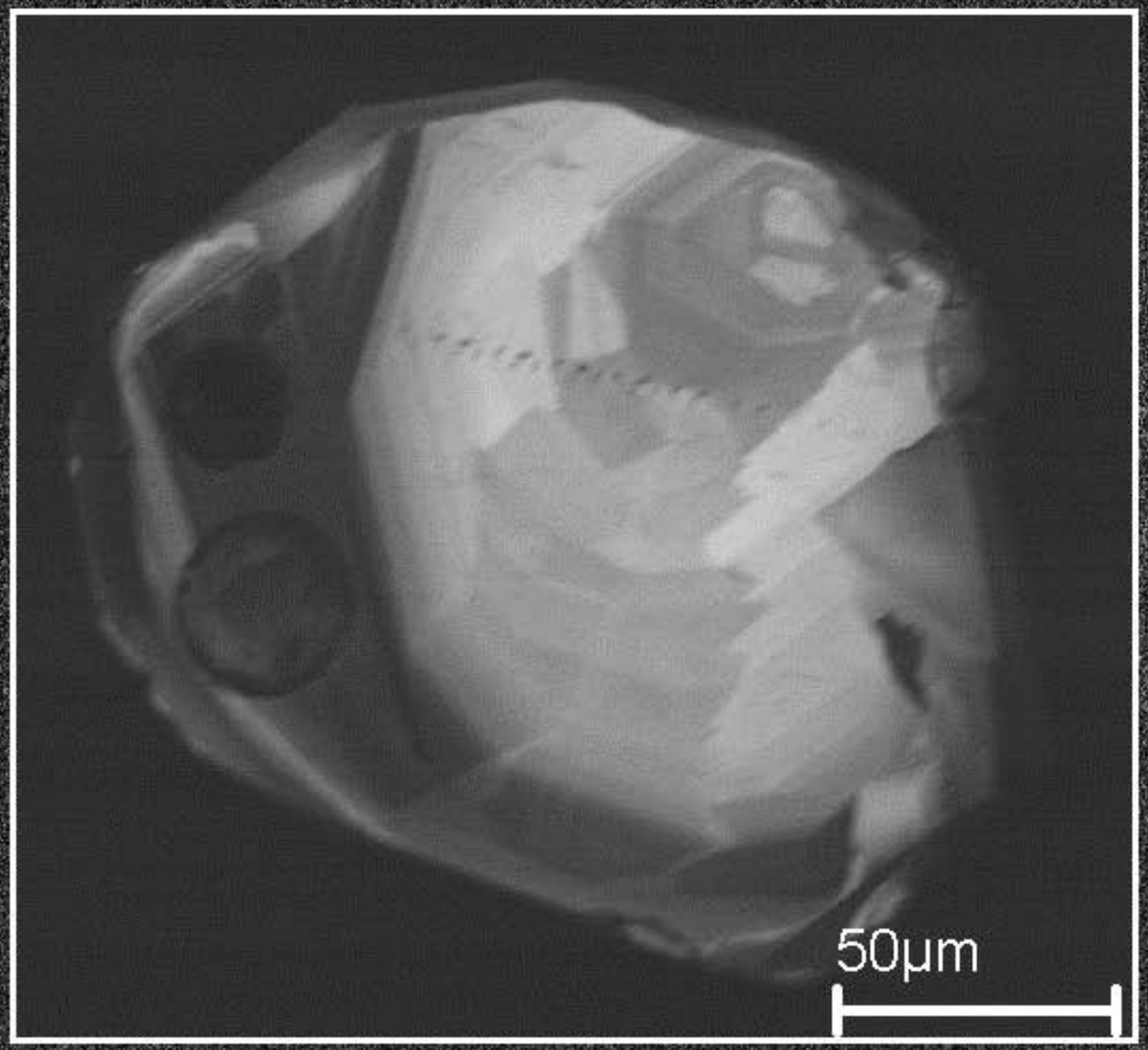

Amostra TQ-14

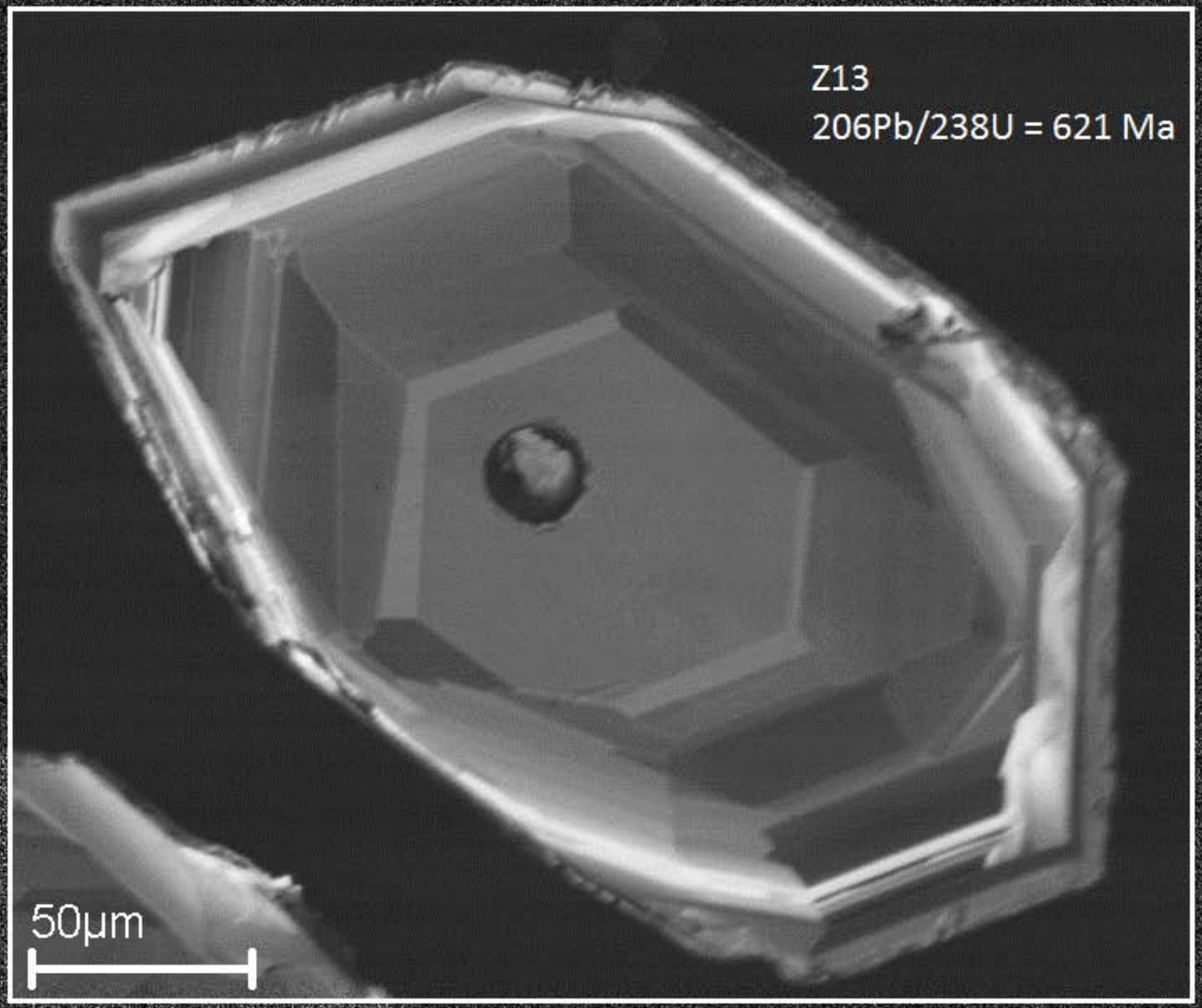

Amostra TQ-14

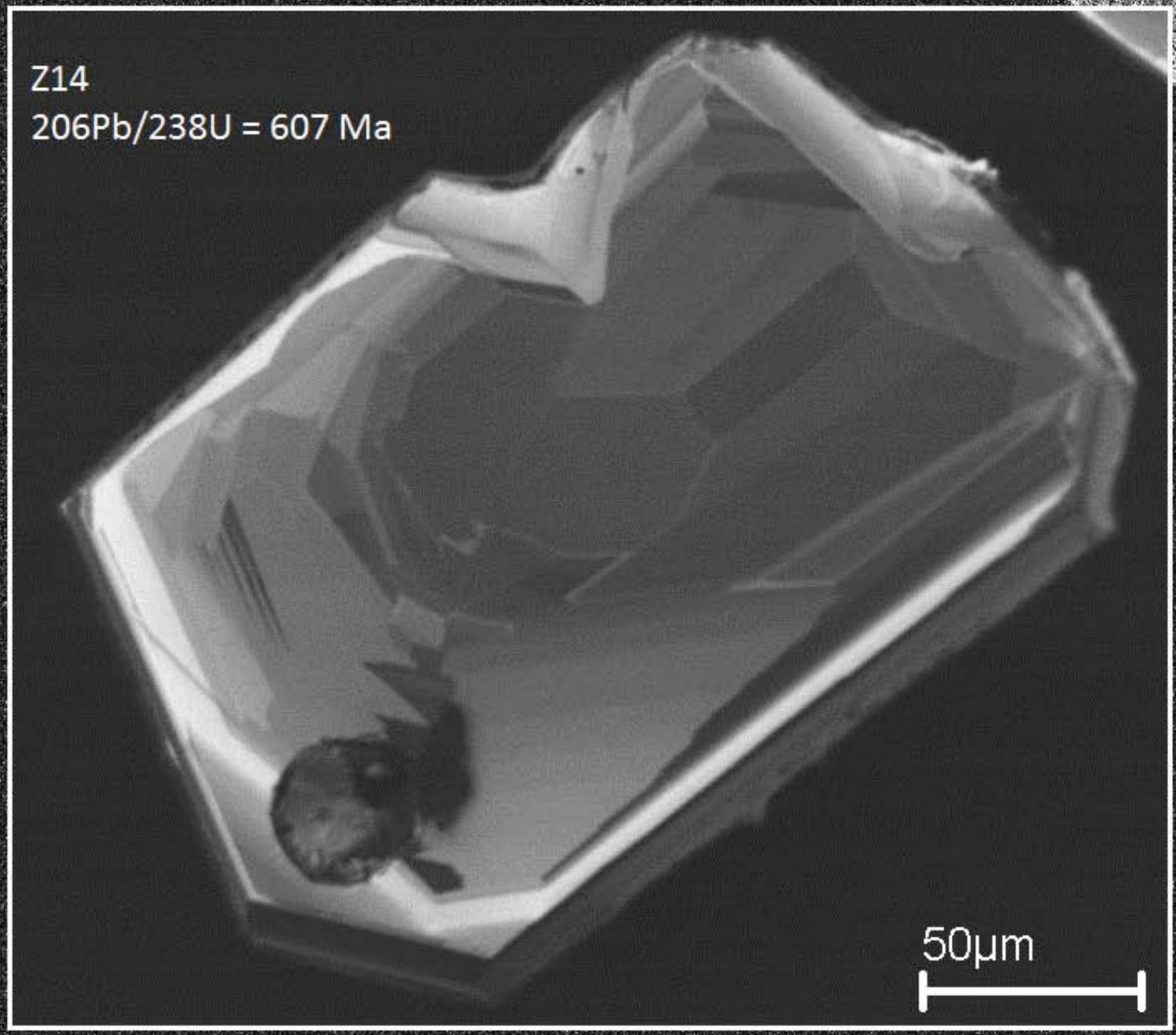

Amostra TQ-14

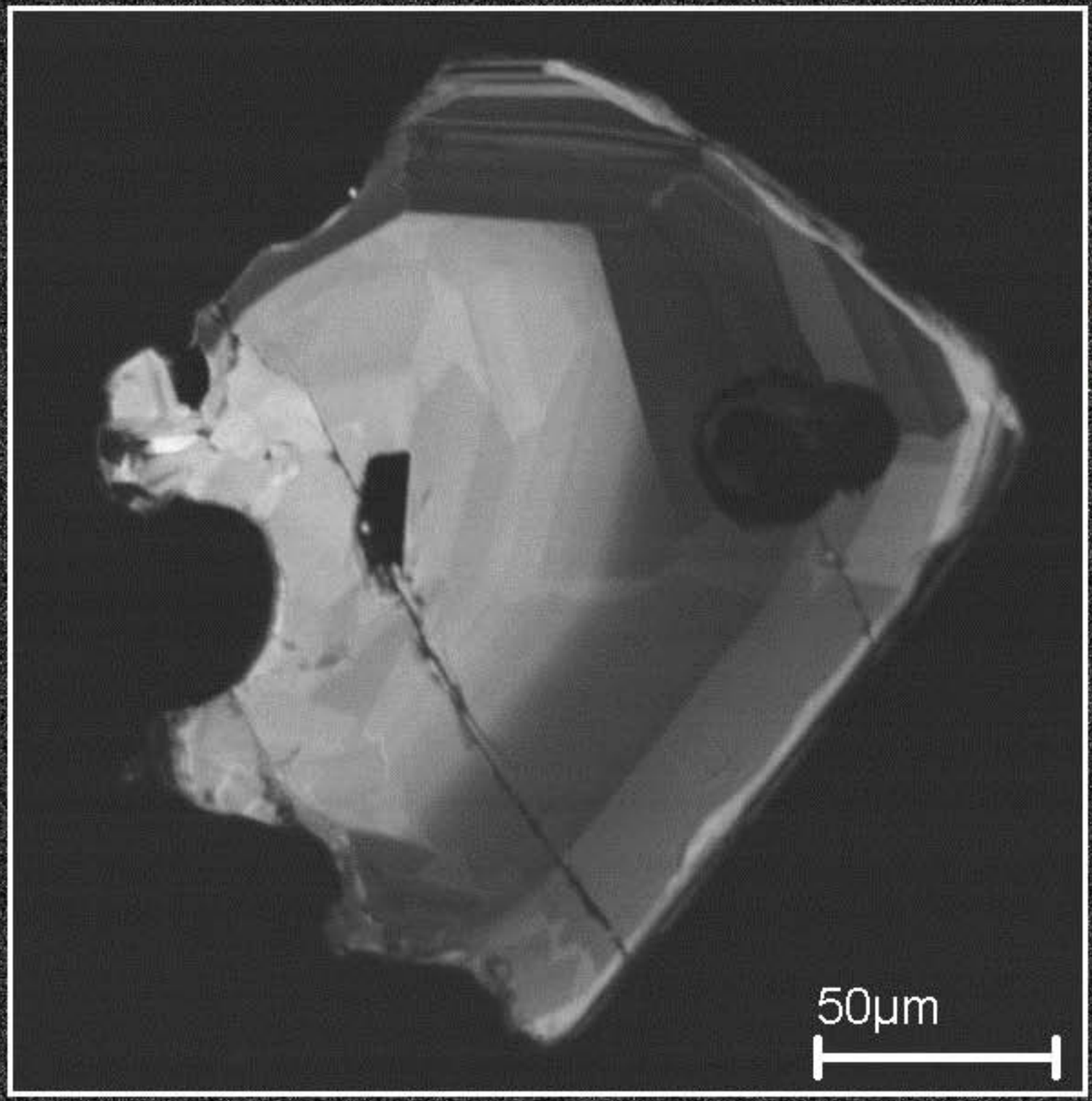

Z15
206Pb/238U = 620 Ma

Amostra TQ-14

Z16

206Pb/238U = 650 Ma

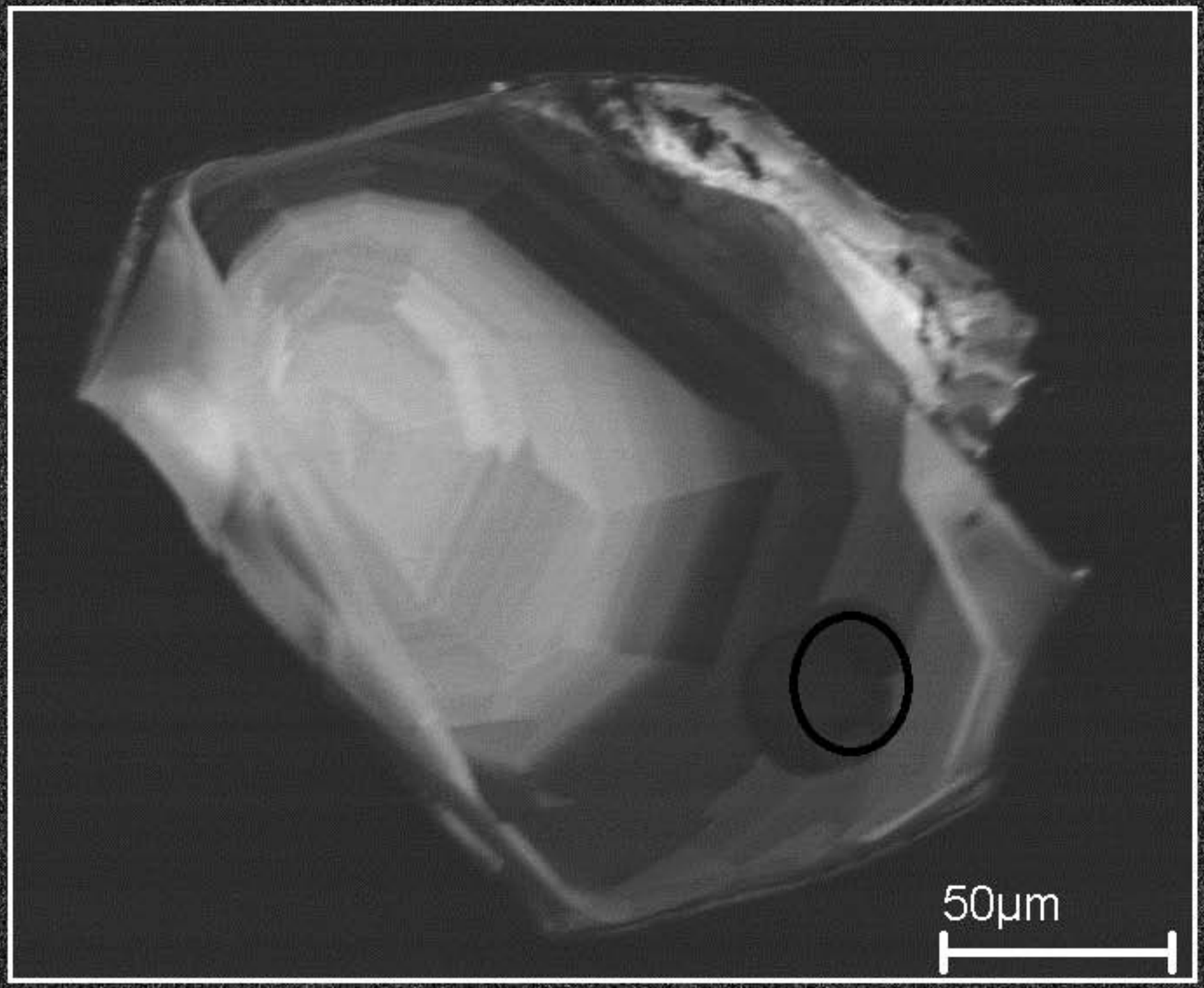

Amostra TQ-14

Z17
206Pb/238U = 624 Ma

Amostra TQ-14

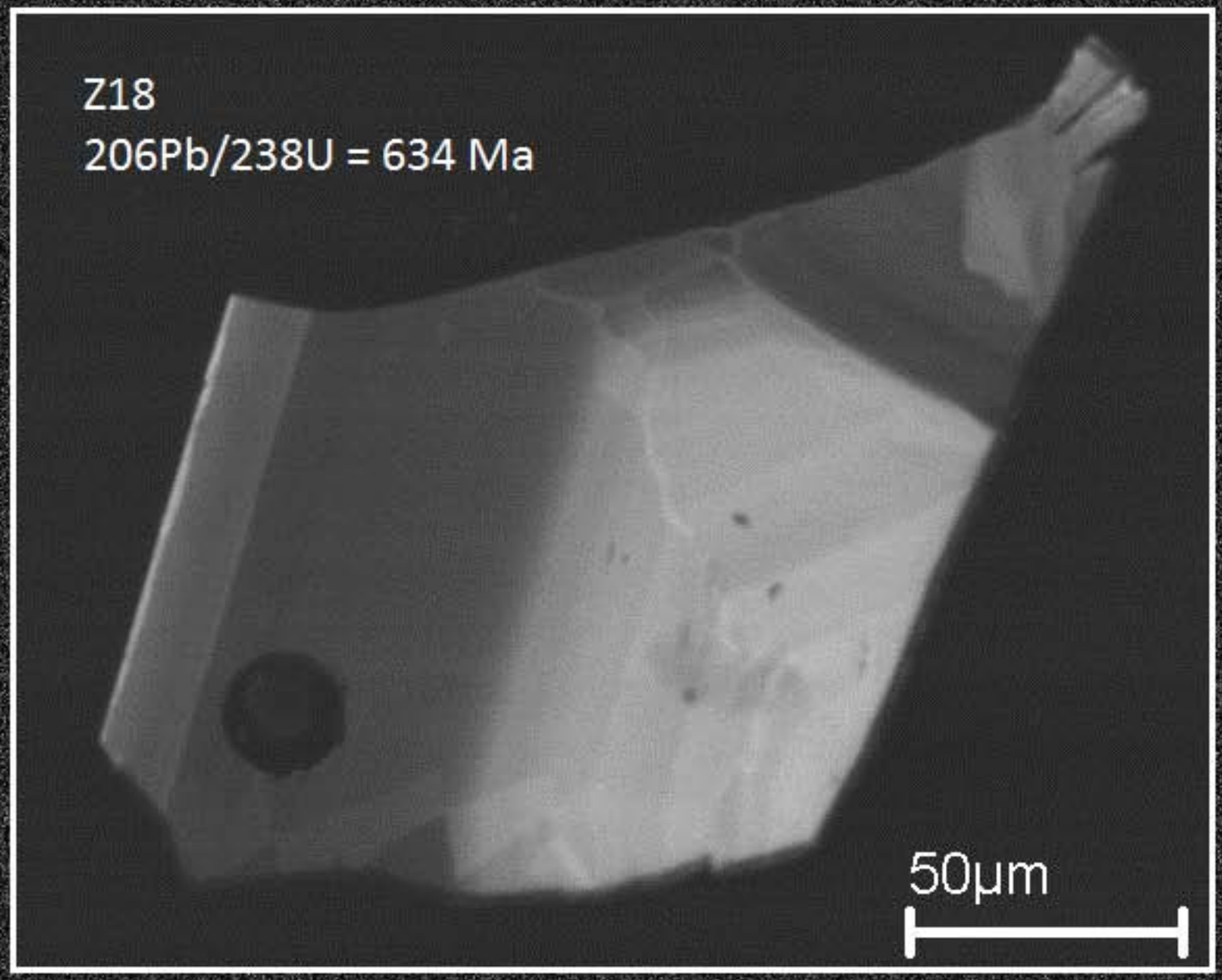

Amostra TQ-14

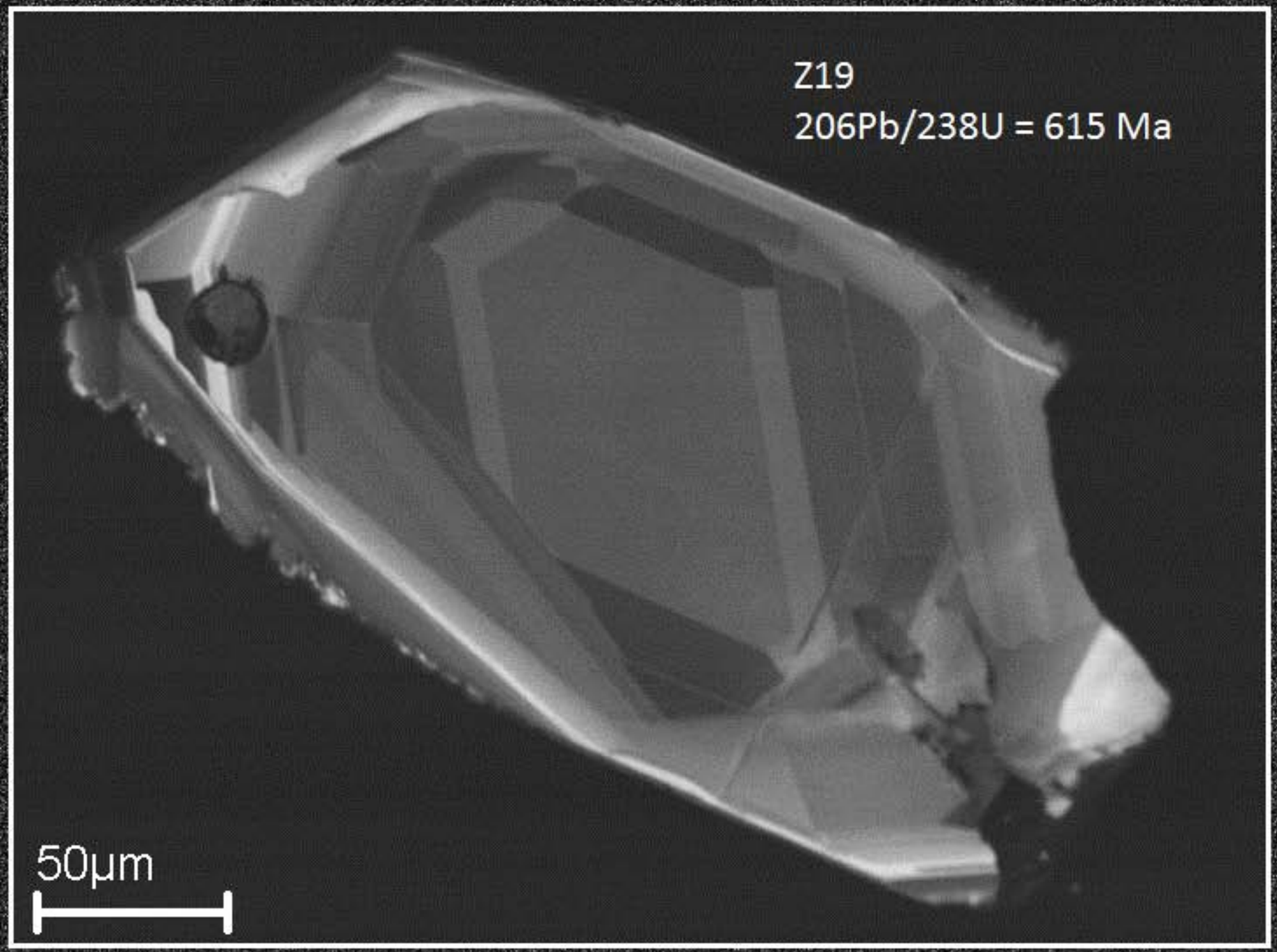

COMPLEXOS MÁFICO-ULTRAMÁFICOS
SERRA DA MALACACHETA E BARRO ALTO

Amostra BAL-09

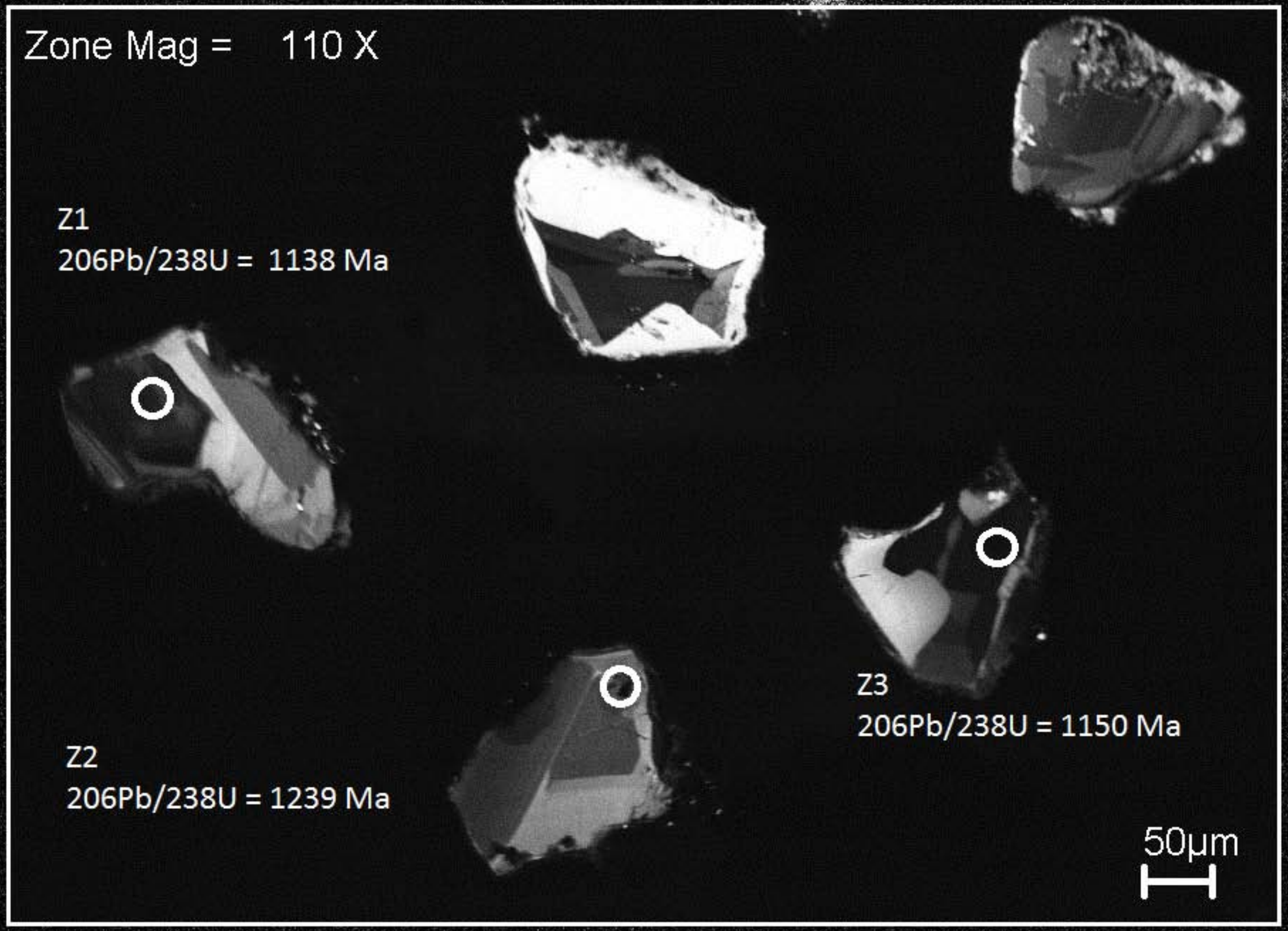

Zone Mag = 190 X

Z4
206Pb/238U = 1224 Ma

Z5
206Pb/238U = 1232 Ma

Z6
206Pb/238U = 1281 Ma

50µm

Amostra BAL-09

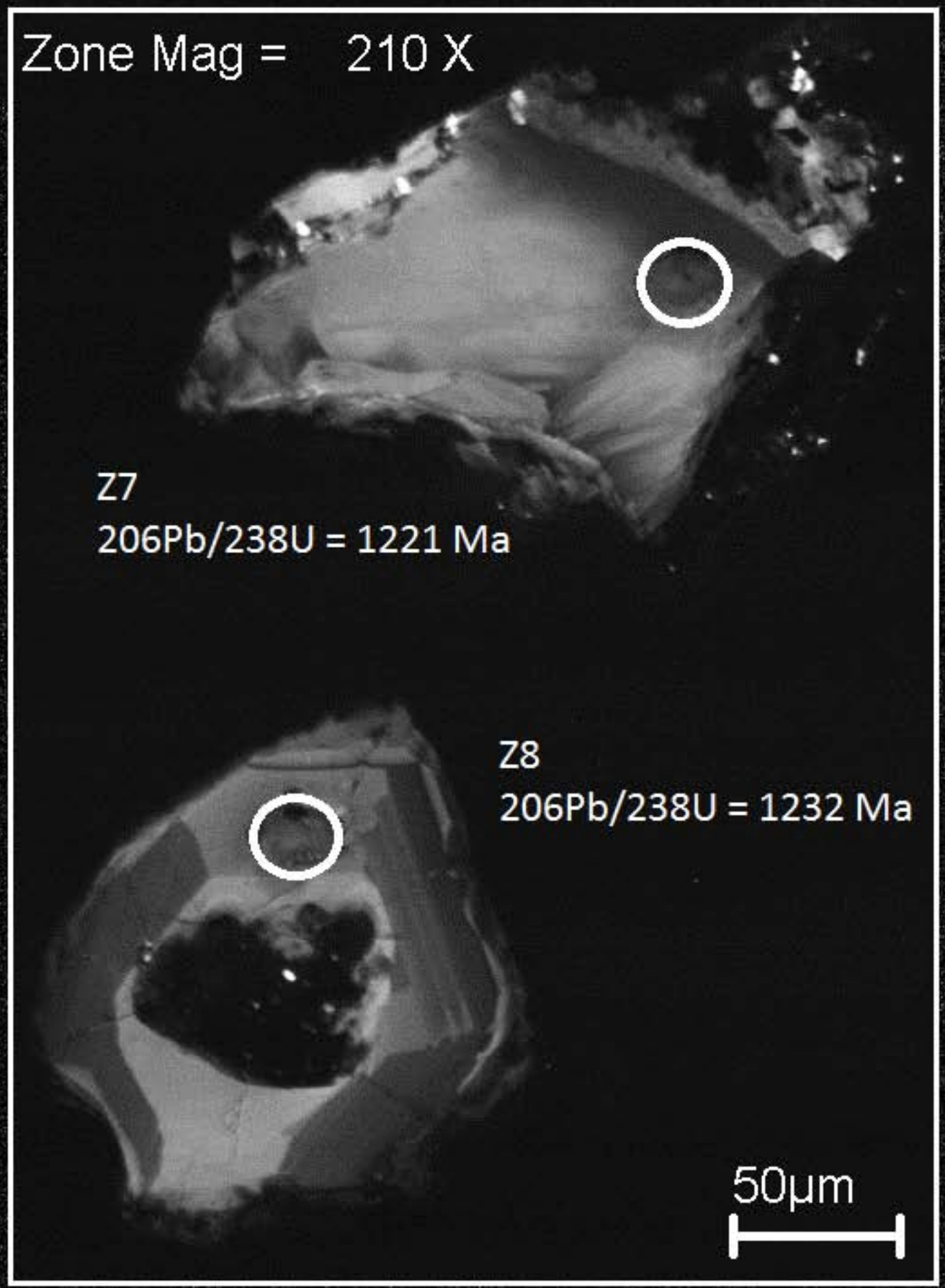

Amostra BAL-09

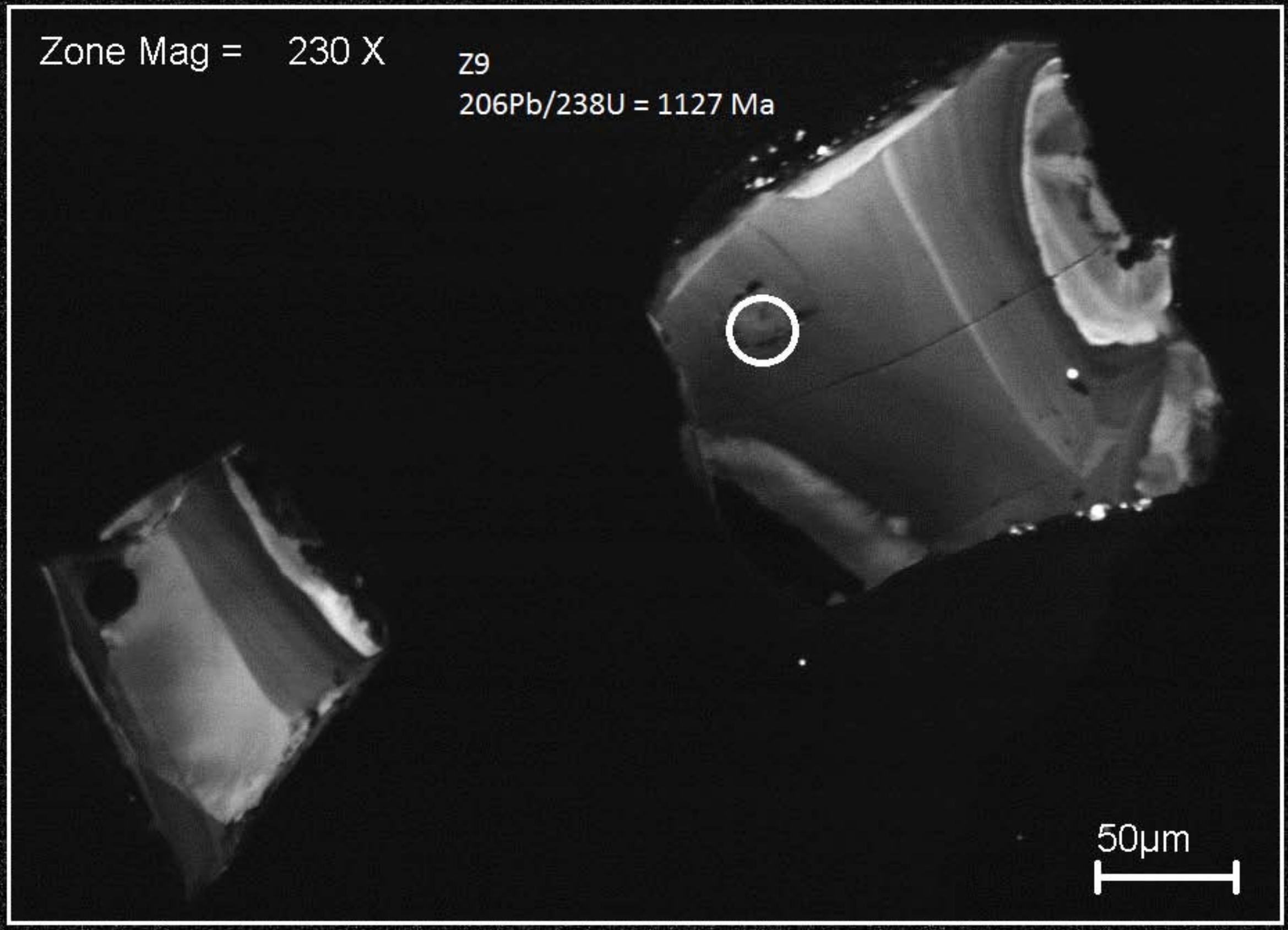

Amostra BAL-09

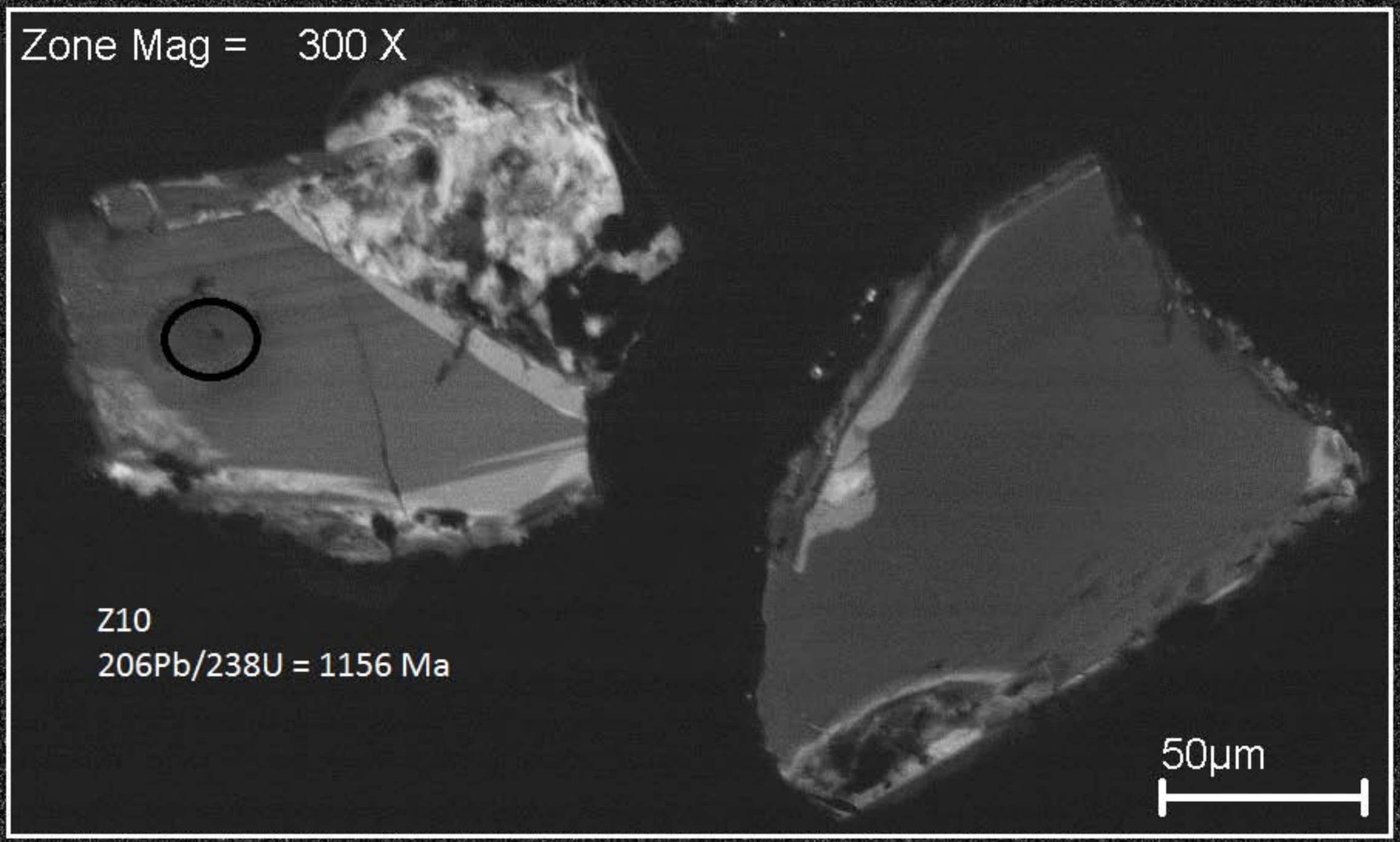

Amostra BAL-09

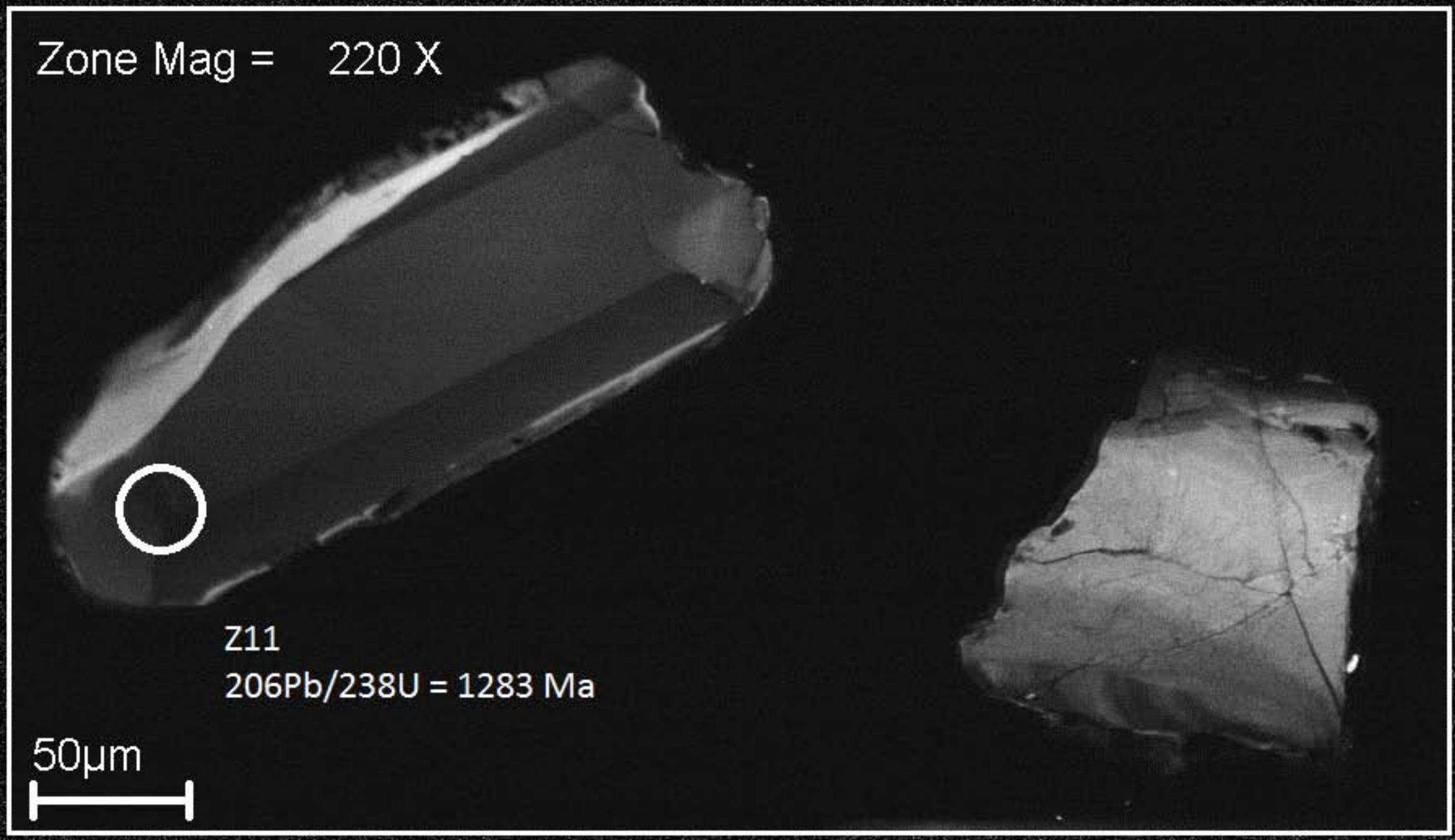

Amostra BAL-09

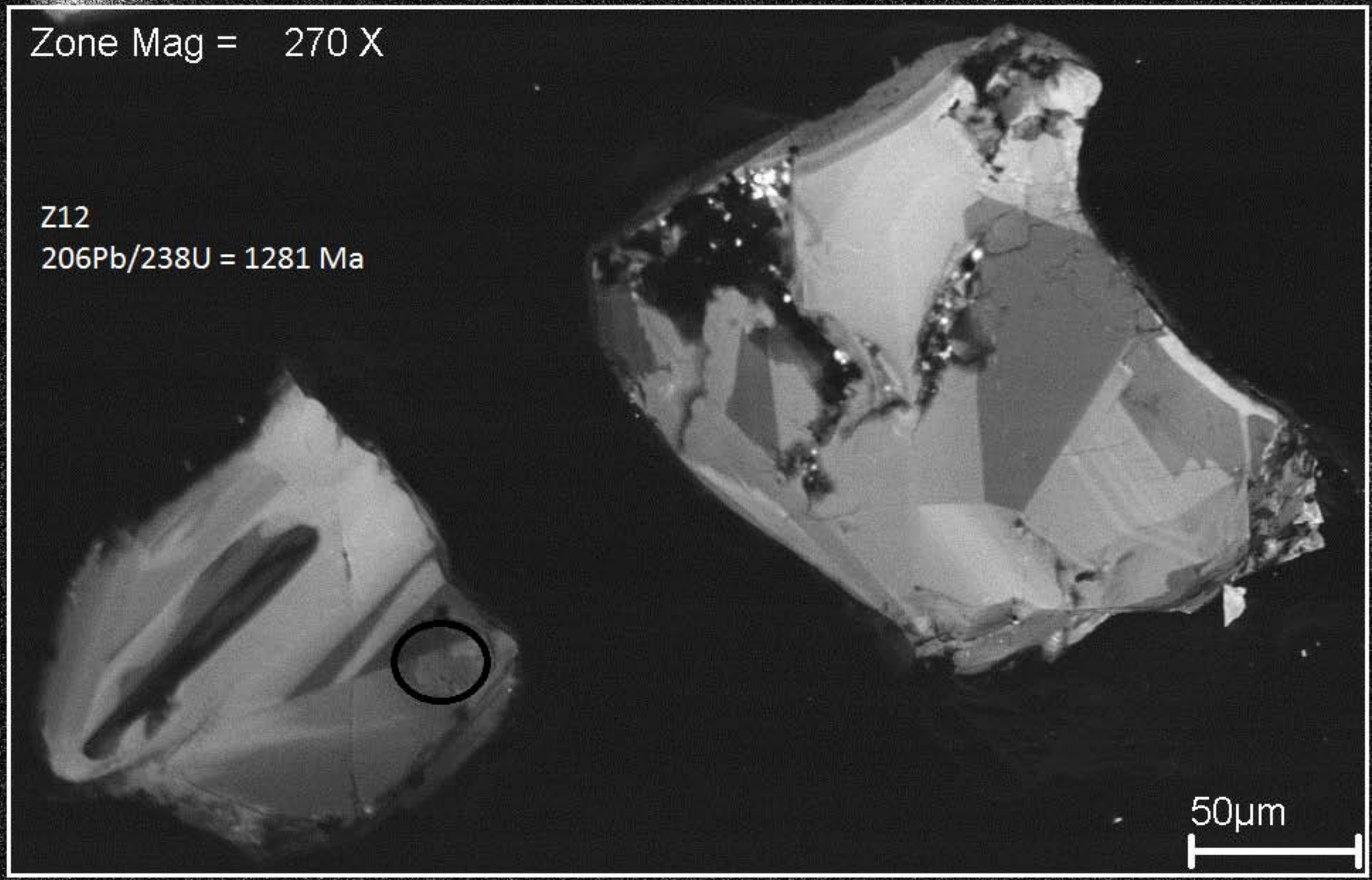

Amostra BAL-09

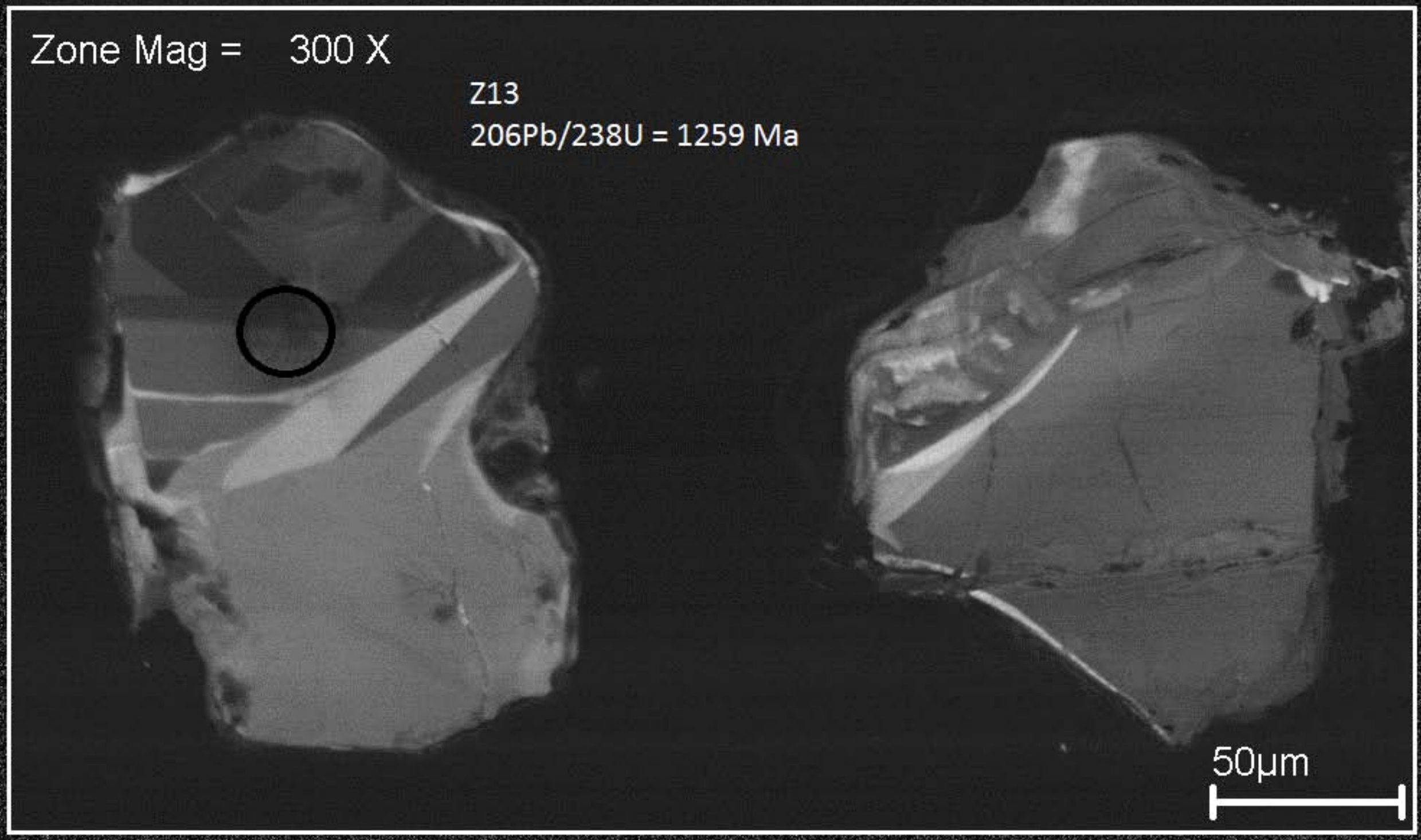

Amostra BAL-09

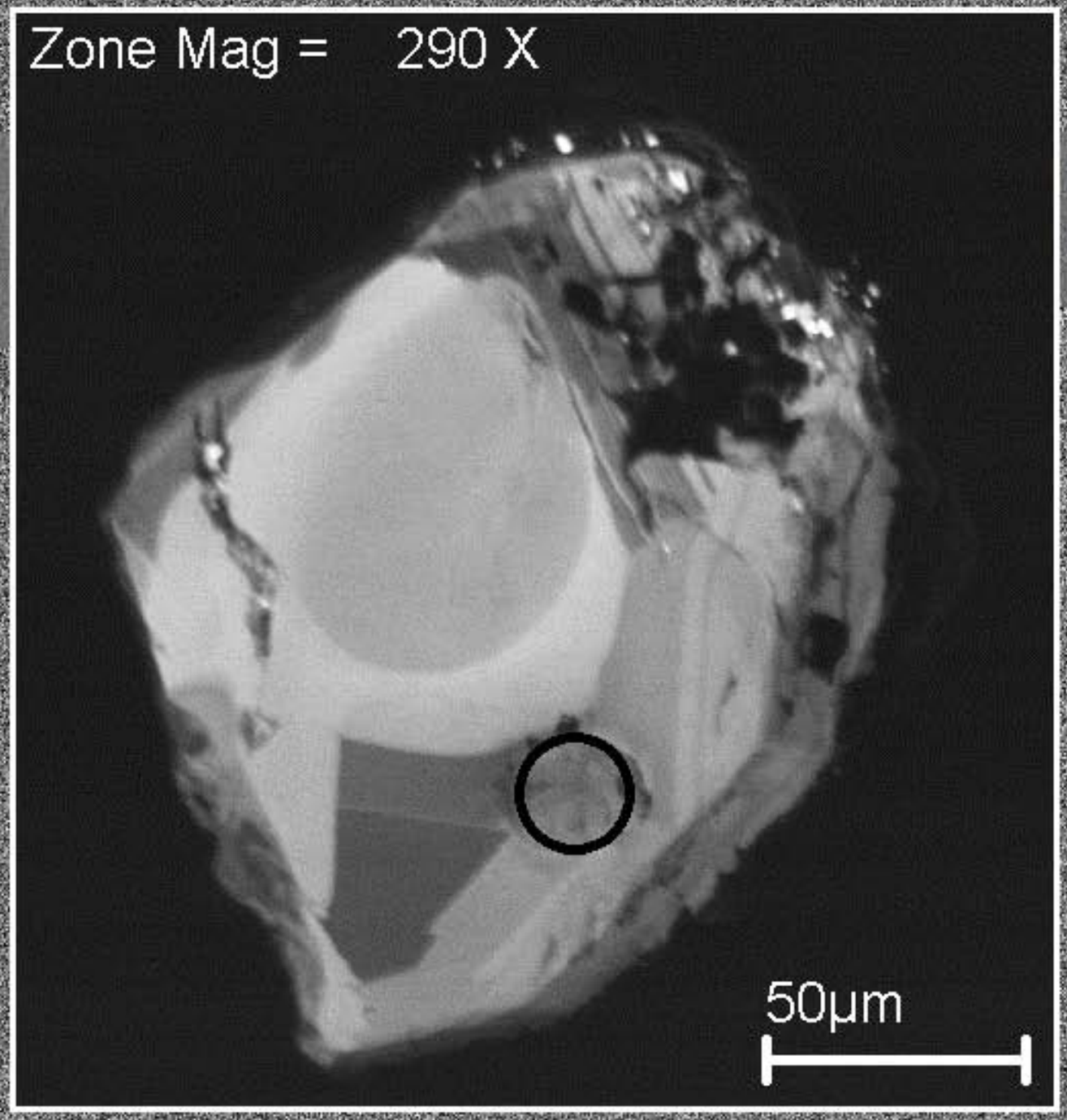

Z14
206Pb/238U = 1301 Ma

Amostra BAL-09

Z15

206Pb/238U = 1264 Ma

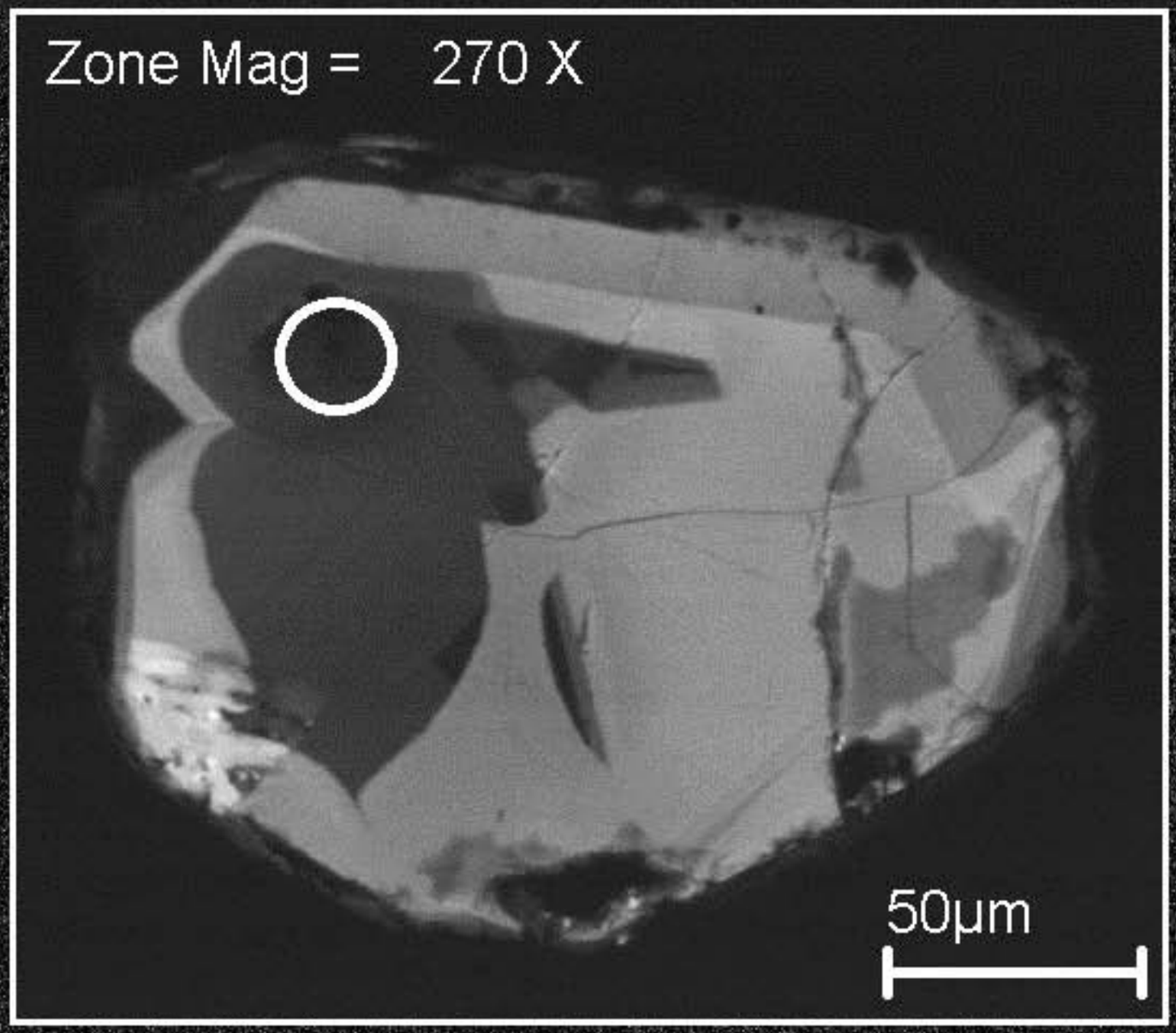

Amostra BAL-09

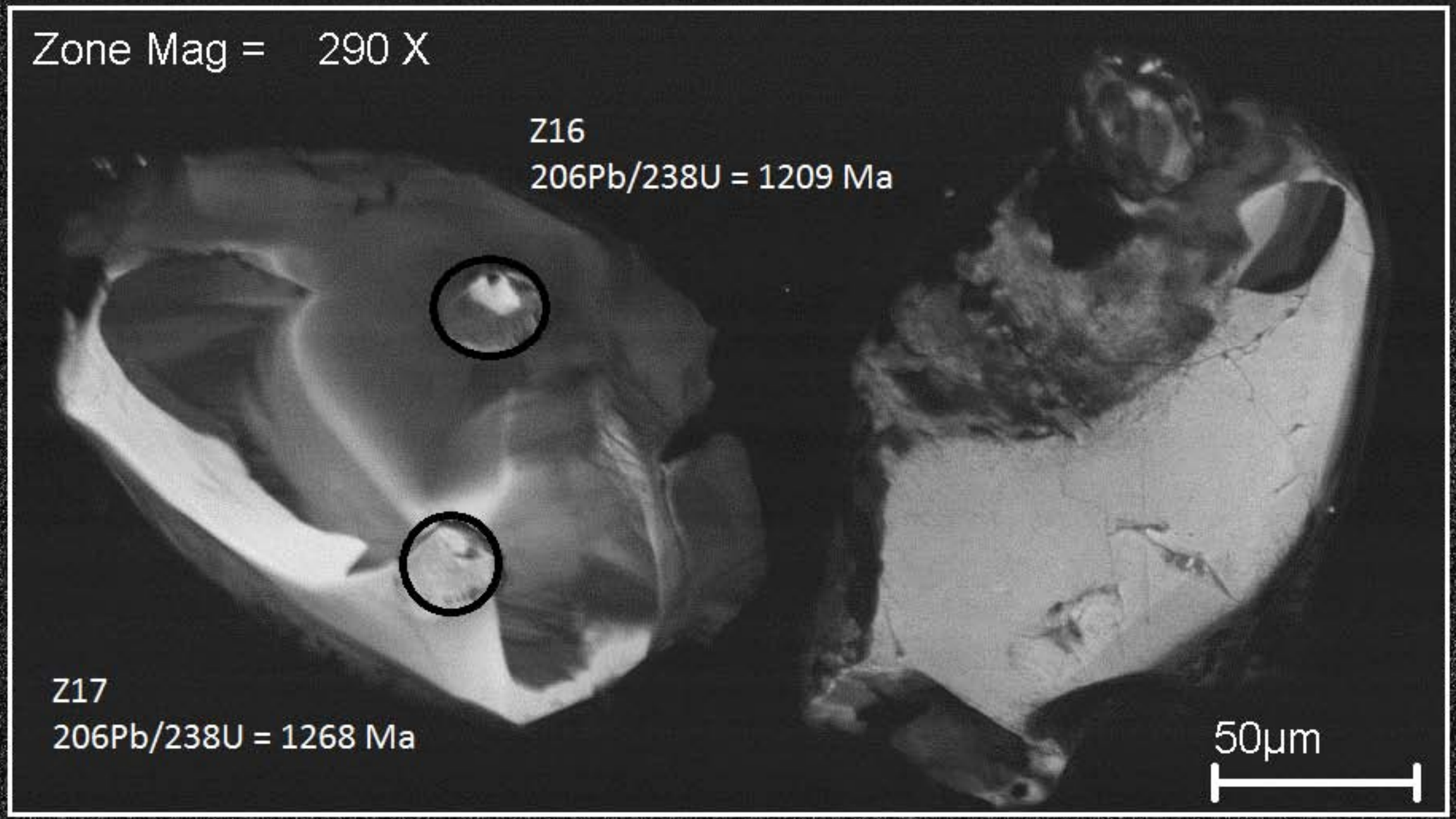

Amostra BAL-09

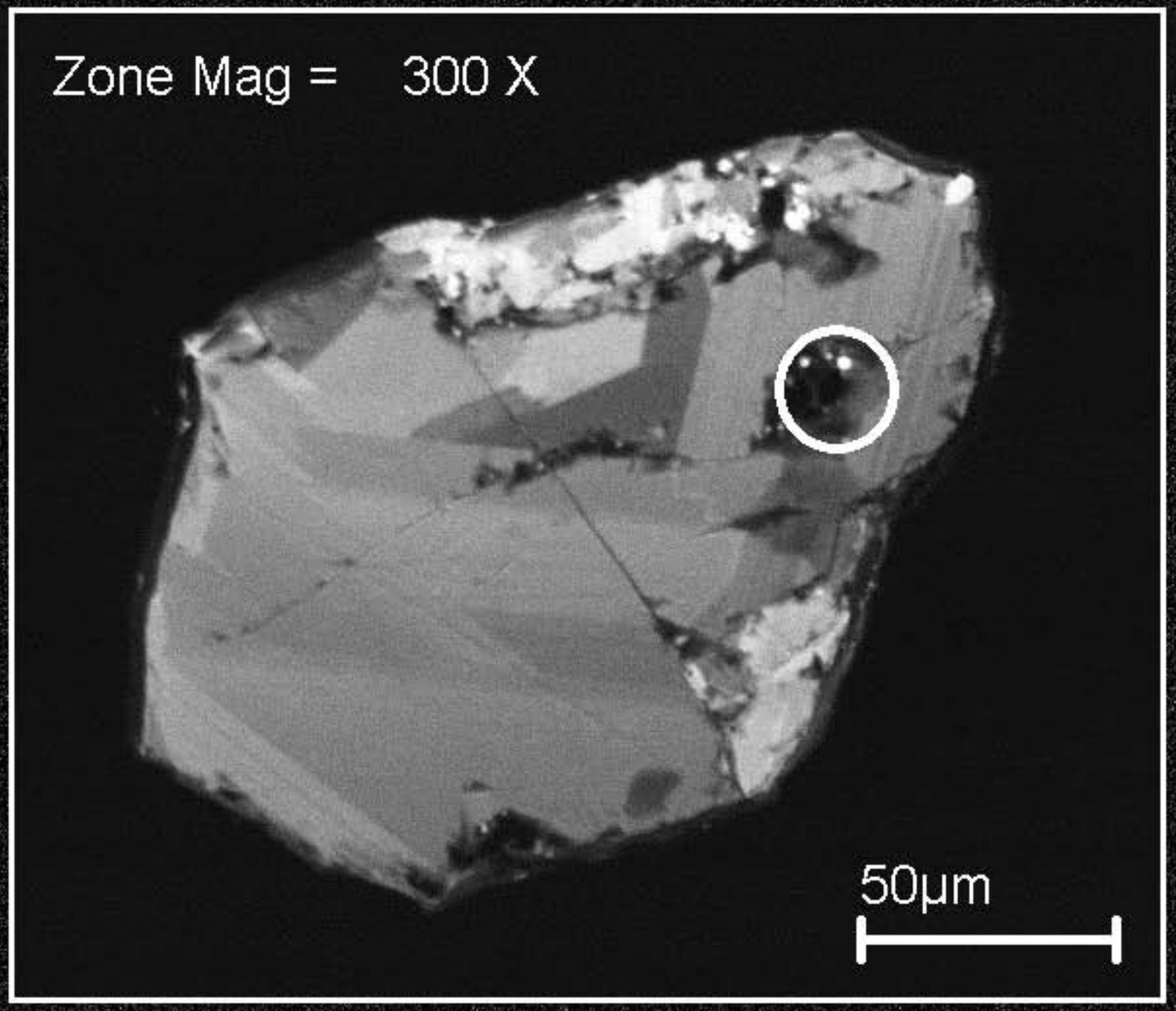

Z18
206Pb/238U = 1293 Ma

Amostra CAFEL

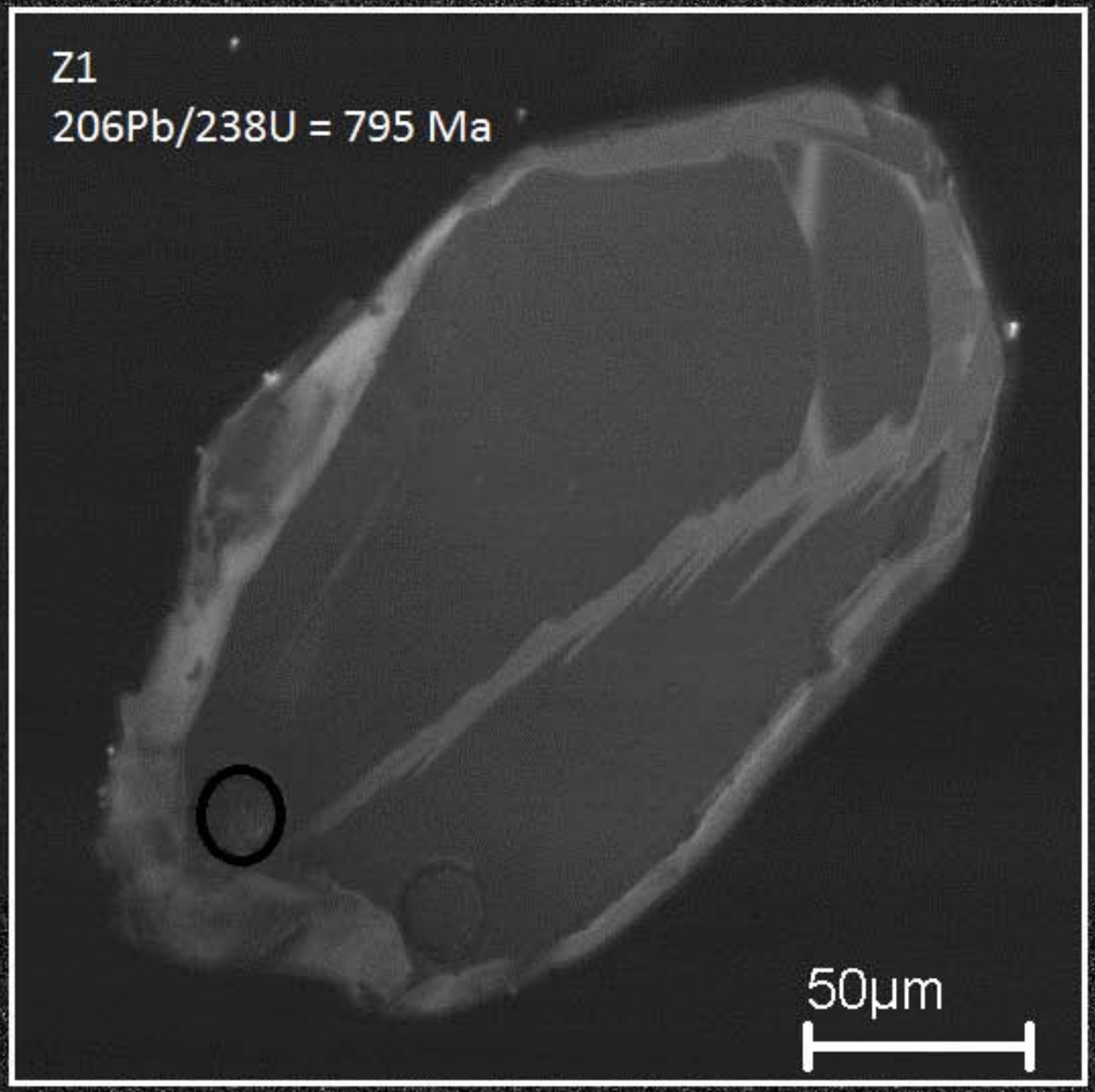

Amostra CAFEL

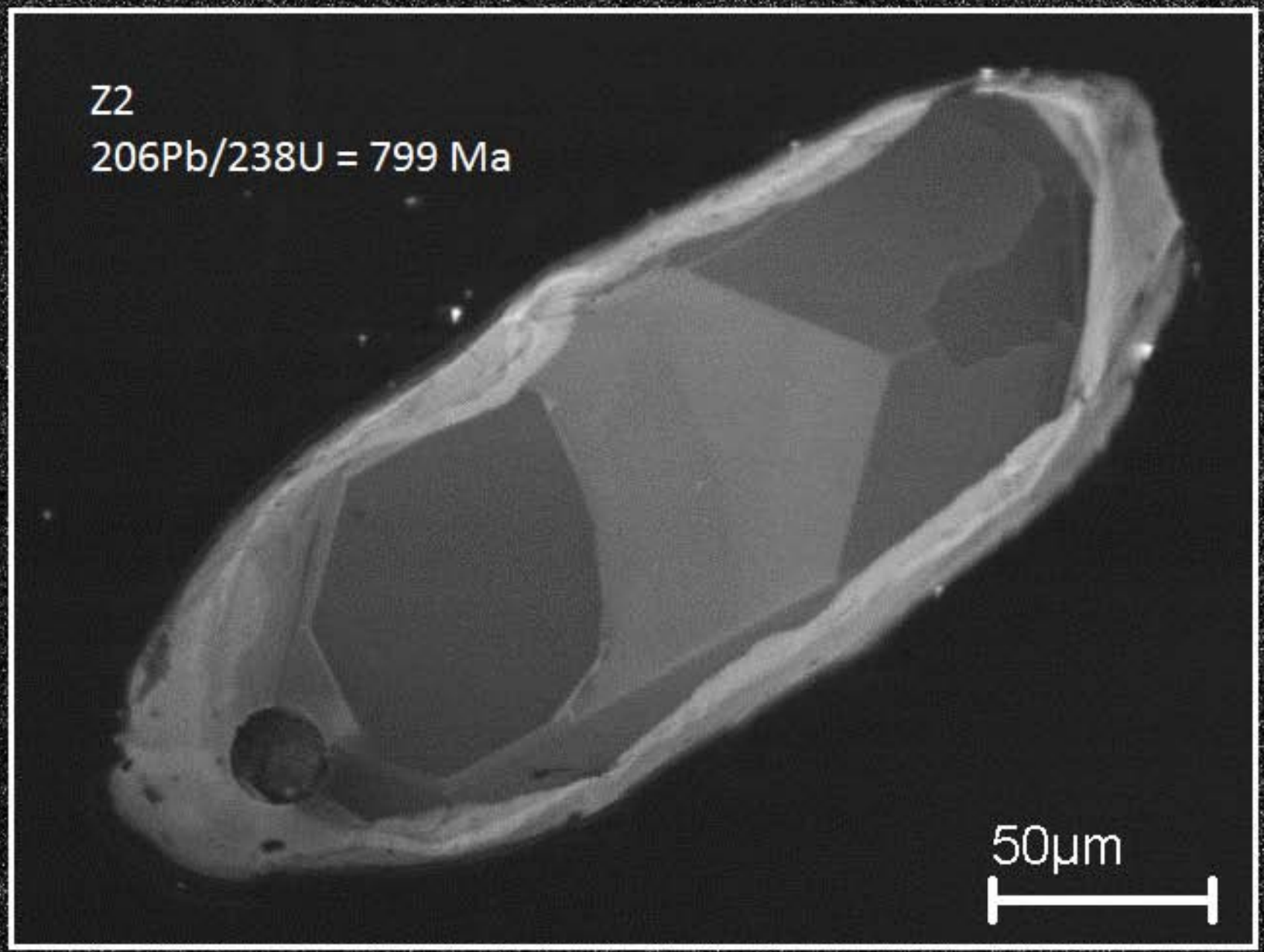

Amostra CAFEL

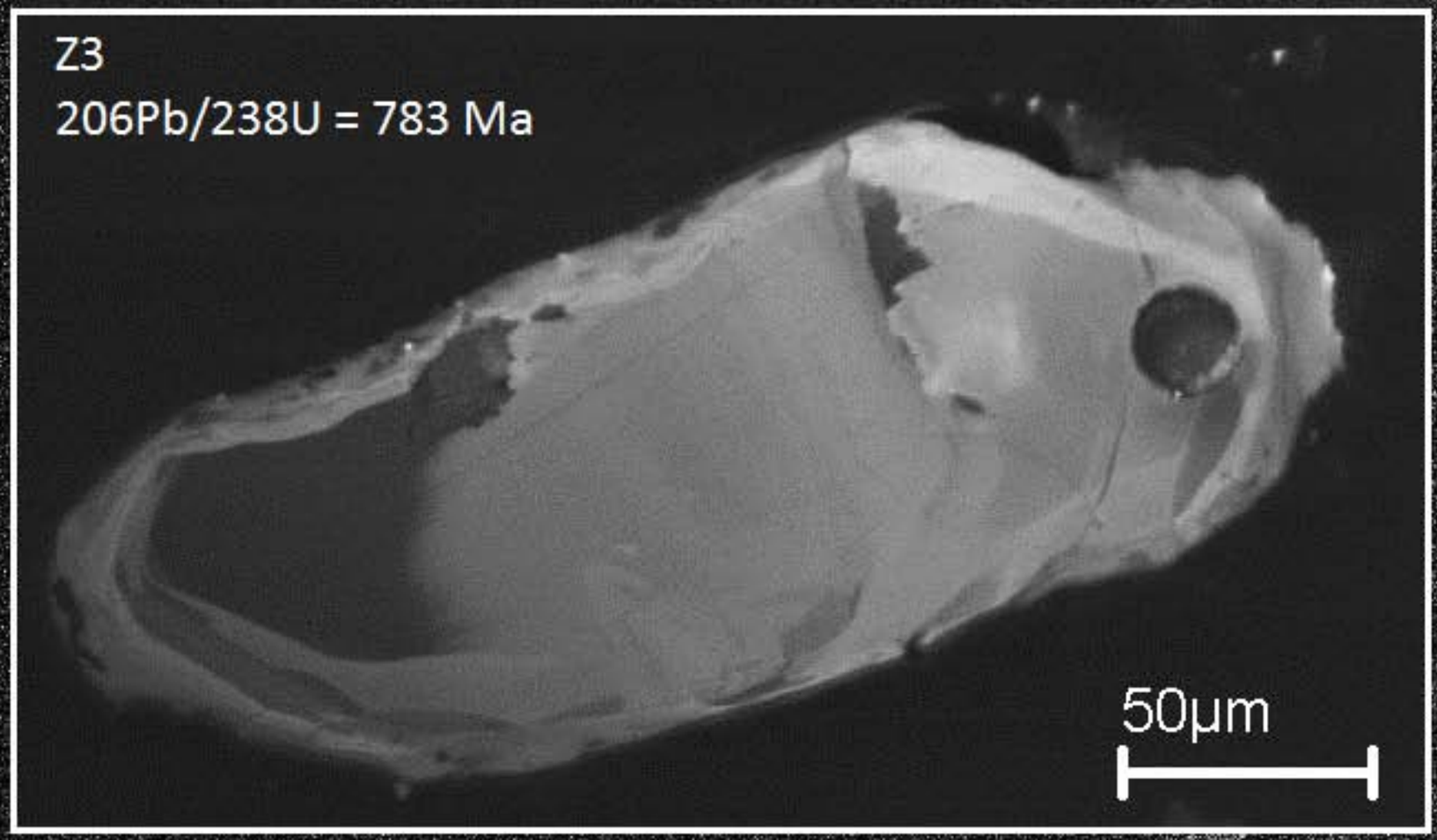

Amostra CAFEL

Amostra CAFEL

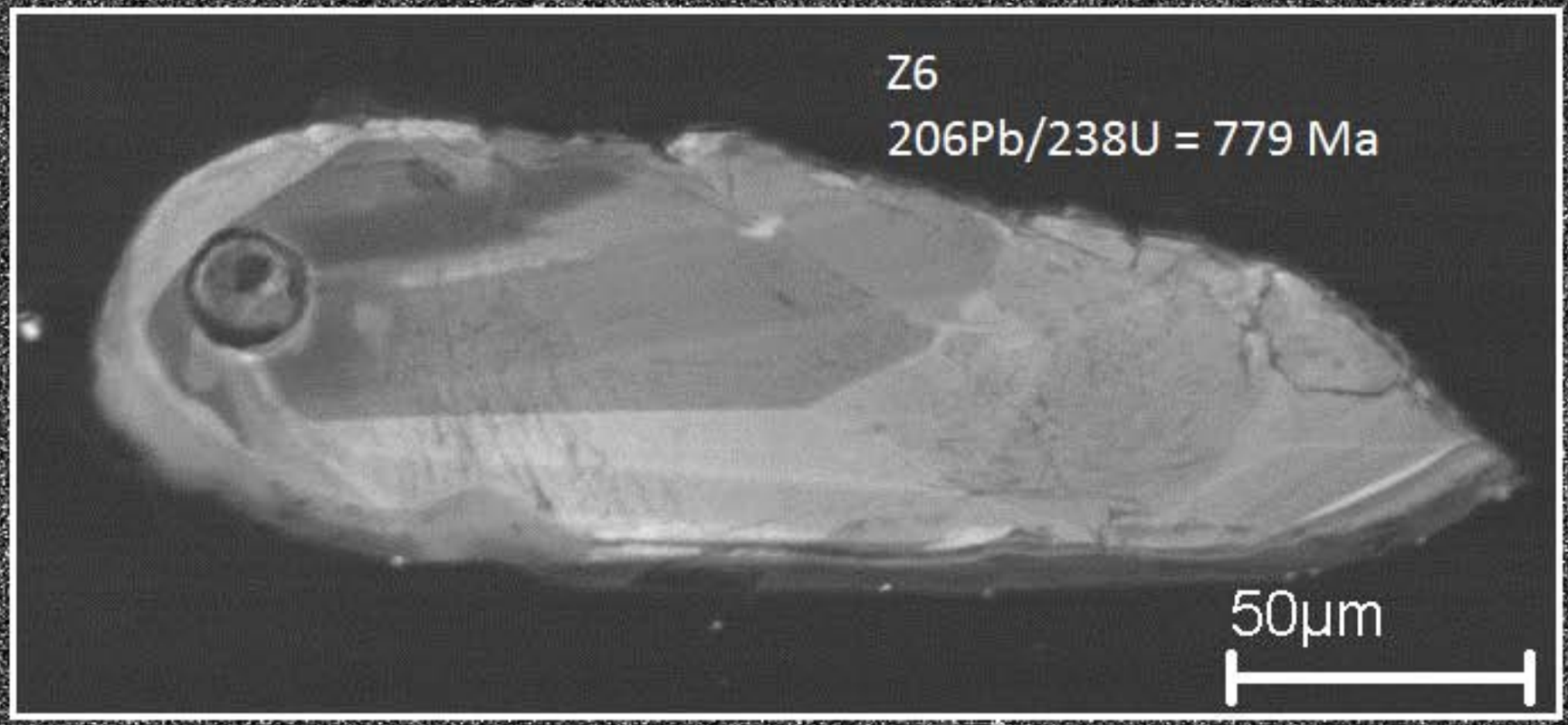

Amostra CAFEL

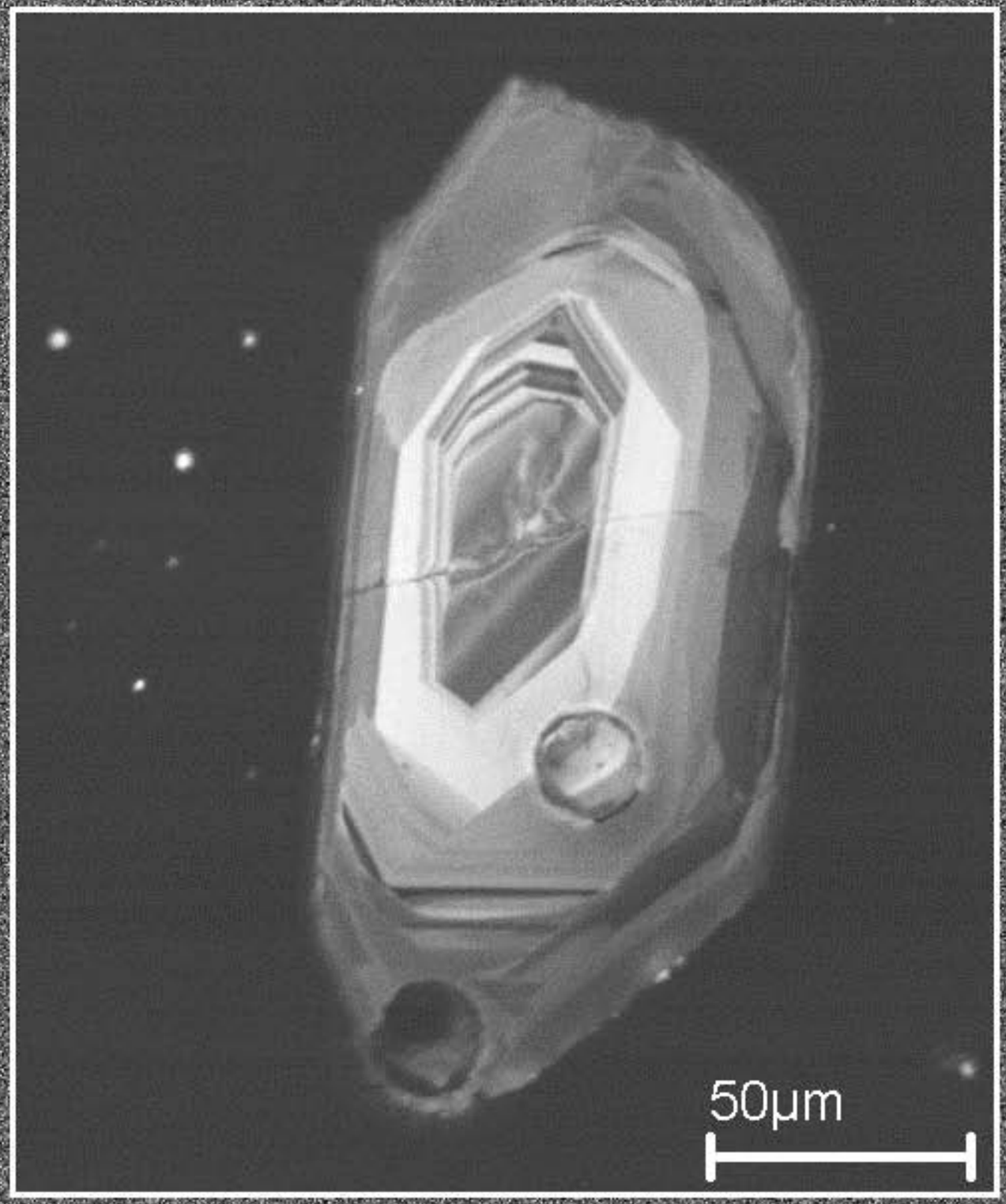

Z7-core
206Pb/238U = 764 Ma

Z7-rim
206Pb/238U = 766 Ma

Amostra CAFEL

Amostra CAFEL

Amostra CAFEL

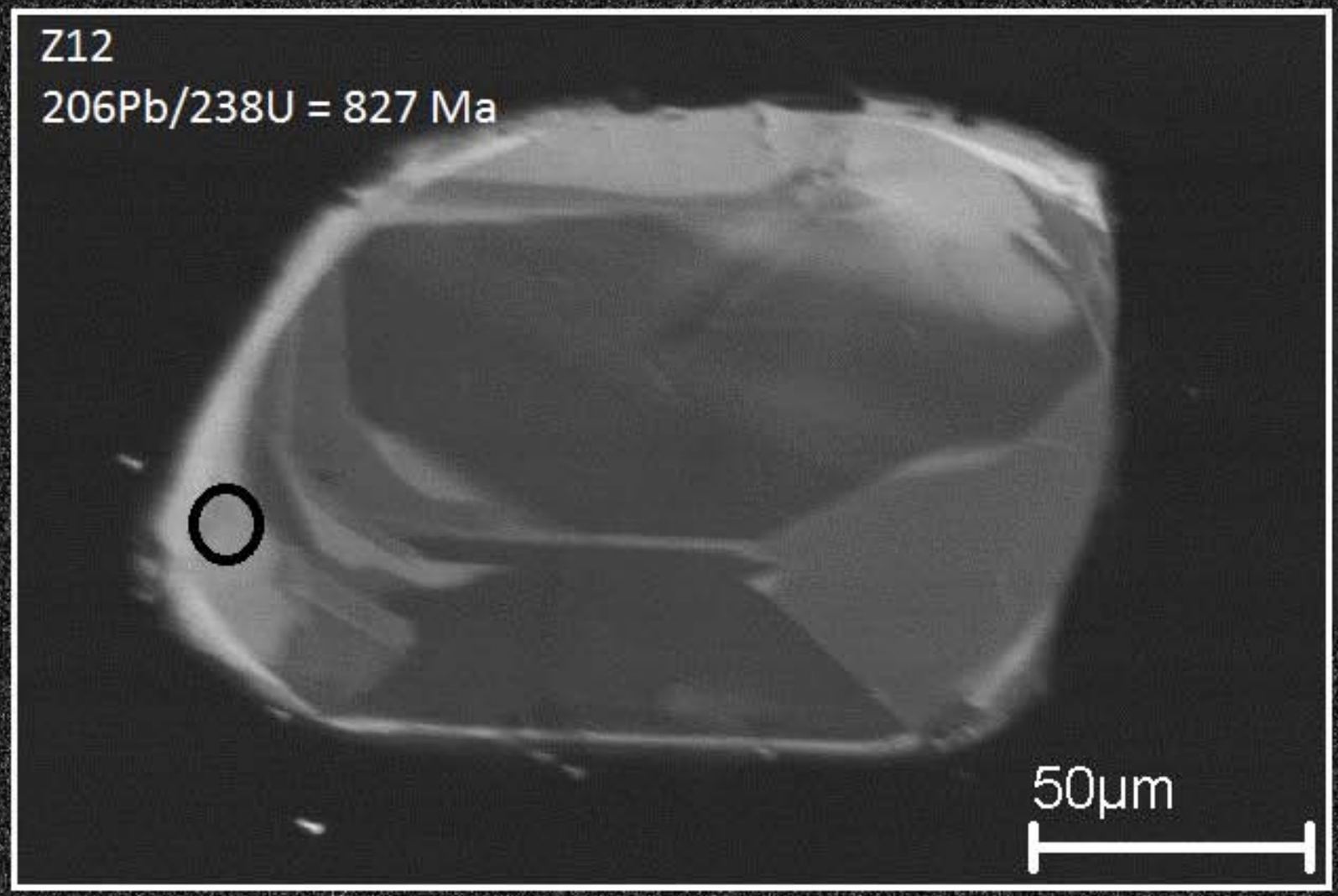

Amostra CAFEL

Z13

206Pb/238U = 779 Ma

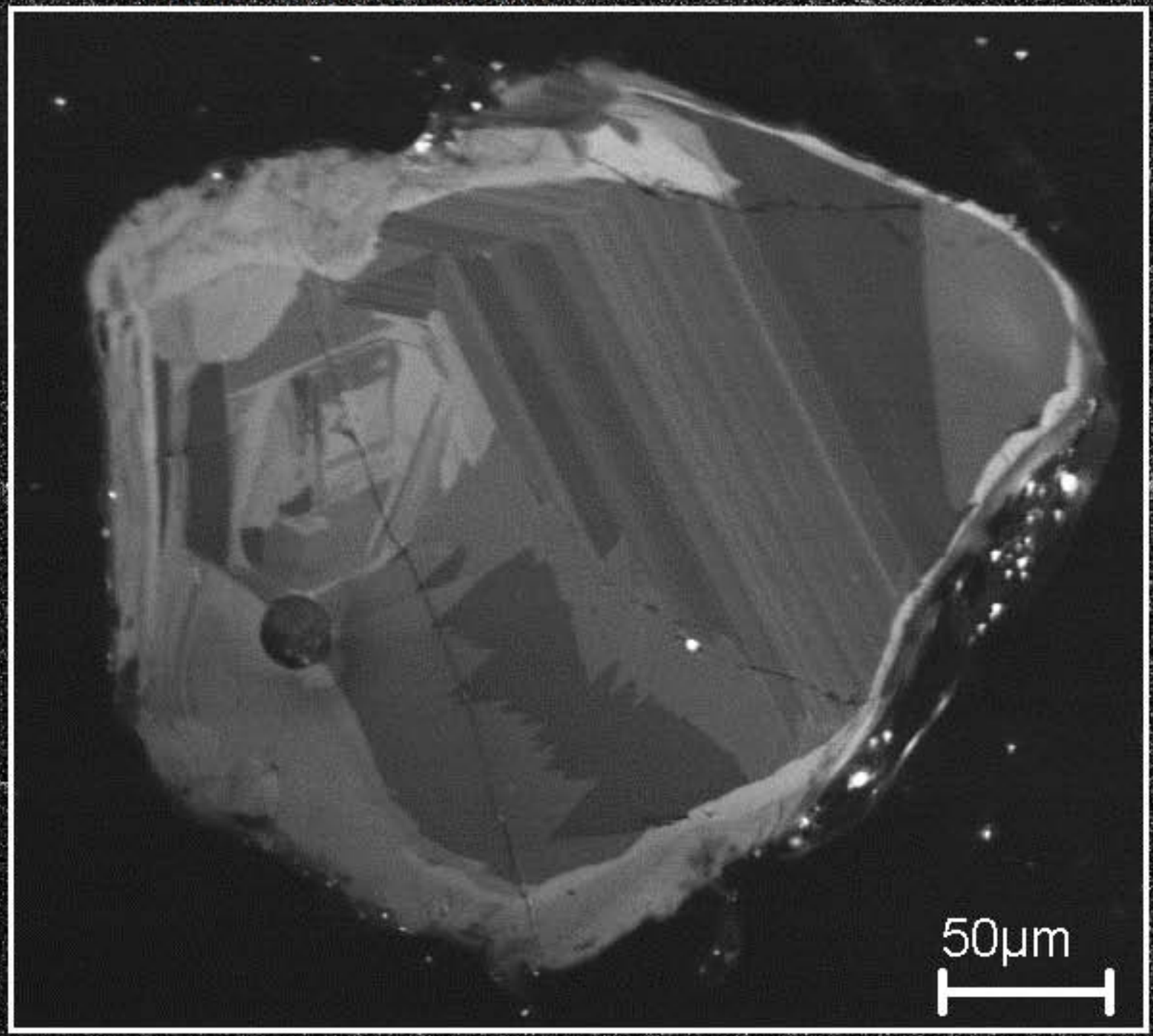

Amostra CAFEL

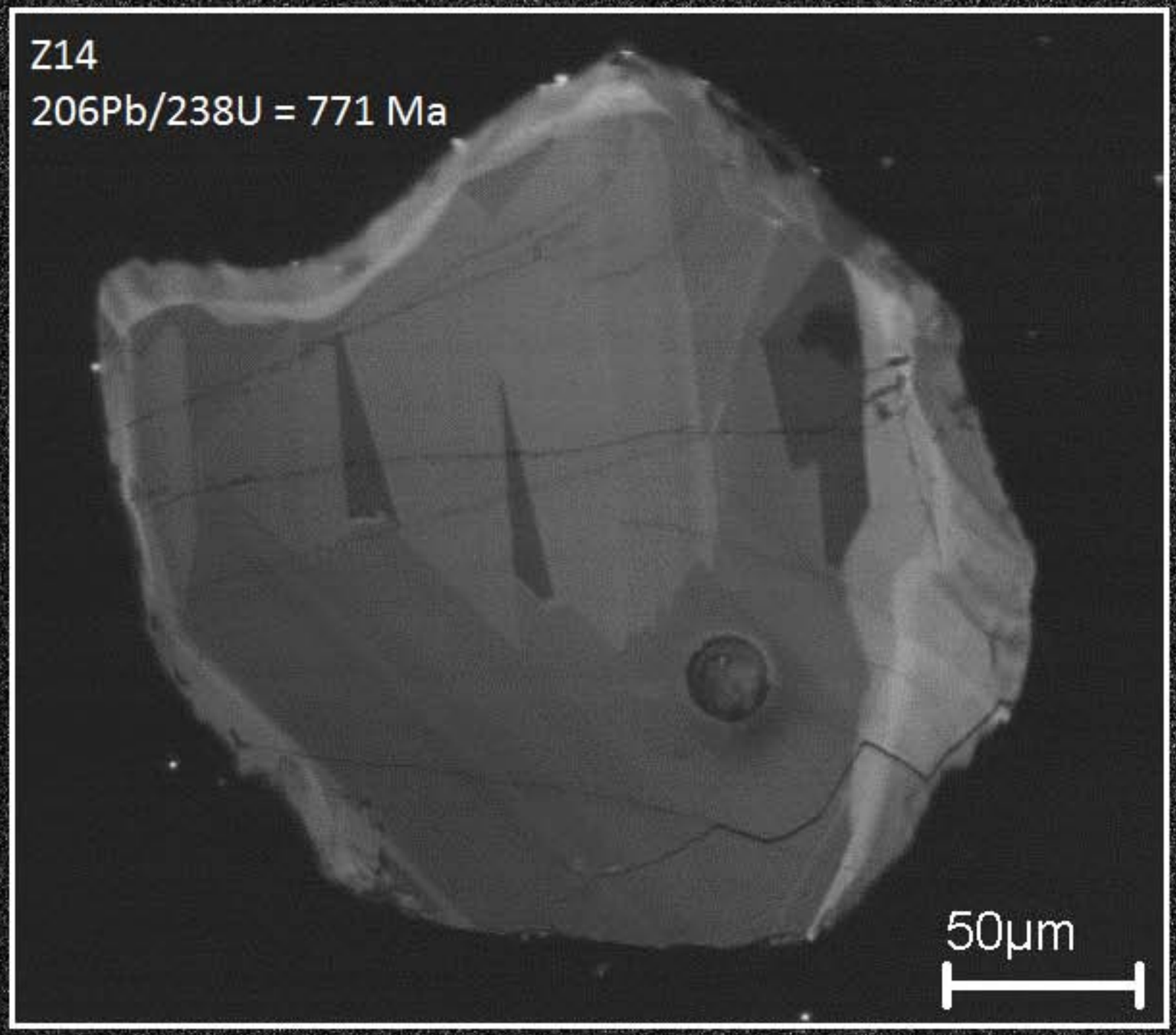

Amostra BAL-05

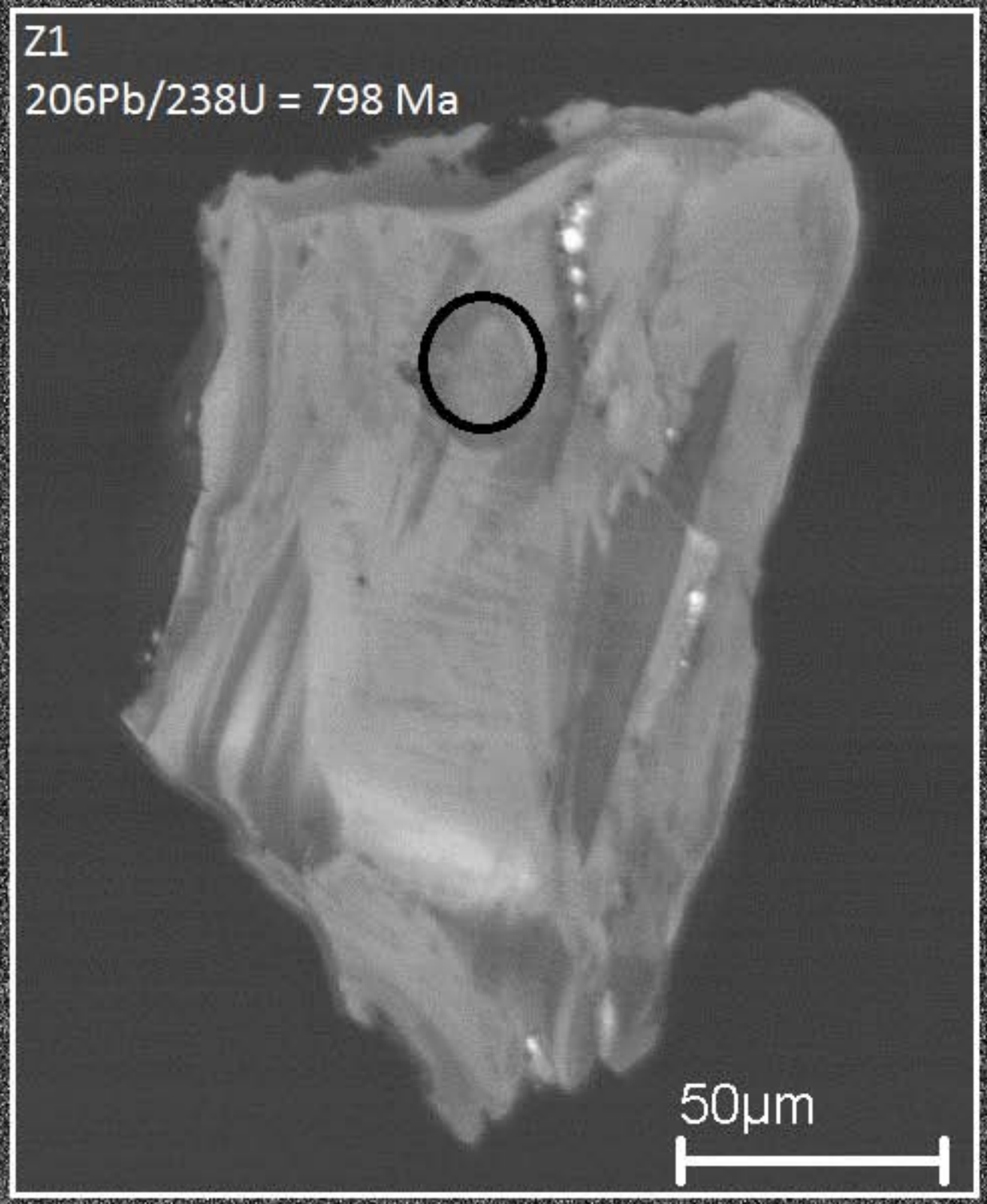

Amostra BAL-05

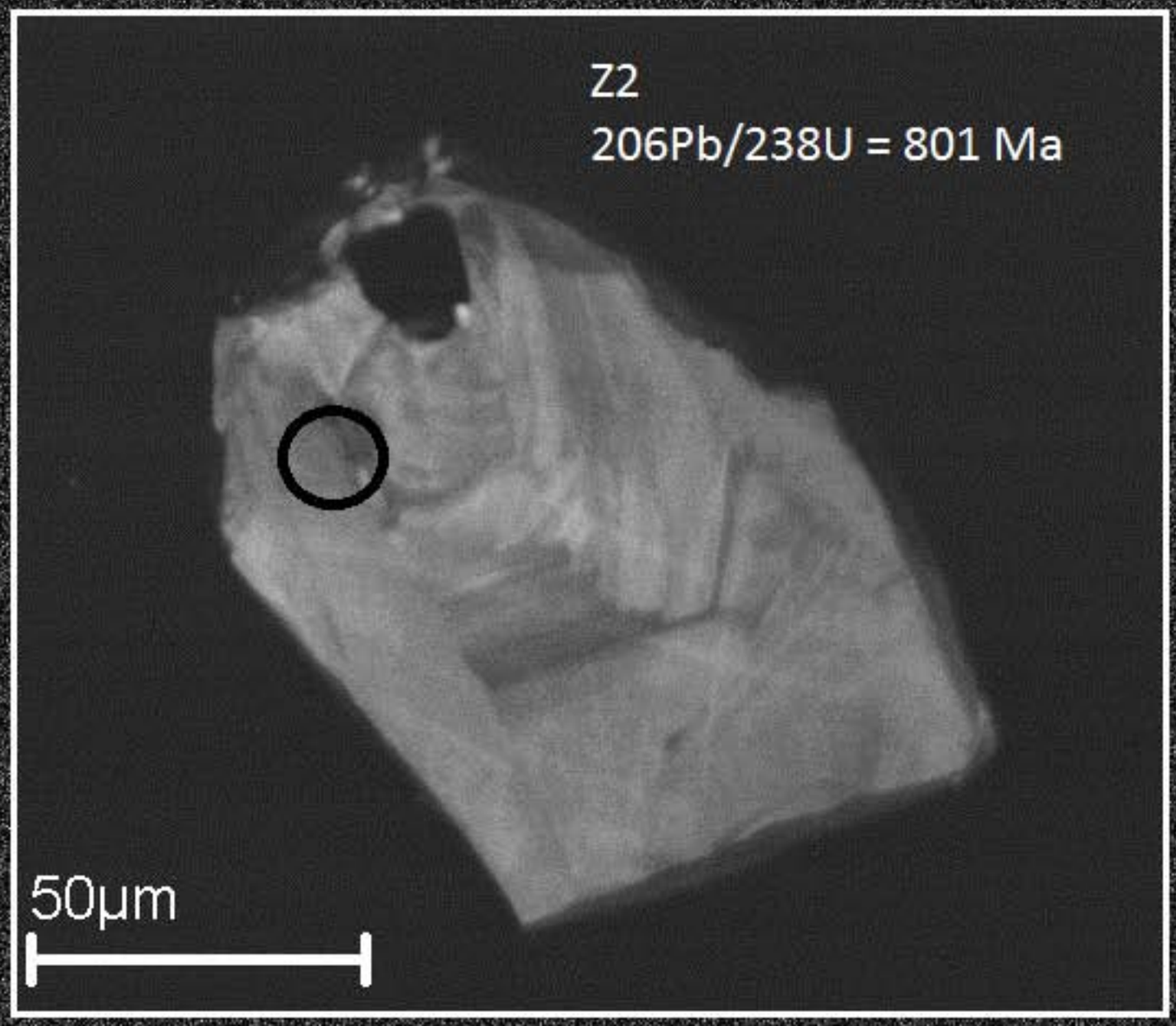

Amostra BAL-05

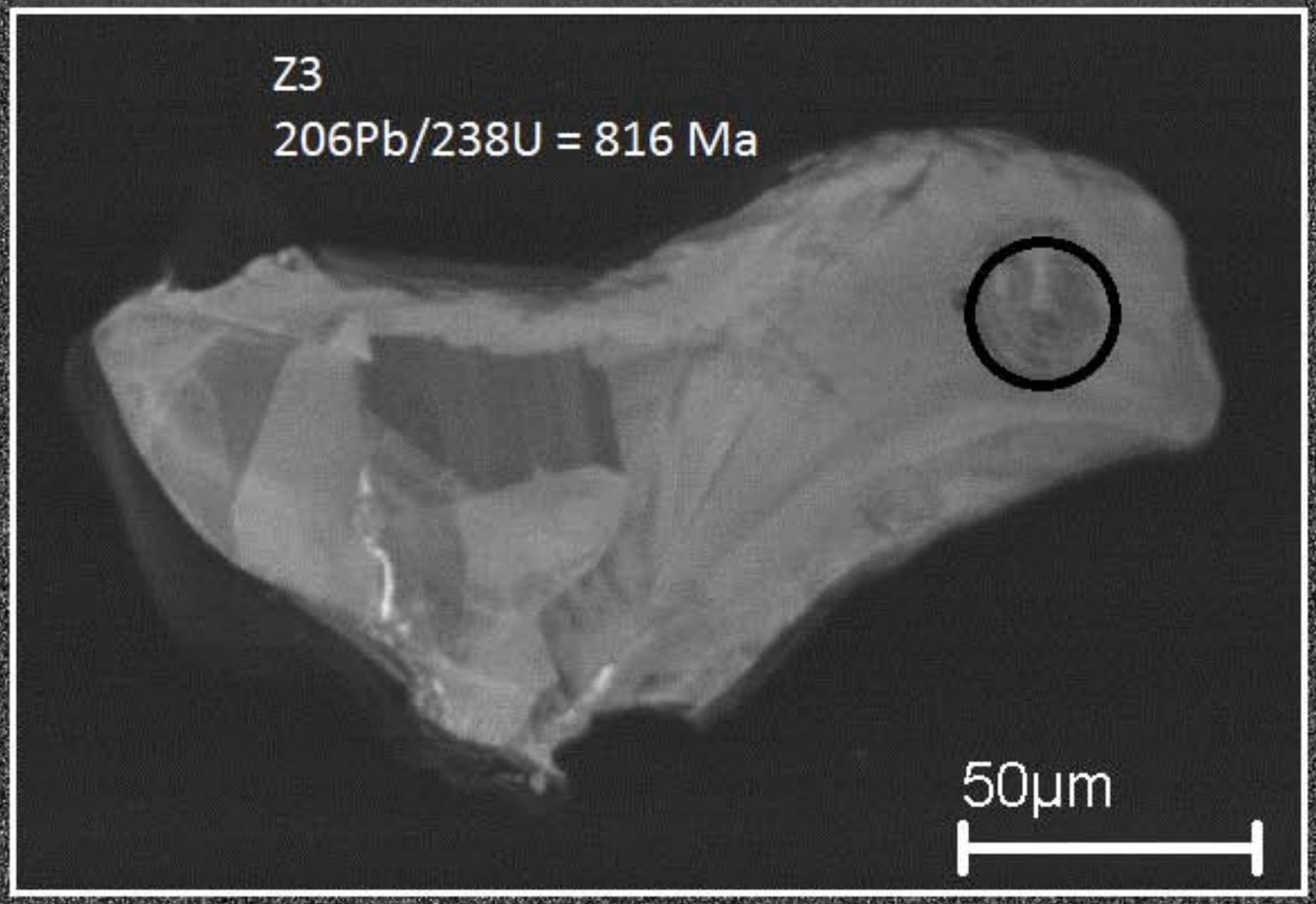

Amostra BAL-05

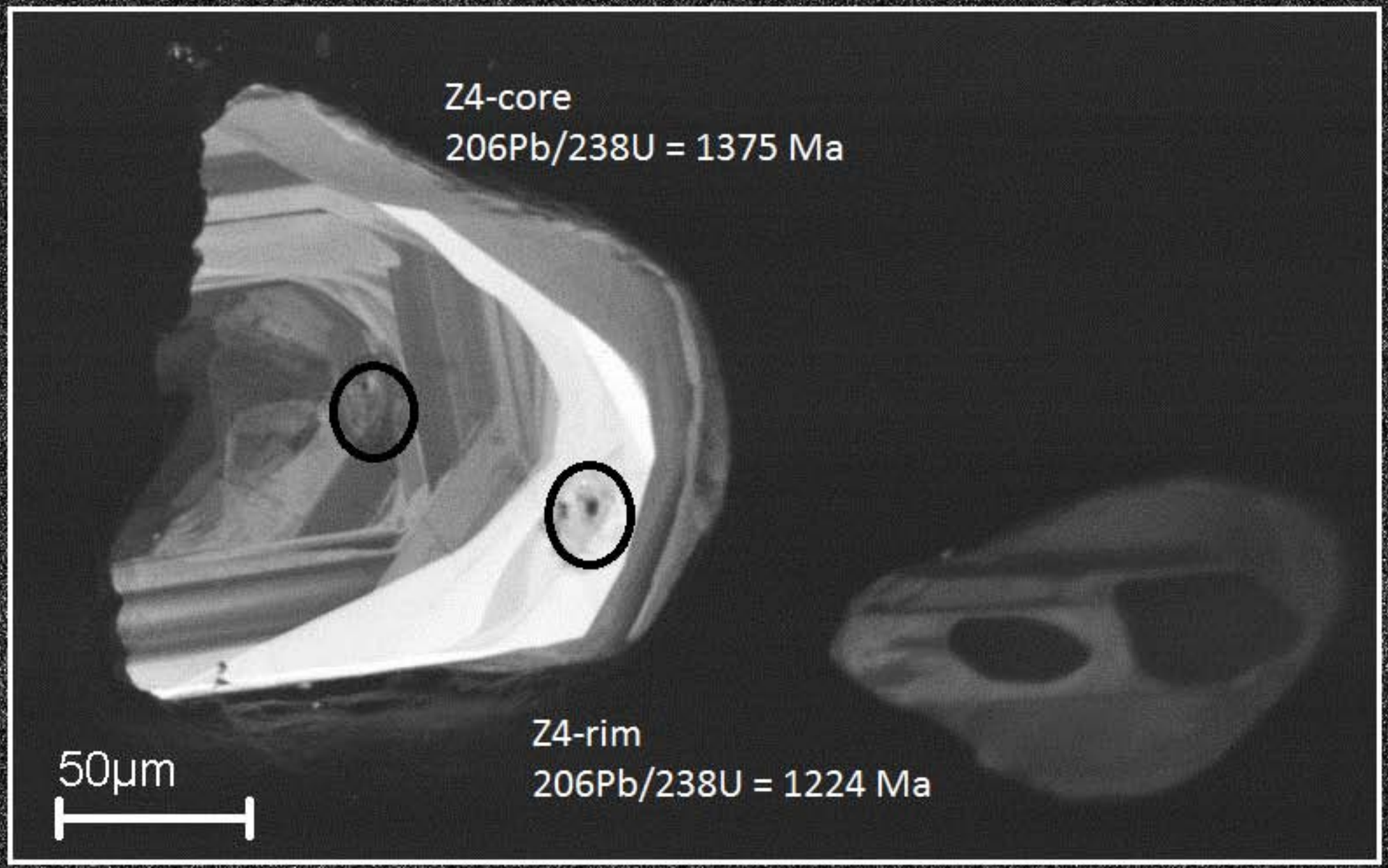

Amostra BAL-05

Amostra BAL-05

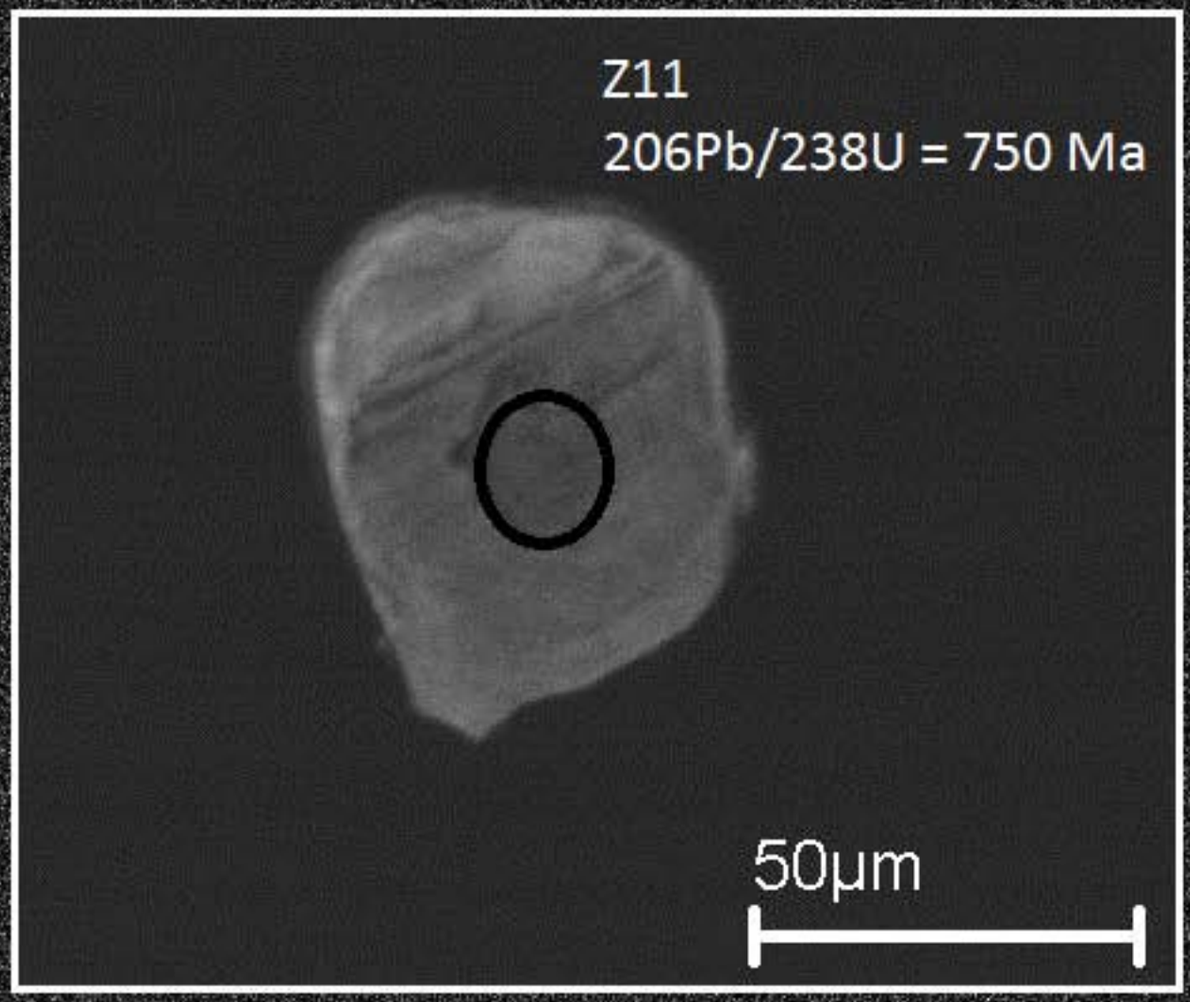

Amostra BAL-05